Multi-Scale Analysis of CUP-SHAPED COTYLEDON Transcription Factors Function

Nathalie Bouré

Thèse de doctorat

NNT : 2021UPASB052

université PARIS-SACLAY

Multi-Scale Analysis of CUP-SHAPED COTYLEDON Transcription Factors Function

Analyse multi-échelle de la fonction des facteurs de transcription CUP-SHAPED COTYLEDON

Thèse de doctorat de l'université Paris-Saclay

École doctorale n° 567 : Sciences du Végétal : du gène à l'écosystème (SEVE)
Spécialité de doctorat : biologie
Unité de recherche : Université Paris-Saclay, INRAE, AgroParisTech, Institut Jean-Pierre Bourgin, 78000, Versailles, France.
Graduate School : Biosphera (Biologie, Société, Ecologie & Environnement, Ressources, Agriculture & Alimentation)
Référent : Faculté des sciences d'Orsay

Thèse présentée et soutenue à Versailles le 26 octobre 2021, par

Nathalie BOURÉ

Composition du Jury

Michel HERNOULD Professeur, INRAE, Université de Bordeaux	Président du jury
Nathalie GONZALEZ Directrice de Recherche, INRAE, Université de Bordeaux	Rapportrice et Examinatrice
Olivier HAMANT Directeur de Recherche, INRAE, Université de Lyon 1	Rapporteur et Examinateur
Marie MONNIAUX Chargée de Recherche, CNRS, Université de Lyon 1	Examinatrice
Jean-Michel DAVIÈRE Maître de Conférences, IBMP, Université de Strasbourg	Examinateur
Nicolas ARNAUD Chargé de Recherche, INRAE, Université Paris-Saclay	Directeur de thèse

Remerciements

Voilà que la fin de la thèse arrive, cependant j'ai le sentiment de ne pas l'avoir vue venir. Mais même si ces trois années sont passées à une vitesse folle, j'ai été entourée comme jamais dans cette aventure d'une vie.

Je me dois de remercier en premier Nico. Tu as su ces trois années trouver comment me gérer dans les bons moments et aussi les plus stressants, et tout ça sans avoir reçu de mode d'emploi. J'ai eu énormément de chance d'avoir un directeur de thèse comme toi, et tous tes futurs thésards connaîtront forcément cette même chance !

Un grand merci également à Magali, j'ai été très heureuse de te partager ma vie et d'écouter la tienne tout au long de ces trois années. Merci aussi à Bernard/Robocop, qui n'aura jamais réussi à me convaincre de faire de la roue sur le parking, mais qui m'aura grandement aidée dans mes nombreux génotypages et autres manips !

Patrick, Véro, Jean-Christophe, je vous remercie d'avoir toujours été présents pour discuter, que ce soit de sciences ou d'autres choses moins sérieuses.

Je tiens à saluer mes co-doctorants préférés, Amélie, Camille, Sami, Thibault ; je vous souhaite une bonne rédaction à tous et beaucoup de bonheur dans la vie ! Mention spéciale à Antoine, pour les sessions team buildings/battage de graines, les retours en voiture, les aller-retours pas prévus en serre, et surtout m'avoir supportée moi et mon sale caractère pendant ces presque quatre ans. Je n'oublie bien évidemment pas Damien, parce que tu as fait tomber toute l'équipe FTA sous ton charme avec ton naturel et ton humour.

Je remercie chacun des membres du sous-sol (et d'ailleurs), même si à la fin de cette thèse nous sommes un peu éparpillés. Merci, dans le désordre, à Philippe A., Éric, Jasmine, Sandrine, Ayoub, Jean-Luc, Marianne, Marine, Jean-Denis, Anaïs, Yannick, Lionel, Michèle, Liudmila, Philippe R., Katia, Cyril, Gladys et tous ceux que j'aurais pu oublier. J'envoie une pensée spéciale à Julien, tout là-haut. Je tiens à remercier mes collègues de la PCSO, dont Emmanuel, Bertrand, Nardjis et bien sûr Valérie. Je pense également à Hélène et Guillaume de la préparation à l'agreg SV-STU. Merci à tous ceux d'Orsay de m'avoir fait faire autre chose que ma thèse, et de m'avoir quelque part préparée à ce qui m'attend l'année prochaine.

Je ne serais pas arrivée au bout de cette thèse sans le soutien indéfectible de ma famille. J'envoie mille baisers à ma maman (d'ailleurs, *lmdNej !*), mon papa, mes frères, ma belle-sœur, mes nièces adorées, et bien entendu Mowgli. Merci à tout le reste de ma famille dont les photos et messages WhatsApp journaliers me donnent toujours le sourire. Un grand merci à tous les copains, qui sont là en semaine comme le weekend pour les jeux, les cocktails, les discussions qui n'en finissent plus, et tout le reste. Merci à mes copains de Blospamm d'avoir partagé vos peines et vos joies, vos cristaux et vos oiseaux.

Victor, je n'ai pas besoin de te dire que sans toi, je n'en serais pas là. Tu es le meilleur mari que l'on puisse avoir, et le meilleur soutien dans la vie dont je puisse rêver. Merci d'être là pour toujours.

Je remercie également chaleureusement les membres de mes comités de thèse, Cécile Raynaud, Patrick Achard et Thomas Blein, pour leurs conseils et avis sur mon travail, ainsi que les rapporteurs de mes présentations de début et mi-thèse à l'IJPB, Sophie Jasinski et Thomas Girin. Je renouvelle mes remerciements à ceux qui ont accepté de relire ce manuscrit de thèse.

Je remercie enfin les membres de mon jury d'avoir accepté de lire et juger mon travail.

à Mémère,

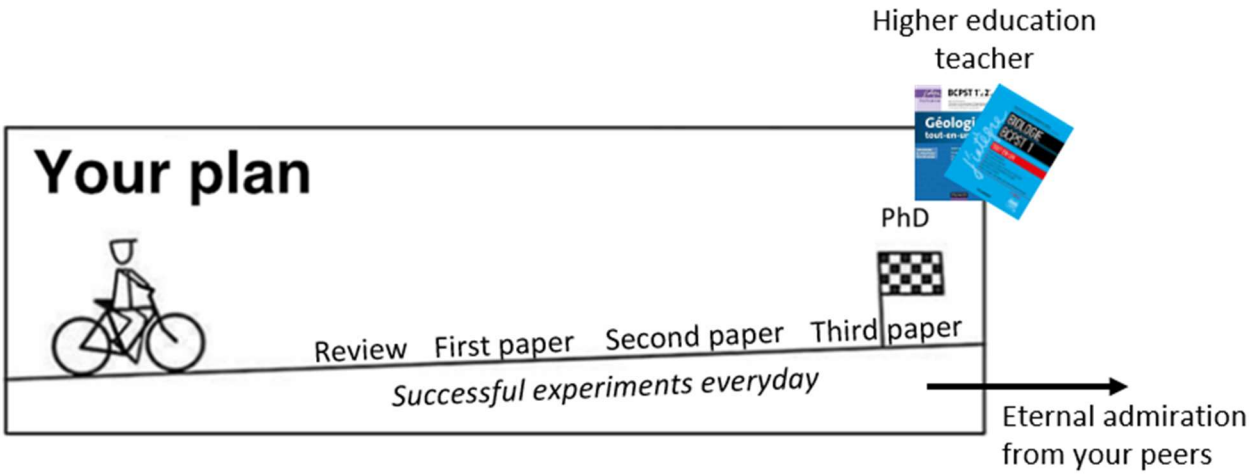
Higher education teacher
Your plan
PhD
Review
First paper
Second paper
Third paper
Successful experiments everyday
Eternal admiration from your peers

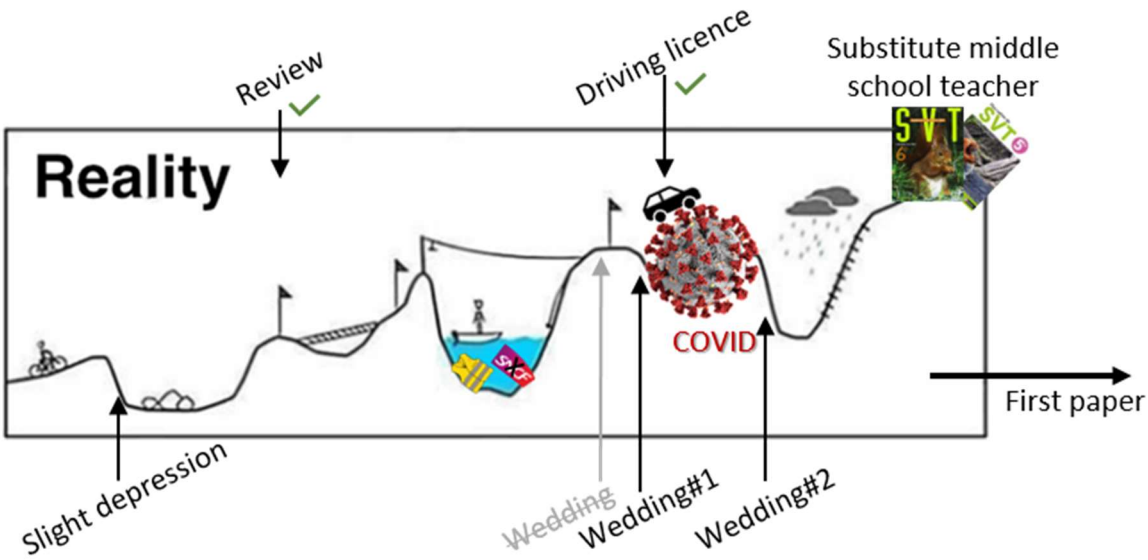
Review
Driving licence
Substitute middle school teacher
Reality
COVID
First paper
Slight depression
Wedding
Wedding#1
Wedding#2

TABLE DES MATIERES

Introduction

FOREWORD: COMPLEX PROCESSES TO PRODUCE REPRODUCIBLE ARCHITECTURES

The diversity of living beings on Earth is so vast, it is thought that a significant part is yet to be discovered (Mora et al., 2011). Plants are as concerned by this fact as animals, since the International Plant Name Index (IPNI) database totals 400,000 described species and it is estimated that there would be twice as many. Most described plants are angiosperms (370,000) and they constitute the most diverse group among plants (Christenhusz and Byng, 2016). Yet, around 2,000 news species are added up each year to the international lists.

Among living species, plants set a large number of world records. For example, the heaviest living being is named Pando, and is a clonal colony of *Populus tremuloides* weighing about 6,000 tons. Likewise, the *Sequoia sempervirens* is known to be the tallest tree on earth and can reach 120-meter heights. Plants also exhibit a tremendous variety in shapes. Yet, just like animals, plants are multi-cellular individuals composed of billions of cells, as a result of a large number of successive cell divisions from a single cell, the zygote. The cellular processes involved in the development of mature organisms are often largely conserved between species. Marginal variations of these processes greatly influence development and yield to a large observable diversity of species.

Cells display a tremendous diversity in plants (Sugimoto-Shirasu and Roberts, 2003). Their size can vary from a few micrometers, like in the shoot apical meristem (SAM), to very large cells like xylem vessels, of which the volume can increase a 30,000-times compared to their initial size (Sperry, 2015). Likewise, plant cells can display a large variety of shapes, like pavement cells in the mature leaf epidermis, the shape of which is reminiscent of puzzle pieces, or trichomes that display a thin, branched architecture. Such complexity and diversity in cell shape can only be achieved through a tightly regulated, asymmetric growth, which occurs along plant development.

Development can be defined as the set of processes that lead to a mature organism from a single cell. In plants, development is both embryonic and post-embryonic, as plants grow new organs continuously through their life. When the seed germinates, dicots display a radicle, a plumule and two cotyledons, which were formed during embryonic development. Shortly after, the shoot apical meristem (SAM) and the root apical meristem (RAM) become active and start to generate news cells and new organs. Aerial vegetative meristems continuously produce new leaves and shoots. Vegetative meristems can also undergo floral transition to produce reproductive meristems, each of which produce a determinate number of flowers.

Morphogenesis is the establishment and growth of organs and distinct parts of an individual. In multicellular organisms with several different cell types, organ formation is based on the establishment of cell identity, which specifies several cell populations, each with a specific role in the development of the organism. Plant development differs from animal development on several points. In animals, the reception by targeted cells of diffusing factors called morphogens, synthesized by organization centers, orient cell fate towards determination and then differentiation (Quante and Wang, 2009). Moreover, cells, or sets of cells, can migrate during embryonic development, allowing contact between different tissues and developmental organizers, and giving rise to a whole new level of cell fate determination. Lastly in animals, programmed cell death has long been recognized as evolutionary conserved for development, as there are very conserved molecular actors determining cell apoptosis (Conlon and Raff, 1999).

Plants, on the other hand, are submitted to a set of particular constraints. Plant cells are surrounded by a cell wall that restricts them in a closed, rigid space. Contrary to animals, no cell migration then occurs in plants except for cases of intrusive growth (Lev-Yadun, 2015). Like in animals, programmed cell death can occur in plants during development (Vaux and Korsmeyer, 1999). Moreover, the existence of morphogens is more and more admitted, as auxin, the first-discovered phytohormone in plants, is required for cell specification during embryonic development (Robert et al., 2015; Smit and Weijers, 2015), and auxin maxima help maintaining cell identity in the Root Apical Meristem (RAM) (Brumos et al., 2018). Similarly, small RNAs can be considered as plants morphogens since they are able to diffuse outside of their expression domain to influence cell fate (Nogueira et al., 2007; Chitwood et al., 2009; Skopelitis et al., 2017; Klesen et al., 2020), which is a morphogens-like activity. Finally, proteins can also diffuse outside of their expression domain through plasmodesmata, and constitute a symplasmic signal for plant

development (Wu et al., 2016). Phytohormones, sRNAs and proteins are therefore able to diffuse in the plant to modify the functioning of gene regulatory networks (GRNs) involved in development. Nonetheless, most of the plant development occurs at the meristems, where identity signals diffuse locally. Then, cell identity is mostly defined as a result of cell position, hence cell lineage. In roots, one can predict the cell type a new cell is going to differentiate based on its position towards the organization center. In shoots, *SHOOTMERISTEMLESS* and *WUSCHEL* genes are expressed by cells from the SAM and define meristem identity. Cell location, which is determined by contacts and signals with neighboring cells, triggers the expression of specific transcription factors, and consequently determines cell fate. The most striking difference between plant and animal is, in my opinion, the ability of plant cells to dedifferentiate and turn back to a stem cell-like state, that produces new cells and new organs by re-entering into the cell cycle (Grafi, 2004). For example, lateral root primordia are formed after root pericycle cells underwent dedifferentiation and rapid periclinal proliferation (Malamy and Benfey, 1997; Dubrovsky et al., 2000).

The result of morphogenesis, after integrating developmental signals and environmental inputs, is a three-dimension, organized individual. The spatial organization of the organs relative to each other is called plant architecture (Reinhardt and Kuhlemeier, 2002). Plant architecture includes branching, position, size and shape of the different plant organs. The development and arrangement of plant organs is species-specific and very reproductible under fixed environmental conditions as morphological traits vary within a small range of values. Although plants respond strongly to their environment (temperature, humidity, stresses, light, nutrient availability…), their response is stereotyped and results in the same set of phenotypes where there is little variation between individuals. For example, wild type dark-grown seedlings all undergo hypocotyl elongation to achieve very similar lengths (Josse and Halliday, 2008). Over and above, plant architecture is one of the critical levers of crop improvement (Reinhardt and Kuhlemeier, 2002). One of the keys to the green revolution was indeed the selection of semi-dwarf, higher-producing mutants like *Rht,* which displays a resistance to growth-promoting gibberellic acid (GA) phytohormone (Peng et al., 1999), or *sd-1* in which GA production is partially impinged on (Monna et al., 2002; Hedden, 2003). Hence, a better understanding of plant development and architecture establishment is critical to agronomics, especially when considering a more and more changing and contrasted environment. In particular, understanding the molecular mechanisms that govern

growth is essential, as differential growth resulting from different cell growth rates overrules morphogenesis.

In the following introduction, I will intend to define and describe the different types of cell growth and the regulatory principles that control growth decision. I will focus on leaf development and polarity establishment. The leaf margins will subsequently be used as a model to describe molecular mechanisms sustaining differential growth.

TO GROW OR NOT TO GROW: GENERAL CONCEPTS ON CELL GROWTH AND ITS CONTROL

Different types of growth

The shape and size of an individual is determined by the number, position and size of cells it is composed of. The starting point of shape acquisition for an organism is cell proliferation. Cell divisions can be symmetric or asymmetric. In animals, cell migration can also trigger the apparition of a certain architecture, but no such movements can be observed along most part of plant development. In order to acquire a complex shape, embryos must break isotropic growth, which means their growth must be oriented in preferential directions instead of all directions. This break of isotropy can be achieved thanks to specific timing of cell divisions, oriented divisions (for example anti-/periclinal divisions, *i.e.* parallel/radially to the stem axis) or asymmetric cell divisions (for example the few first cell divisions of the zygote: the two daughter cells do not have the same cytoplasmic content). In addition, cell anisotropic growth without cell division can give rise to shapes. Anisotropic growth creates differential enlargement between distinct parts of the organism, which in turns gives rise to a shape. In order to explain how differential growth may occur, I must first introduce the different ways cells can grow, the molecular actors involved and how the different types of growth coordinate tightly to allow the robust development of organs.

Beyond cell division, in order to grow an organism must increase the volume of the cells it is composed of. While the number of cells increases through cell divisions, increase in cell volumes is mainly triggered by both cytosolic growth (net gain of cellular components) and cell expansion (cell growth in association with cell wall modification). Endoreduplication is a modified cell cycle where cells undergo replication but skip mitosis; polyploid cells can display much larger

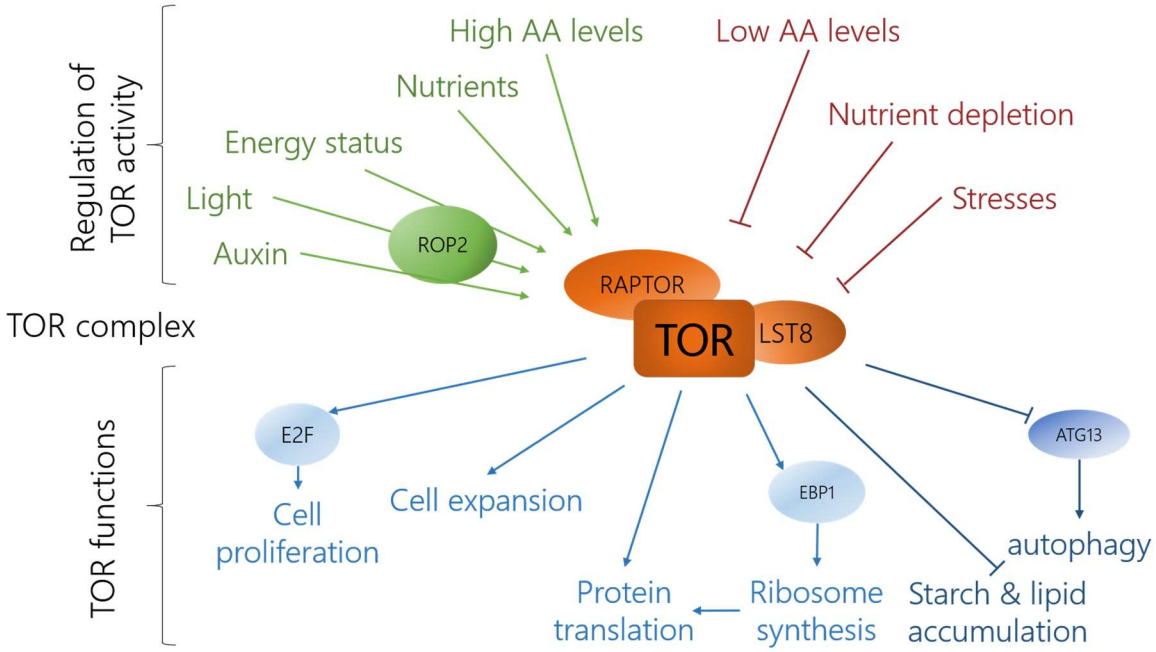

FIGURE I-01: The plant TARGET OF RAPAMYCINE COMPLEX 1 (TORC1)

TORC1 is composed of Regulatory associated protein of TOR (RAPTOR), Lethal with Sec13 protein 8 (LST8) and TOR. This complex controls various metabolic processes and is critical for cytoplasmic growth. Its activity is heavily dependent upon the cell state.

Figure inspired by (Burkart and Brandizzi, 2021)

cell sizes. Increases in cell volume and number are intertwined with one another and the cellular processes involved in their control are tightly coordinated.

Cytosolic growth

Cytosolic growth must first be introduced as an isotropic growth that is different from water uptake-triggered growth in volume. Cytosolic growth is a net increase in cell volume which relies on macromolecular syntheses (ribosomes, metabolism proteins, membranes, cell wall…). It is very energy- and resources-consuming as it uses available molecules to perform various processes of anabolism and accumulate cellular components. Cytosolic growth must hence occur according to proper nutrient availability and energy status.

In plants, the major regulator of nutrient availability sensing is the TARGET OF RAPAMYCINE (TOR) kinase (Robaglia et al., 2012; Dobrenel et al., 2013; Xiong et al., 2013). TOR can be activated by sugar levels and the mitochondrial energy status through the activity of ROP2 GTPase (Li et al., 2017; Schepetilnikov et al., 2017) (Figure I-01). TOR can also be activated by light and hormones, such as auxin (Schepetilnikov et al., 2013; Schepetilnikov et al., 2017). Some amino acid levels can also be used as sensors for the cell energy status (Jewell et al., 2013; O'Leary et al., 2020). In animals, TOR activation upon high amino acid levels promotes protein synthesis and growth, while its inactivation triggered by low amino acid levels is linked to autophagy (González and Hall, 2017). More generally, TOR inactivity in case of nutrient shortage triggers autophagy which recycles cellular components. In plants, TOR activity was shown to promote rRNA accumulation (Ren et al., 2011). TOR also promotes translation and the formation of polysomes (Ren et al., 2011; Xiong et al., 2013). TOR is also a direct regulator of metabolism as it was shown to repress starch accumulation as well as lipid storage to promote growth (Caldana et al., 2013). A recent focus on the relationship between TOR activity and the circadian clock outlined TOR to be a key actor in the coordination between plant growth and day/night alternance (Zhang et al., 2019a). Taken together, the different inputs that trigger TOR activation and the large span of growth-promoting responses it is involved in establish how decisive TOR is for anabolism, hence cytosolic growth (Figure I-01).

Interestingly, TOR was also shown to be involved in the control of stem cell proliferation in response to light and energy status (Pfeiffer et al., 2016; Schepetilnikov and Ryabova, 2018). $E2F^{B}$, which is important for leaf primordia proliferation, is indeed targeted and phosphorylated

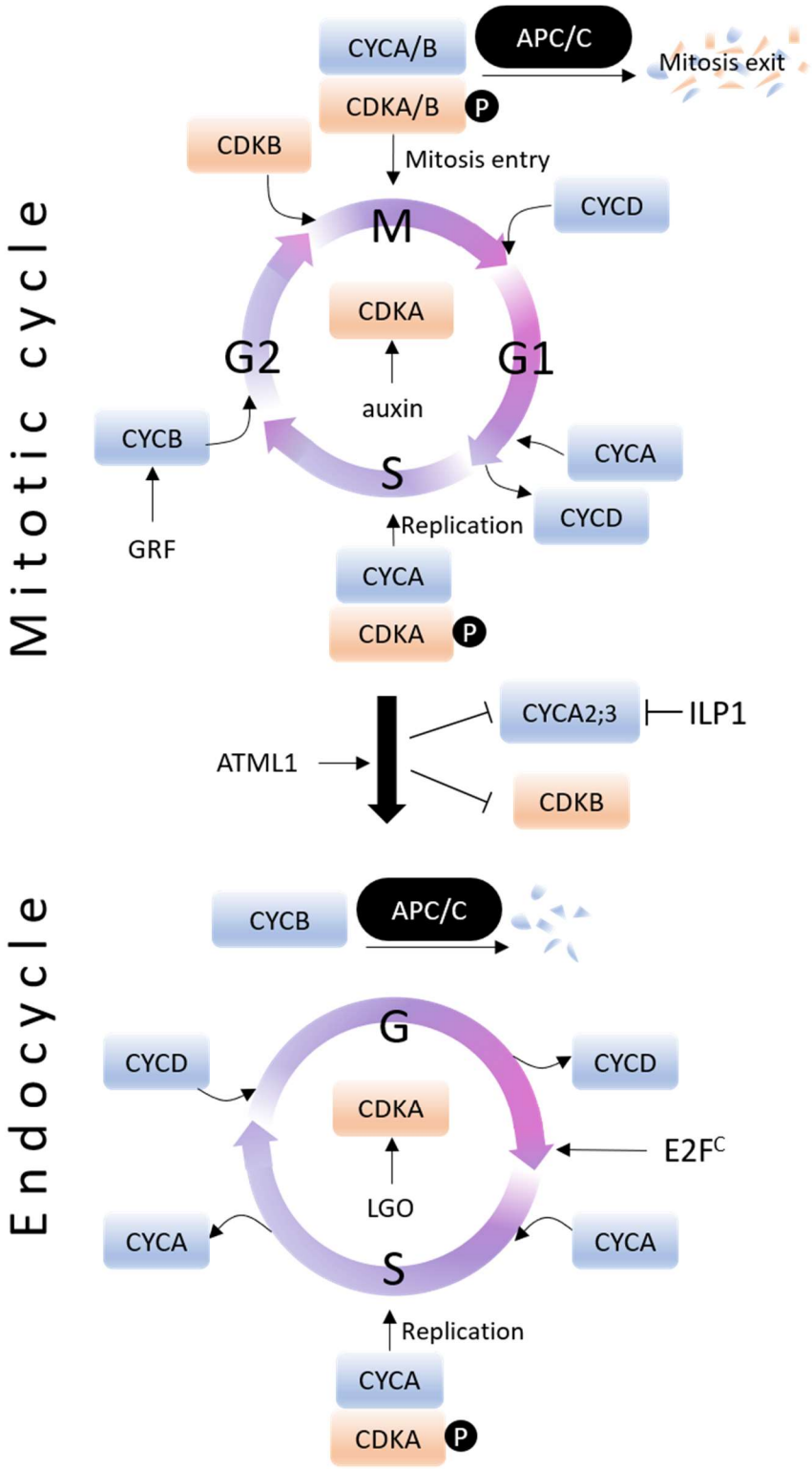

FIGURE I-02: Cell cycle and endoreduplication regulation

Cell cycle is regulated by CYCLIN (CYC) / CYCLIN-DEPENDENT KINASES (CDK) complexes that oscillates through time. CYCD activity is associated with G1/S transition while CYCB activity is associated with G2/S transition. Switch from cell division to cell endocycling can be triggered by alternative CYC/CDK complexes. Multiple developmental processes can promote the mitotic cycle/endocycle switch.

by TOR (Li et al., 2017). TOR could also be an important regulator of the cell cycle as several G1- and S-specific genes have been identified as TOR targets.

Segmentation

Plant growth is achieved through the tightly-regulated coordination of segmentation and other types of cellular growth, which allows the growth of the whole organism. Here, segmentation refers to net cell divisions, independently from cytoplasmic growth. Cell division cannot occur indefinitely in an organ in which cells do not perform cytoplasmic growth, because each symmetrical division reduces the volume of a cell by two times. Likewise, the cytoplasmic growth of a diploid cell is limited by a maximum size (Robinson et al., 2018). Cell division is thus key for the development of plants. Moreover, cell division is essential to shape acquisition as asymmetric divisions are crucial to create new axes of growth (Pillitteri et al., 2016).

The cell cycle divides itself into two main stages, the mitosis and the interphase. The interphase is itself composed of three stages, the gap 1 phase (G1), the synthesis phase (S) during which the genomic DNA undergoes replication, and the gap 2 phase (G2). Each of these steps is characterized by a set of proteins, such as the cyclin-CDK (cyclin-dependent kinases) complexes, for which the activity oscillates throughout the progression of the cell cycle (Figure I-02). In plants, a large variety of Cyclins (CYC) and CDK form complexes that are involved in the control of the cell cycle and act as checkpoints to allow the progression along the cycle. For instance, the entry into mitosis is triggered by the formation of the CDKB/CYCA/B complex. On the contrary, the anaphase-promoting complex/cyclosome (APC/C), which displays a E_3 ubiquitin ligase activity, directly targets CYCB to promote its degradation by the proteasome and subsequently to terminate the M phase (Figure I-02).

CDK activity seems to be essential to the coordination between cytoplasmic growth and segmentation. Interestingly, cell area increases at the SAM in *cycd* mutants, while the duration of the cell cycle remains stable (Jones et al., 2017). Similarly, in CYCD-overexpressing plants, cell areas at the SAM were shown to decrease while displaying a consistent cell cycle duration (Jones et al., 2017). These data suggest that cell size and cell cycle control are strongly coordinated. In the *cycd* mutant, the length of G1 was reduced, which is due to a larger initial cell size at the G1 entry (Jones et al., 2017). The authors concluded that the G1 phase duration depends on cell size.

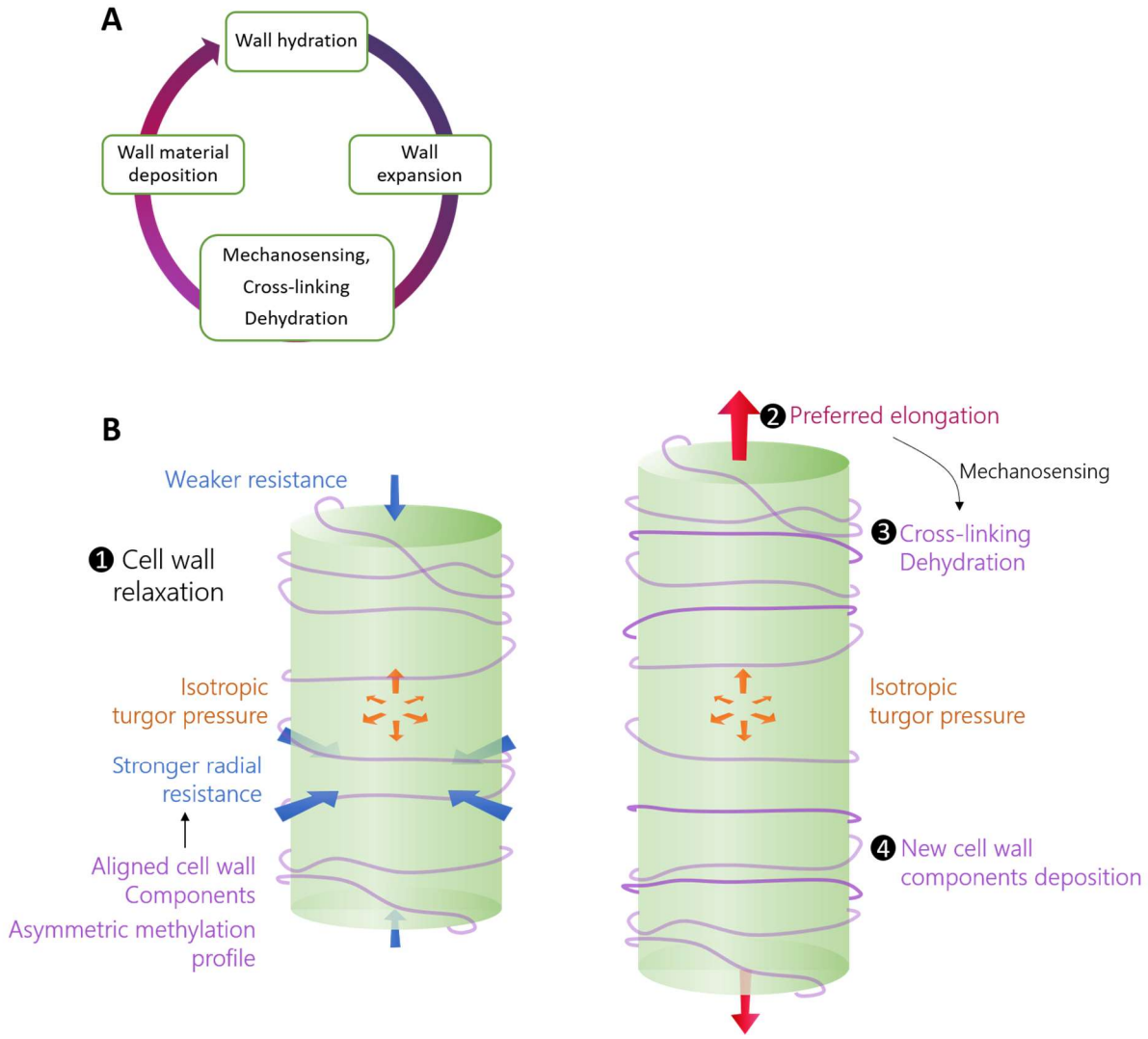

FIGURE I-03: Mechanism of cell expansion: a parietal view

A. Cell expansion is the result of an oscillating cell wall dynamic. Cycle is redrawn after (Wolf et al., 2012). B. Cell expansion is a cyclic process that can be anisotropic as a result of uneven cell wall resistance.. A,B. Wall hydration and acidification results in cell wall relaxation to a point turgor pressure is sufficient to trigger deformation. Aligned cell wall components and an asymmetry in pectin methylation profile results in an uneven cell wall resistance around the cell. Elongation triggers mechanosensing and promotes dehydration and cross linking of the cell wall components, while new components are added to the wall to maintain its thickness and stiffness.

Segmentation is crucial to guarantee the production of the adequate number of cells to form the plant organs. However, the number of cells does not determine the final organ size. Similar organ size can be achieved in leaves for instance with different cell numbers due to compensatory systems that increase cell volume, meaning leaf morphogenesis is a very robust developmental process (Tsukaya, 2002).

Polyploid growth

In addition to segmentation, polyploid growth allows an increase in cell size and represents an important lever of organ shaping and growth. Plant cells can perform a modified cell cycle called endocycle, in which mitosis is bypassed between G1 and G2 phases, leading to an increase in cell ploidy. The shift from cell division to endoreduplication is due to a reorganization of the pool of cyclins, CDKs and regulatory proteins (Figure I-02). For example, mitosis-promoting CYCB are constantly targeted by ubiquitin E3 ligases (the APC complex) and sent to the 26S proteasome for degradation, which ultimately represses the entrance into mitosis. In addition, INCREASED LEVELS OF PLOIDY 1 (ILP1) promote endocycling by repressing the expression of mitosis promoting CYCA2 (Yoshizumi et al., 2006; De Veylder et al., 2011).

More specifically in leaves and sepals, LOSS OF GIANT CELLS (LGO) functions as a CDK repressor, and repress mitosis entrance to trigger endoreduplication, indicating that polyploid growth can be tissue specific (Walker et al., 2000; Churchman et al., 2006; Roeder et al., 2010). The expression of *Arabidopsis thaliana* MERISTEM LAYER1 (ATML1) TF, which is epidermis-specific, can fluctuate between neighboring cells within a tissue. The levels of *ATML1* expression was shown to determine cell fate in a dose-dependent manner, as low *ATML1*-expressing cells still divide while high *ATML1*-expressing cells undergo endocycling (Meyer et al., 2017). The random distribution of cells expressing elevated levels of ATML1 results in the homogeneous spacing of giant cells within the sepals. These data indicate that cell polyploid growth, in association with cell expansion, can also occur in specific cells within a tissue.

Polyploid growth is in most cases associated with a large increase in cell size and volume (Sugimoto-Shirasu and Roberts, 2003). While correlations between epidermis cell surface and ploidy level has long been demonstrated in *Arabidopsis* (Melaragno et al., 1993), more recent data indicate that correlations between cell volume and cell ploidy level is cell-type specific (Katagiri et al., 2016). Furthermore, the level of ploidy was confirmed in sepal epidermis to drive cell size rather than the nucleus volume (Robinson et al., 2018). Hence, since cell size seems to be highly

correlated with cell ploidy level in the epidermis, it must also be considered that cell endocycle regulation represents a critical lever to control overall growth.

Cell expansion

The type of growth that probably contributes the most to plant growth is cell expansion. Cell expansion is a turgor-driven increase in cell size, which requires that the surrounding cell wall, that constricts plant cells within closed spaces, be rendered flexible. Cell expansion occurs when the turgor pressure exceeds the resistance of the cell wall, due to the relaxation of the latter. The balance between these two opposed dynamics is achieved by periodic oscillations (Figure I-03). Cell wall reorganization includes wall hydration, acidification, and modification of polysaccharides branching and tight cohesion (those modifications will be further explained later in this introduction). Next, the inflation of the cell within the cell wall cavity triggers the activation of mechanosensing pathways (Wolf et al., 2012). Finally, synthesized cell wall components are secreted through exocytosis and allow maintenance of the cell wall thickness and density following elongation. This dynamic loop is continuously active thorough organ elongation (Figure I-03).

Study on tip-growing pollen tubes from lily and tobacco showed that cell wall thickness, as well as growth rate, oscillate with time (McKenna et al., 2009). Interestingly, even though they share the same oscillating period, growth rate and cell wall thickness were out of phase, since the oscillation in thickness precedes growth oscillations by about 7 seconds. Detection of cell exocytosis oscillations showed that cell wall components are secreted and take part in increasing the wall thickness (McKenna et al., 2009). The temporal shift between cell wall components secretion and growth rate peak confirms a cyclic functioning of cell elongation in the case of tip growth.

Coordination between different types of growth

During organ development, several developmental dynamics can be observed. A proliferative state implies a certain kind of cellular growth since extensive mitosis requires cytoplasmic growth, which guarantees that cells are not smaller and smaller division after division and preserves cell integrity. In elongating organs, cell expansion is associated with polyploid growth which allows the emergence of giant cells - affecting all cells of a tissue, or only a fraction of it (Roeder et al., 2010; Meyer et al., 2017). In addition, both polyploid growth and cell expansion

are associated with cytoplasmic growth. Thus, the previously described types of growth are deeply interconnected and coordinated to allow proper plant development.

The balance between polyploidy and segmentation is critical to guarantee correct organ development. For example, $E2F^C$ is an endocycle-promoting TF. In the *e2fc-R* RNA-interfered line, leaves were much smaller and exhibited more, smaller cells with a lower level of ploidy (del Pozo et al., 2006). In polyploid cells from *Arabidopsis* stem, cell wall composition was shown to be altered, containing less cellulose and more polysaccharides (Corneillie et al., 2019). Such changes in cell wall composition could be associated with modifications of cell wall mechanical properties and greatly influence the cell wall local extensibility, by increasing cell potentiation to elongate.

The coordination between different types of cell growth was shown to depend on intrinsic cell parameters. For instance in sepal primordia, which exhibit a leaf-like development, the existence of a cell size-related, *JAGGED* (*JAG*)-dependent checkpoint was demonstrated before the start of DNA replication, since abnormally small replicating cells were reported following an ectopic *JAG* expression (Schiessl et al., 2012). It was thus hypothesized that cell size constitutes a G1-S checkpoint for cell cycle progression. In *Arabidopsis*, expression of genomic *AtCYCD2;1* was sufficient to reduce cell size due to acceleration of the G1 phase, which in the end abolished endoreduplications (Qi and John, 2007). These data suggest that a minimal cell size is indeed required to provoke endoreduplication, and link cytosolic growth with mitotic and polyploid growth.

TOR represents a good candidate to explain the coordination between different types of growth. Indeed, down-regulation of TOR yielded differential expression of genes involved in cell wall synthesis and modifications, like expansins, pectin methyl esterases, xyloglucan transglycosylases *etc*… (Caldana et al., 2013). Then, in addition to cytoplasmic and segmentation, TOR is also involved in the control of cell expansion.

Under drought conditions, LGO (also named SMR1 for SIAMESE RELATED 1) accumulates in cells to repress cell proliferation, which ultimately represses leaf growth (Dubois et al., 2018). Hence, growth processes can also be controlled by external parameters like stresses and other environmental inputs.

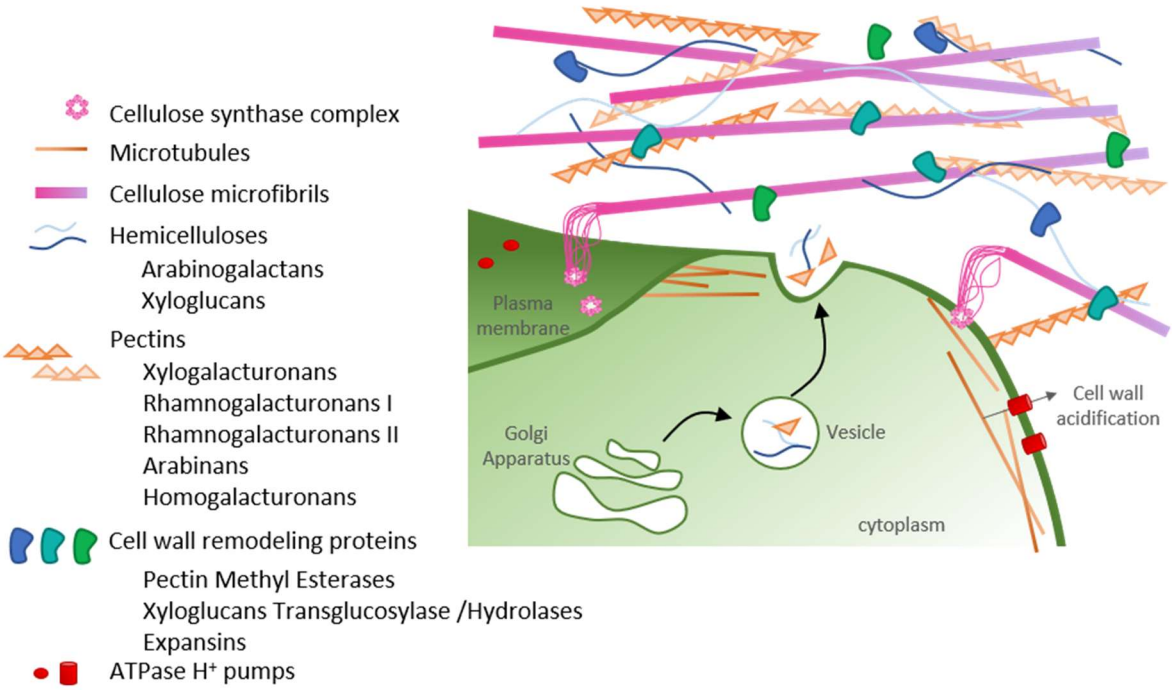

FIGURE I-04: The plant cell wall

Cell wall is a complex structure composed of cellulose microfibrils, hemicelluloses and pectins. While microfibrils are directly secreted in the cell wall thanks to microtubules-guided cellulose synthase complexes, pectins and hemicelluloses are synthesized in the Golgi Apparatus and are secreted by exocytosis. Weak and covalent bonds were demonstrated between the different components of the wall. Cell wall remodeling proteins are able to modify those bonds. Some of their activity depends on the activation of ATPase H^+ pumps triggered by auxin signaling.
Figure inspired by (Cosgrove, 2005).

Mechanisms of cell expansion

Even if most of the components of the cell wall have been known for decades, the fine details of its compositions and organization are still under study in numerous labs in the world. With the rise of more advanced techniques, the study of cell wall mechanical properties has been the subject of renewed interest from researchers. New imaging techniques have also fostered a better understanding of several cellular processes.

To allow a proper plant development, the cell wall has to present a few characteristics, as it must be rigid and resistant to provide support to the rest of the plant, but also malleable to allow cellular expansion and cell divisions. Here I chose to focus on the primary cell wall which is involved in cell expansion.

Composition of the cell wall

The plant cell wall is a complex network mainly composed of cellulose microfibrils (assembly of β1-4 D-glucose polymers). Cellulose microfibrils are embedded in non-cellulosic polysaccharides, namely pectins (that contains diverse homogalacturonans and rhamnogalacturonans) and hemicelluloses (xyloglucans and arabinoxylans). The plant cell wall also contains apoplastic proteins that are crucial for the cell wall dynamic (Figure I-04).

Microfibrils are directly synthesized at the plasma membrane thanks to cellulose synthase complexes (CSCs) that are composed of cellulose synthase (CESA) polymeric complexes (Hill et al., 2014), in which every CESA has a glucose polymerization activity. Unlike microfibrils, pectins and hemicelluloses are synthesized in the Golgi apparatus and undergo exocytosis. Once secreted, they diffuse in the cell wall and integrate themselves into the matrix through enzymatic reactions or cross-linking binding. In the cell wall, hemicelluloses spontaneously bind to microfibrils (Takeda et al., 2002). Xyloglucans were also shown to bind to pectins (Popper and Fry, 2008). Recent data identified the transferases that catalyze the covalent bond between xyloglucans and pectin derivatives (Stratilová et al., 2020). In the wall, different functional domains were identified for xyloglucans, such as cellulose-binding, although some remained inaccessible, buried in cellulose domains (Pauly et al., 1999). Hence, the cell wall can be interpreted as a tight network. Pectins were shown to interact with cellulose (Zykwinska et al., 2005). De-methylesterified pectins can also form self-interacting networks around Ca^{2+} cations, thus forming a hydrated gel that densifies and makes the wall stiffer, *i.e.* less likely to deform (Ridley et al., 2001).

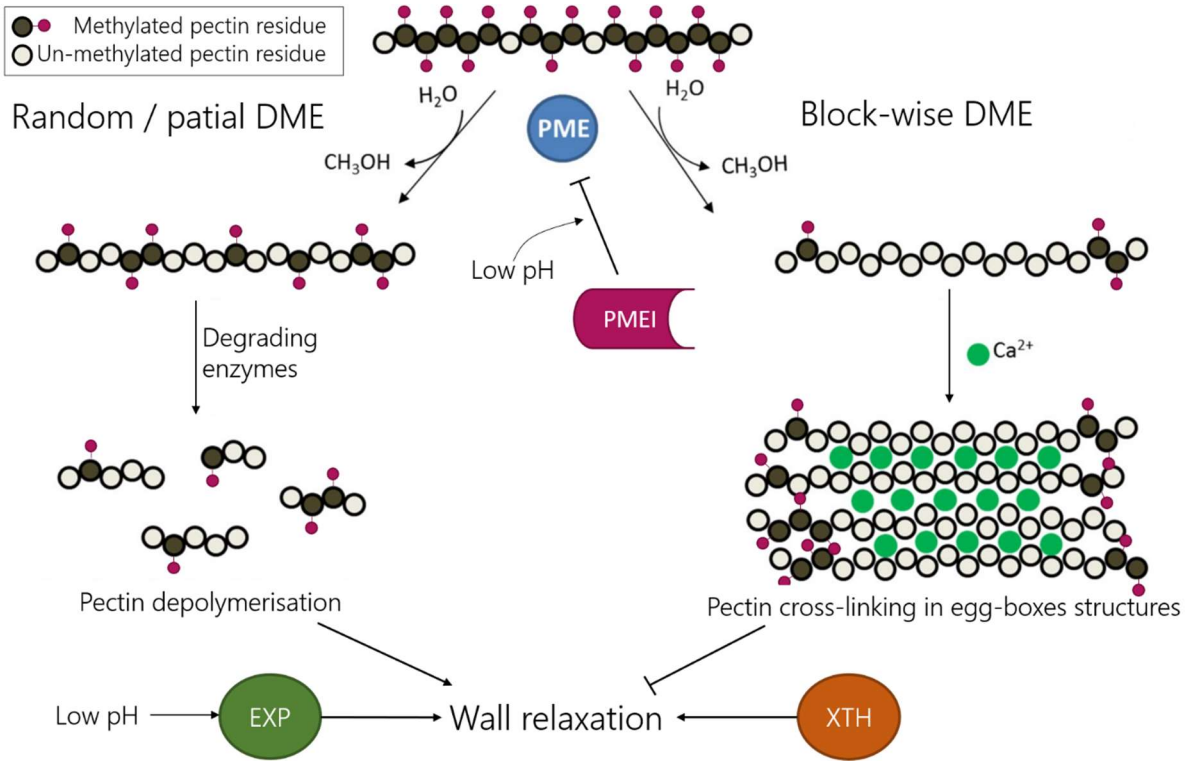

FIGURE I-05: Cell wall relaxation is triggered by cell wall remodeling enzymes.
Pectins de-methyl esterification can either promote or repress wall relaxation depending on the pattern of de-methylated residues. Expansins and Xyloglucan endoTransglucosylase /Hydrolases are other significant apoplastic enzymes that trigger cell wall relaxation. Abbreviations: PME = Pectin Methyl Esterase; PMEI = PME Inhibitor; DME = De-Methyl Esterification; EXP = Expansin; XTH = Xyloglucan endoTransglucosylase /Hydrolases.
Figure is modified from (Wormit and Usadel, 2018)

Cell wall relaxation and growth

Cell wall relaxation is key to balance cell wall resistance and turgor pressure. During cell expansion, the cell wall undergoes several chemical modifications, which in turn greatly modify its mechanical properties and make it deformable.

While they are major components of the cell wall matrix and take part in cell wall stiffening, pectins are also crucial for the control of cell wall porosity (Willats et al., 2001) and are key actors of the cell wall loosening. Methyl-esterified pectins form a tight network in the cell matrix, which can be destabilized through the activity of Pectin Methyl-Esterases (PMEs) that trigger demethyl-esterifications (DMEs). Two types of pectins DME can cause opposite effects on cell wall mechanical properties (Wormit and Usadel, 2018)(Figure I-05). The DME of consecutive residues, also termed block-wise DME, triggers wall stiffening through the formation of egg-boxes-like structures that contain crosslinked un-methyl-esterized pectins around calcium ions and form an hydrated gel (Tibbits et al., 1998; Braccini and Pérez, 2001; White et al., 2014). On the contrary, partial block-wise or random DME triggers pectin saccharification by pectin degrading enzymes which ultimately softens the cell wall.

Free, un-methyl-esterified pectins are mobile in the cell wall and soften the pectin matrix (Cosgrove, 2005; Höfte and Voxeur, 2017). PME inhibitors (PMEI), on the contrary, can bind to PME and prevent pectin DME. PMEI can have opposite effects on cell wall rigidity. A significant increase in root length was reported in a *Atpmei4* mutant, as a consequence of increased *AtPME17* expression and activity (Sénéchal et al., 2015). This suggests that PME17 triggers cell wall softening to allow cell elongation. Conversely, an *AtPMEI2* over-expressing line reduced pectin DME and was associated with longer roots (Lionetti et al., 2007), which suggests that pectin DME can also repress cell elongation. Hence, pectin methylation state can have distinct effects on cell growth. The role of *PME* and *PMEI* families of genes is not fully resolved yet, and specific PME/PMEI pairs could trigger opposing effects on growth (Wormit and Usadel, 2018). The formation of the PME3/PMEI7 complex was shown to be pH-dependent (Sénéchal et al., 2017). Hence, acidic pH prevents PMEI-triggered inhibition of PME which in turn can act to soften the cell wall (Figure I-05).

In addition to PME/PMEI proteins, other proteins are involved in the control of cell wall relaxation. Expansins (EXPs) are proteins that increase the cell wall softening by breaking the hydrogen bonds between cellulose microfibrils and hemicelluloses (Cosgrove, 2005; Cosgrove,

2016). Experiments on expansins applications and depletion in EXP demonstrated that their level correlates with cell elongation (Cho and Cosgrove, 2000). Like PME/PMEI complexes, EXPs activity is enhanced in acidic pH (McQueen-Mason et al., 1992).

The role of cell wall acidification in cell expansion has been known for a long time (Cleland, 1973). Auxin was shown to be responsible for the cell wall acidification and plasma membrane hyperpolarization. Upon auxin induction, early auxin-responsive *SAUR* genes are expressed and were shown to inhibit PP2C-D phosphatase, which normally represses H^+ATPase pumps (Spartz et al., 2014). Hence, auxin triggers cell wall acidification which is necessary to PME and EXP optimum activity.

Hemicellulose branching and composition are also modified upon cell wall loosening. Xyloglucan endoTransglucosylase /Hydrolases (XTHs) act as cell wall loosening enzymes by both catalyzing the cleavage and rejoining of xyloglucan chains (Fry et al., 1992; Van Sandt et al., 2007). Xyloglucan EndoTransglucosylase (XET) activity was demonstrated for most XTHs, including *At*XTH12/13/17/18/19 (Maris et al., 2011). Besides, *XTH18* and *XTH19* overexpressing lines exhibit longer hypocotyls in the dark than the wildtype, indicating that they take part in cell expansion (Miedes et al., 2013). Recent results indicate that modification of both cellulose microfibrils and xyloglucans is necessary to trigger cell wall loosening (Zhang et al., 2019b). Hence, hemicellulose relaxation is also as critical as any other cell wall component modification.

Interestingly, brassinosteroids (BRs) were also shown to trigger rapid cell elongation in the hypocotyl. BR signaling was shown to induce the expression of several XTHs and expansins (Guo et al., 2009). Besides, BR signaling is also involved in cell wall acidification as BR can promote the activity of H^+ATPase pumps through BRI1 kinase activity (Caesar et al., 2011). It thus seems that other growth-promoting hormones can drive cell elongation during development.

Anisotropy of cell expansion

Cell elongation is most of the time oriented towards a specific direction. As cell surface does not expand in all directions, cell expansion is thus said to be anisotropic. The turgor pressure generates a force applied uniformly over the entire contact area between the cell and its surrounding wall. Therefore, anisotropic growth of the cell is related to the characteristics of the cell wall, in particular to the heterogeneity of its strength along certain directions (Figure I-03). Recent data indicate that two cell wall properties synergistically act to establish asymmetric

growth. Cellulose microfibrils are the major components of cell walls and are deposited by cellulose synthase complexes (CSCs) inserted in the plasma membrane and guided by underneath microtubules (MTs) (Burk and Ye, 2002; MacKinnon et al., 2006; Crowell et al., 2010; Chan et al., 2011). Microfibrils deposition was shown to be mostly perpendicular to cell elongation, which creates an asymmetric cell resistance (Crowell et al., 2010). Since the strongest cell wall resistance is oriented radially, cell elongation naturally occurs along the weakest resistance (Figure I-03).

More recent data focused on the break in cell growth symmetry at early developmental stages of hypocotyl growth, and suggest that asymmetric pectin methylation state could precede anisotropic microfibrils deposition (Peaucelle et al., 2015). Longitudinal cell wall softening would trigger longitudinal elongation and influence radial cellulose deposition (Peaucelle et al., 2015). A recent study on hypocotyls established that both cell wall mechanical asymmetry and microfibrils orientation arise from the very first hours after germination (Daher et al., 2018). Modelling of a hypocotyl section yielded that cell wall composition anisotropy is sufficient to induce anisotropic growth, while pectin triggered elastic asymmetry was not. However, both had additive effects on anisotropic cell expansion (Daher et al., 2018). Ultimately, both cell wall material asymmetrization and remodeling seem to act in concert to promote an adequate, oriented growth.

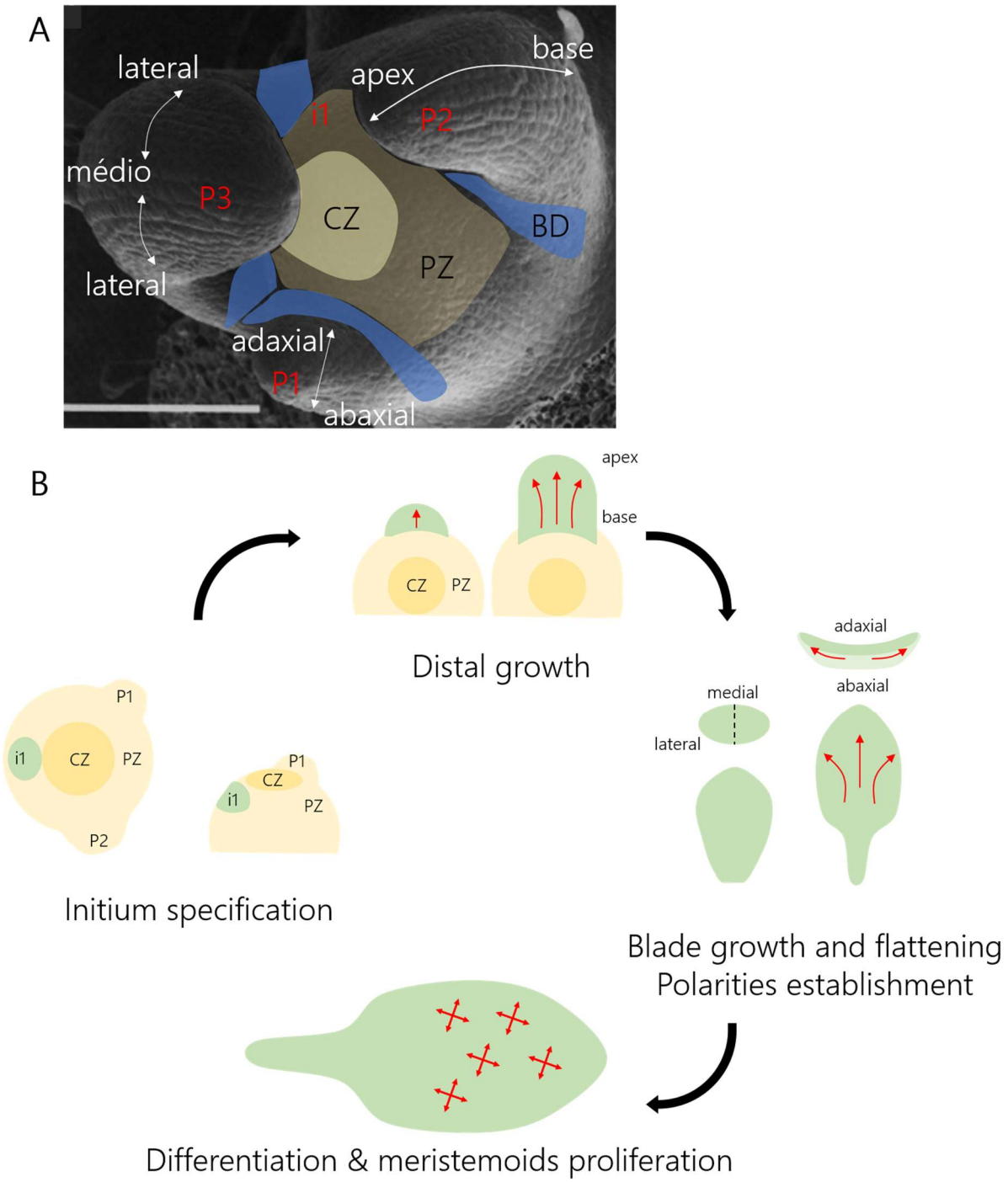

FIGURE I-06: Leaf development from the shoot apical meristem. A. The SAM, which is located at the tip of the shoot, continuously generates leaves during development according to a reproducible spatial pattern called phyllotaxis. Scale bar is 100µm. B. Soon after primordia emerge from the meristem, medio-lateral, abaxial-adaxial and basal-apical polarities are established. Cell proliferation and expansion occur subsequently in the blade and lead to its expansion until it reaches mature area.

LEAF DEVELOPMENT: A ROBUST, CONTROLLED CASE OF MORPHOGENESIS

The SAM continuously produces postembryonic aerial parts, such as stems and leaves. The SAM is composed of different zones, each with cellular and functional characteristics. The central zone (CZ) is made of small cells that slowly divide to renew a pool of more-rapidly dividing stem cells surrounding them. Around the central zone, the peripheral zone (PZ) forms cells that will constitute leaves primordia. After a few initial cells are recruited, they undergo divisions and growth which rapidly forms a bump at the SAM periphery. Next, the primordium extends drastically while proximo-distal, medio-lateral and aba/adaxial polarities are established and allow the formation of an individual blade (Figure I-06). In the following paragraphs, I attempt to roughly describe the events of leaf development, as well as some genetic and hormonal controls in place.

Initiation of a primordium and cellular multiplication

Specification of cell initials

In the SAM, growing primordia are involved in the positioning of the next incipient primordium (Reinhardt et al., 2005; Shi et al., 2017). Micro-ablation experiments were performed on the SAM to isolate primordia from the rest of the SAM, and indeed altered phyllotaxis. Hence, pre-existing primordia are a signal for phyllotaxis (Figure I-07). Auxin maxima repeat periodically around the CZ, their location coinciding with phyllotaxis (Reinhardt et al., 2000; Reinhardt et al., 2003). The PZ cells are competent cells that are able to produce new shoot organs upon specification by these auxin maxima (Reinhardt et al., 2003; Barton, 2010). Those periodic, local auxin maxima are determined by the polarization of PIN1 auxin efflux transporters (Reinhardt et al., 2003; Heisler et al., 2005). N-1-naphthylphthalamic acid (NPA) auxin transport inhibitor is indeed sufficient to prevent leaf initiation at the SAM (Reinhardt et al., 2000). In addition, no floral primordia are initiated in a *pin1* mutant, indicating auxin maxima are critical for organ initiation (Okada et al., 1991; Vernoux et al., 2000).

Additive actors take part in the initium specification and make phyllotaxis a robust developmental trait. For example, four auxin influx transporters AUX1, LAX1/2/3 have been shown to partake in the robustness of SAM auxin-mediated patterning (Bainbridge et al., 2008). Besides, ARABIDOPSIS HISTIDINE PHOSPHOTRANSFER PROTEIN 6 (AHP6), which is a cytokinin signaling

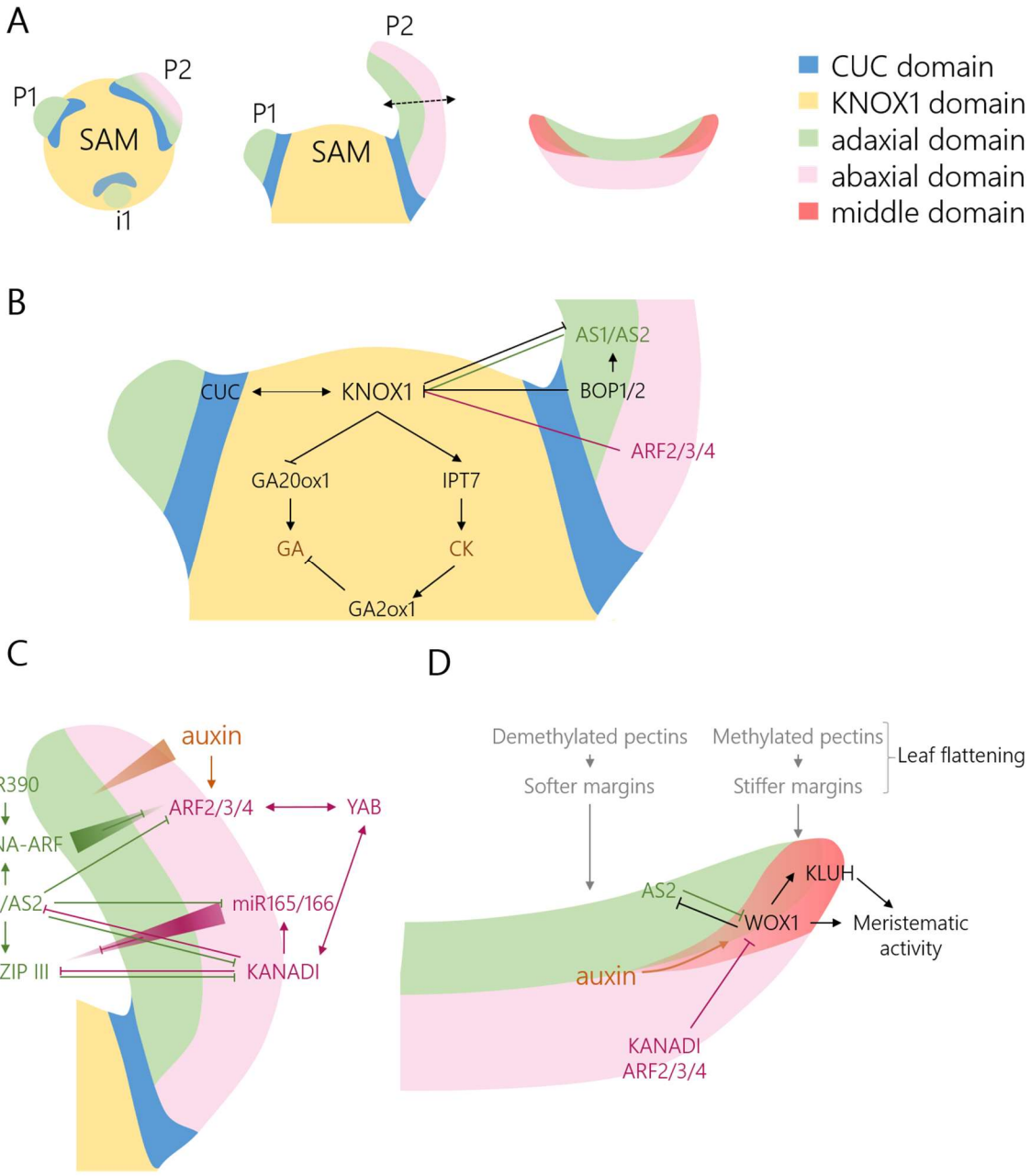

FIGURE I-07: Overview of the gene regulatory networks that trigger leaf initiation and polarities establishment.

A. Schematic representations of the different domains of the SAM seen from the top (left panel), the side (middle panel) and across the P2 (right panel). B. Regulatory network in the meristem at the base of a growing primordium. The respective down-regulation of genes expressed in the SAL *versus* the primordia allows organ separation. C. Abaxial-adaxial polarity establishment is under a sharp control of abaxial and adaxial-specific genes that repress each other. D. A third domain is established at the leaf margin during leaf development. The middle domain has a longer proliferative activity that is crucial for the leaf flattening.

inhibitor activated by auxin, was shown to act in a non-cell-autonomous manner to create CK signaling inhibitory fields (Besnard et al., 2014). This ultimately reinforces phyllotaxis robustness.

Prior to primordia outgrowth, cortical MT organization is disrupted at the SAM periphery because of the local increase in auxin concentration (Sassi et al., 2014). The combination of local cell wall isotropy and low decrease in rigidity then promote the protrusion of an outgrowth at the periphery (Sassi et al., 2014). Accordingly, the contrast between stiffer cells in the CZ and softer cells in the PZ was already reported (Milani et al., 2011; Kierzkowski et al., 2012). It was proposed that this repartition of cell wall mechanical properties contributes to morphogenesis at the SAM by restricting growth at the CZ while controlling it finely at the PZ (Kierzkowski et al., 2012).

Primordia formation and growth

Upon local auxin maxima, specified cells undergo oriented cell divisions and anisotropic cell expansion (Reddy et al., 2004). As a result, a bump appears at the periphery of the meristem: the primordia.

SHOOT MERISTEMLESS (STM), which is a class I KNOTTED-LIKE HOMEOBOX (KNOX1) transcription factor, is expressed in the SAM and specifies meristematic cell fate (Long et al., 1996). STM is down-regulated in the growing leaf through different, independent pathways. ASYMMETRIC LEAF1 (AS1) acts in complex with AS2, by recruiting Polycomb Repressive Complex 2 (PRC2) to repress *KNOX1* genes expressions (*BREVIPEDICELLUS / BP* and *KNOTTED-like from Arabidopsis thaliana2 / KNAT2*) (Hay et al., 2006; Lodha et al., 2013). In parallel, STM also negatively regulates *AS1* (Byrne et al., 2001). Together, these data indicate that *STM* expression domain and *ARP (AS1+AS2)* expression domain exclude each other (Figure I-07B). Furthermore, auxin was also reported to negatively regulate BP (Hay et al., 2006). Similarly, KNOX2 protein is also capable of antagonizing KNOX1 (Furumizu et al., 2015).

The SAM exhibits low bioactive GA levels due to KNOX1 direct repression of GA20ox1 GA biosynthesis enzyme, as well as promotion of GA2ox1 GA catalytic enzyme (Hay et al., 2002; Bolduc and Hake, 2009). In addition, KNOX1 promotes CK signaling in the SAM (Yanai et al., 2005; Scofield et al., 2018), which ultimately represses GA signaling (Greenboim-Wainberg et al., 2005) (Figure I-07B). In rice, *KNOX* gene *OSH1* was shown to down-regulate BR signaling *via* the promotion of expression of BA-catabolic enzymes (Tsuda et al., 2014). As a result, the SAM is depleted in both BR, GA and auxin locally. On the contrary, growth-promoting hormonal signaling

pathways are activated in the primordia where *KNOX1* is repressed. Those data indicate that local hormonal status in the SAM is extensively controlled to prevent cell expansion, while their activation in the primordia is critical to the final leaf size.

Boundary domain at the SAM

From initial cell specification, a frontier appears between the SAM and the primordium, in which cell growth is restrained: the boundary domain. Cells from boundary domains display specific properties. They exhibit slow growth rate and are slowly dividing (Kwiatkowska and Dumais, 2003; Reddy et al., 2004; Heisler et al., 2005). Moreover, boundary domains express a specific set of transcription factors, such as the CUP-SHAPED COTYLEDON (CUC) 1, 2 and 3 (Aida et al., 1997; Hibara et al., 2006). Boundary domains also exhibit specific hormonal status, as they are depleted in growth promoting hormones such as BR (Gendron et al., 2012), which trigger local cell growth repression. In addition to their role in separating growing organs and creating new axes of growth, boundary domains act to maintain meristem activity. Indeed, a *cuc1 cuc2* double mutant forms two cotyledons after which the meristem stops producing new organs (Aida et al., 1997).

The SAM is essential to trigger correct boundary domain patterning, as STM is able to act in a non-cell autonomous manner to control CUCs levels post-translationally (Balkunde et al., 2017). Indeed, non-mobile versions of STM triggered lower expression levels for all three *CUC* genes (Balkunde et al., 2017). Direct up-regulation of *CUC1* and *MIR164* (which targets CUC1/CUC2 mRNAs) by *STM* was demonstrated in the SAM of *Arabidopsis* (Spinelli et al., 2011), indicating that STM finely tunes CUC expression (Figure I-07B).

Combination of MT live imaging and modeling of the mechanical stresses revealed that MTs align along the direction of maximal stress in the SAM (Hamant et al., 2008). Such an orientation of MTs forces the direction of expansion and pushes the primordium away from the SAM. Interestingly, the area of maximum stress coincides with the boundary domain where CUC3 is expressed. However, it has been shown that mechanical stress can also induce CUC3 expression (Fal et al., 2016). Thus, it is conceivable that local mechanical stress may be involved in maintaining the local expression of boundary domains specific factors. In addition, STM was also shown to be stress-induced, which could also be critical for SAM patterning (Landrein et al., 2015).

Polarity establishment and maintenance

While the primordium is growing on the side of the SAM, the young leaves form and acquire basal-apical, abaxial-adaxial, and medio-lateral symmetries, while their size increases dramatically.

Apico-basal polarity

Apico-basal polarity is already present at the initiation of the primordia as the top of the bump prefigures the leaf apex. During the primordia distal growth, the auxin maxima are localized at the tip of the leaf thanks to the localization of PIN1 efflux transporters. Tip-located auxin maxima promote growth and cell proliferation in the growing blade (Reinhardt et al., 2003). Later in the developing leaf, PIN1 localization changes and directs auxin flow into the developing vessels (Benková et al., 2003; Reinhardt et al., 2003; Heisler et al., 2005).

During leaf distal growth, the petiole is specified from the blade through the activity of *BLADE ON PETIOLE1* (*BOP1*) and *BOP2* genes. Indeed, the *bop1 bop2* double mutants exhibit leaves in which the blade invades the part where the petiole is normally located (Ha et al., 2007). BOP1 and BOP2 were found to promote *AS2* as well as *LATERAL ORGAN BOUNDARIES (LOB)* genes expression, and are hence involved in specifying the abaxial-adaxial polarity (Ha et al., 2007). Moreover, BOP were found to repress *KNOX1* expression (Norberg et al., 2005; Ha et al., 2007).

Abaxial-adaxial polarity

Like apico-basal polarity, abaxial-adaxial polarity is established very early during primordia development. A set of genes are specific to both abaxial and adaxial sides of the leaf. REVOLUTA *(REV)* is a member of the class III HD-ZIP gene family that specifies the adaxial domain (Otsuga et al., 2001; Emery et al., 2003). PHAVOLUTA and PHABULOSA, are two other class III HD-ZIP, adaxial-specific proteins (McConnell et al., 2001). As previously cited, AS1 and AS2 also specify adaxial cell identity (Ha et al., 2007) (Figure I-07C).

Other genes are abaxial-specific. *KANADI* (*KAN1,2,3,4*) encode abaxial-specific proteins (Kerstetter et al., 2001; Wu et al., 2008). In particular, KAN1 negatively regulates adaxial *AS2* expression and triggers abaxial-adaxial patterning. The *YABBY (YAB)* TF family is also abaxial-specific and contributes to abaxial-adaxial polarity (Sawa et al., 1999). In addition, abaxial epidermis-expressed miR165 and mir166 are able to diffuse towards the abaxial domain to trigger

the post transcriptional down-regulation of adaxial-specific class III HD-ZIP genes (Juarez et al., 2004). AS2 acts to counteract miR165/166 by negatively controlling their expression (Husbands et al., 2015). ARF2,3 and 4 are three repressive ARFs which redundantly trigger abaxial cell fate (Guan et al., 2017). Besides, the adaxial domain appears to be auxin-depleted while the abaxial domain is not (Qi et al., 2014). Similarly to adaxial fate repression by miR165/166, miR390 is expressed adaxially and indirectly triggers the repression of expression of abaxial ARFs (Fahlgren et al., 2006; Marin et al., 2010). Hence, abaxial-adaxial patterning is very sharply regulated in *Arabidopsis* leaves (Figure I-07C).

Strikingly, abaxial-adaxial polarity is acquired as early as initial cells specification, since REV and KAN1 expression was reported in the SAM before the apparition of a bump in the PZ (Caggiano et al., 2017). REV is expressed in the center of the SAM, while KAN1 pattern of expression forms a ring that surrounds the meristem (Caggiano et al., 2017). Hence, abaxial-adaxial polarity exists even before the primordia is initiated.

Mechanical properties of the growing primordia cell walls were estimated on different sides of tomato and *Arabidopsis* primordia, and revealed that the adaxial domain is stiffer than abaxial in P1 (Qi et al., 2017). Observation of the pectin methyl-esterification state on each side indicated that the abaxial side contains de-methyl-esterified pectins, which is coherent with higher elasticity, while the rest of the leaf primordium has more methyl-esterified pectins, in agreement with measured data. In addition, alteration of pectin methyl-esterification pattern led to aberrant lead polarity, which suggest that the cell wall's mechanical properties and pectin modifications are critical for leaf development and abaxial-adaxial polarity (Qi et al., 2017).

Medio-lateral polarity

As the blade grows away from the SAM, it flattens along the middle region which creates a bilateral symmetry, also called medio-lateral symmetry.

Two *WUSCHEL-RELATED HOMEOBOX* (*WOX*) genes were shown to be critical for margin development following abaxial-adaxial polarity specification (Nakata et al., 2012; Guan et al., 2017). WOX1 and WOX3 are two TFs that are indeed necessary for the flattening of the leaf, as they are expressed at the edges and form a middle domain (Nakata et al., 2012) (Figure I-07D). Indeed, the *wox1 wox3* double mutant exhibits curled, narrower leaves where abaxial-adaxial cell types are altered (Nakata et al., 2012). Auxin signaling converges in the middle domain and this is critical to

establish WOX expression and promote blade flattening (Shi et al., 2017). Both the expression of WOX and flattening of the leaf depend on abaxial auxin signaling, which restricts *WOX* expression through ARF2/3/4 (Guan et al., 2017). *WOX1* expression is also restricted by KAN in the abaxial domain (Nakata et al., 2012). In addition, WOX1 represses adaxial domain through AS2 (Zhang and Tadege, 2015). Hence, WOX determines a middle domain through dynamic regulation of abaxial and adaxial domains (Figure I-07D).

WOX is critical for the blade extension as it promotes cell proliferation. Abaxial ectopic expression of WOX leads to the apparition of protrusions (constituted of mesophyll cells) under the leaves (Nakata et al., 2012). WOX expression allows the maintenance of meristematic activity at the margin while NGATHA (NGA) TFs restrict cell proliferation within the blade (Alvarez et al., 2016). Indeed, the use of a KLUH reporter line revealed that WOX1 promotes the expression of KLUH in the middle domain while no KLUH signal was observed in *wox1 wox3* double mutant (Nakata et al., 2012). Since *KLUH* encodes a P450 cytochrome mono-oxygenase which promotes the maintenance of cell proliferation in a non-cell autonomous manner (Anastasiou et al., 2007), *KLUH* promotion by WOX1 indicates that WOX1 indeed promote cell proliferation in the blade.

Leaf growth and medio-lateral polarity are also associated with specific cell wall reorganization. Indeed, leaf flattening was shown to be dependent on MT orientation. MT visualization established that these align orthogonally to the medio-lateral axis, leading to cells displaying a preferred direction of growth and ultimately promoting blade flattening. (Zhao et al., 2020). The measure of the orientation of division planes in growing primordia treated or not with oryzalin (which depolymerases MT) revealed that cell division planes are preferentially orthogonally oriented to the mediolateral axis (Zhao et al., 2020). No blade flattening was observed in a oryzalin-treated primordia contrary to the mock-treated control, indicating that the orientation of cell division drives the blade flattening (Zhao et al., 2020). Further, mechanical properties of growing primordia cell walls revealed that the middle domain is stiffer than abaxial domain in P2 and stiffer than both abaxial and adaxial domains in P3 (Qi et al., 2017). As the middle domain is critical for the flattening of the leaf, this suggests that local, stiffer cell walls could drive the leaf flattening (Figure I-05).

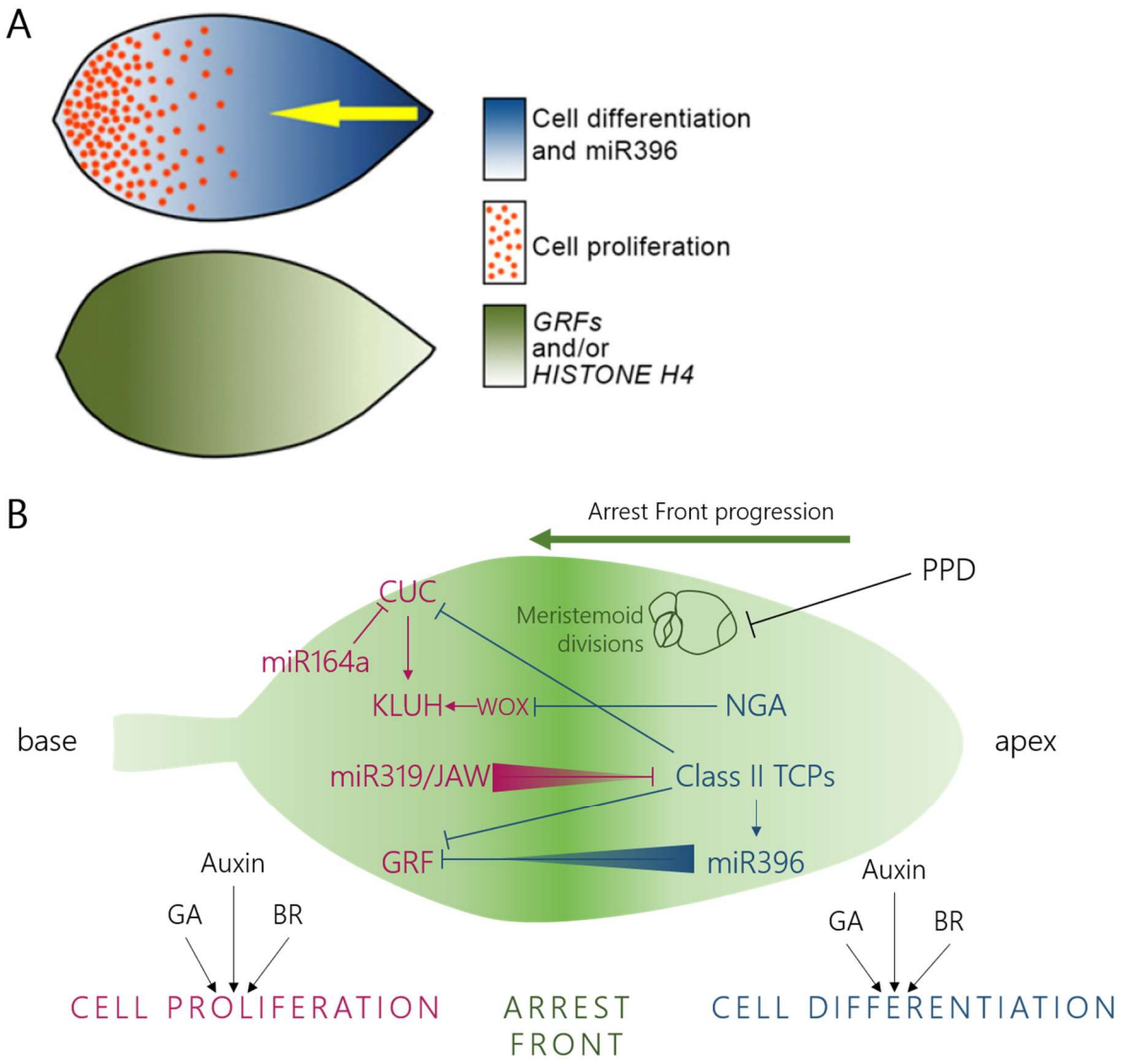

FIGURE I-08: The developing leaf undergoes a tightly regulated proliferation / differentiation switch.

A During development a cell proliferation / cell differentiation switch occurs, appearing first at the leaf apex and then progressing basipetally. Proliferating and differentiating domain each express a specific set of genes. A is from (Das Gupta and Nath, 2015). B. Overview of the regulatory network that sustains the separation of a cell proliferating domain *versus* a cell differentiating domain.

Leaf expansion and control of its final size

The primordium separation from the SAM is followed by a dramatic increase in cell number and size in the blade. Consecutively, a switch from proliferating activity to expansion occurs, starting at the leaf apex and progressing basipetally (Figure I-08A). The progression of the front arrest is a dynamic process, which remains at a constant distance from the leaf base until it disappears abruptly (Kazama et al., 2010; Andriankaja et al., 2012). The expression of several differentiation-promoting genes leads to the emergence and progression of the front arrest. CINCINNATA-class II -TCP (CIN-TCP) transcription factors restrict meristematic activity in the apical domain (Nath et al., 2003; Alvarez et al., 2016). On the contrary, GROWTH-REGULATING FACTORs (GRFs) are expressed closer to the leaf base and prolongs proliferation duration (Kim et al., 2003; Rodriguez et al., 2010). Those two domains have opposite effects and regulate each other reciprocally through miRNAs suppressive activities (Palatnik et al., 2003; Ori et al., 2007; Rodriguez et al., 2010). For example, *miR319* (or *miR-JAW*) is expressed at the base and promotes cell division by repressing class II TCP TFs locally (Palatnik et al., 2003; Ori et al., 2007). Meanwhile, distally-expressed TCP4 induces miR396 expression locally, which restricts GRF activity to the leaf base (Rodriguez et al., 2010). Interestingly, TCP4 also negatively regulates the three CUCs expressions (Koyama et al., 2017) (Figure I-08B).

In spite of the front arrest progression, meristemoid cells are still capable of dividing to form stomatal cells as well as additional pavement cells. Meristemoids highly contribute to the leaf final size as their lineage produces almost half of mature leaf pavement cells (Geisler et al., 2000). PEAPOD (PPD) proteins negatively regulate meristemoid division in the leaf (Figure I-08B). PPD2 binds to CYC_{D3} promoter in a repressive complex that involves KIX proteins and TOPLESS (TPL) and limits cell division (Gonzalez et al., 2015). Recent data further demonstrated that the F-box protein STERILE APETALA (SAP) interacts with KIX8 and KIX9 adaptor proteins as well as PPDs and decreases their stability (Wang et al., 2016; Li et al., 2018). Hence, the PPD-KIX-TPL complex can no longer repress cell division. These findings provide a new mechanism for the control of cell proliferation in the blade and organ size.

Phytohormones are involved in the maturation of the leaf. Indeed, gibberellin signaling contributes to cell proliferation by repressing KIP-RELATED PROTEIN 2 (KRP2) and SIAMESE (SIM) expressions (Achard et al., 2009). Brassinosteroids also control the balance between cell division and cell expansion through CONSTITUTIVE PHOTOMORPHOGENESIS AND DWARFISM (CPD),

the mutant of which is BR-defective (Zhiponova et al., 2013). Finally, auxin promotes cell division by indirectly triggering CYC_{D3} expression through ARF2 (Schruff et al., 2006). Conversely, once the cell switches from division to expansion programs, auxin, GA and BR collectively promote cell elongation (Schruff et al., 2006; Oh et al., 2014) (Figure I-08B).

THE LEAF MARGIN: A CASE OF DIFFERENTIAL GROWTH INDUCED BY CUC TRANSCRIPTION FACTORS

Leaf shape diversity originates from the leaf margins

Not only are leaves the most visible organs of angiosperms, they also display a tremendous diversity in shapes, that is acquired through their development and which mainly is the result of the more or less intense dissection of their edges. Leaves can be compound, and present multiple blades which are called leaflets, or simple like in *Arabidopsis*. The formation of compound leaves requires the maintenance of indeterminate tissues that are still competent for leaflet initiation. Those tissues, namely blastozones, are pseudo-meristematic regions that are located at the primordium margin and are able to initiate new axes of growth. In addition, successive leaflets are separated by boundary domains in which growth is restricted. Multiple reviews very nicely present the processes that lead to the formation of complex leaves (Blein et al., 2010; Bar and Ori, 2015).

Leaves can also display serrations, which correspond to another level of dissection. Serrations do not form individual blades and thus are not assimilated to leaflets. However, the frequency and size of serrations varies extensively, thus triggering a very large diversity in simple leaves shapes (Figure I-09A). The richness of leaf shape terminology truthfully reflects the diversity of their shapes, and leaves are often the main evidence for species identification. In *Arabidopsis*, leaves from wild type plants display serrations at their margins. Those indentations are called teeth, where the tooth tip is surrounded by an upper, close to the leaf apex, and a lower sinus, close to the leaf base (Figure I-09B). At each tooth, a differential growth occurs between the growing tip and the sinuses. In other words, each newly formed tooth grows along an independent growth axis.

All *Arabidopsis thaliana* mature leaves do not display the same degree of serration. This diversity of leaf shape depending on the age of the plant and the rank of the leaf is termed heteroblasty (Figure I-09E). To put it simply, in first approximation, the higher the leaf rank, the more serrated the mature leaf will be (Biot et al., 2016). The environment can also impinge on leaf development and trigger major changes in leaf shape, a process that is called heterophylly (Figure I-09C,D). For example, plants grown in a high temperature environment display specific leaf

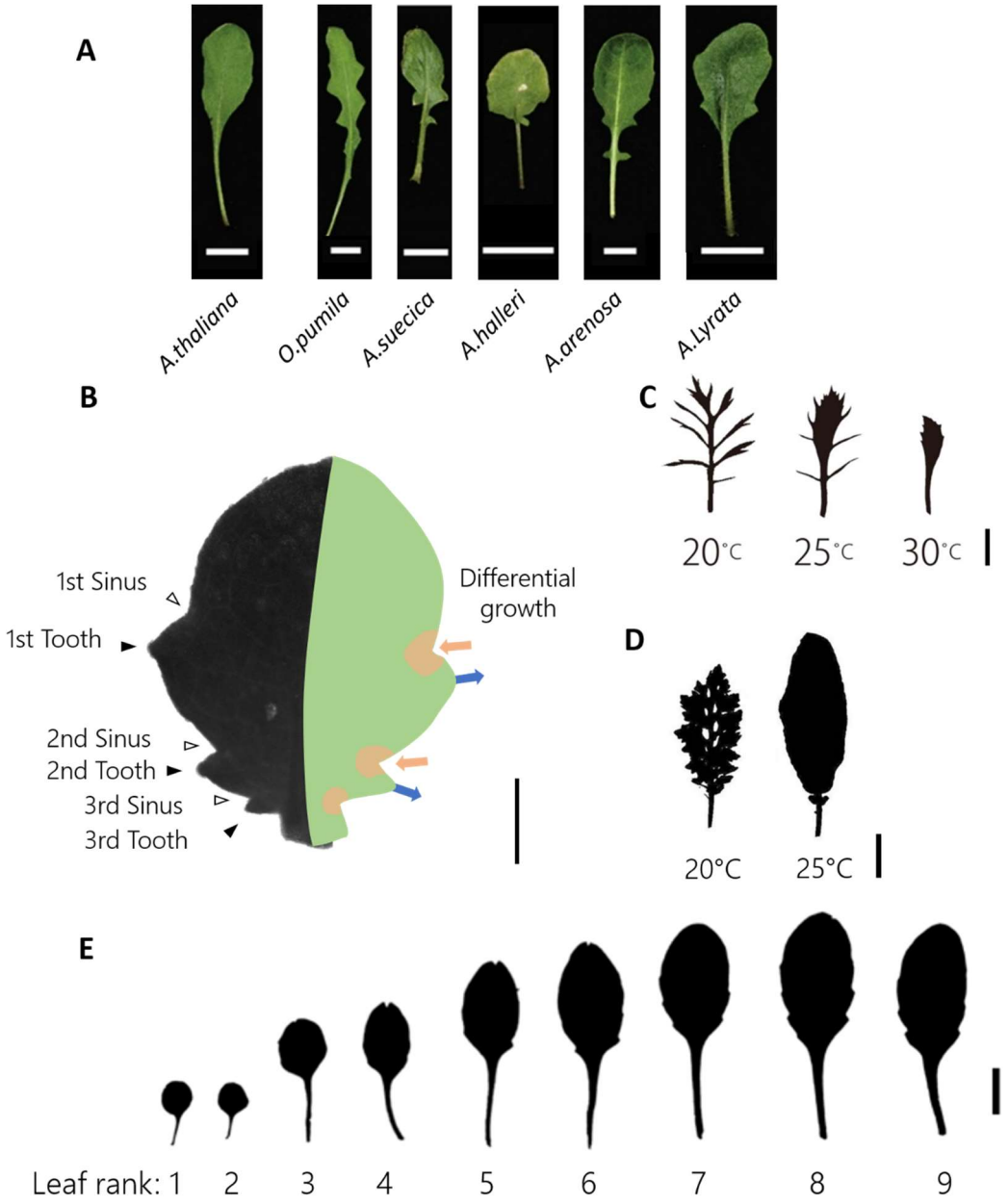

FIGURE I-09: Leaf shape depends on species, leaf rank and environmental conditions. A. leaf diversity across various species from the Bassicaceae family. A leaf of rank 7 is represented (but for *O.pumila*, rank=11). Scale bars are 1cm. Images are from (Piazza et al., 2010). B. Terminology of tooth and sinus on a 35 days-old leaf of rank 11. Differential growth occurs at the margin during development and trigger serration formation. Scale bar is 500µm. C. Leaf shape of a submerged *Roripa aquatica* is heavily dependent on water temperature. Representative leaf silhouette of rank 7 is represented for 20°C, 25°C and 30°C. Scale bar is 1cm. D. Leaf shape of an emerged *Roripa aquatica* plant depends on temperature. Representative leaf silhouette of rank 7 is represented for 20°C and 25°C. Scale bar is 2cm. C,D, are extracts from (Nakayama et al., 2014) and highlight leaf heterophylly in response to environmental conditions. E. Leaf shape in col-0 depends on leaf rank. Representative leaf silhouette is presented for ranks 1 to 9. Scale bar is 1cm. Figure is from (Gonçalves et al., 2017).

phenotypes (Koini et al., 2009; Nakayama and Kimura, 2015). Hence, leaf margins vary in response to variations of environmental parameters.

Because leaves are an accessible organ, on which morphological quantifications can be performed, they constitute a great organ to study development and the effects of various mutations and surrounding conditions on leaf morphogenesis. Indeed, leaves can be assimilated, at least at first, to a two-dimensional object, which facilitates the process of shape quantification and analysis.

Role of *CUC* genes in shaping the leaves

CUP-SHAPED COTYLEDON (CUC) genes were first identified as genes specifically expressed in boundary domains of the SAM (Aida et al., 1997). CUC1, CUC2 and CUC3 redundantly act to specify boundary domains and drive proper organ separation, as combinations of *cuc* mutants leads to severe defects in boundary domain establishment (Aida et al., 1997; Hibara et al., 2006). *CUC* genes belong to the NO APICAL MERISTEM (NAM)/ARABIDOPSIS ACTIVATOR FACTORS (ATAF)/CUC (NAC) TFs family. While CUC1 and CUC2 are regulated post-transcriptionally by *microRNA164 (miR164)*, CUC3 is not. This is probably due to the loss of a miR164 binding site within the *CUC3* sequence, since the *CUC3* lineage separated from the NAM family early after angiosperms emergence (Vialette-Guiraud et al., 2011).

Consistent with *CUC* being expressed in boundary domains, *CUC2* and *CUC3* are expressed in the growing leaf at the boundary between two consecutive growth axes, *i.e.* at the leaf boundary domain or sinus (Nikovics et al., 2006; Hasson et al., 2011). However, *CUC1* is not expressed in leaves. The repetitive expression of *CUC2* and *CUC3* along the leaf margins results in the formation of teeth and sinuses. Besides, the extent of leaf serration directly reflects the levels of CUC2 proteins, since in the *miR164a-4* mutant line, leaves are extensively dissected, while they are smooth in *cuc2* mutants (Nikovics et al., 2006; Maugarny-Calès et al., 2019) (Figure I-10G). Leaf serration is a good model to study CUCs functions in defining boundary domains. Indeed, as no *CUC1* expression was reported in leaves, only the functional redundancy between CUC2 and CUC3 has to be considered.

Even if the role of CUC TFs at defining the leaf margins has been known for a long time, the gene regulatory network (GRN) underlying tooth formation is only beginning to be unraveled.

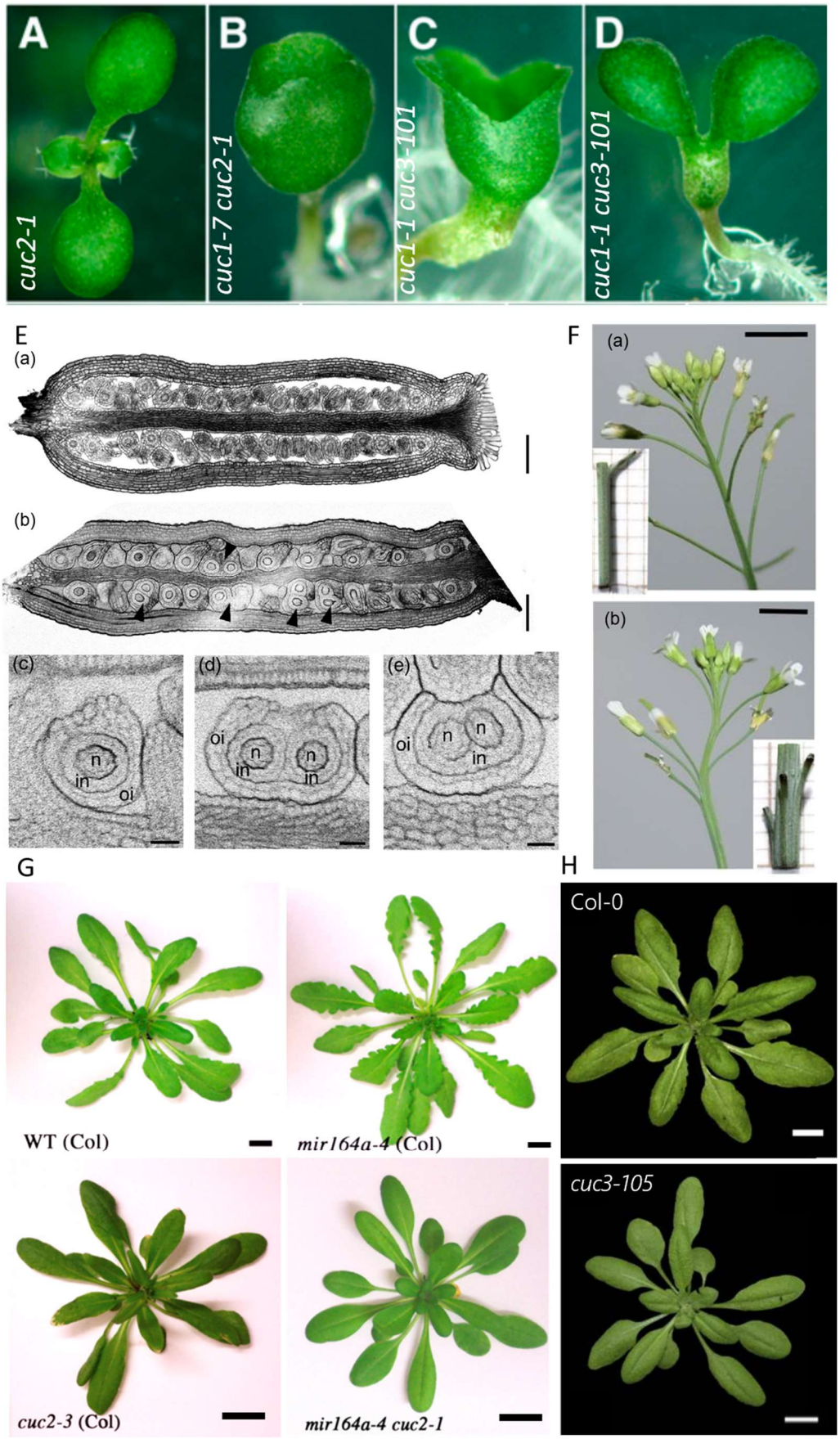

FIGURE I-10: CUC transcription factors are involved in organ separation in various developmental contexts, as well as SAM maintenance. A to D. CUC1/2/3 are partially

redundant, hence combination of *cuc* mutants triggers developmental defects, notably partial cotyledons fusions (heart-shaped seedlings) and total cotyledon fusions (cup-shaped seedlings). Single *cuc2-1* mutant does not exhibit fusions phenotype, on the contrary to *cuc1cuc2, cuc1cuc3* and *cuc2cuc3* (not shown) double mutants. (Hibara et al., 2006) E. Observation of col-0 (a) and *cuc2cuc3* (b), stained carpels at a late stage of development. Black arrowheads point at fused ovules. While col-0 carpels exhibit a single nucellus surrounded by two layers of integuments (c), *cuc2cuc3* double mutants can exhibit carpels in which either the outer integuments are fused (d), or both integuments are fused (e). (a), (b) scale bars are 100 µm; (c), (d), (e) scale bars are 20 µm. n= nucellus, in= inner integument, oi= outer integument. Images are from (Gonçalves et al., 2015). F. Inflorescence of col-0 (a) and *cuc2cuc3* (b), with insets on pedicels separating from the stem. In the double mutant, phyllotaxis is altered and pedicels are partially fused to the stem. Scale bars are 5 mm, insets are 1 mm high. Images are from (Burian et al., 2015). G. Rosettes phenotype at bolting of col-0 (upper left), *cuc2-3* (lower left)*, mir164a-4* (upper right) and *mir164a-4 cuc2-1* (lower right). The intensity of leaf serration reflects the CUC2 proteins level in plants. Absence of serration in the double *mir164a-4 cuc2-1* indicates *miR164a* is epistatic to *CUC2*. Scale bars are 1 cm. Images are from (Nikovics et al., 2006). H. Phenotypes at bolting of col-0 (upper panel) and *cuc3-105* (lower panel). *cuc3* mutant also displays smoother leaves than the wild-type. Scale bar is 1cm. Images are from (Hasson et al., 2011).

The gathered knowledge on the molecular mechanisms controlling serration formation will be extensively described in the introduction of chapter 2.

CUC transcription factors define boundaries broadly in the plant

Not only are CUC TFs crucial for shaping the leaf, they are also involved broadly in the plant to specify boundaries and shaping plant architecture. As said earlier, CUC are critical for cotyledons separation. Almost all *cuc2 cuc3* double mutant seedlings hence display heart or cup-shaped cotyledons. As said earlier, boundary-expressed CUCs are also necessary to the meristem specification as no SAM is established in a double *cuc1 cuc2* (Aida et al., 1997) (Figure I-10A to D).

CUC TFs are also involved in flower development. *CUC2* is expressed at the boundary between the inflorescence meristem and the flower primordia. *CUC2* was also shown to be expressed later between floral whorls as well as between individual forming sepals (Ishida et al., 2000). In *cuc1 cuc2* double mutant, fusion defects appear in developing sepals and stamens and yield the apparition of bulging tissues (Aida et al., 1997; Ishida et al., 2000). More recently, the expression pattern of *CUC* TFs was refined in the gynoecium. While *CUC1* and *CUC2* are expressed in the medial tissue and are necessary for ovule primordia initiation (Galbiati et al., 2013), *CUC2* and *CUC3* are expressed between developing ovules in the placenta (Gonçalves et al., 2015). As *cuc2cuc3* double mutants display fused ovules (Figure I-10E), a semi-redundant role for CUC2 and CUC3 was suggested at separating developing ovules (Gonçalves et al., 2015). In *Medicago truncatula*, CUC homolog NO APICAL MERISTEM (MtNAM) was shown to regulate both organ separation and identity in the flower (Cheng et al., 2012). Further, *NAC* genes were shown to trigger leaflet separation in a set of relatively distant species displaying compound leaves (Brand et al., 2007; Blein et al., 2008; Berger et al., 2009). Hence, the function of NAC family TFs at defining the plant architecture seems to be conserved across evolution. The evolution of the *NAC* genes family has already been reviewed (Maugarny et al., 2016).

CUC TFs are also involved in axillary meristem production, as *cuc3* mutants produce fewer axillary stems than a wild type (Ishida et al., 2000; Hibara et al., 2006). Furthermore, CUCs regulate flower phyllotaxis along an inflorescence meristem. Indeed, a *cuc2cuc3* double mutant exhibits floral pedicels fusions with the stem (termed fasciations) as well as aberrant phyllotaxis (Burian et al., 2015) (Figure I-10F).

Together, these data show that CUCs are essential actors of the global shaping of the plant. Most strong phenotypes require two impaired *cuc* genes to be observable, due to strong redundancy between *CUC* genes. However, in the leaf, both *cuc2* and *cuc3* single mutants are sufficient to prevent serration formation at the leaf margin (Figure I-10 G,H). This suggests that CUC functions are more distinct in the leaf, and that the study of single mutants might lead to the identification of finer roles of both TFs.

MAIN OBJECTIVES OF THE PROJECT

As highlighted in the introduction, CUC TFs are involved in plant architecture development. The team in which I did my PhD has the long-term goal of using the establishment of serrations at the leaf margin to better understand the role of *CUC* genes during development. To do so, we combine mutant lines and treatments to perform precise quantification of leaf morphometric data. Even if new CUC2 downstream elements were recently described (Maugarny-Calès et al., 2019), the precise molecular pathways that subtend the growth differential at the leaf margin remain unclear. During my PhD, I intended to clarify the GRN downstream of CUC2 in order to provide new insights on the pathways that lead to teeth development.

Despite the numerous over-dissected mutants that have been described over the past two decades (Laufs et al., 2004; Blein et al., 2013; Challa et al., 2021), only a few unserrated mutants have been observed (Aida et al., 1997; Nikovics et al., 2006; Maymon et al., 2009; Bilsborough et al., 2011; Tameshige et al., 2016a; Gonçalves et al., 2017). Among these smooth mutants, the reasons for the appearance of these specific leaf phenotypes are not always understood.

In the first part of this manuscript, I intend to finely quantify the *spindly* mutant smooth leaf phenotypes, while investigating a probable interaction with the CUC TFs. In a second part, I use formerly acquired transcriptomic data to focus on the molecular events downstream of CUC and SPY and identify potentially shared targets that encode genes involved in the control of cell wall rigidity. In a third, more exploratory part, I aim at investigating the interactions between CUC2 and two hormonal pathways, gibberellins and auxin, in order to better understand how CUC2 is involved in the regulation of growth in general.

Chapter 1

Multi-scale characterization of *spindly* mutants

INTRODUCTION

CUC transcription factors are crucial for the definition and maintenance of boundary domains in several organs throughout plant development. In *cuc* loss-of-function mutants, organ fusion defects are observed in various developmental contexts, highlighting the contribution of CUCs to the shaping of the whole organism (Hibara et al., 2006; Hasson et al., 2011; Blein et al., 2013; Burian et al., 2015; Gonçalves et al., 2015). These different studies provide an increasingly accurate picture of the functions of the CUC genes. However, despite their fundamental roles in multiple developmental contexts, little is known about the molecular mechanisms and cellular processes they trigger and how they control morphogenesis.

GDP-L-fucose is essential to serration development in *Arabidopsis*

A genetic screen to uncover CUC2 downstream elements

In order to identify new CUC2 downstream targets and to provide a better understanding of the molecular mechanisms involved in CUC2 pathway, a suppressor genetic screen was performed in the lab on *CUC2g-m4* plants. This suppressor screen aimed at selecting EMS mutant lines with less-serrated leaves than the non-mutagenized *CUC2g-m4* line, which would be used as a proxy to identify genes involved in CUC2-dependent leaf serration development (Gonçalves et al., 2017).

Among the identified mutants, the team focused on a mutant displaying rounded, smooth leaves, which they called *folivora* (Gonçalves et al., 2017). *folivora* carries a false-sense mutation in the sequence that encodes the MURUS1 protein. As the progeny of a *folivora X mur1-1* cross retained the suppressor leaf phenotype in the dominant *CUC2g-m4* background, *folivora* was confirmed as a new loss-of-function mutation of the *MUR1* gene (Gonçalves et al., 2017).

MURUS1, an enzyme responsible for GDP-L-fucose synthesis

MURUS1 was previously described as a GDP-D-mannose-4,6-dehydratase necessary to GDP-L-fucose biosynthesis in *Arabidopsis* (Bonin et al., 1997). Hence, *mur1* mutants are fucose-deficient with virtually no fucose in the aerial parts (Reiter et al., 1993; Bonin et al., 1997). In plants, GDP-L-fucose can be incorporated to cell wall components *via N-glycosylation* (*i.e.* glycosylated components, such as xyloglucans, or arabinogalactans) (Rayon et al., 1999; van Hengel and Roberts, 2002; Wu et al., 2010; Wan et al., 2018). In addition, relative abundances of the different xyloglucans were similar between *folivora* and *mur1-1*, which both presented L-galactosyl-carrying

xyloglycans and lacked fucosylated xyloglycans, confirming that *folivora* harbors a mutation at the MUR1 locus that altered the MUR1 function (Gonçalves et al., 2017). Proteins can also be N- and O-glycosylated by fucosyltransferases that use GDP-L-fucose as a substrate (See Box 1-01).

Box 1-01: N-glycosylation and O-glycosylation of proteins.

N-glycosylation is a multi-step addition of glycans to the amide group of an asparagine in an Asn-X-Ser/Thr accessible motif. First, an oligosaccharide is transferred to the protein during its translation in the ER. Then, the glycan is processed and modified in the Cis, Median and Trans Golgi compartments by glycosidases and glycosyltransferases. The number of available glycosylation sites and the different glycans that can be formed drastically increase the functional diversity of proteins that undergo N-glycosylations.

Unlike N-glycosylations, **O-glycosylation**s are enzymatic reactions that sequentially transfer monosaccharides to amino acids in the cytosol. Several amino acids can be involved in specific O-glycosylations : Serine, Threonine, Hydroxyleucine, Hydroxyproline, Tyrosine...(Lis and Sharon, 1993). There are different O-glycosylation types depending on the transferred monosaccharide, that are specific to one or several amino acids. For example, Drosophila POGLUT1 is a glucosyltransferase that transfers a glucose to a Serine residues of Epidermal Growth Factor-like (EGF). (Yu and Takeuchi, 2019). Acetyl-glucosamin and GDP-L-fucose can also be added to proteins.

Fucose is essential to serration development

The study of *CUC2g-m4 mur1-1* and *CUC2g-m4 mur1-2* double mutants leaf phenotypes revealed that the *mur1* mutations are sufficient to reduce the *CUC2g-m4* over-dissected leaf margin (Gonçalves et al., 2017). Moreover, the morphometric parameters of mature L6 leaves from *mur1-1* and *mur1-2* were assessed using MorphoLeaf software (Biot et al., 2016) and revealed that *mur1* mutants fail to develop serrated leaves such as the wild-type col-0 (Gonçalves et al., 2017). These data allow depicting MUR1 as a decisive actor in leaf development.

Interestingly, organ or tissue fusion defects were observed in a *mur1-1 cuc3-105* double mutant, such as fused cotyledons, fused seeds, fasciated stems (Gonçalves et al., 2017). These developmental defects show that *mur1-1 cuc3-105* at least partially phenocopies *cuc2-3 cuc3-105*. However, no such defects were observed in the *mur1-1 cuc2-3* double mutant. These data suggest that MUR1 is involved in CUC2-dependent pathway.

Col-0 and *mur1-1* plants were grown *in vitro* on a medium supplemented with fucose to assess whether GDP-L-fucose is required for proper leaf development. A 10 mM GDP-L-fucose supplementation was sufficient to restore serrations on fucose-deficient *mur1* similar to wildtype, indicating that fucose is somehow required to form a serration at the leaf margin (Gonçalves et al., 2017). This result also proves that the smooth margins observed in *mur1* mutant do not result from an over-accumulation of the substrate of MUR1, GDP-D-mannose, or a reaction intermediate, but from the absence of GDP-L-fucose *per se*.

Because *mur1* worsens *cuc3* phenotypes but not those of *cuc2*, and since fucose is sufficient to re-establish a serration at the leaf margin, one can suggest that fucose deficiency alters leaf boundary development *via* the CUC2 pathway, and that fucose *per se* is necessary for a proper boundary domain definition in the leaf. In order to further describe CUC2 functions, it is now necessary to understand which pathway involving fucose is required to determine boundary downstream of CUC2. A recent focus on mutants has brought our attention back to the post-translational modifications of proteins that use GDP-L-fucose as a substrate (Gonçalves et al., 2018).

Box 1-02: Modification of xyloglucans is not how fucose impinge on serration formation.

Fucose can be used to be incorporated into cell wall components or be a substrate in post-translational glycosylations. Specific fucosyltransferases were identified for different hemicelluloses. For example, FUT4 and FUT6 are non-redundant arabinogalactans-specific fucosyltransferases(Wu et al., 2010; Liang et al., 2013). MUR2 was described as a Xyloglucans (XyG) specific fucosyltransferases (Vanzin et al., 2002). Xyloglucans represent the dominant hemicellulose in plant cell walls as it adds up to 30% of the dry weight (Scheller and Ulvskov, 2010).

The overexpression of the xyloglucan-specific fucosyl-hydrolase AXY8/FUC95A29 is able to reverse the short-hypocotyl phenotype observed in the seedlings of lines with defective auxin responses (Günl et al., 2011). This suggests that XyG fucosylation may curb cell elongation in hypocotyls.

Neither a 35S::AXY8 line, nor the *mur2-1* mutant, both carrying un-fucosylated XyG, impinged on the level of leaf serration unlike in the *mur1-1* mutant, indicating that leaf serrations do not depend on XyG fucosylation(Gonçalves et al., 2018).

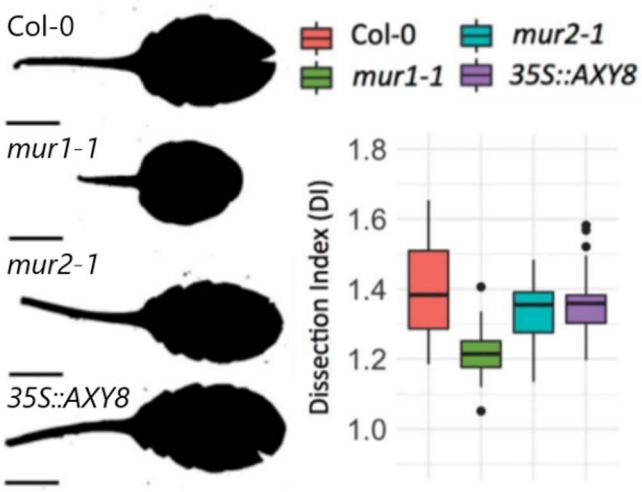

Representative silhouettes of L13 leaves from 8-week-old plants grown in short-day conditions: col-0, *mur1-1*, *mur2-1* and *35S::AXY8*. Leaf shape quantification using dissection index parameter descriptor ($DI=Perimeter_{leaf}^2/(4\pi.Area_{leaf})$)
Adapted from (Gonçalves et al., 2018)

Identification of SPINDLY and its mutant phenotypes

As modifications of the cell wall components do not seem to be responsible for the smooth margins in *mur1* mutants, one other hypothesis is that GDP-L-fucose is used elsewhere in the plant, like in post-translational modifications (see Box 1-02). Most described O-fucosyltransferases are located in the Golgi apparatus where they modify cell wall components that are assigned for exocytosis (Verger et al., 2016; Hooper et al., 2017; Smith et al., 2018). GDP-fucose transporter 1 (GFT1) is a recently identified transporter that is able to translocate nucleotide sugar GDP-L-fucose into the Golgi lumen (Rautengarten et al., 2016). Interestingly, *gft1* t-DNA mutants display severe growth defects, but no smooth margins phenotype was reported on leaves (Rautengarten et al., 2016). A proper quantification of leaf dissection would be interesting in order to confirm that the involvement of fucose in leaf serration is not Golgi-related.

SPINDLY (SPY) is a well-described growth inhibitor that was recently identified as the first O-fucosyltransferase in *Arabidopsis* (Zentella et al., 2017). Unlike most O-fucosyltransferases, SPY is localized in the cytosol and the nucleus (Swain et al., 2002; Wang et al., 2019). Strikingly, a smooth-margin phenotype was reported in several *spy* mutants (Greenboim-Wainberg et al., 2005; Maymon et al., 2009; Steiner et al., 2012), which indicates that SPY is probably a significant piece in the developmental pathway to form serrated leaves. However, the smooth leaf phenotype observed in *spy* mutants was never properly quantified before, neither extensively studied in a developmental context. In the rest of this introduction, I present in depth the *SPY* locus and the gathered knowledge about the functions of the protein.

SPY is a regulator of the GA response pathway

The *SPINDLY* locus was discovered in the course of a mutagenic screen which aimed at revealing new actors involved in the gibberellin response pathway (Jacobsen and Olszewski, 1993) (see Box 1-03). As paclobutrazol inhibits an early stage of gibberellin (GA) biosynthesis, and since GAs are necessary for seed germination, M2 seeds resulting from an EMS mutagenesis that were able to germinate on paclobutrazol were selected and led to the identification of the three first mutant alleles of *SPINDLY* (Jacobsen and Olszewski, 1993).

Besides the extreme dwarf phenotypes that are characteristics of GA-synthesis mutants, there are two different kinds of GA pathway mutant phenotypes (Jacobsen and Olszewski, 1993; Jacobsen et al., 1996). First, GA-insensitive mutants display dwarf and GA unresponsive phenotypes (Harberd et al., 2009; Davière and Achard, 2013). Those phenotypes are related to inhibited GA perception or transduction, since GA signaling is critical for germination, flower development, and above all plant growth (Davière and Achard, 2013). On the other hand, GA constitutive mutants display *slender*, frail, early-flowering phenotypes. The *spy* mutants belong to that second category of GA pathway mutants and were soon categorized as major repressor of GA signaling pathway (Jacobsen and Olszewski, 1993; Wilson and Somerville, 1995; Jacobsen et al., 1996). In particular, the different phenotypes of *spy* mutants are partly reminiscent of GA-sprayed wild type plants phenotypes (Wilson and Somerville, 1995). Hence, *spy* mutants were at first considered as GA-constitutive.

Interestingly, *spy* mutants only allow a partial rescue of GA-deficient phenotypes. First, *spy-4* mutation is partially epistatic to *ga1-2* GA-deficient mutant, as it partially restores its low germinating and extreme dwarf phenotypes (Jacobsen et al., 1996). Then, *spy-4* is completely

epistatic to *gai* (GA INSENSTITIVE, one of the five DELLA proteins in *Arabidopsis*) as *gai spy-4* double mutant displays the same phenotype as a single *spy-4* (Jacobsen et al., 1996), while *spy-5* is only partially epistatic to *gai* (Wilson and Somerville, 1995). However, *spy* mutants and the double *spy-4 ga1-2* still respond to GA treatment (Wilson and Somerville, 1995; Jacobsen et al., 1996). Meanwhile, a closer look at the internodes length or the phyllotaxis of strong *spy-2* and *spy-5* phenotypes demonstrated that *spy* mutation does not completely mimics a GA treated plant (Swain et al., 2001). For example, while dark grown hypocotyls were longer in doubles *ga1-2 spy-2*, *ga1-2 spy-3* and *ga1-2 spy-4* mutants than in the GA-deficient *ga1-2*, all three double mutants led to shorter hypocotyls when repeating the experiment on a medium containing 300µM GA_3 (Swain et al., 2001). A similar experiment was performed under far red light conditions with increasing GA_3 concentration and led to identical results (Tseng et al., 2004). These results suggest that SPY could also have a repressive role on growth, uncoupled from GA signaling.

Both *spy* and REPRESSOR OF *gai1-3* (*rga*) mutants allow the rescue of the dwarf phenotypes of GA-deficient mutants and thus function as inhibitors of the GA pathway (Silverstone et al., 1997). However, neither *spy* nor *rga* mutants restore GA levels in GA-deficient backgrounds, meaning both act on the GA response pathway (Silverstone et al., 2001).

Box 1-03: Biological role and mode of action of GA

Gibberellins (GA) form a large family of tetracyclic diterpenoid phytohormones involved in every step of plant life and development. At least 136 different molecules have been characterized so far as GA, and were found in plants but also fungi and bacteria. In plants, only GA_1, GA_3 and GA_4 are naturally present, and GA_4 is considered as the most bioactive form of GA (Cowling et al., 1998). Bioactive GAs are important for growth as they are involved both in the control of cell proliferation (Achard et al., 2009) and cell elongation in the hypocotyl (Cowling and Harberd, 1999; Sauret-Güeto et al., 2012) as well as the stem (Shibaoka, 1993). Moreover, GA are involved in the control of root growth (Fu and Harberd, 2003; Ubeda-Tomás et al., 2008). GA are also critical for plant life cycle, as they are necessary to start seed germination (Yamaguchi and Kamiya, 2001; Lee et al., 2002; Hauvermale and Steber, 2020) and induce flowering (Blázquez et al., 1998; Mutasa-Göttgens and Hedden, 2009).

DELLA proteins are major repressors of GA signaling pathway in plants (Silverstone et al., 1997; Fleet and Sun, 2005; Achard et al., 2007; Li et al., 2016). There are 5 different DELLA proteins in *Arabidopsis* (GAI, RGA, and three RGA-LIKE proteins RGL1, RGL2, and RGL3). DELLA repress GA responsive genes through various pathways. The DELLA-mediated repression pathways were reviewed elsewhere on multiple occasions (Davière and Achard, 2013; Claeys et al., 2014; Ito et al., 2018; Blanco-Touriñán et al., 2020b; Hernández-García et al., 2021). An increase in bioactive GA levels leads to the degradation of DELLA proteins in cells, hence the de-repression of genes positively regulated by GA signaling (Dill et al., 2001; Willige et al., 2007; Murase et al., 2008; Shimada et al., 2008). The regulation of GA signaling pathway activation leans thereby on whether DELLA proteins are present or active.

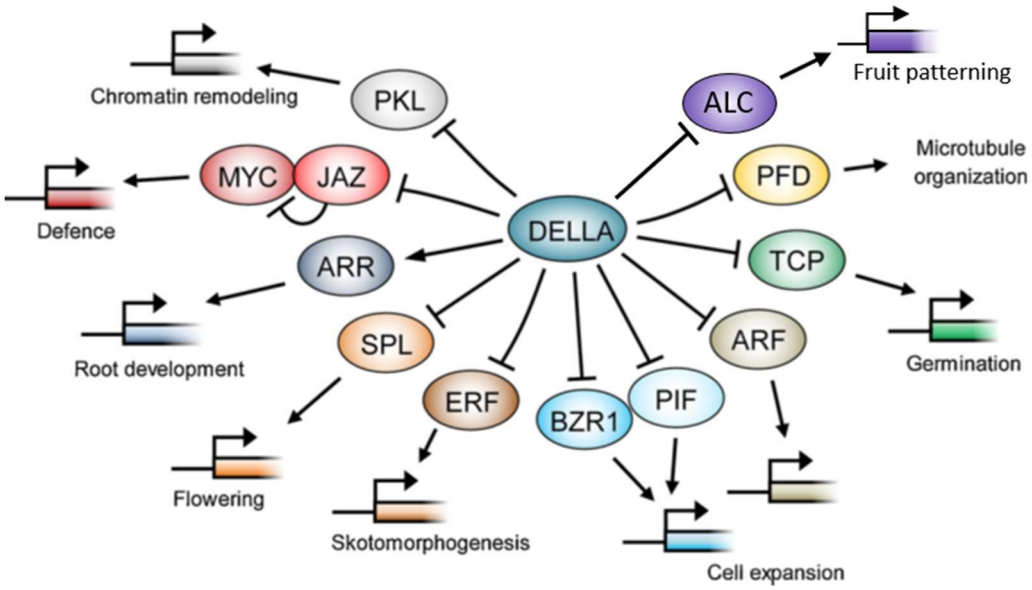

Representative interaction of DELLA with TF and transcription regulators. Arrows indicate a positive effect of DELLA on expression, while T-lines represent negative effects.
ALC, Alcatraz (Arnaud et al., 2010); PFD, Prefoldin (Locascio et al., 2013); TCP, TEOSINTE BRANCHED CYCLOIDEA/PCF1 (Davière et al., 2014); ARF, AUXIN RESPONSIVE FACTOR (Oh et al., 2014); PIF, PHYTOCHROME INTERACTING FACTOR (Feng et al., 2008; de Lucas et al., 2008); BZR1, BRASSINAZOL RESISTANT1 (Bai et al., 2012; Gallego-Bartolomé et al., 2012); ERF, ETHYLENE RESPONSIVE FACTOR (An et al., 2012); SPL, SQUAMOSA PROMOTER LIKE (Yu et al., 2012); ARR, ARABIDOPSIS RESPONSE REGULATORS (Marín-de la Rosa et al., 2015); JAZ, JASMONATE-ZIM DOMAIN (Hou et al., 2010); PKL, PICKLE (Park et al., 2017). Modified from (Hernández-García et al., 2021).

Box 1-03: Biological role and mode of action of GA

GID1 is soluble receptor that, in presence of bioactive GA, is able to bind to DELLA proteins, and to trigger their degradation (Ikeda et al., 2001; Ueguchi-Tanaka et al., 2005; Ueguchi-Tanaka et al., 2007). The binding of the rice DELLA protein SLR1 to GA/GID1 deeply modifies SLR1 conformation and reveals a binding site for GIBBERELLIC ACID INSENSITIVE 2 (GID2) (Hirano et al., 2010; Xiang et al., 2018). Rice GID2 and Arabidopsis SLEEPY1 (SLY1) are SCF E3 Ubiquitin ligases that modify DELLA protein and trigger their 26S proteasome-mediated degradation (McGinnis et al., 2003; Sasaki et al., 2003). CONSTITUTIVELY PHOTOMORPHOGENIC1 (COP1) is a pivotal regulator of temperature and light response pathways. COP1-DELLA interaction was demonstrated in various models and the ubiquitination of RGA by COP1 was reported in vitro, indicating another level of DELLA regulation (Blanco-Touriñán et al., 2020a). In addition, the circadian clock protein GIGANTEA (GI) accumulates in the light and is capable of interacting with RGA, preventing its GA/GID1 complex-triggered degradation. (Nohales and Kay, 2019).

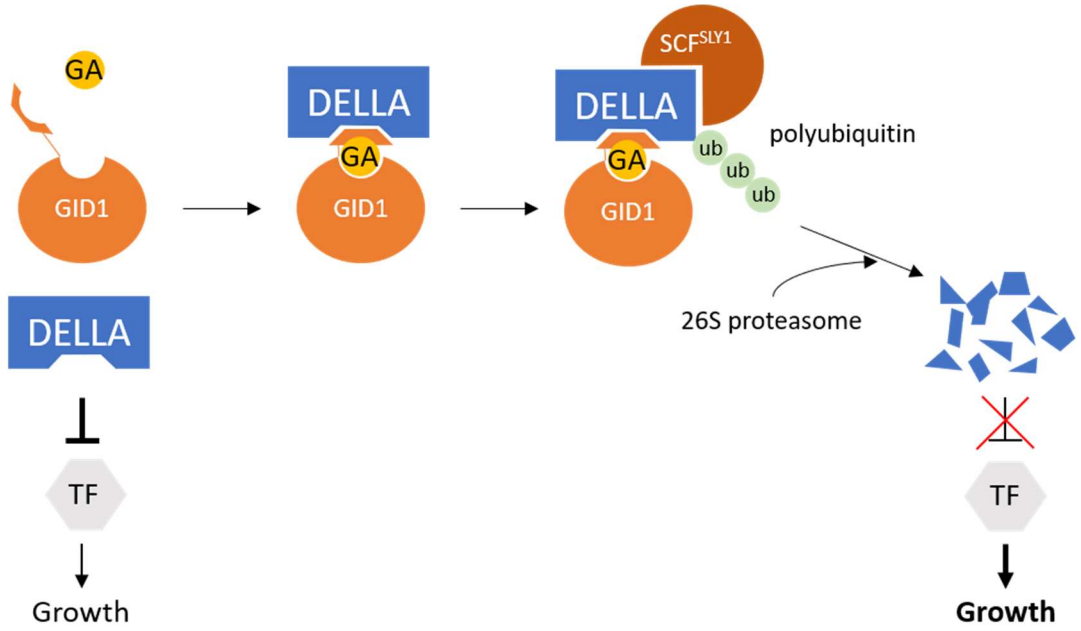

DELLA proteins repress GA responses, like BRZ1 or PIF4. In presence of bioactive GA, GID1 encloses GA in an internal pocket thanks to its N-term lid-like structure. Then the GID1-GA complex can bind DELLA. The formation of the tricomplex enables the binding of SLY1-containing SKIP1-CUL1-F-Box (SCF) E3 ligase which substrate is DELLA. Once polyubiquitinylated, DELLA is recognized and degraded by the 26S proteasome. From then, GA response genes are de-repressed.
Redrawn after (Phokas and Coates, 2021).

In the *rga-Δ17* mutant allele, a DELLA-motif truncated RGA protein is synthesized, which is insensitive to GA-induced degradation. Hence, in the *rga-Δ17* mutant, growth repression is never released and plants display an extreme dwarf phenotype (Dill et al., 2001). Interestingly, the study of the *spy-8 rga-Δ17* double mutant phenotype showed that SPY partially suppresses the *rga-Δ17* mutant gain of function phenotype (Silverstone et al., 2007). However, neither the subcellular location of RGA nor the RGA protein level were modified in the double mutant (Silverstone et al., 2007). Hence, it was hypothesized that SPY can modify RGA trough O-glycosylation and trigger its activation (Silverstone et al., 2007).

Structure and activity of the SPINDLY protein

The use of a *pSPY::GUS* reporter line showed that SPY is widely expressed across the plant (Swain et al., 2002). In addition, a full-length SPY-GFP fusion protein construct under SPY promoter allowed to precise that SPY subcellular localization is both cytosolic and nuclear (Swain et al., 2002). However, whether SPY activities towards growth take place in the cytoplasm, the nucleus or both remain unclear.

SPY protein structure has been extensively described

An analysis of the predicted protein sequence allowed the identification of different substructures, such as 11 tetratricopeptide repeats (34 amino-acids repeats, TPRs) on the N-terminal side of the protein (Jacobsen et al., 1996; Olszewski et al., 2010), and two distinct catalytic domains on the C-terminal half. In addition, there is a predicted phospholipid binding domain (PBD) on the C-terminal end (Olszewski et al., 2010) (Figure 1-01).

The TPR domains are known to mediate protein-protein interactions that can be relevant for various cellular processes (Lamb et al., 1994; Kreppel et al., 1997).

Fast-Neutron and EMS-generated mutants were selected for loss of GA-deficient dwarf phenotype. This allow the identification of additional *spindly* mutant alleles (Silverstone et al., 2007). Interestingly, the identified mutants which mutations were located in the coding sequence were not located evenly. For example, *spy-1, -2, -6, -7, -8, -9, -10* and *-11* were located in the TPR-2, -3 and -5 (numbering from C-term to N-term) while no GA deficiency-suppressing mutants were reported in the other TPRs (Silverstone et al., 2007). Similarly, *spy-3* ,*-12*, *-13*, *-14*, *-15* mutants are located in the first catalytic domain (CDI), while no mutant which mutation is located in the CDII was selected (Silverstone et al., 2007). These data suggest that TPRs 2 to 5 and CDI would be

more important to the function of SPY toward GA signaling, while mutations in other domains are not sufficient to reverse dwarf, GA-deficient phenotypes (Silverstone et al., 2007; Olszewski et al., 2010). Since the other TPRs as well as CDII are still heavily conserved across evolution, one hypothesis is that they are crucial for SPY interactions with other proteins, and other functions of SPY (Olszewski et al., 2010). Finally, since both *spy*-5, *spy-16* and *spy-17*, which all carry missense mutation in the PBD, display *spy*-like phenotypes and partial rescue of *ga1* dwarf phenotype, the PBD must intervene in SPY functions.

To better determine the functional role of the TPR domain, a *35S::TPR* construct was generated and inserted in both Columbia and *spy* mutants. This construct was shown to be sufficient to confer paclobutrazol resistance to wild type plants, even if it was not sufficient to rescue neither *spy-3* (substitution in CDI) nor *spy-6* (substitution in TPR-5) (Tseng et al., 2001). An interaction between full-length SPY and the TPR domain was demonstrated both *in vitro* and in a Yeast-two-hybrid essays, indicating that SPY must be able to form homo or hetero multimeric complexes (Tseng et al., 2001). Additionally, the TPR domain of SPY was shown to be involved in the interaction with other proteins like TCP14 and TCP15 (Steiner et al., 2012) or GIGANTEA (GI) (Tseng et al., 2004).

SEC, homolog of SPY, is an O-GlcNAcetyl transferase

SECRET AGENT (SEC) was identified due to its similarities in protein sequence with SPY and OGT (Hartweck et al., 2002) (see Box 1-04). In *sec*-1 and *sec-2* mutants, leaves were reported to grow at a lower rate than *spy* mutants which are early-flowering (Hartweck et al., 2006). This result indicates that *spy* and *sec* mutations can have opposing effects on plant development. While *sec* mutants do not display other obvious developmental phenotype, the combination of *spy* and *sec* mutation was lethal, indicating that both proteins intervene in the same pathway, and that their glycosyltransferase activity is essential to plant development (Hartweck et al., 2002). Like SPY, SEC is expressed widely in the plant. However, on the contrary to SPY, its O-GlcNAc transferase activity was demonstrated in multiple studies. In particular, SEC was shown to O-GlcNAcetylate RGA in several studies (Hartweck et al., 2002; Zentella et al., 2016; Zentella et al., 2017).

Box 1-04: Conservation of SPY across evolution.

Sequence BLASTs revealed that SPY shares great similarities with other proteins of the living kingdom. In monocots SPY seems to be conserved as a homolog of SPY (65% conserved DNA sequence, 76% protein identity) was identified in barley (Robertson et al., 1998) and in rice (74% amino acid identity between AtSPY and OzSPY) (Shimada et al., 2006). Similarly, the homolog of SPY in *Petunia hybrida* is very conserved (83% of protein identity) especially in the TPR domains (Izhaki et al., 2001). Subsequently, a strong homology was found with the O-GlcNAc transferases (OGT) of rat, *C.elegans* and *H.sapiens* (Kreppel et al., 1997; Thornton et al., 1999). SEC also has a strong sequence homology with SPY, and it was hypothesized that multiple OGT in plants are the result of an ancient gene duplication that predates eukaryotes (Olszewski elt al., 2010). Indeed, the OGT phylogeny yields to the identification of a SPY-like clade versus a SEC-like clade (Olszewski elt al., 2010). Interestingly, SEC catalytic domain shows higher similarity with Human OGT (41% amino acid identity) than SPY (24% identity) (Zentella et al., 2016). Moreover, SPY lacks a Histidine that is essential to the activity of both SEC and HsOGT (Zentella et al., 2016), which could explain why no O-GlcNAcetylation was ever reported for SPY, on the contrary to SEC (Hartweck et al., 2002; Zentella et al., 2016; Zentella et al., 2017).

Due to its close homology with SEC, SPY was thought to be an O-GlcNAcetyl transferase for a very long time, before recent data pointed out its catalytic activity (Zentella et al., 2017).

SPY is an O-fucosyltransferase that modifies RGA

MS/MS analysis revealed that RGA can be mono-O-fucosylated on Ser-Thr residues close to the DELLA domain. Besides, the fucosylation of RGA was reduced in *spy-8* but not in *sec-3* indicating this post-translational modification is SPY-dependent (Zentella et al., 2017). MS analysis on SPY+DELLA co-infiltrated tobacco leaves showed only RGA and RGL1 can be modified by SPY (Zentella et al., 2017). Moreover, *spy-8, spy-15* and *spy-19* (Figure 1-01) all rescue short hypocotyl phenotypes observed in the *ga1-3* ga-deficient line, meaning that growth repression in *ga1-3* mutant required SPY (Zentella et al., 2017). Since hypocotyl growth was shown to be driven by the BAP module (Oh et al., 2014; reviewed in Bouré et al., 2019), where RGA acts as a negative switch, it was hypothesized that SPY O-fucosylates RGA to trigger its repressive activity. Pull-down assays confirmed that RGA binding to BRZ1 and PIF3/4 is reduced in *spy-8, spy-15* and *spy-19*, meaning RGA is less able to prevent its targets from binding DNA (Zentella et al., 2017). Finally, co-infiltration in tobacco leaves of fixed RGA and SPY quantities with increasing quantities of SEC, followed by MS analysis, demonstrated that the more SEC there is, the more the Fuc/GlcNAc-modified RGA ratio decreases, indicating that SEC and SPY competitively target RGA to modify it (Zentella et al., 2017). Zentella *et al.* finally proposed a model in which SPY and SEC competitively

act to modify RGA and trigger its activation/inhibition (see Box 1-05). In that model, RGA fucosylation modifies its conformation leading to an open, active form of the protein. On the contrary, O-GlcNAcetylation by SEC triggers a closed, less active form.

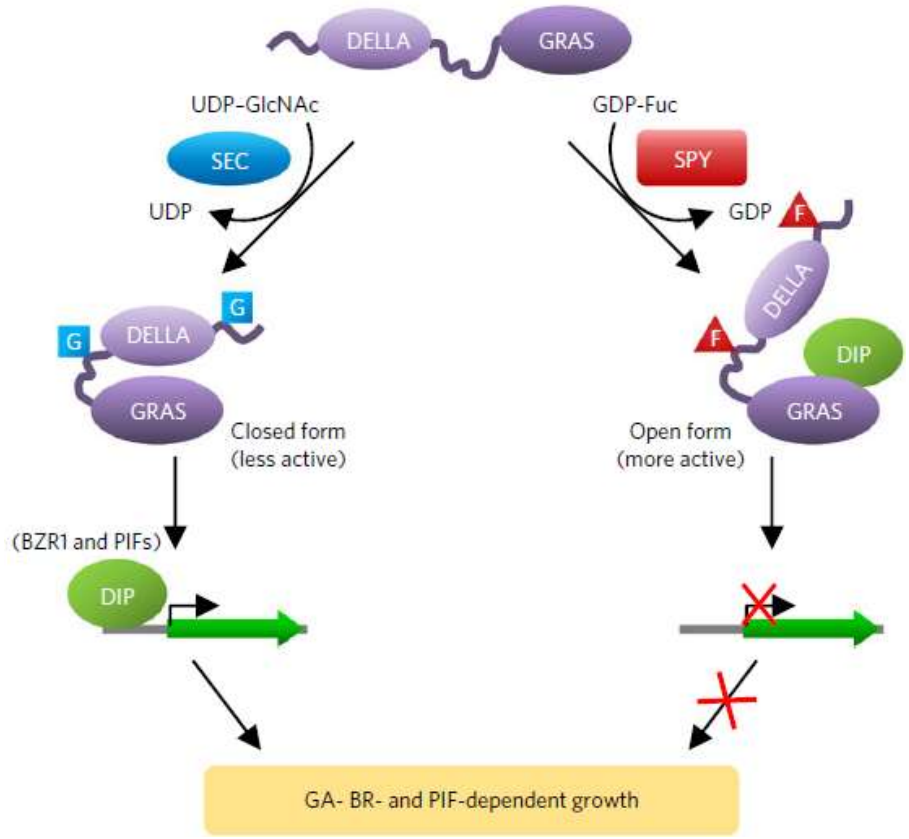

Box 1-05: Conservation of SPY across evolution.

Model proposed by Zentella *et al.* to describe the role of SPY in GA signaling. As SPY modifies RGA to trigger its activation, it globally acts as a GA repressor. F = Fucose. G = GlcNAc. DIP = DELLA interacting protein. From (Zentella et al., 2017)

Other known and supposed roles for SPY in *Arabidopsis*

As previously reported, SPY does not completely mimics a GA-treated plant phenotype (Swain et al., 2001). Indeed *spy* mutants display additional phenotypes, like glabrous sepals (Jacobsen and Olszewski, 1993), which was not reported as a GA-related phenotype. In addition, leaves exhibiting low serration level were already reported in *spindly* mutant in past work (Greenboim-Wainberg et al., 2005; Maymon et al., 2009; Steiner et al., 2012), even if most *spy* mutations were generated in the Landsberg *erecta* ecotype, which displays smooth leaves due to

the presence of the *erecta* mutation (Tameshige et al., 2016a). Several studies have highlighted other roles for SPY, particularly in relation to cytokinins and the control of the circadian cycle.

SPY promotes CK signaling

Treatments with various phytohormones revealed that *spy* mutants do not respond to cytokinins (CK), indicating SPY is essential to CK response (Greenboim-Wainberg et al., 2005). In addition, the expression of *ARABIDOPSIS REPONSE REGULATOR 5 (ARR5)*, a primary CK response gene, was inhibited both by GA_3 treatment and in the *spy-4* mutant (Greenboim-Wainberg et al., 2005). This result suggests SPY might play a central role in GA/CK crosstalk. Similarly, CK-induced *GLABROUS INFLORESCENCE STEMS 2 (GIS2)* and *GLABROUS1 (GL1)* response was suppressed in *spy-4*, and SPY was shown to act upstream of both CK-responsive genes (Gan et al., 2007). These data suggest SPY acts early in the CK response pathway.

More recent data show that SPY interacts with Class I TCP 14 and 15 in Y2H and pull down essays and that SEC can O-GlcNacetylate TCP14 and TCP15 in *E.coli* (Steiner et al., 2012). TCP14 and 15 were shown to be involved in the promotion of early CK responses downstream of SPY (Steiner et al., 2016). Researchers demonstrated that SPY is necessary to prevent 26S proteasome-mediated degradation of TCP14, and it was hypothesized that SPY modifies TCP14 to inhibit its proteolysis and keep a high CK sensitivity (Steiner et al., 2016). Strikingly, *tcp14tcp15* double mutant displays smooth, un-serrated leaves similarly to those of *spy-4* (Steiner et al., 2012)(see Box1-06), while no smooth margins phenotypes were reported in GA-deficient mutants. This could suggest that the role of SPY in serration formation lies in the CK response pathways rather than the GA pathway.

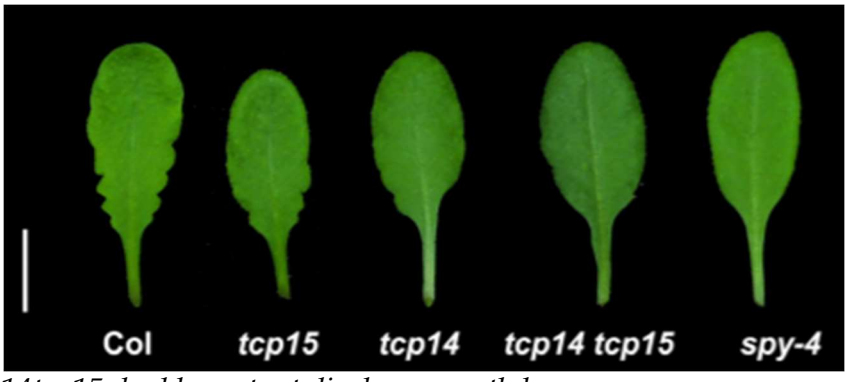

Box 1-06: tcp14tcp15 double mutant displays smooth leaves

L7-ranked leaves from col-0, *tcp15*, *tcp14*, *tcp14tcp15* and *spy-4* grown in short-day condition. Figure from (Steiner et al., 2012)

SPY is involved in the control of circadian clock

In addition to its function in the GA response pathway, SPY interacts with GIGANTEA(GI) both in Y2H and pull down-assays (Tseng et al., 2004). GI is a nuclear protein involved in the control of the circadian clock that acts upstream of CONSTANS (CO) and FLOWERING LOCUS T (FT) to promote flowering. Similarly to *gi-2* mutant, *spy-4* displays an altered circadian clock with unsynchronized cotyledon movements and modified leaf transpiration in continuous light after light entrainment (Sothern et al., 2002; Tseng et al., 2004). In addition, *spy-8, spy-15* and *spy-19* all display an elongated circadian period compared to wild type Ler (Wang et al., 2019). It was thus hypothesized that SPY and GI act in concert to regulate circadian clock parameters. More recently, protein-protein interactions were demonstrated between GI and all five DELLA proteins in *Arabidopsis*, adding a new levels of GA response fine-tuning (Nohales and Kay, 2019).

Another study recently demonstrated that the TRP domain of SPY interacts in the nucleus with PSEUDO-RESPONSE REGULATOR 5 (PRR5), one of the core circadian clock components (Wang et al., 2019). SPY catalytic activity was shown to be involved in PRR5-mediated degradation as PRR5 protein levels were higher in *spy-3* (Wang et al., 2019).

Together, these data suggest that SPY can modify its targets post-translationally to trigger either their stabilization, or their degradation. One can hypothesize that proteins can be fucosylated on target domains required for ubiquitination, thus fucosylation by SPY would prevent proteasome-dependent degradation. On the contrary, SPY could target proteins for degradation by promoting E_3 ligases recognition of fucosylated domains. In addition, SPY could modify only the activity and not the stability of its targets, like it seems to be the case for RGA (Silverstone et al., 2007; Zentella et al., 2017).

SPY appears to be involved in a plethora of different pathways in which it interacts with and potentially modifies many proteins. The phenotypes of SPY are numerous and are not limited to that of GA-treated plants but seem to correspond to several independent pathways. Indeed, a transcriptomic analysis on *spy-3* mutants compared to col-0 revealed than most SPY up- and down-regulated genes are not differentially expressed upon GA treatment (Qin et al., 2011). Nevertheless, the role of SPY in defining border domains has never been questioned until now, even though spy mutants exhibit smooth leaves, and even though defects in cotyledon fusion have been reported (spy-23, unpublished data). Although smooth leaves have been reported among the phenotypes of spy mutants, they have never been thoroughly quantified or studied

in a developmental context. Furthermore, their relationship with CUC transcription factors, which regulate the establishment of serration at the leaf margin, has not been studied. Finally, since fucose has been shown to be essential for serration, SPY fits naturally as the ideal candidate to link CUCs, fucose and leaf serration.

Here, I characterized in depth the leaf phenotypes of *spindly* mutants at organ/tissue/cellular levels in order to understand the contribution of SPY to leaf development. Accordingly, I identified a genetic link between SPY and the CUC transcription factors.

RESULTS

SPINDLY regulates leaf morphogenesis

Previous studies reported that *spy* mutant rosette leaves display a smooth margins phenotype (Greenboim-Wainberg et al., 2005; Maymon et al., 2009; Steiner et al., 2012). However, all previous descriptions of *spy* mutant leaf phenotype were qualitative. New tools now exist and allow a fine morphometric characterization to quantify leaf phenotypes, at different scales (Barbier de Reuille et al., 2015; Biot et al., 2016). In order to better understand the role of SPY in leaf serration development, we chose to use the loss-of-function *spy-3* mutant (Jacobsen and Olszewski, 1993). The *spy-3* mutant carries a G to A substitution, which on the protein leads to a false-sense mutation as the Glycine residue at the position 593 is converted into a Serine (Jacobsen and Olszewski, 1993) (Figure 1-01). This mutation is likely to lead to a loss-of-function mutant as the full conservation of SPY first catalytic domain was shown to be critical for SPY function (Silverstone et al., 2007). In addition to *spy*-3 and in order to detect a potential allele bias, we also used *spy-22* and *spy-23* in our study. The *spy-22* mutant (SALK09058) carries a T-DNA insertion in the 5'-UTR (Figure 1-01), and was previously described (Mutanwad et al., 2020). The *spy-23* mutant (WiscDsLox241C03) carries a t-DNA insertion within the forth exon and has been characterized in the present work.

Real time RT-PCR mRNA quantifications were performed on the different *spy* mutants. Transcript levels are at least ten times lower in *spy-22* and *spy-23* mutants than in the wild type, indicating that both insertional mutants may lead to a very severe reduction of *SPY* expression (Figure 1-01). In *spy-3*, an EMS-generated loss-of-function mutant, *SPY* transcript levels are as high in as in the wild type, which confirms former molecular characterizations (Figure 1-01).

In order to specify SPY role in serration development at the leaf margins, we performed a mature leaf shape analysis on 6-week-old short days grown leaves from rank 11, 12 and 13 for both *spy-3* and the wild type col-0. Qualitatively, *spy-3* displays a smoother margin phenotype than the wild type col-0 (Figure 1-02). We then performed a morphometric characterization using the Morpholeaf software, in order to evaluate *spy-3* leaf phenotype quantitatively (Biot et al., 2016) (see methods). Visualization of mean leaf shape for 19 col-0 leaves and 20 *spy-3* leaves confirms the qualitative description on single leaves. Focusing first on global leaf parameters, we measure that leaf area is significantly bigger in the wild type than in *spy-3* (241.2 mm^2 ± 38.5mm^2 for col-

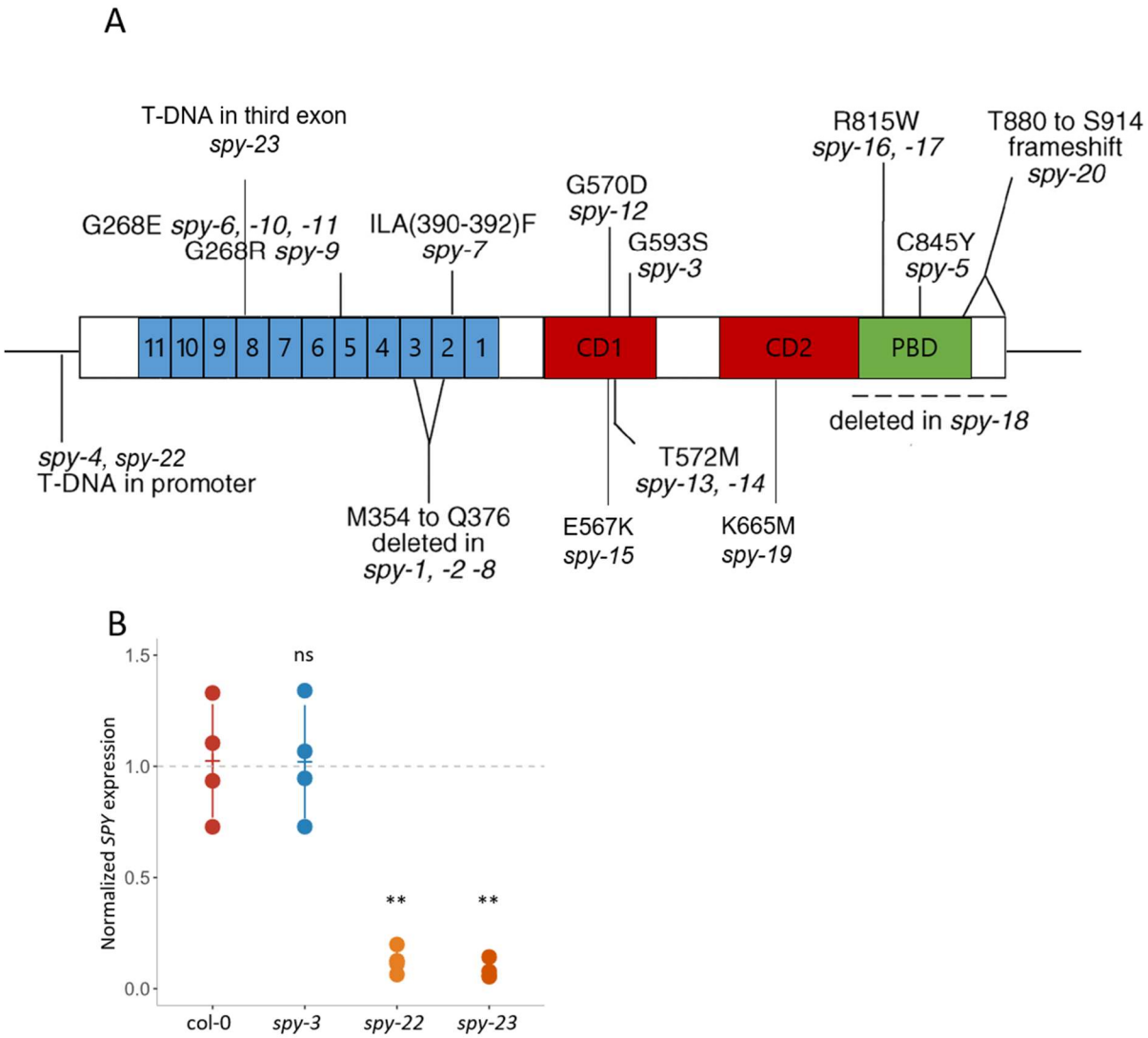

FIGURE 1-01: Diversity of protein defects in various *spindly* mutants and molecular characterization of *spy-3*, *spy-22* and *spy-23* mutant alleles.

Schematic representation of nature and localization of 21 *spy* mutations. Localization of *spy-19* point mutation and *spy-22* t-DNA insertion were added compared to the original figure (Zentella et al., 2016; Mutanwad et al., 2020). The *spy-23* is a novel insertion allele that we characterized in this study. The 11 TPRs were relabeled from the C-term end to the N-term end following the convention used in (Olszewski et al., 2010). CD = catalytic domain, PBD = Phospholipid binding domain.

Adapted from (Silverstone et al., 2007).

B. Expression level of *SPY* in col-0, *spy-3*, *spy-22* and *spy-23*. Each dot represents a biological RNA sample. *SPY* transcript levels were measured by real-time quantitative RT-PCR normalized by *EF1α* and *qREF*. Statistical significance (Student's test) is designated by ns=not significant, ** $p<0.01$.

0 and 192.2 mm² ± 40.5 mm² for *spy-3*, t-test p-value = 0.000427). This difference in leaf blade area is mainly due to a difference in leaf width, as col-0 is wider than *spy-3* (11.6 mm ± 1.3mm for spy-3 and 13.7 mm ± 1.3mm for col-0, t-test p-value = 3.531e-06) rather than a difference in length of the blade, as both *spy-3* and the wild type show equivalent blade lengths (25.3 mm ± 2.2mm for col-0 and 24.3 mm ± 3mm for *spy-3*, t-test p-value = 0.2198) (Figure 1-03). We did not focus on global leaf shape differences between the two lines, but accordingly chose to use a normalization step that would take those differences into account in a characterization of the margin's phenotype. Hence, for each leaf blade examined in this study, leaf complexity was described as a convex hull-normalized dissection index (DI) (see methods). Therefore, *spy-3* yielded smoother leaf shapes than col-0 since the normalized DI is significantly lower than in the wild type (col-0 DI was 1.25 ± 0.02, *spy-3* was 1.19 ± 0.03, t-test p-value 3.175e-09) (Figure 1-02).

In *Arabidopsis*, which exhibits simple leaves, leaf serration level is the result of both serration intensity and quantity of teeth (Blein et al., 2013). When comparing mature leaves from different lines, I chose to compare the second tooth height between col-0 and *spy-3* because it can still be identified precisely at that late stage of development, while the first tooth has been extensively modified along leaf growth. As a result, second teeth in col-0 are significantly higher, with 693µm ± 186µm high, than those in *spy-3* serrations are only 347µm ± 97µm high (t-test p-value = 2.32e-14). The exact number of teeth product in both genotypes cannot be determined using mature leaf shapes, as older teeth are not visible anymore at this stage, but will be exanimated later.

In order to confirm the observed leaf phenotype is not biased by the *spy-3* allele, a morphometric characterization was also performed in two additional *spy* T-DNA insertion lines, *spy-22* and *spy-23* (Mutanwad et al., 2020). Qualitatively, both mutant alleles display smoother leaf shapes (Figure 1-04). Global leaf parameters were also analyzed for these mutants. Like before, *spy* mutations yielded to a significant thinner width than in the wild type (col-0 was 15.8 mm ± 0.7 mm, *spy-22* was 13.5 mm ± 1.0 mm, *spy-23* was 13.7 mm ± 1.1 mm, One-way ANOVA analysis followed by Tukey comparison test) while the blade length was equivalent (col-0 was 32.0 mm ± 2.0 mm, *spy-22* was 31.9 mm ± 2.1 mm, *spy-23* was 31.4 mm ± 2.5 mm). Consequently, blade areas were smaller in *spy-22* and *spy-23* (col-0 was 331.5 mm² ± 27.3 mm², *spy-22* was 287.6 mm² ± 34.1 mm², *spy-23* was 311.0 mm² ± 42.9 mm²) (Figure 1-05). In addition, we used a *spy-22* mutant that was complemented with a *pSPY::SPY-FLAG* construct, and observed a restored wild-

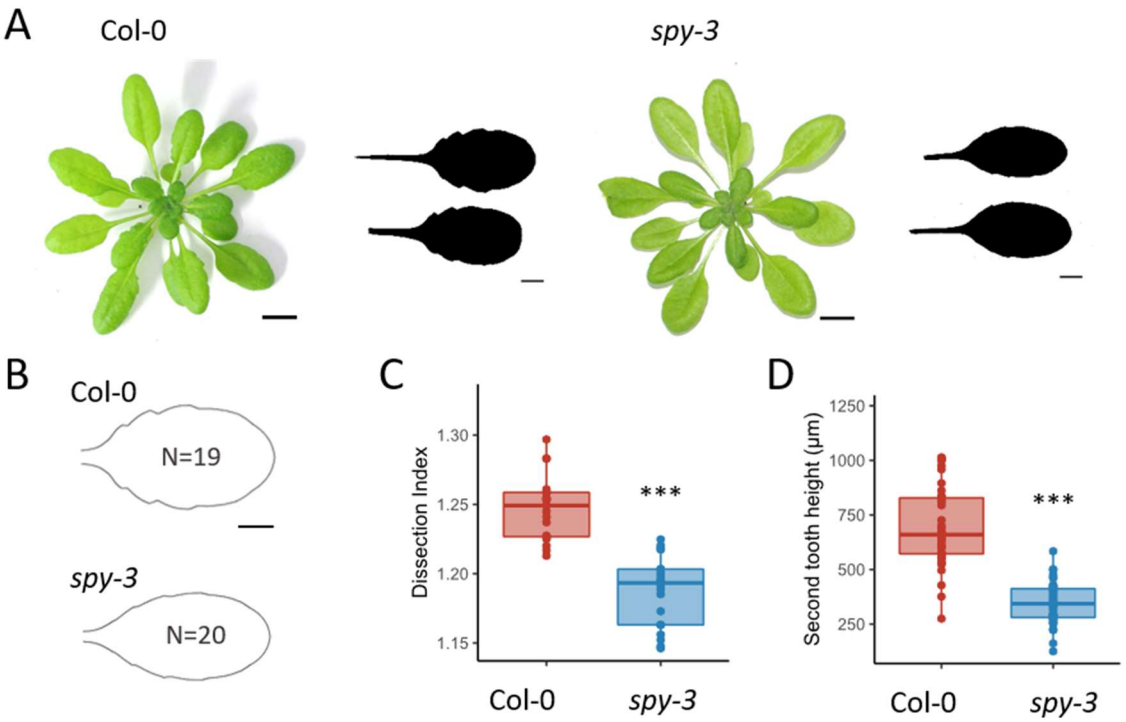

FIGURE 1-02: Morphometric characterization of *spy-3* mature leaf shape

A. Wild type and *spy-3* mutant rosette from plants grown in short-day condition for 6 weeks. Representative silhouettes from mature leaves ranked L11, L12, L13 are also represented. Scale bar are 1cm. B. Mean shape of mature leaves of col-0 and *spy-3*. Scale bar is 1cm. C. Quantification of alpha-hull normalized dissection index of col-0 and *spy-3* mature leaves. D. Quantification of the height in µm of the second tooth from col-0 and *spy-3* mature leaves. B,C,D. col-0 (N=19) and *spy-3* (N=20) 6 weeks-old leaves grown in short-day condition L11/12/13. Statistical significance (Student's test) is designated by *** $p<0.0001$.

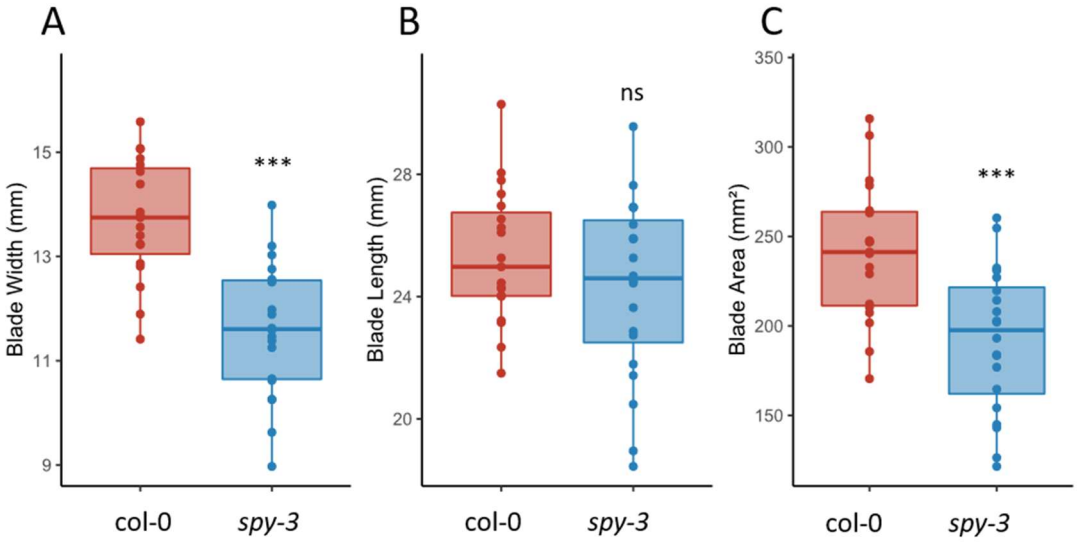

FIGURE 1-03: Morphometric characterization of *spy-3* global leaf parameters.

A. Maximal blade width of col-0 and *spy-3* (mm) B. Blade Length of col-0 and *spy-3* (mm) C. Blade area of col-0 and *spy-3* (mm^2). A, B, C. col-0 (N=19) and *spy-3* (N=20) 6 weeks-old leaves grown in short-day condition L11/12/13 were used. Statistical significance (Student's test) is designated by ns=not significant, *** $p<0.001$.

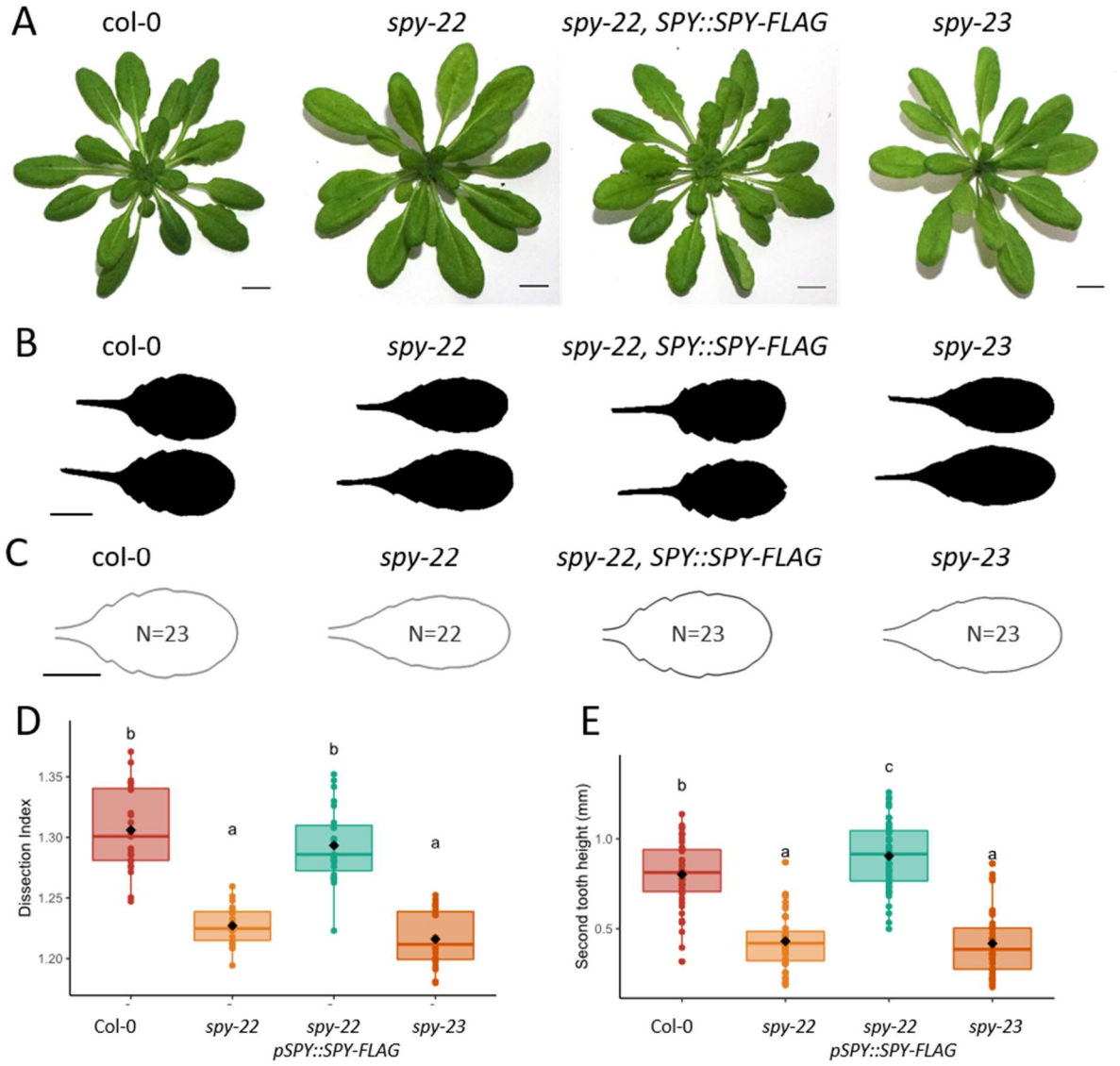

FIGURE 1-04: Morphometric characterization of *spy-22, spy-23* and *spy-22* complemented with *pSPY::SPY-FLAG* leaf shape and dissection index.

A. Wild type, *spy-22, spy-23*, and the complemented *spy-22 pSPY::SPY-FLAG* line rosettes from plants grown in short day condition for 6 weeks. Scale bars are 1cm. B. Representative silhouettes from leaves L11, L12 and L13. Scale bar is 1cm. C. Mean shape of mature leaves L11, L12 and L13 (col-0 N=23, *spy-22* N=22, *spy-22 pSPY::SPY-FLAG* N=23, *spy-23* N=23). Scale bar is 1 cm. D. Quantification of alpha-hull normalized dissection index of col-0 (N=23), *spy-22* (N=22), *spy-22 pSPY::SPY-FLAG* (N=23) and *spy-23* (N=23) mature leaves. E. Quantification of the height of the second tooth for col-0 (N=23), *spy-22* (N=22), *spy-22 pSPY::SPY-FLAG* (N=23) and *spy-23* (N=23) mature leaves. Statistical one-way ANOVA analysis, followed by Tukey comparison test.

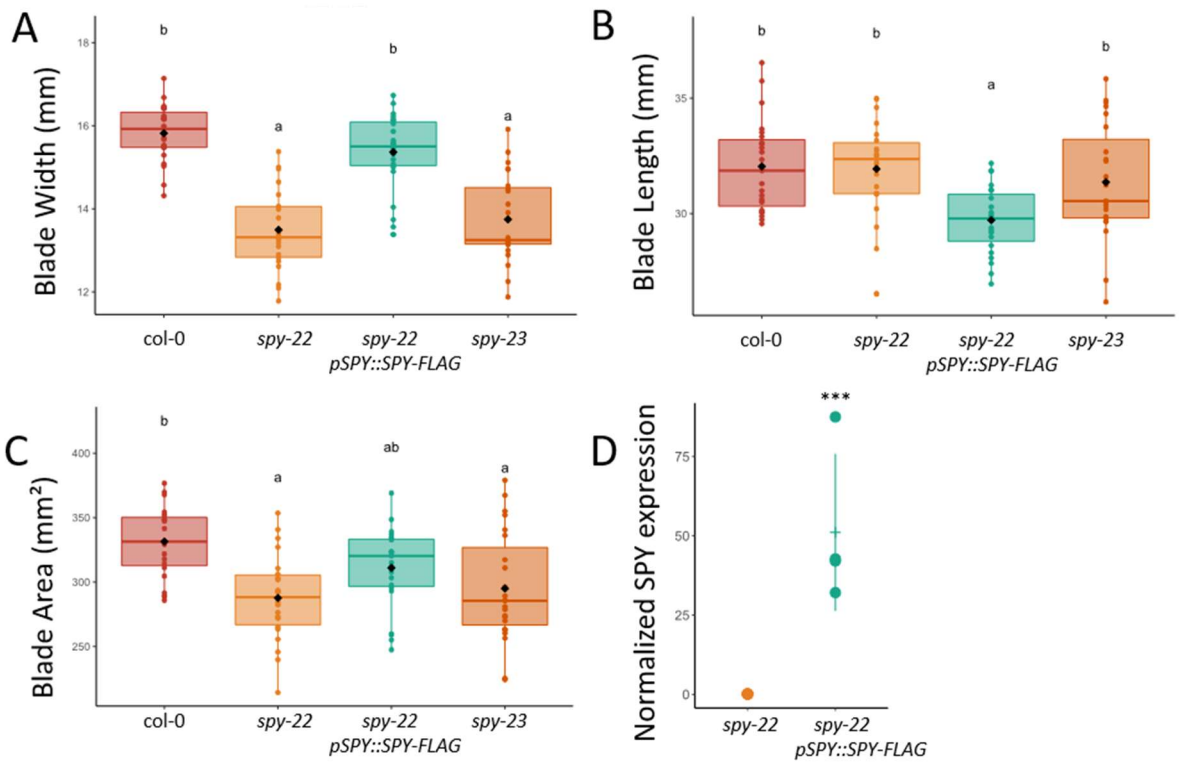

FIGURE 1-05: Morphometric and molecular characterization of *spy-22, spy-23* and *spy-22* complemented with *pSPY::SPY-FLAG*.

A. Maximal blade width in mm of col-0 (N=23), *spy-22* (N=22), *spy-22 pSPY::SPY-FLAG* (N=23) and *spy-23* (N=23) mature leaves. B. Blade Length of col-0 (N=23), *spy-22* (N=22), *spy-22 pSPY::SPY-FLAG* (N=23) and *spy-23* (N=23) mature leaves (mm). C. Blade area of col-0 (N=23), *spy-22* (N=22), *spy-22 pSPY::SPY-FLAG* (N=23) and *spy-23* (N=23) mature leaves (mm^2). For A, B and C, 6 weeks-old short-day condition L11/12/13 were used. Statistical one-way ANOVA analysis, followed by Tukey comparison test. D. Expression level of SPY in *spy-22* and *spy-22 pSPY::SPY-FLAG.* Each dot represents a biological RNA sample. *SPY* transcript levels were normalized by *EF1α* and *qREF.* Statistical significance (Student's test) is designated by *** $p<0.001$.

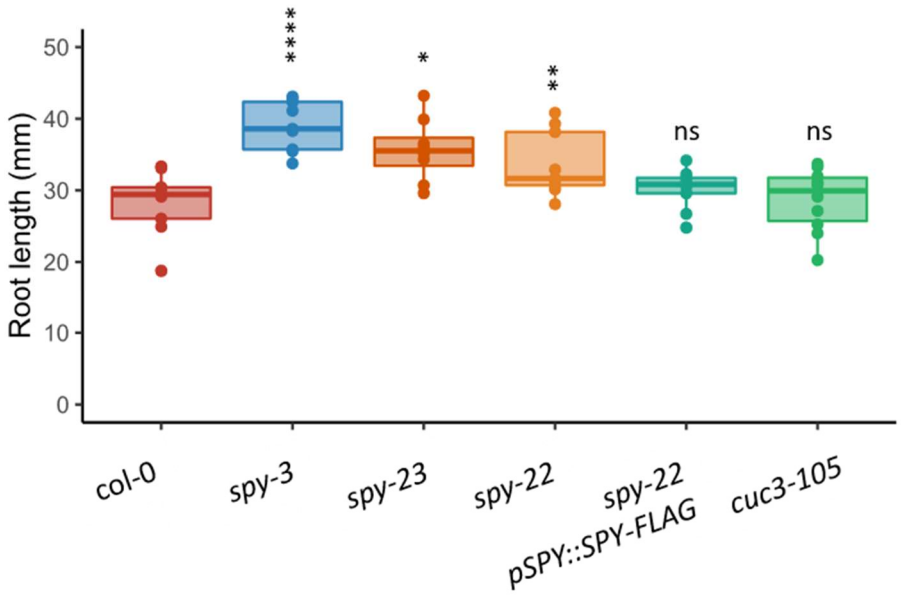

FIGURE 1-06: Mean length of the primary root of *spy* and *cuc3* mutants.
Primary root length in mm for col-0 (N=9), *spy-3* (N=9), *spy-23* (N=7), *spy-22* (N=9), *spy-22 pSPY::SPY-FLAG* (N=9), and *cuc3-105* (N=10) of plants grown in vitro for XX days. Statistical significance (Student's test against wild type) is designated by ns=not significant, * p≤0.5, ** p<0,01, **** p<0.0001.

type leaf shape phenotype (Figure 1-04). *spy-22 pSPY::SPY-FLAG* had a blade width similar to that of wild type (15.4 mm ± 0.9 mm), while its blade length was slightly smaller (29.7 mm ± 1.4 mm). However, no significant difference was observed for the blade area between the wild type and the *spy-22 pSPY::SPY-FLAG* line (295.0 mm^2 ± 31.4 mm^2). Let's note that the SPY complementation was verified by real time RT-PCR quantification to confirm that SPY expression was retrieved (Figure 1-05). Like before, an α-hull-normalized dissection index was calculated, taking these variations of global leaf shape into account. Like for the *spy-3* mutant, *spy-22* and *spy-23* displayed reduced dissection index (Figure 1-04). This phenotype was fully restored in the complemented line *spy-22 pSPY::SPY-FLAG*. Likewise, second tooth height were found to be smaller in *spy-22* and *spy-23* than in col-0, while the complementation triggered a restoration of the phenotype. Taken together, our results show that SPY *per se* is involved in the development of leaf serrations.

SPINDLY is involved in the control of the primary root length

In order to further characterize the *spy* mutant phenotypes, the main root length was measured on *spy* mutants *spy-22* complemented line and the wild type col-0 10-day-old seedlings vertically grown *in vitro* under long-day conditions (Figure 1-06). The main root length in the three different *spy* mutant alleles is longer than in the wild type control, suggesting that SPY inhibits the primary root growth. In addition, this root phenotype is restored in the complemented *spy-22 pSPY::SPY-FLAG* line, which confirms that SPY is responsible for this effect on root length. Previous data showed that GA signaling promotes root elongation *via* DELLA destabilization (Fu and Harberd, 2003). Moreover, several experiments demonstrated that both Auxin promotion of root elongation and Ethylene repression of root elongation are triggered by effects on DELLA degradation and/or stabilization (Achard et al., 2003; Fu and Harberd, 2003). Hence, it is possible that the root length-promoting effect in *spy* mutant is due to non-fucosylated, thus inactive, DELLA proteins, that are not able to exert their repressive effects on root growth. In studies where the principal root length was measured in various DELLA mutants in a GA-deficient background established that DELLA protein are indeed involved in the control of root elongation in response to GA (Fu and Harberd, 2003). Nevertheless, another study found that the repression of root elongation in response to cytokinin treatment is abolished in a *spy-4* mutant (Greenboim-Wainberg et al., 2005), meaning the CK-promoting role of SPY could also be involved in the control of root elongation. The fact that *rga-24 gai-t6* double mutant failed to respond to root growth repressing effect of ACC (the precursor of ethylene) is consistent with DELLA being

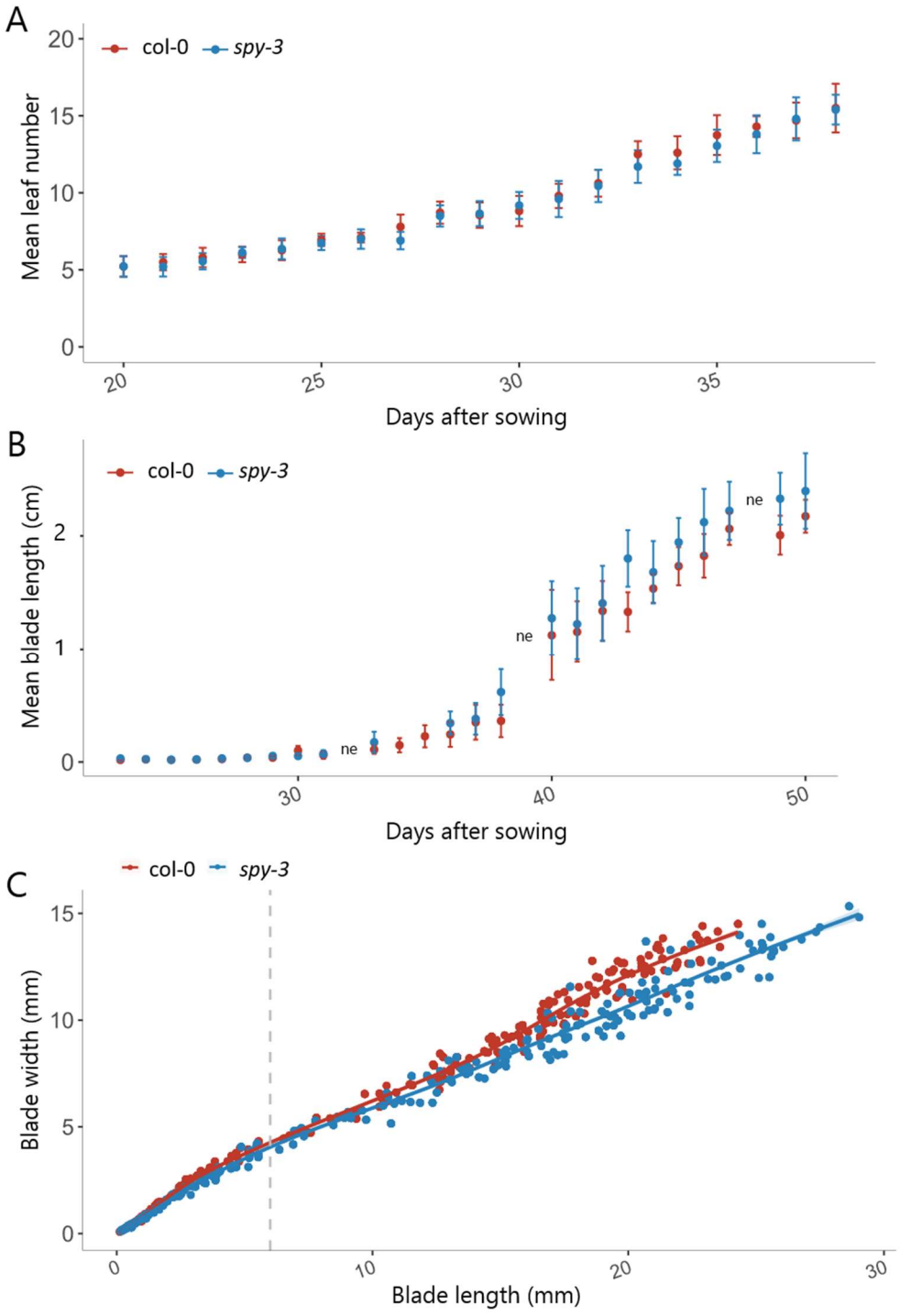

FIGURE 1-07: Wild-type and *spy-3* leaf initiation and growth parameters.

A. Wild-type and *spy-3* (N=10 per day per genotype) leaf primordia appearance in short days conditions from D20 to D38 after sowing. Error bars represent standard deviation. B. Wild-type and *spy-3* blade length along leaf development. Error bars represent standard deviation. ne = not estimated. C. Blade width evolution in function of blade length along leaf development for col-0 and *spy-3*. Grey bar represents the 6mm blade length threshold used subsequently in our experiments. B,C. col-0 (N=282) and *spy-3* (N=288).

mediators of growth repression in roots in response to CK (Achard et al., 2003). In addition, recent data indicate that SPY is critical for proper root hair patterning independently from its effects on RGA activity (Mutanwad et al., 2020), suggesting that SPY role on roots could also be GA-independent.

SPINDLY is required for growth serration maintenance rather than for early serration development.

Next, we aimed at defining the role of SPY at defining serration along leaf development. Mature leaf shape is the result of various growth and differentiation processes that add up throughout leaf development. Determining the exact parameters that vary between col-0 and *spy-3* and the exact moment in leaf development these differences occur would pinpoint more precisely the role of SPY in developing a serration at the leaf margin. To do so, we performed *spy-3* developmental kinetics in short-day conditions using leaf of ranks 11-12-13 from 23 days after sowing to 50 days, which roughly includes leaves from ≈80µm to 3cm for both *spy-3* and the wild type. A total of 282 col-0 and 288 *spy-3* leaves were dissected under a stereomicroscope, mounted and imaged to be used in this experiment.

Prior to perform this kinetics, we assessed global plant growth parameters to ensure that *spy-3* and col-0 developmental kinetics can be compared. First, the primordia apparition rate was calculated by counting every day the total number of visible leaves (about 1 mm long) for ten plants of each phenotype (Figure 1-07A), and yielded similar results between the wild type and *spy-3* in the culture conditions, showing that leaves appear at similar rates in both genotypes. Similarly, leaf elongation rates were assessed by measuring leaf length for all dissected leaves and plotting it against the days post-sowing. No significant difference was observed in terms of blade length between the two genotypes over leaf development, which is compatible with the mature leaf phenotypes that were evaluated earlier (Figure 1-07B), meaning the overall leaf elongation rates are comparable. Finally, blade width was plotted against blade length to assess the evolution of the overall blade shape. At early developmental stage, leaf width from col-0 and *spy-3* are not distinguishable from one another, while from 15 mm long, col-0 leaves are wider than *spy-3* leaves, which again is consistent which mature leaf phenotype (Figure 1-07C). Thereafter, a subset of the kinetics (the 6 first millimeters) was used to evaluate tooth growth parameters acutely, thus minimizing the impact of this global change on tooth growth.

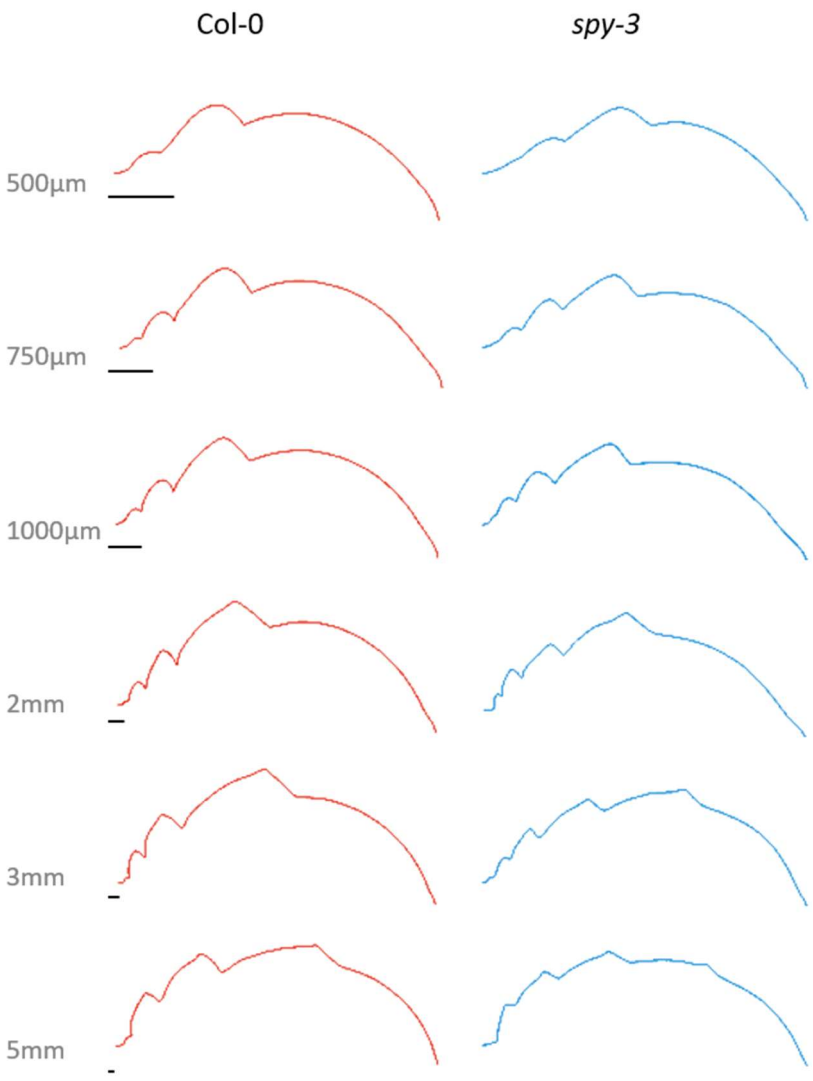

FIGURE 1-08: Teeth growth kinetics for col-0 and *spy-3*

Mean half contours of developing leaves from col-0 (N=282) and *spy-3* (N=288) generated with Morpholeaf (Biot et al., 2016), using moving average computation normalization method, with twenty neighbor rank (*i.e.* 20 different leaf samples contribute to the construction of each of the average shapes) and user-defined targeted lengths (500µm, 750µm, 1000µm, 2mm, 3mm and 5mm). Half contours were symmetrized prior analysis. Scale bars are 100 µm.

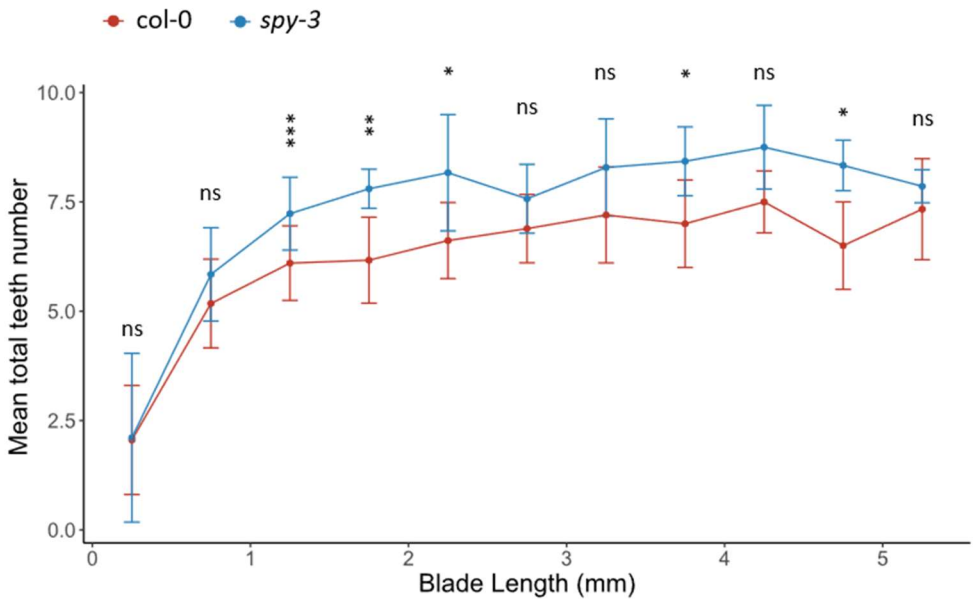

FIGURE 1-09: Evolution of mean total teeth number along col-0 and *spy-3* development.

Mean total teeth number in short day-grown col-0 (N=190) and *spy-3* (N=194) plotted against blade length. 500 µm-wide blade length classes were made to perform statistical analysis. Statistical significance (Student's test) is designated by ns=not significant, * p<0.05, ** p<0.01, *** p<0.001.

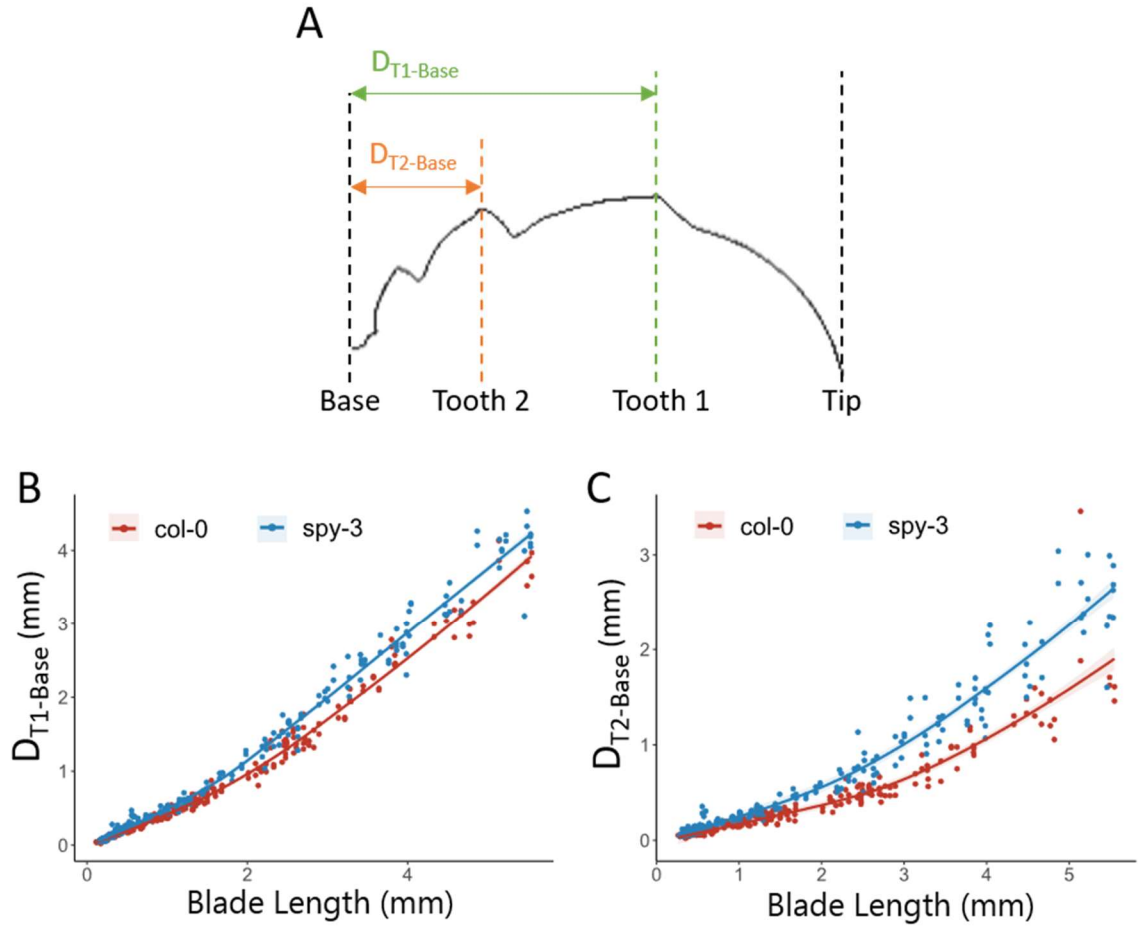

FIGURE 1-10: Evolution of first and second tooth position on the proximo-distal axis for col-0 and *spy-3*.

A. Definition of tooth-tip and tooth-base distances for the first and second teeth, used in the four following graphs. B. Tooth 1 base-distance in mm plotted against blade length. C. Tooth 2 base-distance in mm plotted against blade length B, C. Leaves of ranks 11-12-13 up to 6mm-long from short day condition col-0 (N=190) and *spy-3* (N=194) were used. Each tooth is represented by a point, and a LOESS curve is shown for visual interpretation.

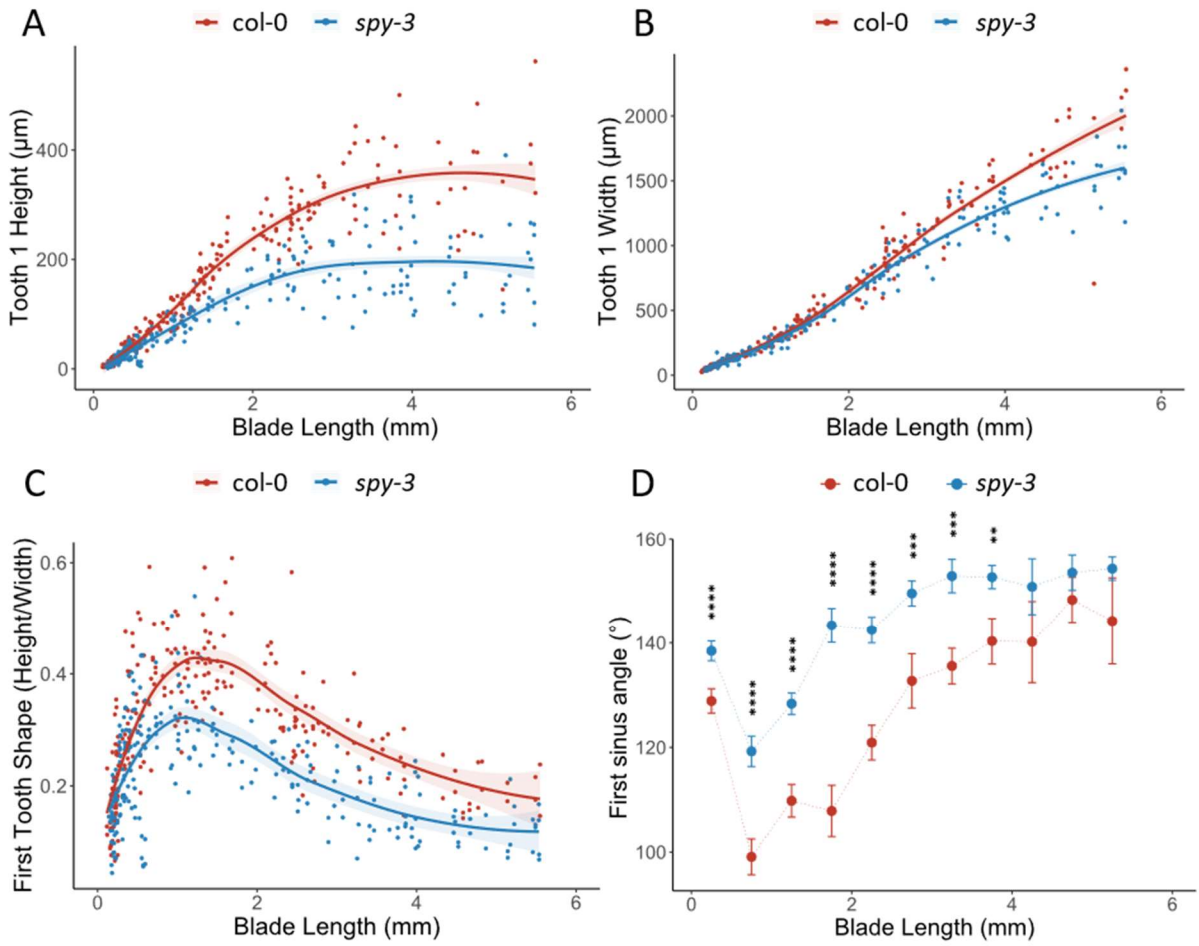

FIGURE 1-11: First tooth kinetics for col-0 and *spy-3*

A. First tooth height plotted against blade length for wild-type and *spy-3*. B. First tooth width plotted against blade length for wild-type and *spy-3*. C. Tooth shape of the first tooth, calculated as tooth height over tooth width plotted against blade. A,B,C. L11-12-13 from col-0 (N=190) and *spy-3* (N=194) plants grown in short-day conditions were used. Each tooth is represented by a point, and a LOESS curve is shown for visual interpretation. D. Mean first sinus angle measured in short day-grown col-0 (N=190) and *spy-3* (N=194) and plotted against blade length. 250 µm-wide classes were made to perform statistical analysis. Statistical significance (Student's test) is designated by ** p<0.01, *** p<0.001, **** p<0.0001.

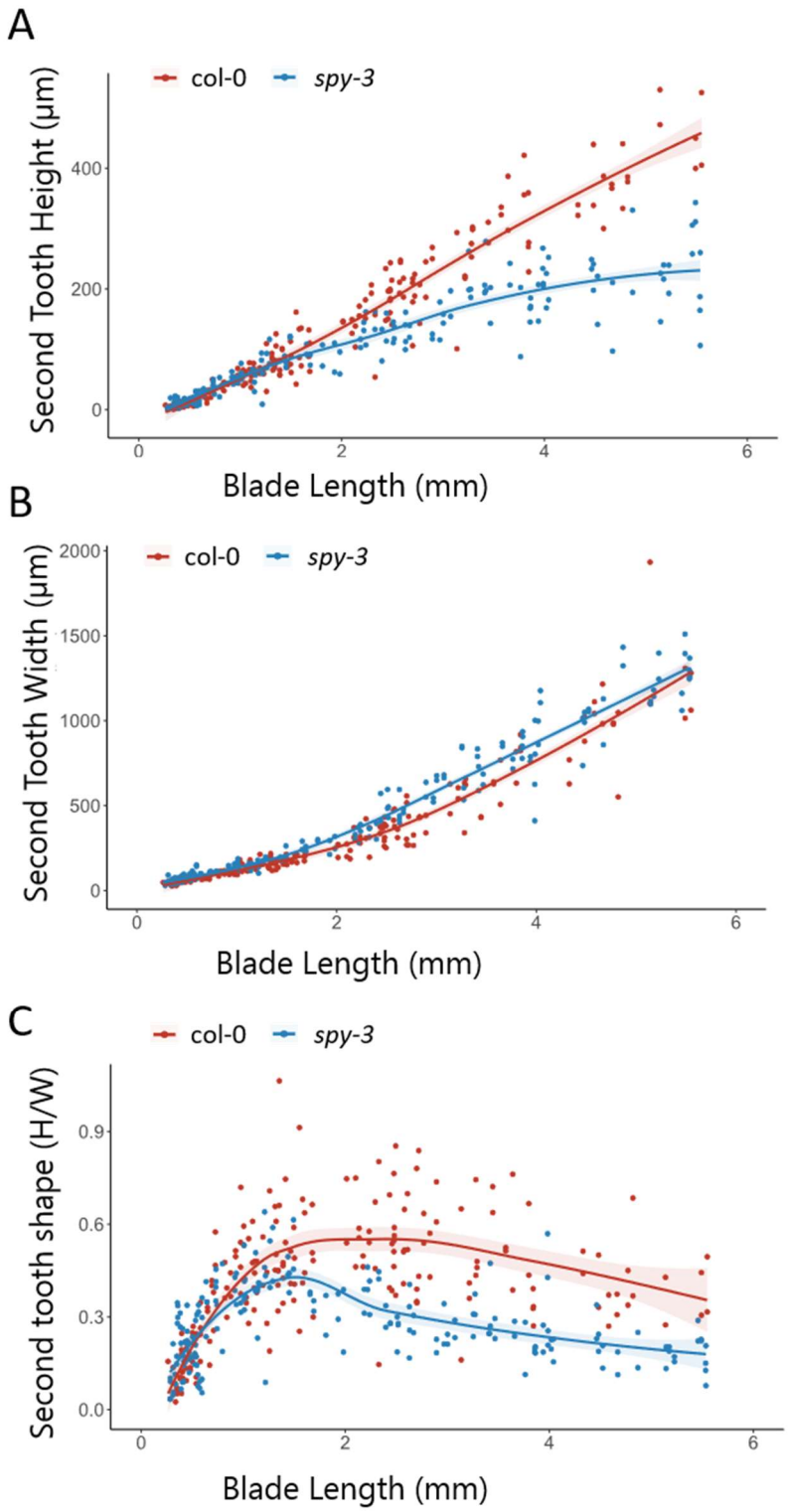

FIGURE 1-12: Second tooth kinetics for col-0 and *spy-3*

A. Second tooth height plotted against blade length. B. Second tooth width plotted against blade length. C. Tooth shape of the second tooth, calculated as tooth height over tooth width plotted against blade length. A, B, C. L11-12-13 from col-0 (N=190) and *spy-3* (N=194) plants grown in short-day conditions were used. Each tooth is represented by a point, and a LOESS curve is shown for visual interpretation.

Mean contours were generated to provide a visual, qualitative view of the kinetics. In *spy-3*, teeth are still initiated at very early stages of leaf development with no significant differences with the wild type control (Figure 1-08 and Figure 1-09). Hence, a defect in teeth initiation is not responsible for the smooth phenotype we observed in mature leaves. Moreover, it seems that *spy-3* generates teeth more often and/or more rapidly that col-0, since *spy-3* leaves display more teeth from 1 mm of total length (Figure 1-08 and Figure 1-09). The difference between *spy-3* and the wild type in terms of teeth number is not always significant thorough leaf growth, although *spy-3* mean teeth number is always higher than that of col-0. To explain this, we can either suppose, since that *spy-3* generates the same total amount of teeth than col-0 but earlier in the development, or that *spy-3* generates teeth at a quicker rate than the wild type along development and ends up with more teeth. As *spy-3* displays as many teeth as col-0 from 6000 µm of total blade length, the former hypothesis is favored.

When looking qualitatively at averaged half contours generated over leaf growth, *spy-3* teeth look both lower in height and sharper than the wild type (Figure 1-08). For equivalently-long half contours, the teeth positions seem to differ between col-0 and *spy-3*. From 2mm-long leaves, on half contours the distance between the first tooth and the leaf tip is indeed shorter in *spy-3* than in col-0. Put in another way, teeth are positioned closer to the apex in the *spy-3* leaf mutant. To verify this quantitatively, we used Morpholeaf that allows to quantify teeth positions. We measured the distance between the peak position and the leaf base for the two first teeth (see explicative scheme in Figure 1-10A). For both teeth1 and teeth 2, the distance between the projected peak position and the projected leaf base positions increases as a result of overall leaf growth. Interestingly, both *spy-3* teeth are farther from the leaf base than the wild type from around 2 mm of total blade growth (Figure 1-10). This quantitative measure confirms the qualitative description made earlier. As for the teeth number, we can hypothesize that *spy-3* initiates teeth at a faster rate and that it starts initiating teeth earlier in the development. However, in younger mean contours (*i.e.* less than 1.5 mm), no difference can be observed in terms of tooth position.

On mean half contours, the height of the first tooth looks smaller in *spy-3* than in the wild type control. A plot of its height against the blade growth reveals that col-0 indeed produces higher first teeth than the mutant from about 800µm-long leaves (Figure 1-11A). Wild type and *spy-3* display comparable first tooth width values until approximately 2,5mm of leaf growth, where

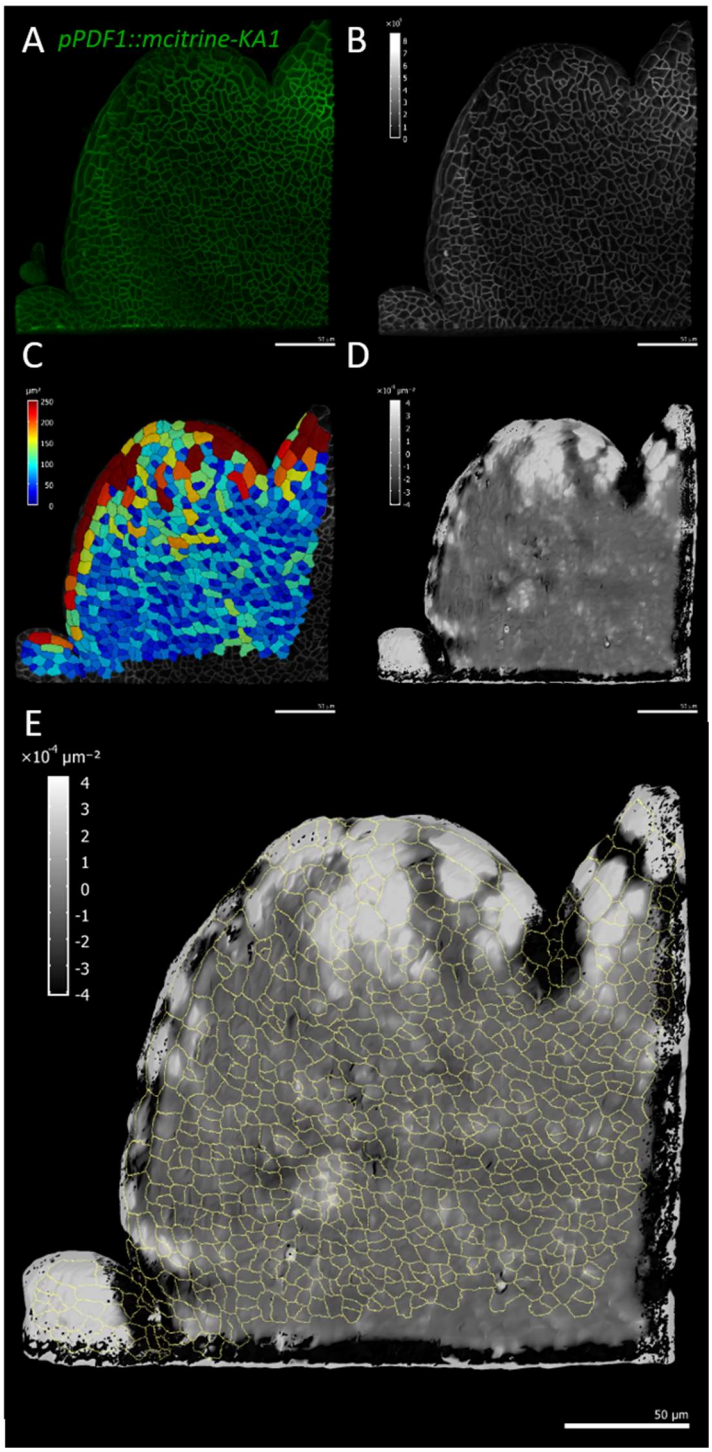

FIGURE 1-13: Determination of cell projected area in the first tooth sinus.
A. *pPDF1::mcitrin-KA1* plasmic membrane signal observed in the first tooth of a col-0 leaf. B. [2-6] µm-wide *pPDF1::mcitrin-KA1* signal projection on shape-calculated surface. C. Heat map of projected cell area. D. Gaussian curvature calculated with a 16µm neighboring radius. Black areas indicate concave gaussian curvatures, while white areas indicate convex gaussian curvature. E. Superposition of segmented cell borders over gaussian curvature projection. Only cell within a negative gaussian curvature, used as a proxy for cell within sinuses, were used in projected cell area quantifications. Scale bars are 50 µm.

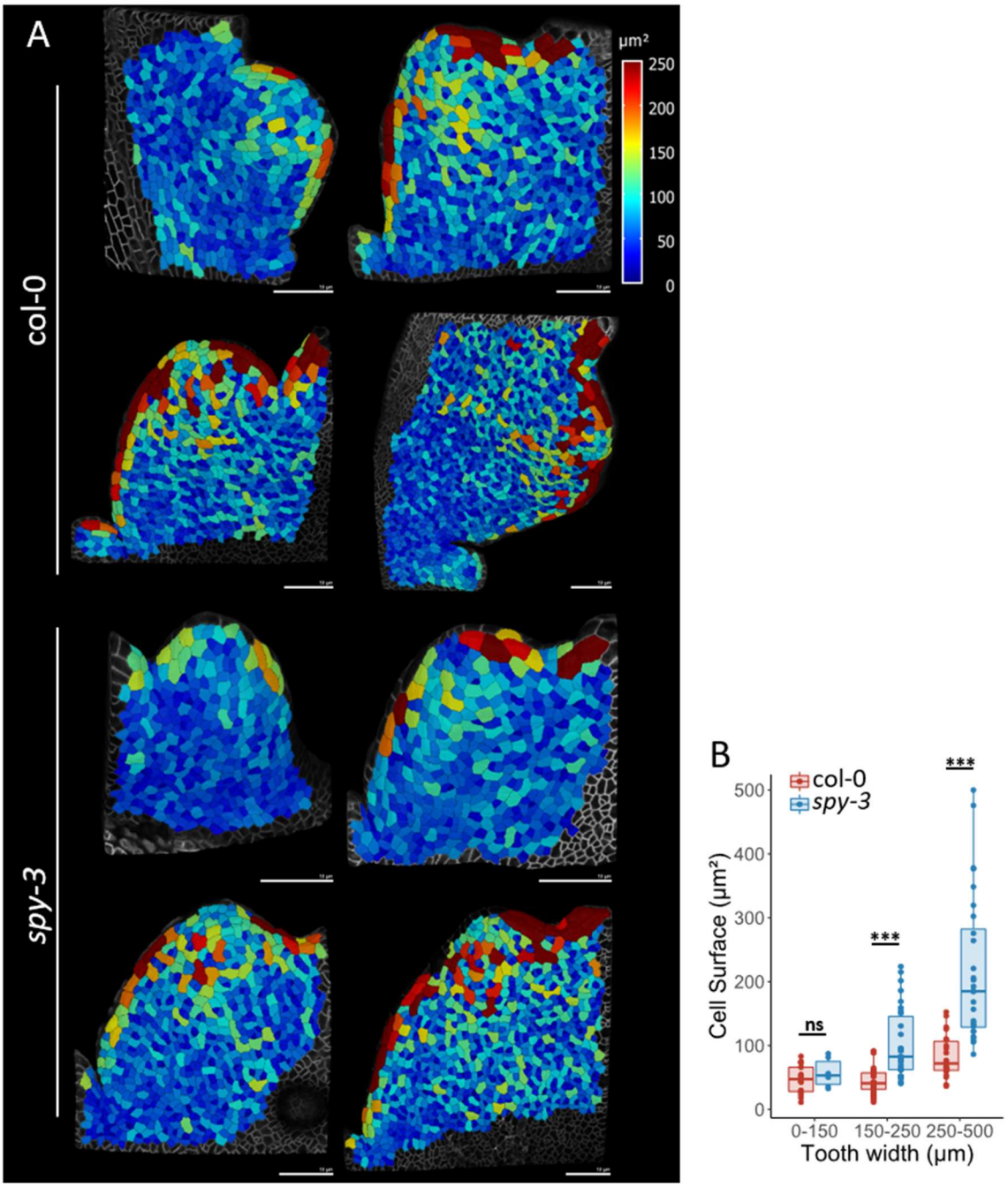

FIGURE 1-14: Representative heatmaps for col-0 and *spy*-3 and projected surfaces quantification from the first tooth sinus cells.

A. Representative heatmaps of teeth segmented in the cell surface estimation experiment. A total of 20 teeth were segmented for each genotype. The four col-0 teeth are 145 µm, 219 µm, 221 µm and 293 µm large. The four *spy-3* teeth measure respectively 136 µm, 177 µm, 222 µm, 316 µm. Scale bars are 50 µm. B. Projected areas of the sinus cells were divided into 3 classes according to the width of the tooth and plotted according to these categories. N_{col-0} = 17, N_{spy-3} = 6 in [0-150] µm. N_{col-0} = 37, N_{spy-3} = 30 in [150-250] µm. N_{col-0} = 22, N_{spy-3} = 28 in [250-500] µm. Statistical significance (Student's test) is designated by ns=not significant, *** $p<0.001$.

col-0 tooth 1 starts to grow larger than of *spy-3* tooth 1 (Figure 1-11B). To better describe the evolution of the tooth morphology, the tooth shape was calculated as the height over width ratio (Figure 1-11C). From the very beginning col-0 grows more marked first teeth than the mutant, as a consequence of a more intense increase in tooth height in col-0 than in *spy-3* while tooth width values remain comparable. Around 1,5mm of blade growth though, the shape ratio stops increasing and even starts to decrease, as a result of the global leaf growth parameters that impose a specific growth rate to the teeth. Around 2,5mm of blade length, the leaf keeps on growing, however the tooth outgrowth stabilizes. As a consequence, the first tooth shape ratio keeps decreasing. In *spy-3* the level of shape ratio is always lower than in the wild type, indicating the first tooth is never as pronounced as in the wild type. Interestingly, it seems that the slowing down of the tooth ratio that occurs around 1,5mm of leaf growth starts earlier in *spy-3*. Thus, not only *spy-3* forms lower teeth but also the outgrowing of the tooth stops earlier in the development.

The same measurements were performed using the second tooth of both *spy-3* and col-0 (Figure 1-12). Like before, col-0 grows higher teeth than the mutant, even if this difference is only visible from 1,5mm of total blade growth, and since the second tooth develops later in the development. There are no significative differences between col-0 and *spy-3* second tooth width up to 6 mm-long leaves. In addition, the shape ratio displays a similar dynamic along leaf development as before, though the curve inflexion is less visible.

Together, our data suggest that SPY is involved in teeth growth maintenance rather than tooth initiation promotion. Yet, tooth outgrowth maintenance was previously associated with the maintenance of boundary domains at the sinuses (Hasson et al., 2011; Maugarny-Calès et al., 2019; Serra and Perrot-Rechenmann, 2020). Accordingly, we chose to focus on the dynamics of the first sinus angle (see Figure 1-21), as a cue to infer local growth repression at the sinus. The first sinus angle was measured for *spy-3* and col-0 in the first 6 mm of leaf growth (Figure 1-11). According to what was described earlier (Maugarny-Calès et al., 2019), the first angle decreases as long as the tooth shape ratio increases, meaning the tooth is forming sharper and sharper. Later, while the tooth shape ratio decreases, the angle reopens as a result of the tooth smoothening. 250µm-wide classes were established to compare col-0 and *spy-3* first tooth sinus angle throughout leaf development, using t-test statistical analysis. Up to 4mm-long leaves, *spy-3* always displayed significantly more open angles than the wild type. This result is also quite visible in averaged half

contours (Figure 1-08). Very early during leaf development, first sinus angle is not the same between col-0 and *spy-3* even if other global parameters exhibit similar values. This probably means that from very early developmental stages, SPY in involved in the shaping of the teeth, and particularly the bending of the sinus. These data suggest that the alteration of leaf shape may partially results from local defect in boundary domain definition in the spy-3 mutant.

SPINDLY is required to inhibit sinus cells growth during leaf development.

To go further in the study of the role of SPY at defining the sinus, it is then necessary to reach for cellular scale, as differences in cellular growth rate are responsible for differential growth at the leaf margin which lead to the formation of proper serration (Serra and Perrot-Rechenmann, 2020). To do so, we used the *pPDF1::mCitrine-KA1* reporter line, which allows plasma membrane visualization (Simon et al., 2016; Verger et al., 2018). We imaged young leaves from the *pPDF1::mCitrine-KA1* reporter line with a confocal microscope, either in col-0, or in the *spy-3* mutant background. Subsequent cell segmentations and analyzes were performed with the *MorphoGraphX* software (Barbier de Reuille et al., 2015). The projected cell surface was estimated for the epidermis of first teeth from col-0 and *spy-3* leaves from rank 11, 12 and 13 grown in short-day conditions (Figure 1-14). Then, a pipeline based on negative gaussian curvature was applied to pick the cells that belong to the sinus only (see methods, Figure 1-13)(Serra and Perrot-Rechenmann, 2020). Importantly, leaves within 100 µm to 1 mm of total blade length were used in this experiment, which corresponds to a developmental window where the first tooth heights significantly differ between genotypes, while on the contrary, neither the global leaf parameters (leaf length and width, teeth number, Figure 1-07) nor the tooth position on the margin (Figure 1-10) differ between col-0 and *spy-3*. Thus, we can suppose that a potential difference in cell area between genotypes will be more the results of a difference in cell growth than of differential organ growth regimes.

In order to perform statistical analysis, the measured cells were separated into three classes according to measured tooth width (0-150 µm, 150-250 µm, 250-500 µm). Such a separation into categories is possible, since the analysis of the first tooth width against blade length did not reveal any difference between the mutant and the wild type for leaves shorter than 2mm (or teeth under 750 µm in width, Figure 1-11). For first teeth up to 150 µm wide, sinus cell sizes of early leaf primordia were not significantly different between *spy-3* and the wild-type. Later,

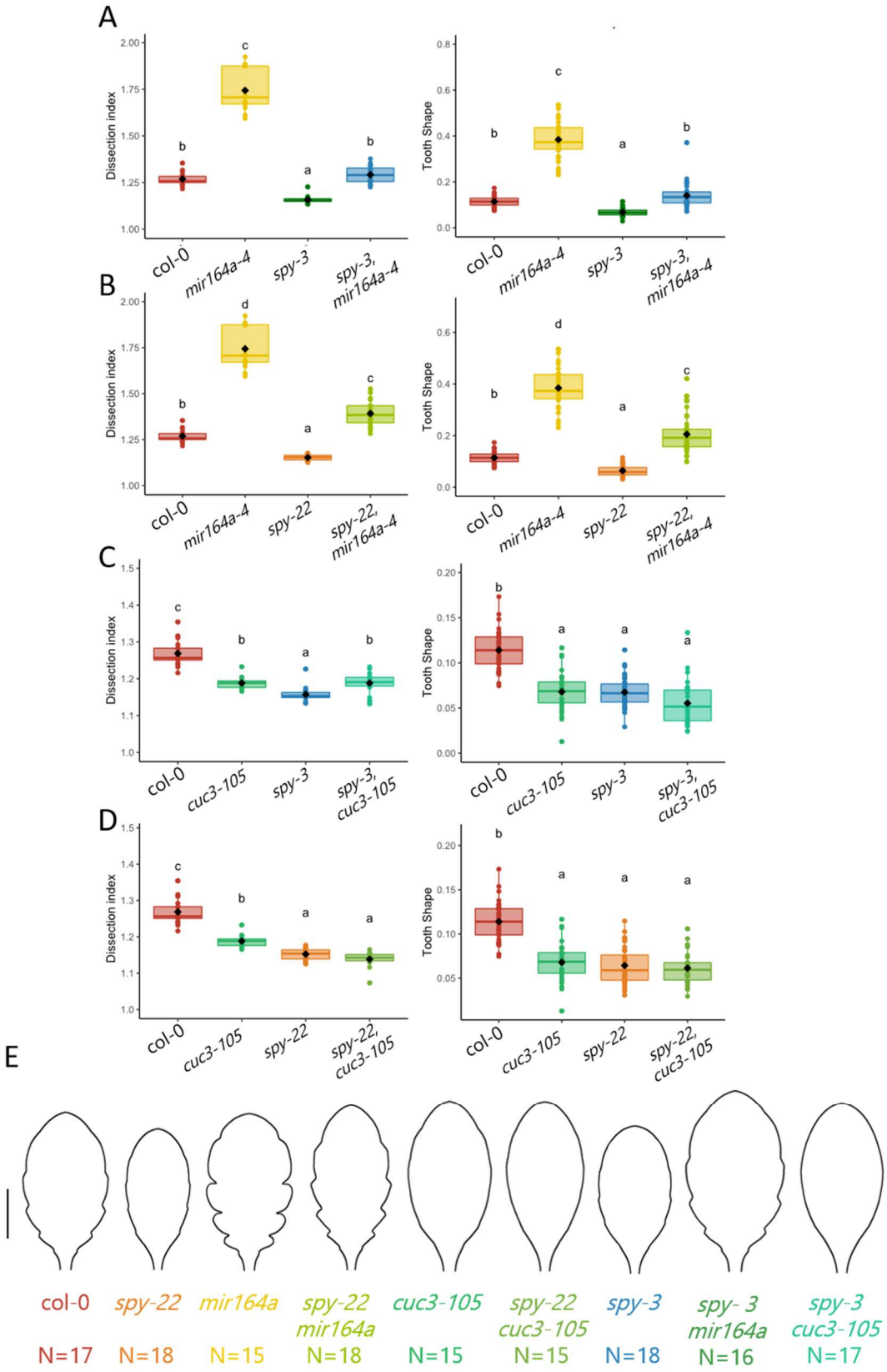

FIGURE 1-15: Morphometric characterization of mature leaf shape to evaluate the interaction between *spy-3* and *-22, cuc3-105* and *mir164a.*

A. alpha-hull normalized dissection index and tooth shape (defined as tooth 2 height over its width) of col-0 (N=17), *mir164a* (N=15), *spy-3* (N=18), *spy-3 mir164a* (N=16).

B. alpha-hull normalized dissection index and tooth shape of col-0, *mir16a, spy-22* (N=18) and *spy-22 mir164a* (N=18). C. alpha-hull normalized dissection index and tooth shape of col-0, *cuc3-105* (N=15), *spy-3* and *spy-3 cuc3-105* (N=17) D. alpha-hull normalized dissection index and tooth shape of col-0, *cuc3-105, spy-22* and *spy-22 cuc3-105* (N=15). E. Mean shape of mature leaves. Scale bar is 1 cm. A,B,C,D: mature leaves of rank 11-12-13 from 6 weeks-old plants grown under short-day conditions. Data and averaged shapes were both generated using Morpholeaf software (Biot et al., 2016).

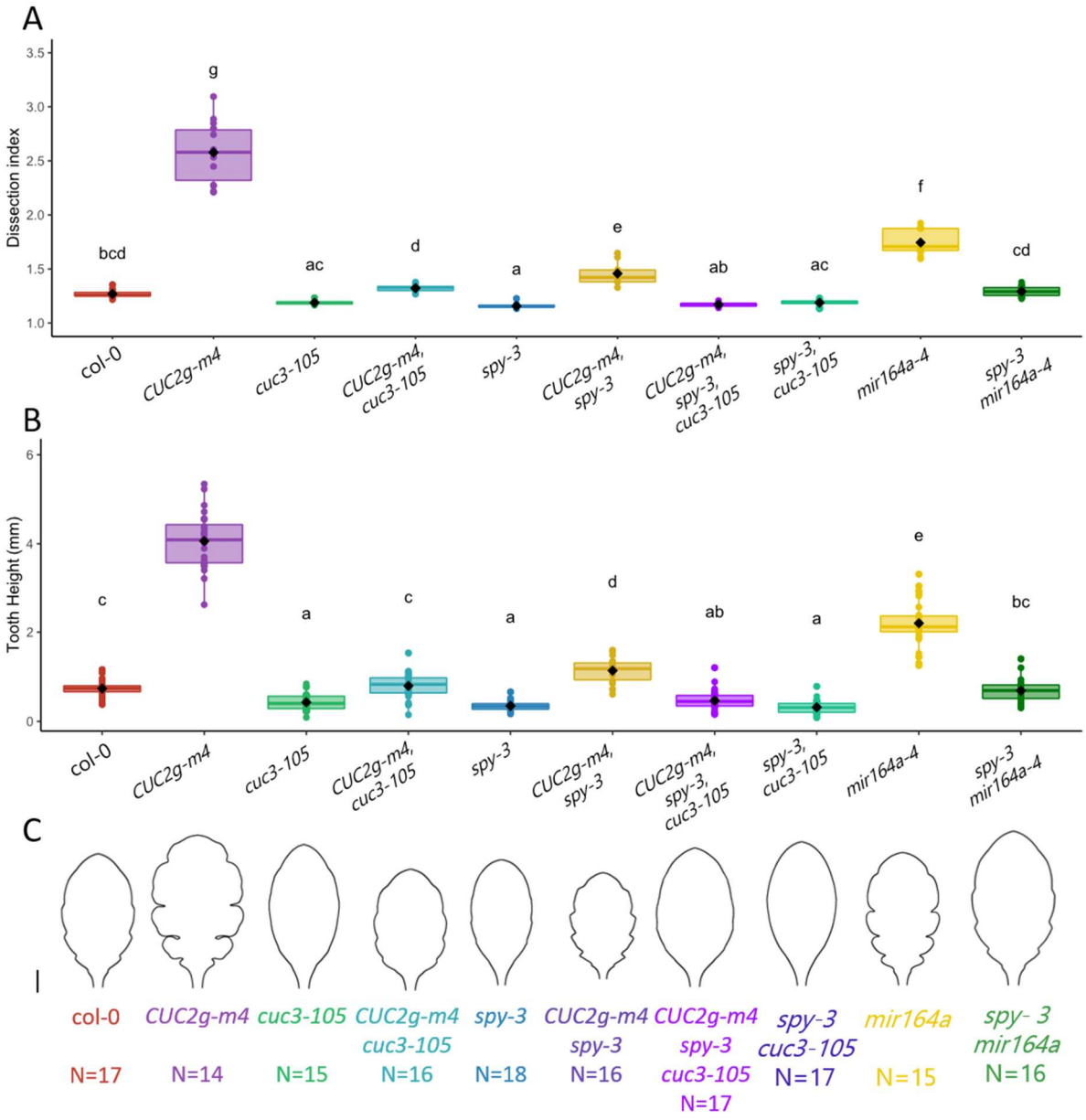

FIGURE 1-16: Morphometric characterization of mature leaf shape to evaluate the interaction between *spy-3, CUC2g-m4, mir164a* and *cuc3-105.*

A. alpha-hull normalized dissection index of col-0 (N=17), *CUC2g-m4* (N=14), *cuc3-105* (N=15), *CUC2g-m4 cuc3-105* (N=16), *spy-3* (N=18), *CUC2g-m4 spy-3* (N=16), *CUC2g-m4 spy-3 cuc3-105* (N=17), *spy-3 cuc3-105* (N=17), *mir164a* (N=15) and *spy-3 mir164a* (N=16) mature leaves of rank 11-12-13. B. Height in mm of the second tooth. C. Mean shape of mature leaves L11-12-13. Scale bar is 1 cm. A,B,C: mature leaves of rank 11-12-13 were collected from plants grown under short-day conditions for 6 weeks. Data and averaged shapes were generated on Morpholeaf software (Biot et al., 2016).

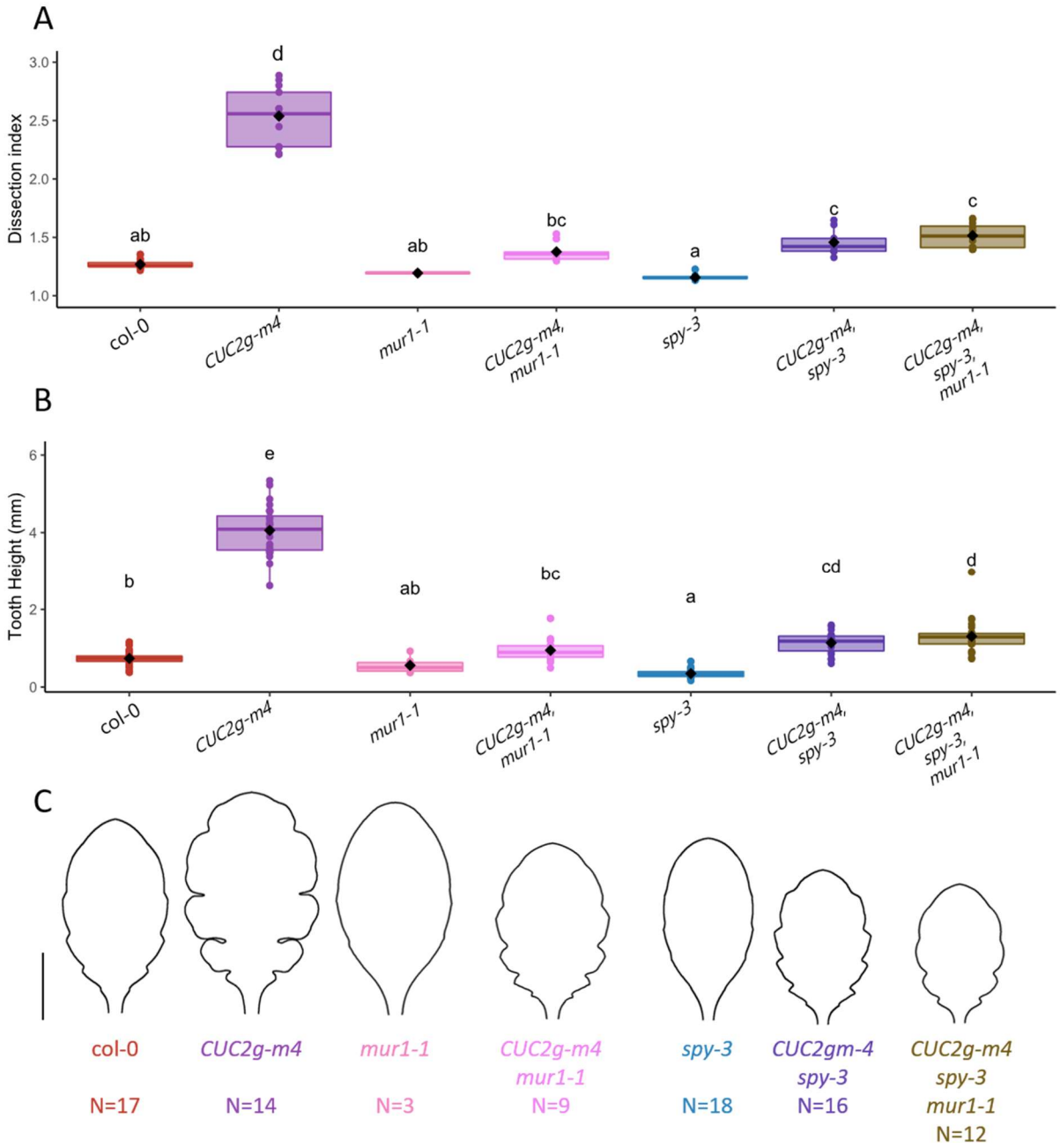

FIGURE 1-17: Morphometric characterization of mature leaf shape to evaluate the interaction between *spy-3, CUC2g-m4* and *mur1-1*

A. alpha-hull normalized dissection index of col-0 (N=17), *CUC2g-m4* (N=14), *mur1-1* (N=3), *CUC2g-m4 mur1-1* (N=9), *spy-3* (N=18), *CUC2g-m4 spy-3* (N=16) and *CUC2g-m4 spy-3 mur1-1* (N=12) mature leaves of rank 11-12-13. B. Height in mm of the second tooth. C. Mean shape of mature leaves L11-12-13. Scale bar is 1 cm. A,B,C: mature leaves of rank 11-12-13 were collected from plants grown under short-day conditions for 6 weeks. Data and averaged shapes were generated on Morpholeaf software (Biot et al., 2016).

for teeth within [150-250] µm and [250-500] µm intervals, sinuses of *spy-3* mutant leaves are constituted of larger cells than wild-type cells (Figure 1-14). Very large cells can indeed be observed on the heatmaps of older teeth from *spy-3* (Figure 1-14). On the contrary, cell growth seems to be slower in sinuses, which is consistent with previous analysis on cell sizes in leaves (Kierzkowski et al., 2019; Serra and Perrot-Rechenmann, 2020). Our data show that SPY is required to maintain restricted sinus cell growth at late stages of tooth development. Interestingly, large cells at the sinus were also reported in the *cuc3-105* loss-of-function mutant due to local release of cell growth (Serra and Perrot-Rechenmann, 2020). Thus, *spy-3* and *cuc3-105* mutants display very similar sinus cell phenotypes, which suggests that *SPY* and *CUC* transcription factors may function through a common pathway to coordinate growth restriction of sinus cells.

SPINDLY interacts genetically with CUC2

At multiple scales, our in-depth characterization of *spy-3* mutant leaf shape phenotypes revealed similarities with *cuc* transcription factors mutants. Indeed, *spy-3* displays smooth margins as previously described for *cuc* mutants (Nikovics et al., 2006), and phenocopies the cellular phenotype observed recently in the sinuses of the *cuc3-105* mutant (Serra and Perrot-Rechenmann, 2020). As *spy-3* and *cuc3-105* exhibit very similar phenotypes both at the organ scale and at the cellular scale, we hypothesized that SPY is involved in the same pathway as CUCs to control boundary cell growth in sinuses.

Since leaf serration directly reflects CUC2 levels (Nikovics et al., 2006), we tested whether *spy* mutation can impinge upon over-serrated leaf phenotypes from the *mir164a-4* line. Indeed, MIR164 regulated leaf shape through the post-transcriptional regulation of CUC2 mRNA levels (Laufs et al., 2004; Nikovics et al., 2006). To do so, mature leaf phenotypes were investigated in *spy-3 mir164a-4* and *spy-22 mir164a-4* double mutants. An α-hull normalization of DI yielded that *mir164a-4* leaves exhibit a higher level of dissection ($DI_{mir164a-4}$=1.74±0.11 compared to wild type DI_{col-0}= 1.27±0.03), confirming previously reported data (Nikovics et al., 2006). Similarly, the second tooth is much higher in *mir164a-4* than in the wild type. In the *spy-3 mir164a-4* double mutant, both DI ($DI_{spy-3\ mir164a-4}$= 1.29±0.05) and the second tooth height are decreased compared to *mir164a-4*, meaning that *spy-3* mutation is sufficient to reduce *mir164a-4* over-dissected phenotype. The *spy-22 mir164a-4* double mutant confirms this result as both DI ($DI_{spy-22\ mir164a-4}$= 1.39±0.07) and the second tooth height are decreased compared to *mir164a-4*. However, it is possible that this result is biased by the other up-regulated genes in a *mir164a-4* mutant, as it

was shown several genes are upregulated (*i.e. CUC1*, *CUC2, NAC1*, *At5g07680*, *At5g39610*, and *At5g61430* (Nikovics et al., 2006)).

In order to investigate whether CUC3 and SPY belong to the same pathway, we performed an analysis on *spy-3 cuc3-105* and *spy-22 cuc3-105* double mutant mature leaf shape (Figure 1-15). *spy-22 cuc3-105* exhibited a DI similar to that of *spy-22* but lower than *cuc3-105* ($DI_{spy\text{-}22\ cuc3\text{-}105}$ = 1.14±0.02; $DI_{spy\text{-}22}$ = 1.15±0.02; $DI_{cuc3\text{-}105}$ = 1.19± 0.02). Conversely, *spy-3 cuc3-105* leaf DI was similar to that of *cuc3-105* and higher than *spy-3* ($DI_{spy\text{-}3\ cuc3\text{-}105}$ = 1.19±0.03; $DI_{spy\text{-}3}$ = 1.16±0.02). These results are quite contradictory with one another, which can be explained by the fact that leaves are extremely smooth in those mutants as it can be seen on averaged shapes (Figure 1-15). Hence, using DI as a tool is not conclusive with those mutants. Second tooth height is not an ideal tool either to decipher whether SPY and CUC3 act in the same pathway, as *spy-22 cuc3-105* is not different from either single mutants ($H_{cuc3\text{-}105}$ = 0.43±0.18 mm, $H_{spy\text{-}22}$ = 0.31±0.12 mm, $H_{spy\text{-}22\ cuc3\text{-}105}$= 0.38±0.16 mm) while *spy-3 cuc3-105* exhibits lower second teeth than *cuc3-105* but not than *spy-3* ($H_{spy\text{-}3}$ = 0.35±0.10 mm, $H_{spy\text{-}3\ cuc3\text{-}105}$= 0.32±0.15 mm). This is probably due to the fact that both single mutants are very smooth already, so it is not possible to form even lower teeth. To overcome this issue, we proposed to perform the experiment in a *CUC2g-m4* over-dissected background.

We first analyzed the leaf morphology of a *spy-3 CUC2g-m4* line. The *CUC2g-m4* line, expresses a mutated version of CUC2, in which the miR164-targeted site involved in CUC2 mRNA degradation is modified and made resistant to degradation, thus triggering a local over-expression of CUC2 (Nikovics et al., 2006). Accordingly, as leaf serration level heavily depends on CUC2 protein levels, *CUC2g-m4* displays very serrated leaves ($DI_{CUC2g\text{-}m4}$=2.58±0.28) with very high second teeth ($H_{CUC2g\text{-}m4}$ =4.06±0.62mm, Figure 1-16) (Nikovics et al., 2006; Maugarny-Calès et al., 2019). Previous studies that established that CUC3 acts as a local functional relay for CUC2 showed that *cuc3-105* partially suppresses the *CUC2g-m4* over-dissected leaf phenotype (Hasson et al., 2011; Maugarny-Calès et al., 2019). This result was once again confirmed in those growth conditions and with αhull DI normalization, since *CUC2g-m4 cuc3-105* exhibited a reduced DI and lower second teeth than *CUC2g-m4* ($DI_{CUC2g\text{-}m4\ cuc3\text{-}105}$= 1.32±0.03, $H_{CUC2g\text{-}m4\ cuc3\text{-}105}$=0.80±0.27mm). Similarly, *spy-3* mutant partially suppressed *CUC2g-m4* phenotype both in term of dissection and second tooth height ($DI_{CUC2g\text{-}m4\ spy\text{-}3}$= 1.46±0.11, $H_{CUC2g\text{-}m4\ spy\text{-}3}$=1.14±0.29mm). In addition, *spy*-3 mutation was also able to lower the *mir164a* over-dissected phenotype down DI ($DI_{spy\text{-}3\ mir164a\text{-}4}$=

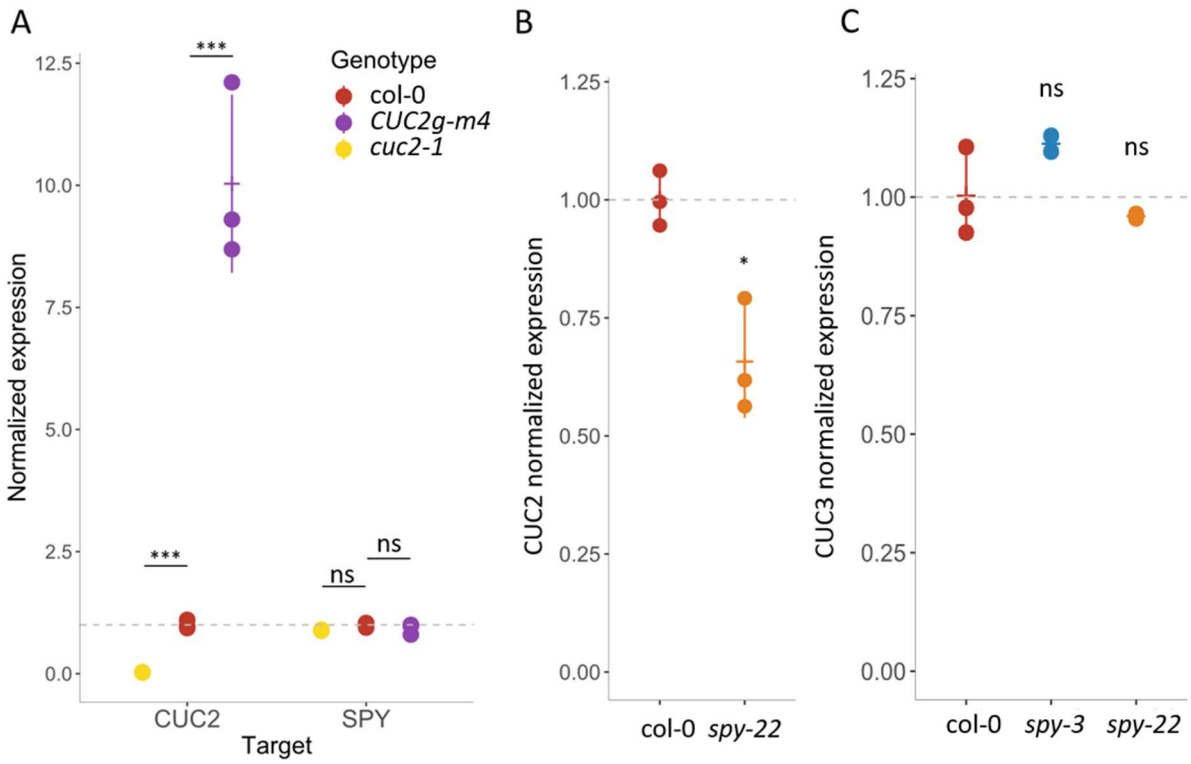

FIGURE 1-18: CUC2, CUC3 and SPY expression levels in various mutant contexts

A. Real-time RT-PCR quantification on CUC2 and SPY transcript level in *cuc2-1* null mutant, col-0 and *CUC2g-m4*. *CUC2* and *SPY* transcript levels were normalized by *EF1α* and *Actin2*. B. Real-time RT-PCR quantification on CUC2 in col-0 and *spy*-22. *CUC2* transcript levels were normalized by *EF1α, qREF* and *Actin2*. C. Real-time RT-PCR quantification on CUC3 in col-0, *spy-3* and *spy*-22. *CUC3* transcript levels were normalized by *EF1α, qREF* and *Actin2*. A,B,C. Each dot represents a biological RNA. Statistical significance (Student's test) is designated by ns=not significant, * $p<0.05$, *** $p<0.001$.

1.29±0.05, $H_{spy\text{-}3\ mir164a\text{-}4}$= 0.69±0.23 mm) This would tend to support the idea that *spy-3* impinges upon CUC2 effect on serration the same way that *cuc3-105* does. However, the averaged shapes of the two double mutants seem to differ as teeth look sharper in *CUC2g-m4 spy-3*, indicating both smoother mutant affect serration differently. Please note that *CUC2g-m4 spy-3* exhibited smaller leaves in that particular experiment due to germination issues and not as a reproductible phenotype. This experiment has been reproduced for these particular genotypes leading to the same conclusions, but are not represented here as it does not encompass the full set of genotypes described in Figure 1-16. In addition, the triple mutant yielded a DI and a second tooth height both significantly lower than the two double mutants, indicating *spy-3* effects on leaf serration are additive with those of *cuc3-105* ($DI_{CUC2g\text{-}m4\ spy\text{-}3\ cuc3\text{-}105}$= 1.17±0.02, $H_{CUC2g\text{-}m4\ spy\text{-}3\ cuc3\text{-}105}$=0.46±0.21mm). It seems that the combination of both *spy-3* and *cuc3-105* completely suppressed *CUC2g-m4* phenotype, as DI is comparable between the double and the triple mutant.

Taken together, our data suggest either that SPY and CUC3 have additive, independent effects on serration development, or that both belong to the CUC2 downstream pathway. To test the latter hypothesis, we measured *SPY* transcript levels in lines exhibiting different levels of CUC2 by real time RT-PCR. While CUC2 transcript levels varied from ten times lower in the *cuc2-1* null mutant to ten times higher in *CUC2g-m4* than the wild type, *SPY* transcript levels remained unaffected in all three genetic backgrounds (Figure 1-18A). This shows that SPY expression is not modulated by CUC2 levels in plants, suggesting that SPY does not act downstream of CUC2. Curiously, we obtained a subtle decrease in *CUC2* transcript level in the *spy-22* background (Figure 1-18B). Conversely, expression data in other *spy* mutants were not significant (data not shown). *CUC3* transcript levels was also quantified in two *spy* mutants (Figure 1-18C). Neither *spy-3* nor *spy-22* displayed an altered *CUC3* expression.

SPINDLY could act downstream of MUR to trigger serration formation

Since the role of GDP-L-fucose for leaf serration was demonstrated (Gonçalves et al., 2017), we aim at understanding the molecular processes that involve GDP-L-fucose to form teeth at the leaf margin. Our current hypothesis is that SPY, which is an O-fucosyltransferase, uses the GDP-L-fucose synthesized by MUR1 and modify other proteins to trigger serration formation. To do so, we propose to observe the leaf phenotype of a *spy-3 mur1-1* double mutant. However,

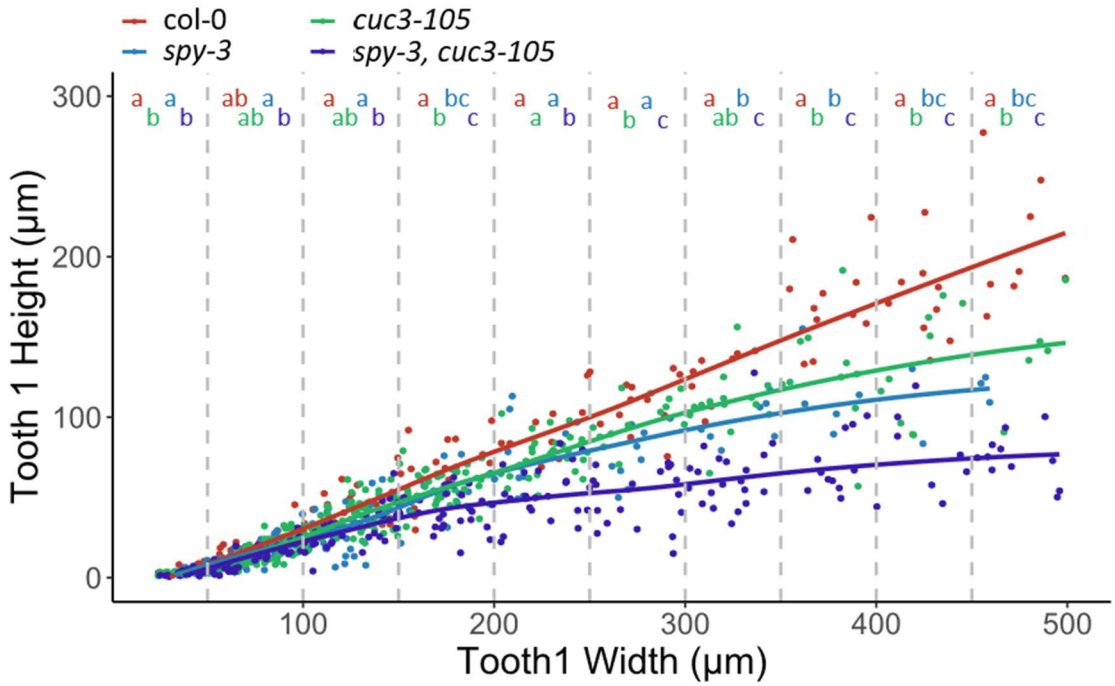

FIGURE 1-19: Interaction of *spy-3* and *cuc3-105* during first tooth shape development. First tooth height in µm from col-0 (N=190), *spy-3* (N=194), *cuc3-105* (N=213), *spy-3 cuc3-105* (N=191) plotted against 50µm-wide first tooth width classes. SD-grown plants from DAS 22 to 50 were used. Statistical analysis: one-way ANOVA analysis were performed within each class, followed by Tukey comparison test.

since both single mutants are very smooth, the quantification was performed in a *CUC2g-m4* over-dissected background (Figure 1-17). Even if quantification of the dissection index and second tooth height are not sufficient to yield significance between genotypes, *mur1-1* leaves clearly appear smoother than the wild type leaves, as reported previously (Gonçalves et al., 2017). Please note that very few data were available for *mur1-1* genotype due to germination issues, but the few data we obtained was coherent compared to previous quantifications on this mutant. We retrieved a decreased dissection index and tooth height in a *CUC2g-m4 mur1-1* line compared to *CUC2g-m4* ($DI_{CUC2g\text{-}m4\ mur1\text{-}1}$= 1.38±0.08, $H_{CUC2g\text{-}m4\ mur1\text{-}1}$=0.95±0.29mm), in accordance to previously published data (Gonçalves et al., 2017). In the *CUC2g-m4 spy-3 mur1-1* line, dissection index was not significantly different to that of *CUC2g-m4 spy-3* ($DI_{CUC2g\text{-}m4\ spy\text{-}3\ mur1\text{-}1}$= 1.52±0.10), nor was the second tooth height ($H_{CUC2g\text{-}m4\ spy\text{-}3\ mur1\text{-}1}$=1.30±0.45mm). The fact that the *mur1-1* mutation does not further suppress *CUC2g-m4 spy-3* phenotype suggests that MUR1 and SPY belong to the same pathway. This is coherent with SPY using the GDP-L-fucose that is synthesized by MUR1.

Taken together, our data show that *spy-3* and *mur1-1* phenotypes are not additive concerning DI and second tooth height in a *CUC2g-m4* background. Hence, we suggest that SPY uses the fucose that is biosynthesized by MUR1 to modify other proteins that consecutively lead to serration formation promotion.

SPINDLY acts redundantly with CUC2 and CUC3 to define boundaries

In order to test whether SPY and CUC3 have independent effects on leaf serration, we performed a leaf developmental trajectory on a double *spy-3 cuc3-105* mutant (Figure 1-19). Since previous results demonstrated CUC3 maintains cell growth repression in sinus cells locally, we chose to use the first tooth height as a proxy for CUC3 activity (Hasson et al., 2011).

Strikingly, when tooth height of T1 was measured for different tooth width classes, *cuc3-105* and *spy-3* displayed comparable quantitative phenotypes in almost all classes (within [50-250] µm and [300-500] µm intervals of T1 width) while the combination of the two mutations had additive effects on T1 height. The double *spy-3 cuc3-105* had significantly smaller T1 than *cuc3-105* from 150-200 µm-wide T1. In addition, *spy-3 cuc3-105* displayed significantly smaller teeth than *spy-3* within [0-150] µm and [200-400] µm intervals. The wild type was significantly different from all the other genotypes within [150-200] µm and then from 350 µm (Figure 1-19). This can be

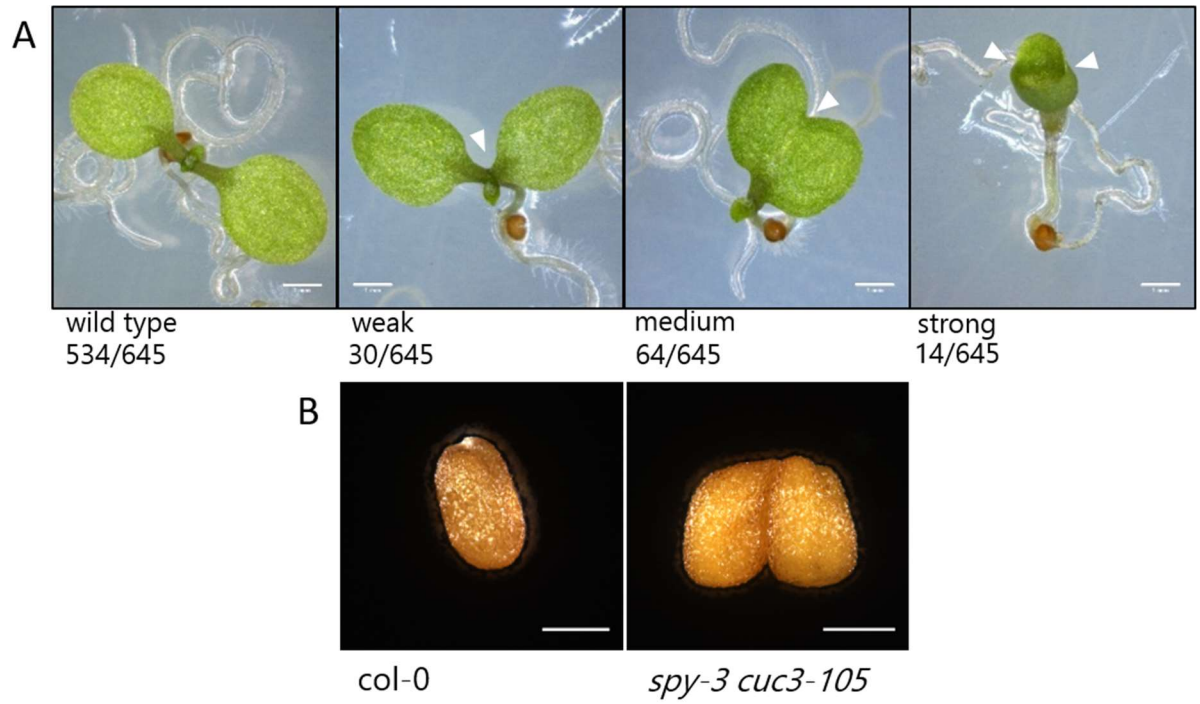

FIGURE 1-20: Fusion defects observed in the *spy-3 cuc3-105* double mutant line in different developmental contexts.

A. Fusion phenotypes observed in 6 days-old *spy-3 cuc3-105* seedlings *in vitro*. Wild type phenotype corresponds to symmetrically opposed cotyledons. Weak phenotype corresponds to seedlings in which cotyledons are oriented towards an angle due to partial fusion of their petioles. Medium phenotype is for heart-shaped cotyledons. Strong phenotype is for cup-shaped cotyledons. B. seed fusion phenotypes occasionally observed in *spy-3 cuc3-105.*

Genotype	Phenotype				total seedling
	wild type (%)	weak (%)	mild (%)	strong (%)	number
col	99,37	0	0,63	0	315
cuc3-105	99,52	0	0	0,48	631
spy-3	100	0	0	0	317
spy-3 cuc3-105	82,79	4,66	10,39	2,17	645
cuc2-1	100	0	0	0	320
spy-3 cuc2-1	82,57	6,59	10,52	0,31	637

TABLE 1-01: Fusion defects quantification in seedlings cotyledons to evaluate the interaction between *spy-3, cuc2-1* and *cuc3-105.*

explained by the large heterogeneity that can be found within leaves of plants grown in similar conditions (Maugarny-Calès and Laufs, 2018). Even if the ANOVA analysis did no yield statistical significance in each and every classes thorough the kinetics, qualitative assessments – *i.e.* the general shape of the curves throughout the chosen developmental window - always put the double mutant T1 height dynamic smaller than the three other tested genotypes.

Taken together, our data suggest that SPY and CUC3 have additive effects on tooth height and DI both in early stages of leaf development and in mature leaves. In other words, a SPY-dependent pathway seems to be able to restrict growth at the sinus independently from CUC3. As both CUC2 and CUC3 act to control serration development, and since CUC3 acts as a local relay for CUC2 (Maugarny-Calès et al., 2019), one possibility is that SPY could be involved in a novel CUC2-dependent pathway to act in serration establishment.

No developmental trajectory was performed on a *spy-3 cuc2-1* double mutant as CUC2 is necessary for serration establishment (*cuc2-1* does not initiate any teeth) (Nikovics et al., 2006). In order to analyze the relative contribution of SPY, CUC2 and CUC3 to boundary cell growth, we then decided to analyze their roles during cotyledon and ovule separation rather than during leaf development (Figure 1-20). Both double mutant *spy-3 cuc3-105* and *spy-3 cuc2-1* displayed stronger cotyledon fusion phenotypes compared with the corresponding simple mutants and the wild type, since the total number of fusion defects (partial petiole fusion, heart-shaped and cup-shaped cotyledons) increased in those double mutants (total of 108/645 for *spy-3 cuc3-105* and 111/645 for *spy-3 cuc2-1*) (Table 1-01). This result shows that SPY acts redundantly with CUC2 and CUC3 to define boundaries.

SPY is therefore enhancing both *cuc2* and *cuc3* cotyledon fusion defects. This data suggest that CUC2 *per se* could act directly on serration growth maintenance in addition to its well-documented role on serration initiation (Nikovics et al., 2006). Furthermore, these data also show that SPY controls the development of boundary domains in different developmental contexts. This reinforced our previous observations suggesting that global growth regimes of the leaf are not sufficient to explain the leaf margins defects we observed in *spy* mutants.

DISCUSSION

Over this in-depth characterization of *spy* mutants, especially *spy-3*, we demonstrated that *spy-3* smooth, mature leaves are the result of developmental defects on tooth growth throughout leaf development. Indeed, comparison of the wild type with *spy-3* yielded to differences in both tooth position and developmental dynamics. As we found giant cells in the first sinus of *spy-3* mutant, we assume that SPY is involved in sinus cell growth repression, similarly to CUC3 (Serra and Perrot-Rechenmann, 2020). However, both mature leaf phenotypes of double and triple mutants, and the double *cuc3-105 spy-3* developmental trajectories indicate SPY acts independently from CUC3. Since *spy-3* worsened CUC2 and CUC3 fusion defects in other developmental contexts, we suggest that multiple routes exist to trigger boundary establishment and tooth development. Our data even suggest that CUC2 could have growth-repressing activities independently of CUC3.

SPINDLY has a minor role in the control of overall leaf shape

In the mean contours description, we pointed out earlier that the tooth position and rate of teeth apparition are altered in the *spy-3* mutant. We suggest spy-3 initiates teeth at a faster rate and/or that it starts initiating teeth earlier in the development.

A possible explanation for this is that the leaf differentiation front is altered in *spy-3*. As seen in the introduction, SPY is a major repressor of GA signaling (Jacobsen et al., 1996; Swain et al., 2001). Moreover, GA is involved in the proliferation/differentiation switch that occurs during leaf development. In *Arabidopsis*, DELLAs were shown to increase the transcript levels of *Kip-related protein 2 (KRP2)*, *SIAMESE (SIM)* and *SIM Related 1* and *2 (SMR1 and SMR2)*, which are all involved in cell cycle progression inhibition (Achard et al., 2009). As SPY was shown to activate RGA (Zentella et al., 2017), we can hypothesize that in *spy-3* mutant cell cycle progression is less repressed, triggering a faster proliferation to differentiation switch during of the leaf. In addition, in a *GA20ox1* overexpressing line, in which bioactive GA levels are very high, a larger leaves phenotype was reported and linked to more and larger cells (Gonzalez et al., 2010). This result suggest that GA levels control both cell expansion and cell proliferation in leaves, and could explain the tooth position phenotype we reported in *spy-3* (Achard et al., 2009).

Former studies pointed out that SPY has also a role in CK signaling promotion (Greenboim-Wainberg et al., 2005; Gan et al., 2007; Steiner et al., 2012). Yet, it was shown that CK

promote cell proliferation and that reduced CK levels lead to a decrease in cell divisions and consequently to smaller organs (Holst et al., 2011). Moreover, a recent study revealed that a CK/GA balance is responsible for leaf complexity in tomato as it controls morphogenesis/differentiation switch (Israeli et al., 2020). Hence, it is also possible that CK signaling is partially impaired in the *spy-3* mutant and as a consequence modifies the serration growth dynamics.

The independent effect of *spy-3* and *cuc3-105*

The leaf developmental kinetics of the double *cuc3-105 spy-3* mutant led us to note that CUC3 and SPY have additive effects on serration development. The mature leaf phenotype of the triple *CUC2g-m4 cuc3-105 spy-3* supports the same conclusion as *cuc3-105* and *spy-3* have additive effects at decreasing leaf over dissection that is normally observed in the *CUC2g-m4* line.

As smooth phenotypes are more complicate to qualitatively and quantitatively estimate, performing an experiment in an over-dissected leaves phenotype context gave us better chances to achieve quantitative measurements. In addition, as both *cuc3-105* and *spy-3* mutants display very smooth mature leaves already, the additivity effect would not have been visible. Indeed, it is not possible to get even smoother than already smooth. This is particularly true in the measure of mature leaves DI of the *spy-3 cuc-105* and *spy-22 cuc3-105* double mutants, in which data did not allow us to form hypotheses over the relation between SPY and CUC3.

Previous data indicate that CUC2 targets CUC3 in sinuses to trigger tooth growth along leaf development (Hasson et al., 2011; Maugarny-Calès et al., 2019). However, the mature leaf phenotype of the double *CUC2g-m4 cuc3-105* is more dissected than the *cuc3-105* mutant, and since *cuc3-105* is likely to be null (Hasson et al., 2011), it was suggested that another route must be responsible for serration development. This route would trigger serration independently from CUC3, since CUC3 alone cannot entirely suppress CUC2g-m4 phenotype. CUC3 was shown to trigger cell extension repression in sinuses (Serra and Perrot-Rechenmann, 2020). Yet, as CUC2 holds a dual effect at promoting growth at distance and repressing growth locally (Nikovics et al., 2006; Biot et al., 2016), we can suggest that CUC3 is predominantly involved in the latter effect of CUC2. Thus, in a *CUC2g-m4 cuc3-105* double mutant, slight teeth would emerge as the result of a remote growth promotion by CUC2 without CUC3-triggered cell repression in sinuses. Since SPY appears to be involved in a process independent of CUC3, and since SPY is expressed throughout the leaf margin in contrast to CUC3 (Swain et al., 2002), it can be assumed that SPY-

related promotion of growth is mediated by CUC3-independent pathways. The fact that teeth in the *CUC2g-m4 spy-3* double mutant have a very different shape than those of *CUC2g-m4 cuc3-105* is consistent with this. However, the fact that the cells are significantly larger in the sinuses of *spy-3* means that SPY is probably also involved in growth repression. In view of these assumptions, it is possible to suggest that SPY is a sinus cell growth repressor which acts independently of CUC TFs. Transcriptomic analysis performed with *spy-3* mutant identified genes that were differentially expressed in the mutant when compared to the WT control line (Qin et al., 2011). The content of *spy-3* up-regulated genes will be studied and compared to CUC2 in the following chapter, to investigate their role in cell extension repression.

Finally, as the triple *CUC2g-m4 cuc3-105 spy-3* managed to completely smooth the leaf margin in a *CUC2g-m4* over-dissected background, we can hypothesize that SPY and CUCs are two indispensable components of tooth formation in *Arabidopsis*.

The interest of a *spy-3 cuc2-1* cuc3-*105* line

The quantification of fusion defects in doubles *spy-3 cuc3-105* and *spy-3 cuc2-1* helped showing that the *spy-3* mutation worsens the cotyledon fusion phenotypes that can be observed in both *cuc3-105* and *cuc2-1* single mutants (Hibara et al., 2006). In order to determine whether SPY acts in the same pathway as CUC2 and CUC3, we planned on quantifying fusion defects in the triple *spy-3 cuc2-1 cuc3-105* mutant.

If the triple mutant had exhibited as many fusion defects as in a double *cuc2-1 cuc3-105*, we would have proposed that SPY acts to define boundary domains within the CUC2/CUC3 pathways. Then, CUC2 and CUC3 would have been part of the same pathway. Since we demonstrated that SPY and CUC3 act independently to repress growth in sinuses, SPY would be part of a new growth control pathway downstream of CUC2. However, this is not consistent with the fact that *SPY* transcript levels are not modified upon CUC2 level variations (Figure 1-18). On the other hand, if *spy-3* and *cuc2-1 cuc3-105* have had additive effect on fusion defects, it would suggest that SPY activity on growth repression is additive and independent to that of CUC2/3. Thus, SPY would constitute a novel CUC2-independent pathway for cell growth control.

However, we did not manage to produce that triple mutant as it seems that it fails to maintain a meristematic activity post germination. The fact that the combination of these three mutations is lethal in the seedling stage has not been yet demonstrated experimentally. To do so,

one would have to quantify the lethality rate in the progeny of a *cuc2-1* heterozygous, *spy-3 cuc3-105* homozygote and compare it to the lethality rate of the progeny of a *cuc2-1+/- cuc3-105-/-* (the same quantification would be repeated by interverting the *cuc* mutant alleles). In the next population, we would have 25% *cuc2-1-/- cuc3-105-/-*, 25% *cuc3-105-/- cuc2-1+/+* and 50% *cuc3-105 -/- cuc2-1+/-* with or without the *spy-3-/-* allele. If the triple mutant indeed is lethal, one would expect at least 25% more of seedling lethality from the *spy-3-/- cuc2-1+/-cuc3-105-/-* progeny. This experiment is under preparation and will be performed shortly, as the sesqui-mutant lines *cuc3-105+/- cuc2-1-/-* and *cuc3-105-/- cuc2-1+/-* have not been produced yet. Another potential solution to this would be to use the *cuc2-3* allele instead of *cuc2-1*, since it is a weaker allele in which low *CUC2* expression is still observed (Hasson et al., 2011). It is then possible that a triple *spy-3 cuc2-3 cuc3-105* will be able to grow and produce progeny.

Hypotheses towards SPY mode of action.

In our experiments, we show that the *mur1-1* mutation does not intensify the effect on *spy-3* mutation on highly serrated *CUC2g-m4* leaves. This result suggests that MUR1 and SPY act in a joint pathway, hence that the GDP-L-fucose that is synthesized by MUR1 is used by SPY which transfers it onto other proteins to modulate its stability/activity. Indeed, SPY was demonstrated to be an O-fucosyltranferase *in vitro* only recently, that modifies RGA and RGL1 in the nucleus (Zentella et al., 2017). Interestingly, the POFUT activity of SPY was demonstrated using a 3-TPR truncated form of the protein, which indicates only that part of the protein is necessary to its catalytic activity. Indeed, the first TPRs were shown to be necessary to GA-related functions of SPY (Silverstone et al., 2007). Strikingly, no protein-protein interaction was detailed so far between SPY and RGA in the literature. Yet, a mapping of the interaction domains of RGA and SEC was performed using Y2H assays and demonstrated that the N-term half of SEC is involved in the protein-protein interaction (Zentella et al., 2016). Considering SEC as the paralog of SPY, one can suppose that SPY would also interact with RGA on its TRP domains. Moreover, the interaction of SPY was very demonstrated with PRR5, more precisely on its TPR domains (Wang et al., 2019). This suggest that SPY indeed interacts with other proteins thanks to its N-term part. Interestingly, the chromatin remodeling factor SWI3C was shown to interact with both DELLA and SPY in the nucleus (Sarnowska et al., 2013). Since no interactions were demonstrated so far *in vivo* for SPY and DELLA, we can imagine SPY-involving complexes can be formed in the nucleus.

In cells, SPY protein is present both in the nucleus and the cytosol (Swain et al., 2002). Interestingly, the specific subcellular localization of the protein seems to trigger distinctive pathways. For example, nuclear-localized SPY interacts with PRR5 to control circadian clock (Wang et al., 2019). Moreover, SPY could act in the cytosol to repress GA signaling, as a *35S::GFP-SPY-NES* (NES= Nucleus Excluding Signal) construct manages to restore paclobutrazol response in a *spy-3* mutant (Maymon et al., 2009). However, the fucosylation of RGA by SPY is thought to happen in the nucleus (Zentella et al., 2017), which indicates that the physiological roles of SPY are still poorly understood in regards to its localization. A *35S::GFP-SPY-NES* managed to restore serrations at the leaf margin in a *spy-3* mutant while a *35S::GFP-SPY-NLS* did not, which demonstrates that SPY role towards tooth growth lies in the cytosol (Maymon et al., 2009). Hence, if CUC2 and SPY independently trigger the activation of shared targets, SPY must interact in the cytosol with an as-yet-unknown actor that acts as a relay between the cytosol and the nucleus.

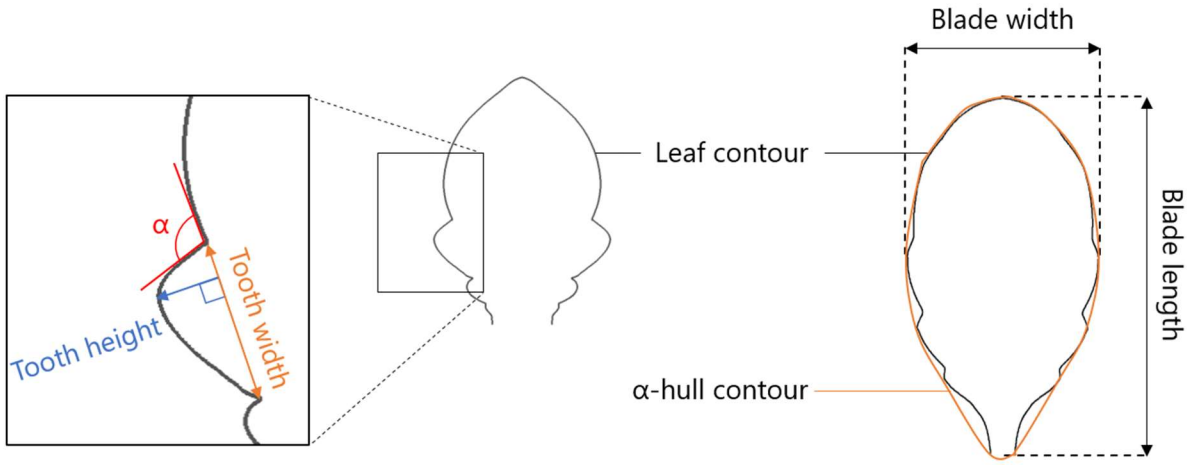

FIGURE 1-21: Morphometric characterization of leaf parameters.

Definition of tooth height and width, sinus angle (α), blade length and width measurements used in this manuscript. The α-hull contour is a linearized convex envelop that results from the closure of the union of all possible segments between the existing points of the input contour.

MATERIALS AND METHODS

Plant material and growth conditions

All plants used in this study were in the Columbia (Col-0) background except the *cuc2-1* mutant which was originally obtained in the Landsberg (Ler-0) background and back-crossed 5 times to Col-0 (Hasson et al., 2011). The *cuc2-3* and *cuc3-105* mutants lines were previously described (Hibara et al., 2006), as well as *mir164a-4* (Nikovics et al., 2006). *T*he transgenic line *CUC2g-m4* (Nikovics et al., 2006) was also previously described. The *spy-3* (CS6268 (Jacobsen and Olszewski, 1993)) mutant line was provided by Utpal Nath (Indian Institute of Science Bangalore). Doris Lucyshyn (BOKU, Vienna, Austria) provided *spy-22* (SALK09058 (Mutanwad et al., 2020)) and *spy-23* (WiscDsLox241C03) mutants, as well as the pSPY::SPY-FLAG *spy-22* and the pSPY::SPY-GFP lines.

For morphometric analysis, seeds were immersed in distilled water for two days in the dark at 4°C before sowing on soil. Then plants were grown under short days (SD) conditions (6 hours day [21°C, hygrometry 65%, light 120 µM/m^2/s], 1-hour dusk [21°C, hygrometry 65%, light 80 µM/m^2/s], 16 hours night [18°C, hygrometry 65%, dark conditions], 1-hour dawn [19°C, hygrometry 65%, light 80 µM/m^2/s]. For in vitro cultures, seeds were sown on Arabidopsis medium (Gonçalves et al., 2017), stratified for 48 hours in the dark at 4°C then transferred to long day conditions (21°C, 16 hours day / 8 hours night, light 50µM/m^2/s).

Expression data

15-day-old seedlings grown in LD conditions on plates were pulled in 1.5 mL ependorf tubes up to 100µm of total mass and instantly immersed in liquid nitrogen. Total RNAs were isolated using RNAeasy Plant Mini Kit (Qiagen) following the manufacturer recommendation for plant tissue. Reverse transcription was performed using RevertAid H Minus M-MuLV Reverse transcriptase (Fermentas) followed by a RNAse H treatment was performed for 20 min 37°C to eliminate DNA-RNA duplexes. Real time PCR analysis was performed on a Bio-Rad CFX connect machine using the SsoAdvance Universal SYBR Green Supermix with the following PCR conditions: 95˚C 3min; (95˚C 10s; 63˚C 10s; 72˚C 10s) x45 cycles. Primers used for real time PCR analysis are available in S1 Table. Expression data were normalized using the ΔΔCt method using at least two independent reference genes (qREF and EF1α).

Morphometric Analysis

For morphometric analysis of mature leaves, leaves from rank 11, 12 and 13 from 6-week-old SD-grown plants were harvested and glued on a paper sheet prior to scanning using a Perfection V800 Photo scanner (Epson) at 1600dpi. For morphometric analysis of developing leaves, young leaf primordia (rank 11, 12 and 13) were dissected using a stereomicroscope throughout development starting at day 22 after sowing. Leaves were mounted between a slide and a coverslip in a buffer containing TrisHCL, 10mM, pH = 8.5, Triton 0.01% (v/v) and imaged using an Axio Zoom.V16 microscope (Carl Zeiss Microscopy, Jena, Germany; http://www.zeiss.com/). From around 5mm of total blade length, developing leaves of rank 11-12-13 were treated as mature leaves for morphometric analysis. Depending on the developmental stage imaged, either the chlorophyll fluorescent signal or the brightfield signal were collected. Averaged leaf contours and measurements were obtained using the Morpholeaf software which allows semi-automatic leaf segmentation and the extraction of relevant biological parameters (Biot et al., 2016). Dissection index was calculated as DI = $Perimeter_{blade}^2/Area_{blade}$ and normalized by the α-hull DI. The α-hull DI is directly calculated after the α-hull contour, which is a convex envelop that results from the

closure of all possible segments between the existing points of the input contour (see Figure 1-22). Leaf parameters measured in Morpholeaf and used in this thesis manuscript are explained on figure 1-21. Graphs were plotted using R software. Mature average contour was calculated with a bin-based normalization resampling all positioned landmarks. Averaged contours of developing leaves from col-0 (n=282) and *spy-3* (n=288) were generated using moving average computation normalization method, with twenty neighbor rank (*i.e.* 20 different leaf samples contribute to the construction of each of the average shapes) and user-defined targeted lengths (500µm, 750µm, 1000µm, 2mm, 3mm and 5mm). First tooth angle was manually measured on all samples under 6mm of total blade length using ImageJ software. The main root length was semi-automatically measured on 10-days old seedlings grown in LD conditions on plates using NeuronJ plugin on ImageJ. Leaf silhouettes were generated using a binary filter on FIJI software. Rosettes pictures were acquired with a Pentax K-r camera with standard parameters.

Cell size quantification

For cellular parameters quantification, we used the *pPDF1::mCitrine-KA1* (Stanislas et al., 2018) line in order to visualize the plasma membrane in the leaf epidermis. 26 to 31-day-old Col-0 and *spy-3* plants containing the *pPDF1::mCitrine-KA1* construct were grown under short days conditions prior to dissecting, mounting in a buffer containing TrisHCL, 10mM, pH = 8.5, Triton 0.01% (v/v) and direct imaging with a Leica SP5 inverted microscope (Leica Microsystems, Wetzlar, Germany; http://www.leica-microsystems.com/). Samples were excited using a 514 nm laser and fluorescence was collected with a hybrid detector at between 569 and 611 nm. TIF images were rotated using TransformJ plugin. Maps and cell surface measurements were then obtained using the MorphoGraphX (MGX) software (http://www.mpipz.mpg.de/MorphoGraphX/) following previously described protocols (Barbier de Reuille et al., 2015; Serra and Perrot-Rechenmann, 2020). A [2-6] µm-wide signal projection was used to generate signal surface. Cells corresponding to tooth sinus were identified as the cells displaying a fully negative signal when projecting a 16 µm-neighboring Gaussian curvature of the surface (Serra et al., 2020).

Chapter 2

Towards a better understanding of the molecular and cellular processes that drive CUC2-dependent serration development

INTRODUCTION

In the previous chapter, we performed an extensive phenotypic characterization of *spy-3* to provide a better understanding of SPY involvement in leaf morphogenesis. Our in-depth characterization suggested that *SPY* locally represses cell growth in the sinus similarly to CUC3. Furthermore, the *spy-3* mutation worsens the fusion phenotypes previously described in seedlings of *cuc2-1* and *cuc3-105* mutants. This suggests that SPY -beyond its role during leaf morphogenesis – might be involved in boundary domain definition in various developmental contexts.

The developmental kinetics we performed on *spy-3 cuc3-105* double mutant showed that SPY acts independently from CUC3 to control serration development.. As CUC3 and SPY seem to hold similar roles during development, and since CUC2 acts upstream of CUC3, we investigated how SPY is linked with CUC2 to control growth and establish teeth at the leaf margin. To do so, it is necessary to understand the genetic and molecular events that are involved in the control of tooth formation downstream of CUC2 and SPY. In the following introduction, the current knowledge on the molecular mechanisms triggering tooth growth establishment is presented.

Serration as the result of an auxin/CUC signaling alternate dynamics

Arabidopsis thaliana carries simple, serrated leaves. These serrations or teeth are sequentially formed at the base of the leaf throughout leaf development. In other words, each new pair of teeth that forms is basal to the previous pair. As said in the introduction, at the tissue level, serrations can be assimilated to the repetition of multiple differential growths between teeth, where growth is promoted, and sinuses, where growth is restricted. Hence, each tooth constitutes a new growth axis. Teeth are formed as a result of the repetitive expression of CUC2 and CUC3 transcription factors (Nikovics et al., 2006; Hasson et al., 2011). A Pro_{CUC2}:GUS transcriptional reporter line revealed a regularly spaced expression pattern of CUC2 at the sinuses (Nikovics et al., 2006) from early stage of leaf development. Likewise, a Pro_{CUC3}:GUS transcriptional reporter line determined that CUC3 is also expressed in sinuses (Hasson et al., 2011). The use of DR5 reporter constructs as an auxin response reporter established that auxin signaling is activated both at teeth and at leaf apices (Hay et al., 2006; Bilsborough et al., 2011). In addition, the use of PIN1:GFP fusion protein reporter line indicated that the auxin maxima could be generated by a convergent polarization of PIN1 auxin efflux transporters towards the teeth (Bilsborough et al., 2011) (Figure2-01). Since both *cuc2-1* and *pin1-En134* null mutants fail to initiate teeth (Nikovics et al., 2006; Bilsborough et al., 2011), CUC2 activity and auxin transport both seem to be critical for leaf morphogenesis. In fact, experiments of continuous expression of CUC2 in the epidermis and continuous auxin (2,4-D) treatment along the leaf margin both led to smoother leaves, indicating that the discontinuities of CUC2 expression and auxin signaling are both necessary to form a serration (Bilsborough et al., 2011). In addition, auxin was demonstrated to inhibit CUC2 expression both transcriptionally and through *MIR164a* up-regulation (Bilsborough et al., 2011). Thus, auxin down-regulates *CUC2* locally, participating in serration patterning. Likewise, CUC2 was shown to be necessary to reorient PIN1 polarity towards outgrowing teeth (Bilsborough et al., 2011), which drives auxin maximum responses away from CUC2-expressing domains. Together, these interactions form two feedbacks loops which creates interspersed CUC2 activity and auxin signaling and leads to serration patterning and formation.

CUC2 has a dual role at defining leaf shape

The first visible tooth arises very early after leaf initiation as it is discernable in leaves as small as 100-150µm of total blade length (Biot et al., 2016) (Figure 1-11A). Using a CUC2-inducible

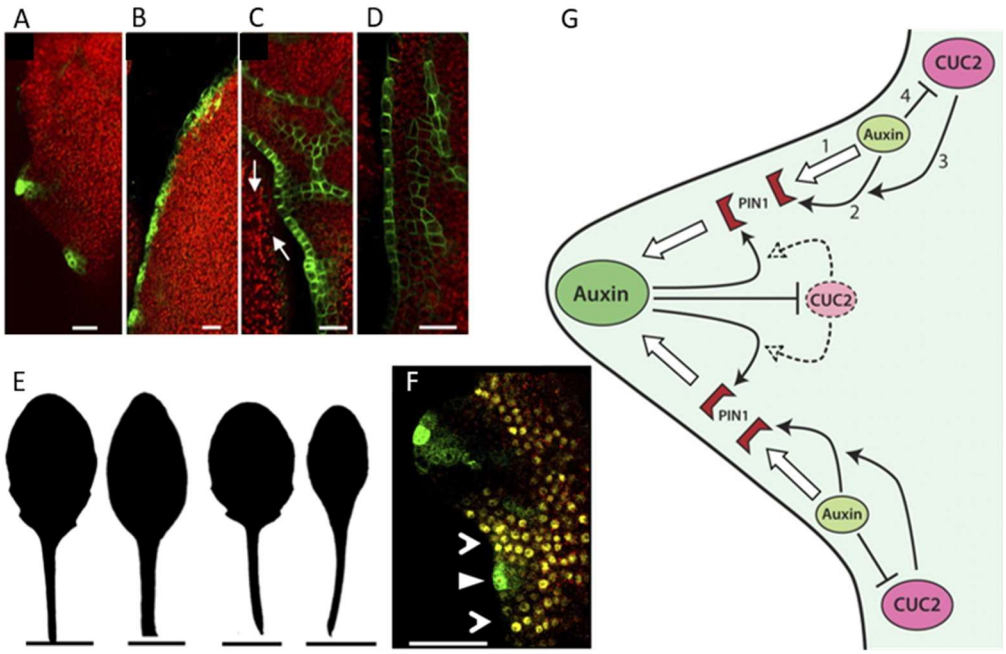

FIGURE 2-01: Serration formation as a result of discontinuous, interspersed CUC2 expression and auxin response maxima.

A-D. Confocal micrographs on *pDR5:GFP* (A,B) and *pPIN1:PIN1-GFP* (C,D) reporter lines in the margin of 500µm-long sixth rosette leaf from wild type plants (A,C) and in *cuc2-3* plants (B,D). Scale bars are 25µm. E. Fifth rosette leaf silhouette of, left to right: col-0, *pAtML1:CUC2:VENUS,* mock-treated col-0 and 10µM 2,4-D-treated col-0. Scale bars are 1 cm. F. Confocal micrograph of *pCUC2:CUC2-VENUS* (empty arrowhead, yellow), *pDR5:GFP* (full arrowhead, green) reporter line on a 130µm-long, fifth leaf. Scale bar is 25µm. G. Model proposed by Bilsborough *et al.* to explain the establishment of interspersed expression of CUC2 and DR5. In that model, auxin inhibits CUC2 locally (4) while CUC2 is involved in the relocalization of PIN1 auxin efflux transporters away from is expression domain (3). Thus, CUC2 and the domain responding to auxin are able to separate in space. All panels are from (Bilsborough et al., 2011).

construct (*CUC2i*) based on ethanol-switch strategy, CUC2 was transiently expressed in *cuc2-1* mutant (Maugarny-Calès et al., 2019). An 8 hour-long induction of *CUC2* was sufficient to induce tooth initiation in the mutant, which confirms the role of CUC2 at patterning the leaf margin and initiating teeth (Maugarny-Calès et al., 2019). Furthermore, this experiment shows that transient *CUC2* expression is sufficient to allow tooth development implying that CUC2 acts through functional relays to maintain its activity over time.

To infer what happens at early stages of leaf development, leaf shape was compared between col-0 and the *cuc2-1* null mutant that doesn't initiate any teeth (Nikovics et al., 2006; Maugarny-Calès et al., 2019). Consequently, the *cuc2-1* mutant displays a smooth, entirely convex mean shape. Developmental growth trajectories have been reconstructed for both col-0 and *cuc2-1* mutant and averaged contours were generated to compare leaf growth dynamics of these genotypes. Superposition of contours with a targeted blade length of 175 µm revealed that col-0 forms two slight depressions prior to any tooth outgrowth (Biot et al., 2016). This result indicates that CUC2 acts to define serration first by repressing growth at the leaf sinus. However, when contours of 225 µm-long blades were placed on top of each other, a tooth outgrowth was observed as col-0 mean contour exceeded *cuc2-1* contour limits (Biot et al., 2016). This means that CUC2 also promotes growth at distance in a second step of tooth formation. Hence, Biot *et al.* suggest a dual role for CUC2, first by repressing growth locally and then triggering its promotion at distance.

Despite this model of a dual effect, other studies have shown contradictory data, which means the precise mode of action of CUC2 is still a subject of debate. For example, a comparison of leaf outlines of col-0 compared to the *cuc2-3* mutant yielded that the *cuc2-3* mutation prevents the outgrowth only (Kawamura et al., 2010). However, the experiment was performed on 800-900µm-long leaves, which may have hidden the dual effect of CUC2. Furthermore, the sinuses in *cuc2-3* do seem lower than in the wild type, but this feature is not commented any further in the study, probably due to the size of leaf (Kawamura et al., 2010).

In order to test whether local growth repression drives morphogenesis at the margins, an artificially induced growth repression was triggered using a DEX-inducible construct in which KIP-RELATED PROTEIN 1 (KRP1) was expressed under the CUC2 promoter (Malinowski et al., 2011). Because KRP1 is a cell cycle inhibitor, growth was inhibited in the CUC2 domain as a result of cell proliferation repression. The induction of KRP1 in the CUC2 domain led to the formation of leaflet-

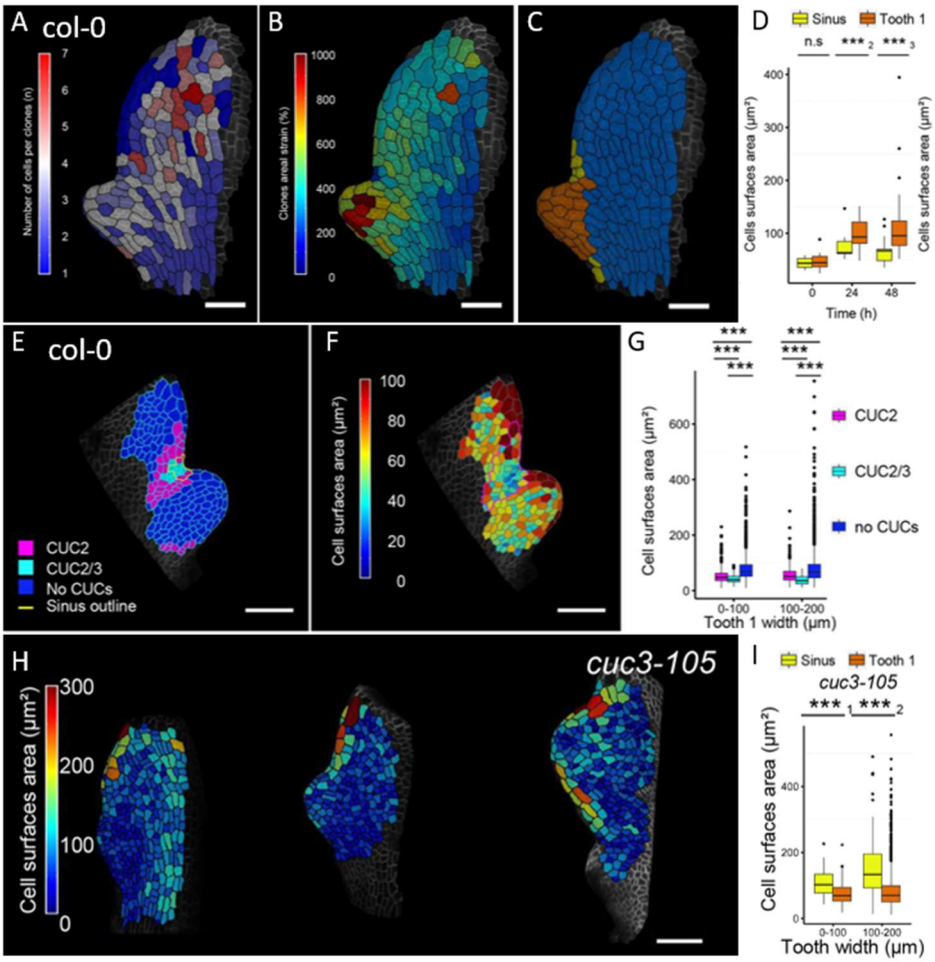

FIGURE 2-02: Cell parameters at the leaf margin and role of CUC3

A. Heatmap of clone divisions after 48 hours-long time lapse imaging on col-0 plants. The blue-to-red scale represents the number of cells that derive from a single clone at the beginning of the time lapse. B. Heatmap of the clonal areal strain after a 48 hour-time lapse experiment, defined as the area increase in % of each clone over the time lapse duration. A [0-1000] % rainbow scale is used to aid visual interpretation. C. Clone type assignment on the fully segmented surface at the end of the time lapse. Orange and yellow stands for cells assigned to tooth and sinuses, respectively. D. Cell surface areas in µm² measured in tooth and sinuses-labeled cells at each point of the time lapse. E. Clone type assignment on the fully segmented surface at the end of the time lapse, established after *pCUC2:RFP* and *pCUC3:CFP* signals were projected on the calculated surfaced. Pink and cyan cells express *CUC2* only and both *CUC2* and *CUC3*, respectively. Blue labeled cells do not express CUC genes. F. Heatmap of the cell surface areas in µm² for the col-0 leaf represented in E. A [0-100] µm² rainbow scale is used to aid visual interpretation. G. Cell surface areas in µm² measured in *CUC2*- and *CUC2/CUC3*-expressing cells for two classes of tooth widths. H. Heatmaps at the three time points of the time lapse of the cell surface areas in µm² on representative *cuc3-105* leaves. [0-300] µm² rainbow scale is used to aid visual interpretation. I. Cell surface areas in µm² measured in tooth and sinuses-labeled cells for two classes of tooth widths. A-C, E,F,H : scale bars are 50µm. All panels are from (Serra and Perrot-Rechenmann, 2020).

like structures, indicating a more complex leaf shape (Malinowski et al., 2011). Hence, the authors suggested that growth repression can trigger leaf morphogenesis and serration. These results are consistent with the findings that CUC2 may first trigger growth restriction of sinus cells.

CUC3 role is to maintain growth restriction in sinuses

On the contrary to *cuc2-1* mutant that does not initiate any teeth, *cuc3-105* mutants produce teeth at their leaf margin but fail to maintain them over leaf development (Hasson et al., 2011; Maugarny-Calès et al., 2019), which means that CUC3 role at defining teeth relies at maintaining a growth differential at the margin. Although quantitative morphogenic analyses have clarified CUC2 and CUC3 respective contributions to serration development at the organ level, the biological processes they trigger at the cellular levels were still unclear. To precise CUC3 role, early leaf development has been characterized using time-lapse imaging experiments were performed on wild type plants and *cuc3-105* mutants. Cell parameters have been obtained, followed by a projected surface segmentation of the epidermal cells (Serra and Perrot-Rechenmann, 2020) (Figure 2-02).

In the wild type, cell lineage over 48h revealed that cell divisions are uniform across the epidermis in the experiment time frame (Kierzkowski et al., 2019; Serra and Perrot-Rechenmann, 2020) (Figure 2-02A). This indicates that the differential growth between the tooth and sinuses is not a result of dividing cells, but other types of cell growth (see introduction). Moreover, over the time frame of the experiment, the study of clone surfaces evolution suggests that cells in sinuses grow to a slower expansion rate than the neighboring cells (Kierzkowski et al., 2019; Serra and Perrot-Rechenmann, 2020) (Figure 2-02B-D). These results indicate that cell growth is reduced in cells in the sinuses (Serra and Perrot-Rechenmann, 2020). However in the *cuc3-105* mutant, the cells from the sinus exhibited significantly larger surfaces, while still no change was observed in cell division between the sinus and other parts of the leaf (Serra and Perrot-Rechenmann, 2020) (Figure2-02H, I). This suggests that CUC3 mediates the reduction of cell expansion in sinuses. Inducible ectopic CUC3 expression – using a *p35S:CUC3-GR* line - demonstrated that CUC3 is able to repress dark-induced growth in the hypocotyl. As dark-grown hypocotyl elongation results more from de-repression of cell elongation rather than increase in cell proliferation (Gendreau et al., 1997), this confirms that CUC3 can inhibit cell expansion. In addition, highly serrated leaves were observed in induced *p35S:CUC3-GR* plants, and cell areas within the sinuses were very small, which supports the idea that CUC3 restricts growth in sinuses. Time lapse experiments at later

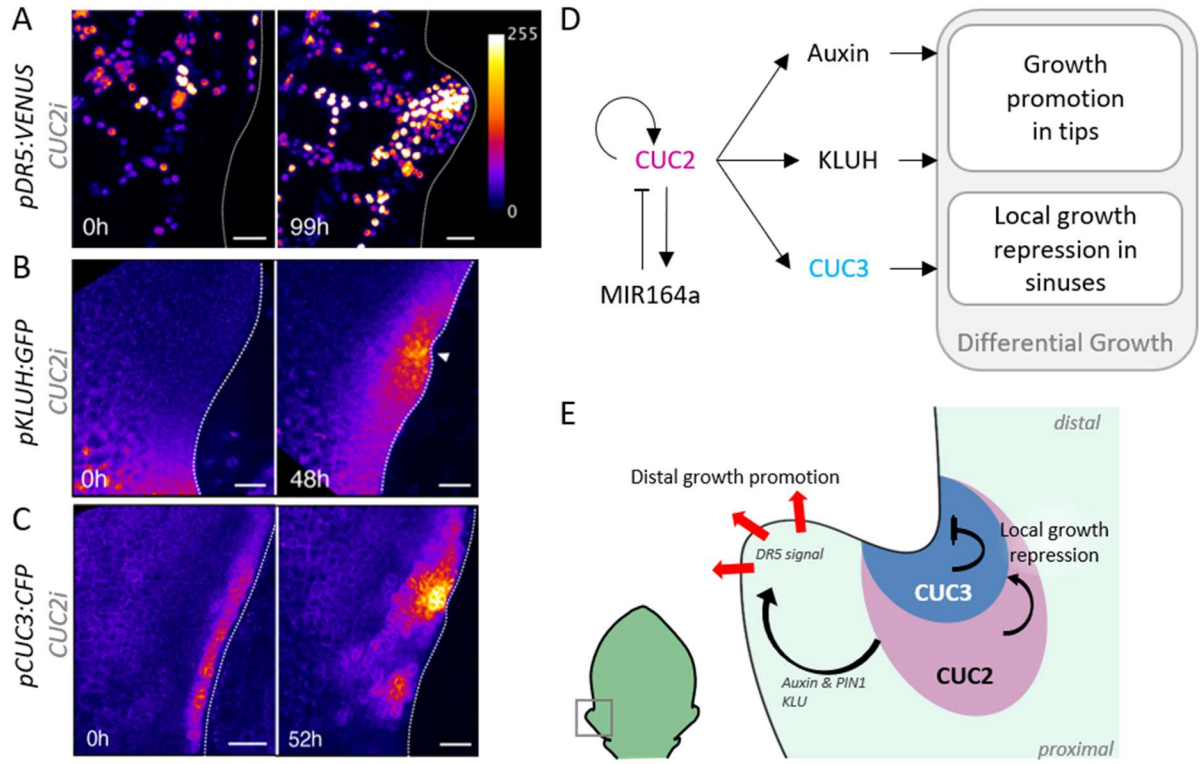

FIGURE 2-03: CUC2 induction can trigger the expression of DR5 at distance, KLUH and CUC3 proximally and provides a paradigm on serration development.

A-C. Confocal micrographs on *pDR5:VENUS* (A), *pKLUH:GFP* (B) and *pCUC3:CFP* (C) in a CUC2-inducible background *CUC2i*, following an 8 hours ethanol induction. 0h corresponds to an uninduced control, while 99h, 48h and 52h refer to the time the induction started. A Fire LUT is used to represent signal intensity and aid visual interpretation. Scale bars are 20µm. D. Current paradigm of CUC2 mode of action in plants. CUC2 promotes the expression of *MIR164a* which in turn provokes its mRNA degradation, creating a negative feedback loop. CUC2 also promotes the expression of *KLUH* locally and acts on auxin maxima in the tip to promote growth, while it triggers the expression of CUC3, which is able to repress growth locally at the sinus. E. Representation of CUC2 dual effect on serration development in the leaf: CUC2 promotes growth at distance through KLUH and auxin signaling, and locally represses cell extension *via* CUC3. A-C are from (Maugarny-Calès et al., 2019).

stages of blade growth and CUC3 signal quantification using a *pCUC3::CFP$_{er}$* line showed that the tooth smoothing that naturally occurs along leaf development coincides with a decrease in CUC3 signal at the sinus (Serra and Perrot-Rechenmann, 2020). Prolongating the duration of CUC3 activity would be an interesting tool to confirm that the decrease in CUC3 signal is responsible for the tooth smoothening. Accordingly, in 15% of the lines in which a *Pro$_{CUC2}$:CUC3* construct was introduced, and where a very high *CUC3* expression was reported, strongly serrated leaves were observed (Hasson et al., 2011). In other words, in plants in which *CUC3* is more strongly and widely expressed (supposing pCUC2 activity is both stronger and wider than pCUC3), the differential growth between teeth and sinuses is more pronounced. This result is consistent with a growth-repressive role for CUC3.

The CUC2 downstream network

CUC2 is a TF which is able to pattern leaf development and to induce serration initiation, but seems dispensable to tooth growth uphold (Maugarny-Calès et al., 2019). Indeed, CUC2 transient induction promotes the expression of several relays, which act to maintain interspersed patterning of the margin and differential growth (Figure2-03). So far, a few of CUC2 direct targets have been uncovered. The identification of CUC2 direct targets would therefore provide a better glimpse of the gene regulatory network downstream of CUC2. To achieve this goal, previous data obtained before I started my PhD, have started to uncover the regulatory network acting downstream of CUC2 (Nicolas ARNAUD, personal communication). RNAseq data following CUC2 induction with or without Cycloheximide (CHX) - an inhibitor of *de novo* protein synthesis - has provided with a list of plausible targets of CUC2. The validation of the identified targets has been performed before and during the course of my PhD.

Among the identified CUC2-targets, we found MIR164A, one of the three genes in Arabidopsis encoding MIR164, which is regulating CUC2 expression. This interaction has been validated using both an independent heterologous system as well as Chromatin-Immunoprecipitation followed by RNAseq (ChIPseq) data, demonstrating that CUC2 is directly able to induce *MIR164A* expression (Nicolas Arnaud & Magali Goussot, unpublished data). In addition, CUC2 ectopic induction was shown to promote endogenous CUC2 expression (Li et al., 2020). Therefore, CUC2 regulates its own transcriptional activity and thus targets MIR164A to trigger its own regulation at the post-transcriptional level hence forming a negative feedback loop that may fine-tunes the CUC2 expression domain and/or levels.

In addition, CUC3 seems to acts as a functional relay for CUC2. Indeed, *pCUC3:CFP$_{er}$* expression intensifies following local CUC2 induction using transgenic line where CUC2 is ethanol-induced under the control of the endogenous CUC2 promoter (CUC2i) (Figure2-03C). Accordingly, *CUC3* transcript levels are higher in microdissected leaf margins from *CUC2i*-induced plants (Maugarny-Calès et al., 2019). Furthermore, numerous quantifications of tooth shape demonstrate that CUC3 is essential for serration formation. Sinus angle - as a proxy a sinus growth repression - is wider in a *cuc3-105* mutant due to larger cells, suggesting that CUC3 can act as a local growth repressor (Maugarny-Calès et al., 2019; Serra and Perrot-Rechenmann, 2020). The highly serrated leaf phenotypes of *CUC2g-m4* and *mir164a-4* lines, in which *CUC2* mRNA levels are elevated, is partially suppressed in *CUC2g-m4 cuc3-105* and *MIR164a-4 cuc3-105* mutants. Hence, CUC3 acts downstream of CUC2 to reinforce and maintain tooth growth. In addition, cells in sinuses expressing both CUC2 and CUC3 were shown to exhibit smaller projected area than the neighboring cells that express CUC2 only, indicating that a combination of CUC2 and CUC3 may have a stronger effect on cell growth repression (Serra and Perrot-Rechenmann, 2020). Alternatively, CUC2 could be more expressed in the cells that also express CUC3. Furthermore, Y2H experiments indicated that CUC2 and CUC3 can interact with one another (Gonçalves et al., 2015). Together these observations suggest that CUC2/3 proteins act as homo- and/or heterodimers and thus may bind differentially to their DNA targets or even bind to different set of targets.

The *pDR5:VENUS* is an auxin-response reporter line, that was used together with the inducible *CUC2i* line in leaves, and helped showing that a CUC2 pulse is sufficient to induce activation of the auxin signaling concomitantly with the initiation of a pair of teeth (Maugarny-Calès et al., 2019) (Figure 2-03A). The use of *pDR5:VENUS* reporter line in *mir164a-4* and *CUC2g-m4* genetic backgrounds showed that elevated CUC2 mRNA levels trigger a higher auxin response activation compared to the wild type (Maugarny-Calès et al., 2019). Hence, auxin response pathway is activated in teeth in a CUC2 level-dependent way. A time-lapse experiment based on PIN1 polarity and intensity showed that PIN1 allows to orient growth polarity locally in a wild type background (Kierzkowski et al., 2019). PIN1 is hence thought to act downstream of CUC2. Those results are consistent with the serration formation model developed in (Bilsborough et al., 2011). Whether CUC2 expression precedes auxin responses for correct tooth patterning remains to be determinated. Quantitative spatiotemporal characterization of gene expression patterns using

CUC2, CUC3, and DR5 reporter lines, currently being performed in the lab, will be a key experiment for understanding the early stages of serration development. This way, it will be possible to see which of CUC2 or auxin signaling begins first during tooth patterning.

CYP78A5/KLUH is also a novel identified relay for CUC2, as *KLUH* transcript levels increase in microdissected leaf margins in which *CUC2* was induced, using the *CUC2i* line (Maugarny-Calès et al., 2019) (Figure 2-03B). Accordingly, the reporter line *pKLUH::GFP* yielded higher signal intensity following a pulse of CUC2 (Maugarny-Calès et al., 2019). As shown previously with CUC3, *KLUH* is expressed in teeth sinuses, and *kluh-4* mutant plants display smaller and smoother leaves than the wild type. In addition, *kluh-4* is able to partially suppress the over-dissected phenotypes from both *mir164a-4* and *CUC2g-m4* (Maugarny-Calès et al., 2019). The *KLUH* gene encodes a cytochrome P450 protein which was shown to regulate cell cycle duration in a non-cell autonomous way (Anastasiou et al., 2007; Eriksson et al., 2010). It was hypothesized that KLUH is able to produce a mobile growth factor (MGF) (Kazama et al., 2010). As no changes in hormonal-regulated gene expression was observed in a *klu* loss-of-function mutant, it was hypothesized that KLUH acts independently of the classical hormonal pathways. Hence, it was proposed that KLUH produce a mobile growth factor (MGF) (Kazama et al., 2010) (Anastasiou et al., 2007). Such a MGF could be involved in CUC2-triggered promotion of cell growth at distance, even if no difference in cell division rate was reported in the teeth (Serra and Perrot-Rechenmann, 2020). Alternatively, it is still possible that KLU may impact development through classical hormonal pathways that do not trigger dramatic changes of gene expression levels. For instance, if KLU acts on PIN1 remobilization, it can dramatically impact development by allowing local differential gene expression that are not easily detectable using global gene expression measuring methods.

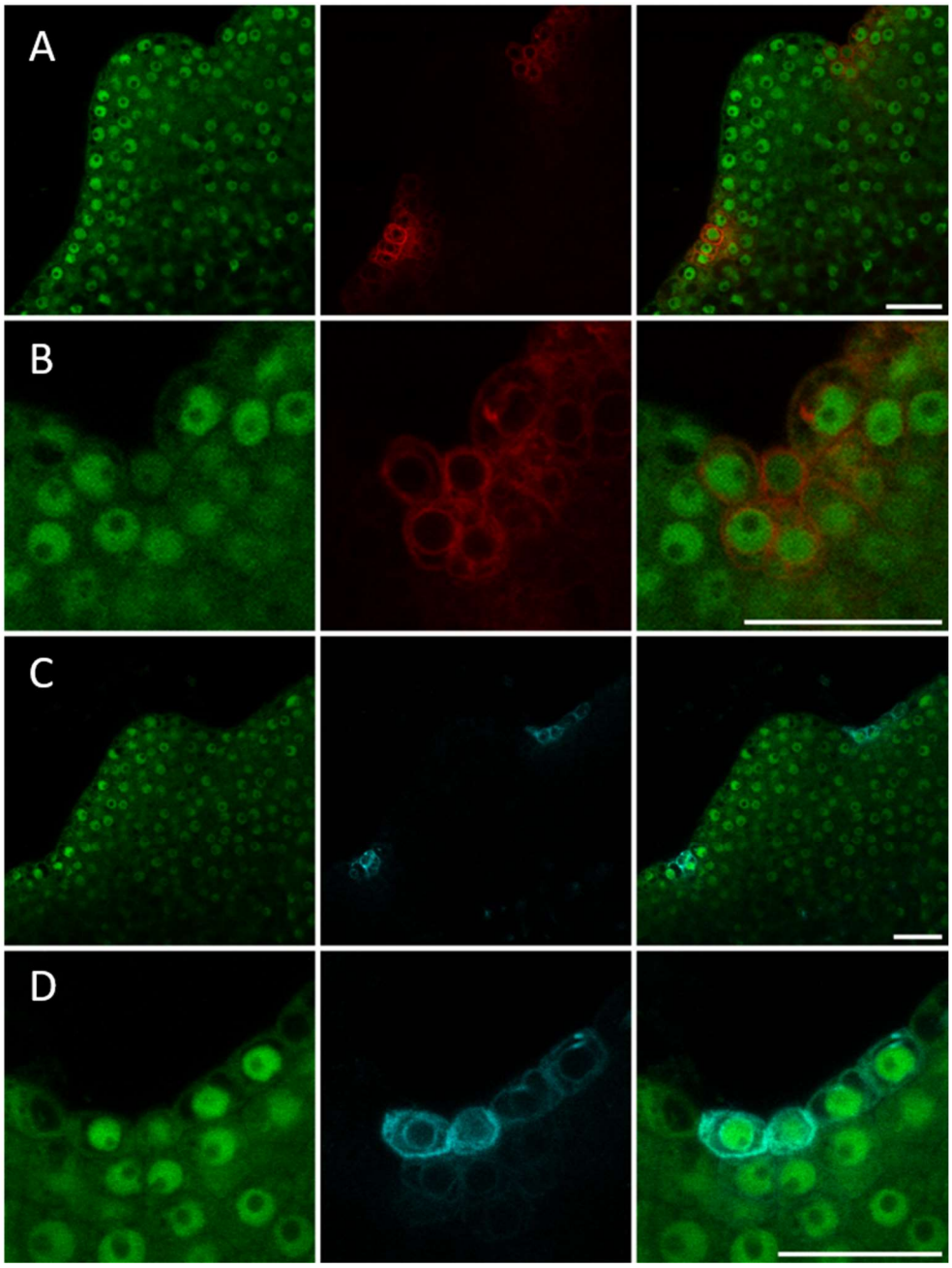

FIGURE 2-04: SPY, CUC2 and CUC3 co-express in cells from the sinus.
A-D. Confocal micrographs on the progeny of a crossing between *pSPY:SPY-GFP spy-23* and *pCUC2-RFP* (A-B), and *pCUC3:CFP* (C-D). From left to right, *pSPY:SPY-GFP* (green), *pCUC2-RFP* (A-B) or *pCUC3:CFP* (C-D), and merged images. A-C, visualization of a full first tooth. B-D. Close-up on the first sinus. Scale bars are 20 µm.

RESULTS

Our data suggest that SPY is able to repress boundary cell size in the leaf. Hence, we propose that SPY controls serration by a pathway different from the CUC pathway, that yet may converge on common downstream factors. Following this, we propose that SPY interferes in the leaf development to control leaf margin differentiation, or shares a certain number of targets with the CUC2 pathway. In order to better understand how the SPY and the CUC pathway are linked to control boundary cell development, we focused on the molecular events downstream of CUC and SPY using transcriptomic data.

SPINDLY and CUC2 act through a common molecular network to restrict sinus cell growth

Our genetic analysis suggests that the CUC pathway and SPY are able restrict boundary domains cell growth independently, as double mutants exhibited additive phenotypes. SPY and CUC2 could either act on separate set of genes, or share several targets. Hence, we tested whether SPY and CUC2 act on the same targets to trigger growth repression.

First, we investigated whether CUCs and SPY can act simultaneously within the same cells by using confocal imaging on reporter lines. To do so, a *pSPY:SPY-GFP* in a *spy-23* background was crossed either with a *pCUC2:RFP* or a *pCUC3:CFP* reporter line. Fluorescence was directly observed in the population resulting from this crossing (Figure 2-04). Like what was reported before, *SPY* is widely expressed in leaves (Swain et al., 2002). Meanwhile, CUC2 and CUC3 are expressed in sinuses (Nikovics et al., 2006; Hasson et al., 2011). A focus on the first tooth of about 500µm/1mm -long leaves, as well as a zoom on the first sinus, confirmed that CUC2 and SPY on the one hand, and CUC3 and SPY on the other hand can be expressed in the same cells.

To test if SPY and CUC2 can act in synergy on local growth restriction by acting on the same targets, we used transcriptomic data from a previous analysis, that unraveled genes that are up- and down-regulated in a *spy-3* mutant compared to a wild type control line (Qin et al., 2011). In addition, a transcriptomic analysis was also performed in the lab prior to my thesis project in order to identify genes that are differentially expressed over CUC2 expression. To do so, a *p35S:CUC2-GR* inducible line was used (see Material and methods). Since both SPY and CUC2 seem to act as growth repressors, genes that are up-regulated in *spy-3* loss-of-function mutant were compared to down-regulated genes of the *p35S:CUC2-GR* gain-of-function line (Figure 2-

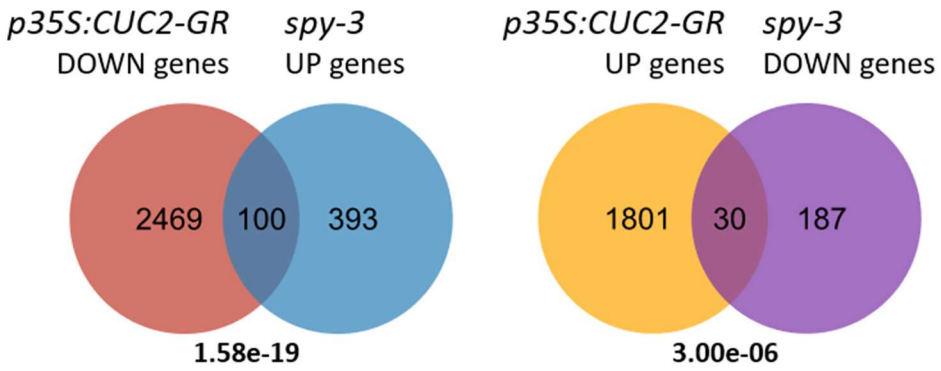

FIGURE 2-05: Venn diagrams of common DEX-induced *p35S:CUC2-GR* up/down-regulated and *spy-3* up/down-regulated genes.

A total of 2,569 and 1,831 genes were respectively down- and up-regulated in DEX-induced *p35S:CUC2-GR.* 493 up-regulated genes and 217 down-regulated genes from *spy-3* mutant were filtered from (Qin et al., 2011) by removing all genes not matching an AGI locus. Numbers below Venn diagrams correspond to hypergeometric probability ($N_{total\ At\ genes}$ = 33,602) (over-enrichment based on the cumulative distribution function (CDF) of the hypergeometric distribution).

05). In addition, alternative lists comparisons (*p35S:CUC2-GR* up-regulated genes *versus spy-3* down-regulated genes, *etc*.) were also performed. Prior comparing lists, *spy-3* up- and down-regulated genes from (Qin et al., 2011) that did not correspond to any AGI locus were filtered-out. A total of 100 genes were common between the 493 up-regulated genes in *spy-3* and the 2569 down-regulated genes from DEX-induced *p35S:CUC2-GR* (FDR<0.05), which represents a significant overlap (p-value=1.58e^{-19}, see appendix 1). In addition, 30 genes were common between *p35S:CUC2-GR* up-regulated genes and *spy-3* down-regulated genes (p-value=3.00e^{-11}, see appendix 2). To infer whether a family of genes is significantly represented among those identified genes, a gene ontology analysis was then performed and yielded an enrichment in genes related to plant cell walls (GO:0009505, enrichment 9.65, raw p-value = 4.31E-05 (Fisher exact test), FDR=4.45E-02) in the intersection of *spy-3* up-regulated genes with *p35S:CUC2-GR* down-regulated genes. In addition, an enrichment in genes associated with cell wall organization and biogenesis was also observed (GO:0071554, enrichment 7.38, raw p-value = 1.13E-06 (Fisher exact test), FDR=6.75E-03). Genes identified in gene ontology study are highlighted in appendix 1. Conversely, no significant family of genes were over-represented in any other intersection under study. This suggests that, if SPY and CUC2 act jointly in the same direction, they probably act on growth repression-related processes associated with cell wall biogenesis which is consistent with their proposed function during leaf margin development.

Among the identified genes, we identified genes coding for several xyloglucan endotransglucosylases/hydrolases (XTH4, XTH15, XTH18 and XTH19), arabinogalactans proteins (AGP4, AGP7, AGP9 and AGP12) as well as two genes coding for expansin-like proteins (EXLA1 and EXLA2). XTH18 and XTH19 were both previously shown to be involved in the control of hypocotyl growth, as overexpressing lines for XTH18 and XTH19 both promoted hypocotyl growth in the dark (Miedes et al., 2013). In addition, AGP4,7,9,12 were identified in a large-scale gene expression pattern study on fast-growing seedlings as robust markers of growth (Kohnen et al., 2016). Similarly to what was observed for XTH proteins, an EXLA2 overexpression is able to increase growth in dark-grown hypocotyls (Boron et al., 2015). In addition, a biomechanical analysis of the EXLA2 overexpressing line showed the cell wall resistance was decreased in the hypocotyl, suggesting EXLA2 may modify the cell wall organization and composition (Boron et al., 2015). It thus seems that among the union of CUC2 and SPY differentially expressed genes, several genes contribute to the cell wall relaxation. This suggests that cell wall modifying enzymes

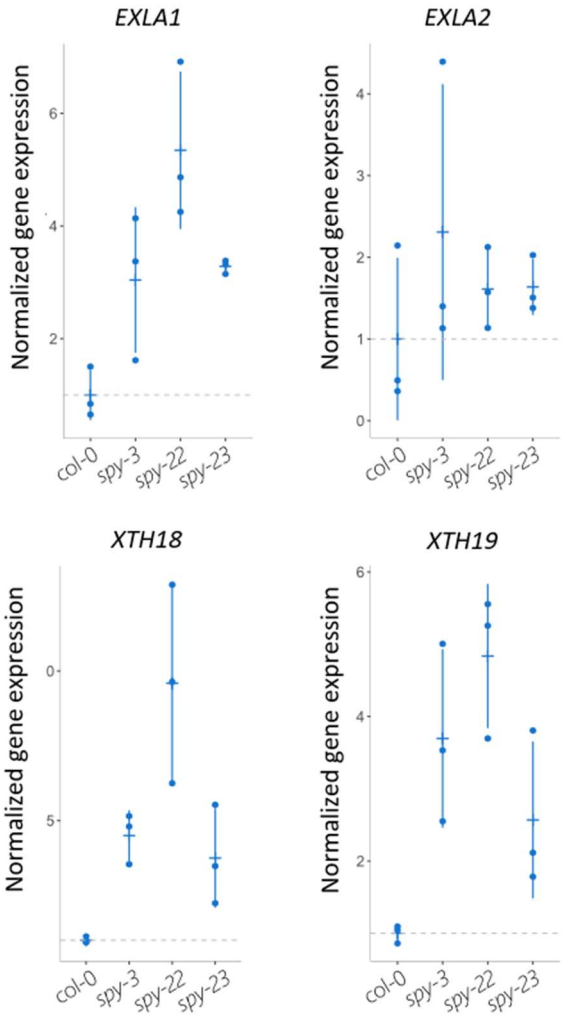

FIGURE 2-06: Quantification of cell-wall extension-related gene expression in *spy* mutants.

Expression level of genes identified as commonly down-regulated by SPY and CUC2 in col-0, *spy-3*, *spy-22* and *spy-23.* Each dot represents a biological RNA sample. *EXLA1, EXLA2, XTH18* and *XTH19* transcript levels were measured by real-time quantitative RT-PCR normalized by *EF1α* and *Actin2*.

could act downstream of both CUC and SPY genes, to impinge on cell expansion. This is consistent with the proposed role for CUC3 and SPY in sinuses (Serra and Perrot-Rechenmann, 2020).

The expression of *XTH18*, *XTH19*, *EXLA1* and *EXLA2* was quantified in *spy-3*, *spy-22* and *spy-23* and compared with wild type (Figure 2-06). For all observed targets, expression in *spy* mutant seem to be higher than in the wild type, thus confirming previous results established by transcriptomics (Qin et al., 2011).

In order to test whether CUC2 overexpression may indeed repress cell expansion, we used the *p35S:CUC2-GR* line to be able to induce CUC2 ectopically in dark-growing hypocotyls. Indeed, in the epidermis of dark grown hypocotyls, almost no cell divisions occur and growth is mainly the result of basipetal cell elongation only (Gendreau et al., 1997). These experiments were conducted in a *cuc2-3* weak allele background, even if no expression was reported in the hypocotyl (Figure 2-07). Three days-old, dark-grown and DEX-treated seedlings – from the *p35S:CUC2-GR* line displayed significantly shorter hypocotyls than the MOCK-treated seedlings consequently of CUC2 induction (N_{DEX}=49 L_{DEX}=5,48±0.92 mm, N_{MOCK}=50 L_{MOCK}=8.46±1.01 mm, p-value < 2.2e-16). Conversely, DEX treatment had no effect on the *cuc2-3* mutant dark-grown hypocotyl length (N_{DEX}=55 L_{DEX}=8.93±0.91 mm, N_{MOCK}=53 L_{MOCK}=9.14±1.42 mm, p-value = 0.3602). To verify the growth differences at a cellular scale, several hypocotyls were retrieved and the cell wall were colored to be imaged with confocal imaging. Cell lengths in the first millimeter above the collet were measured. Cell elongation was reduced upon CUC2 induction (N_{DEX}=53 L_{DEX}=248±86 µm, N_{MOCK}=34 L_{MOCK}=382±87 µm, p-value = 1.016e-09), while no significant differences were observed in the control (N_{DEX}=41 L_{DEX}=400±90 µm, N_{MOCK}=28 L_{MOCK}=413±78 µm, p-value = 0.5085). Then, we measured gene expression levels for *EXLA1* and *EXLA2* and found out that both transcript levels were reduced upon CUC2 induction. Since both EXLA were previously associated with cell wall plasticity, this result is coherent with a decrease in cell elongation as observed before. Taken together, our data suggest that an ectopic CUC2 expression is sufficient to repress a set of genes involved in cell wall relaxation, thus providing a plausible framework for CUC2 downstream activity.

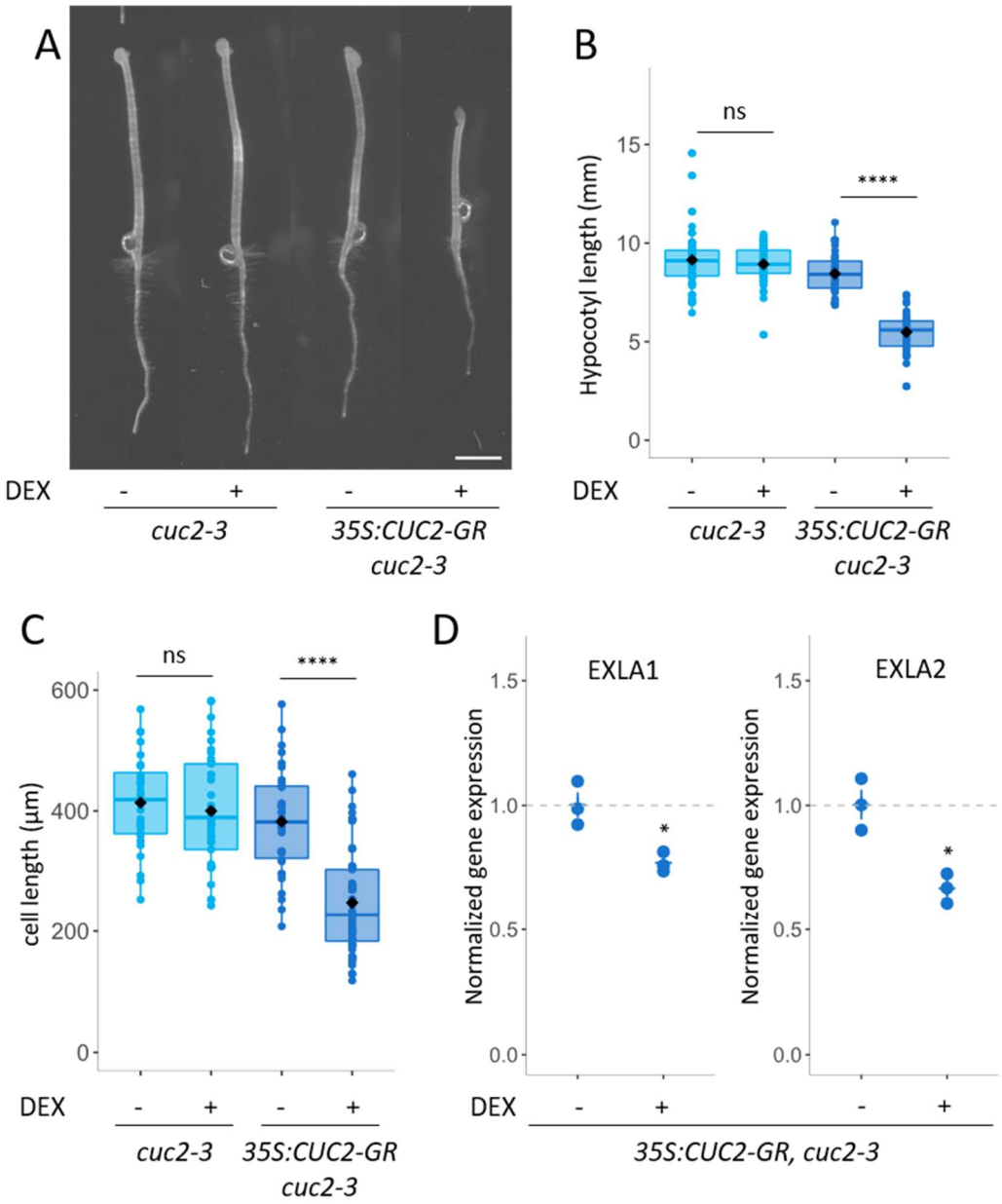

FIGURE 2-07: Quantification dark-grown hypocotyl lengths and cell-wall related genes expressions in a *35S:CUC2-GR cuc2-3*.

A. Phenotype of 3-days-old dark-grown hypocotyls from *cuc2-3* or *35S:CUC2-GR cuc2-3* treated with mock treatment or with 10µM DEX. B. Hypocotyl length quantification. C. Cell length quantification. Cells were measured within the first millimeters over the collet. D. Expression level of *EXLA1* and *EXLA2* in a *35S:CUC2-GR cuc2-3* line grown for 3 days in the dark, treated either with mock treatment or with 10µM DEX. Each dot represents a biological RNA sample. *EXLA1* and *EXLA2* transcript levels were measured by real-time quantitative RT-PCR normalized by *EF1α* and *Actin2*. Statistical significance (Student's test) is designated by ns=not significant, * $p<0.05$, **** $p<0.0001$.

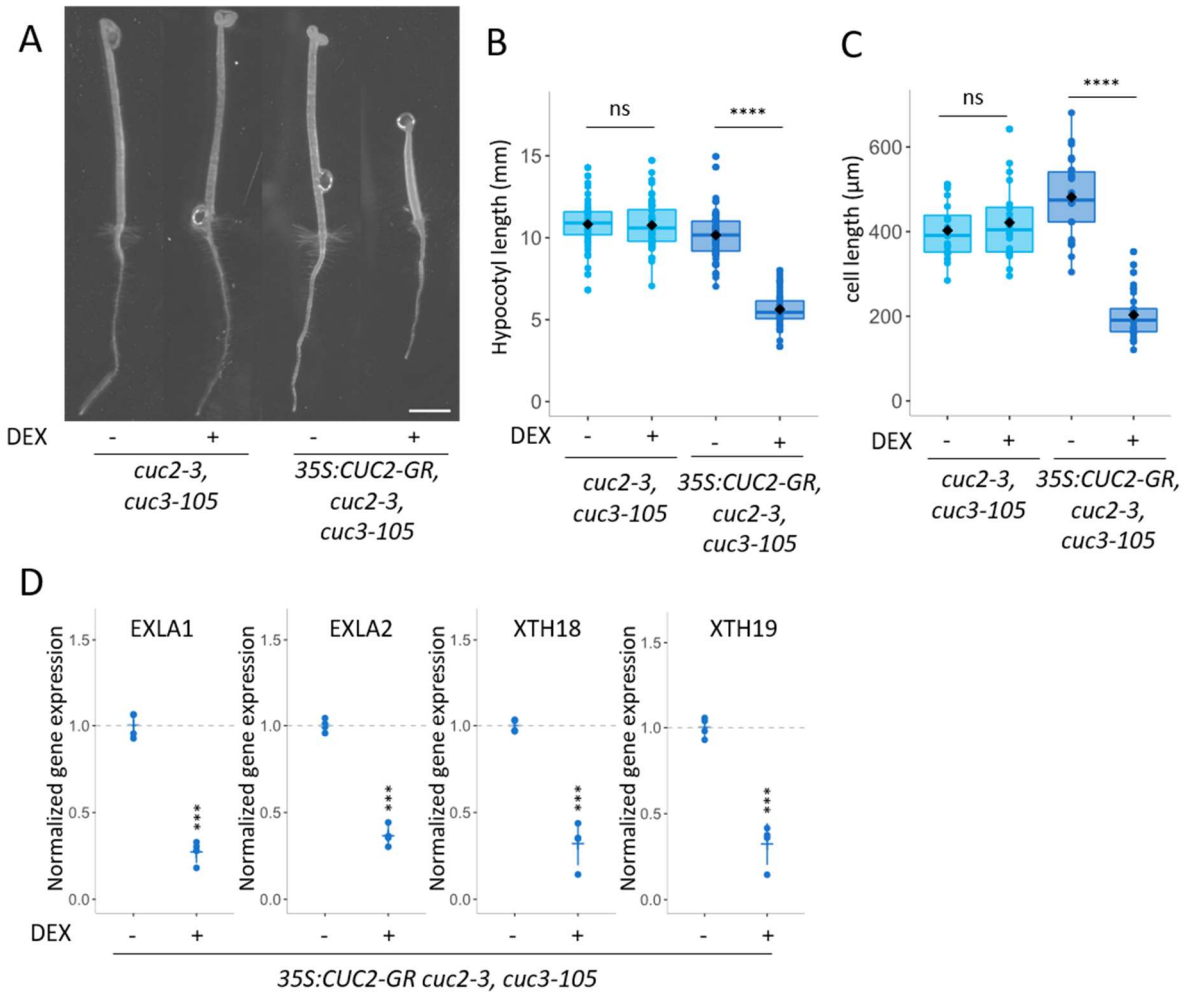

FIGURE 2-08: Quantification dark-grown hypocotyl lengths and cell-wall related genes expressions in a *35S:CUC2-GR cuc2-3 cuc3-105*.

A. Phenotype of 3-days-old hypocotyls from *cuc2-3 cuc3-105* or *35S:CUC2-GR cuc2-3 cuc3-105* treated with mock treatment or with 10µM DEX. B. Hypocotyl length quantification. C. Cell length quantification. Cells were measured within the first millimeters over the collet. D. Expression level of *EXLA1*, *EXLA2*, *XTH18* and *XTH19* in a *35S:CUC2-GR cuc2-3* line grown for 3 days in the dark, treated either with mock treatment or with 10µM DEX. Each dot represents a biological RNA sample. Transcript levels were measured by real-time quantitative RT-PCR normalized by *EF1α* and *Actin2*. Statistical significance (Student's test) is designated by ns=not significant, *** p<0.001, **** p<0.0001.

CUC2 represses cell elongation and promotes cell wall stiffening independently of CUC3.

The activity of CUC2 is mediated by CUC3 which acts as a molecular relay for its activity (Maugarny-Calès et al., 2019). CUC2 and CUC3 redundantly control boundary domain development, therefore it is possible that CUC2 alters cell elongation independently of CUC3. As no serrations are initiated in a *cuc2* loss-of-function mutant, this hypothesis has been difficult to test during leaf development.

Here, we decided to use a *p35S:CUC2-GR* construct in a *cuc2-3 cuc3-105* double mutant background in order to establish whether the CUC2-dependent growth repression we observed earlier in dark-grown hypocotyls requires CUC3 (Figure 2-08A,B). When CUC2 was DEX-induced in a *cuc3-105* null mutant background, dark-grown hypocotyls were shorter than in the control (N_{DEX}=57 L_{DEX}=5,6±1,0 mm, N_{MOCK}=58 L_{MOCK}=10,2±1,5 mm, p-value < 2.2e-16). No difference was observed in the *cuc2-3 cuc3-105* double mutant control, neither with DEX nor with MOCK treatment (N_{DEX}=52 L_{DEX}=10,8±1,4 mm, N_{MOCK}=53 L_{MOCK}=10,8±1,4 mm, p-value = 0.8386). Like before, cell elongation was quantified and yielded shorter cells in the CUC2-induced experiment (N_{DEX}=37 L_{DEX}=203±54 µm, N_{MOCK}=26 L_{MOCK}=482±92 µm, p-value = 2.659e-16) while no difference was observed in the control (N_{DEX}=20 L_{DEX}=421±90 µm, N_{MOCK}=20 L_{MOCK}=402±66 µm, p-value = 0.4534) (Figure 2-07, Figure 2-08C). These results show that CUC2 acts independently of CUC3 to regulate cell elongation in the dark-grown hypocotyl model. In order to infer whether the differences in cell elongation is associated with cell wall-specific genes differential expression, we measured *XTH18*, *XTH19*, *EXLA1* and *EXLA2* gene expression upon CUC2 induction (Figure 2-08D). For all four genes, transcript level was significantly reduced when CUC2 was induced, suggesting that CUC2 inhibits their expression independently from CUC3.

Together, our data suggest that both CUC2 and SPY inhibit cell wall relaxation-related gene expression.

Cell wall mechanics at the leaf margin

Our molecular data support a role for CUC2 in the control of cell wall properties. This CUC2 function has been uncovered using an inducible system in dark grown hypocotyl but might also be at stake during leaf development. Since the genes we identified as negatively regulated by both SPY and CUC2 are involved in the control of plant cell wall plasticity, we then suggested

that the cell wall mechanical properties might be affected depending on CUC2. Therefore, we conducted experiments on an atomic force microscope (AFM) in order to first estimate the stiffness of cell wall along the leaf margin and second, to calculate the apparent Young's modulus to quantify cell wall mechanics. Young's modulus can be defined as the proportionality coefficient between the force required to deform an object and the area of the indentation. In other words, the more rigid an object is, the less elastically it deforms under stress, and the higher the Young's modulus. This value depends on several parameters such as the diameter and the stiffness of the bead used.

We used AFM to measure the cell wall stiffness of the cell wall in the sinus - where CUC2 is expressed - and compare with the stiffness of the cell wall in teeth - where CUC2 is not expressed. CUC2 is expressed very early during leaf development, as it is key to pattern the leaf margin. In young leaf primordia, cells within the margin domain do not display different sizes between sinus and teeth domains (Figure 1-14). Yet, sinus and teeth showed a differential stiffness: cell sinus walls being stiffer than the cell tooth walls (Figure 2-09). This is consistent with both the expression pattern of CUC2 (Nokovics et al., 2006) and our molecular data showing that CUC2 inhibits the expression of genes known to allow cell wall loosening. To validate these data, we quantified the Apparent Young's modulus (Ea) in another set of experiment analyzing cell wall stiffness in 11 independent young dissected leaves for the WT and show once again that sinuses domains are consistently stiffer than tooth domains (Figure 2-09F). This result highlights the fact that CUC2 links patterning and growth throughout leaf development and may provide a mechanical framework for the development and maintenance of boundary domains in various developmental contexts.

As CUC2 is required to initiate teeth, it is difficult to use the *cuc2* loss-of-function to assess whether CUC2-dependent inhibition of cell expansion occurs also at the leaf margin. The *spy-3* mutant initiates teeth but their growth is not maintained due to local cellular changes at the sinus during teeth development. Thus, SPY represses the expression of a common set of genes with CUC2 that are related to the cell wall properties. We therefore used the *spy-3* mutant to check whether the reduced expression of cell wall genes acting downstream of CUC2 is sufficient to change the mechanical properties of the cell wall at the leaf margin. Although the stiffness of walls of sinus-located cells was reduced in *spy-3* when compared with the stiffness of the walls of teeth-located cells, relative stiffness measurements on *spy-3* young leaf primordia yielded to lower

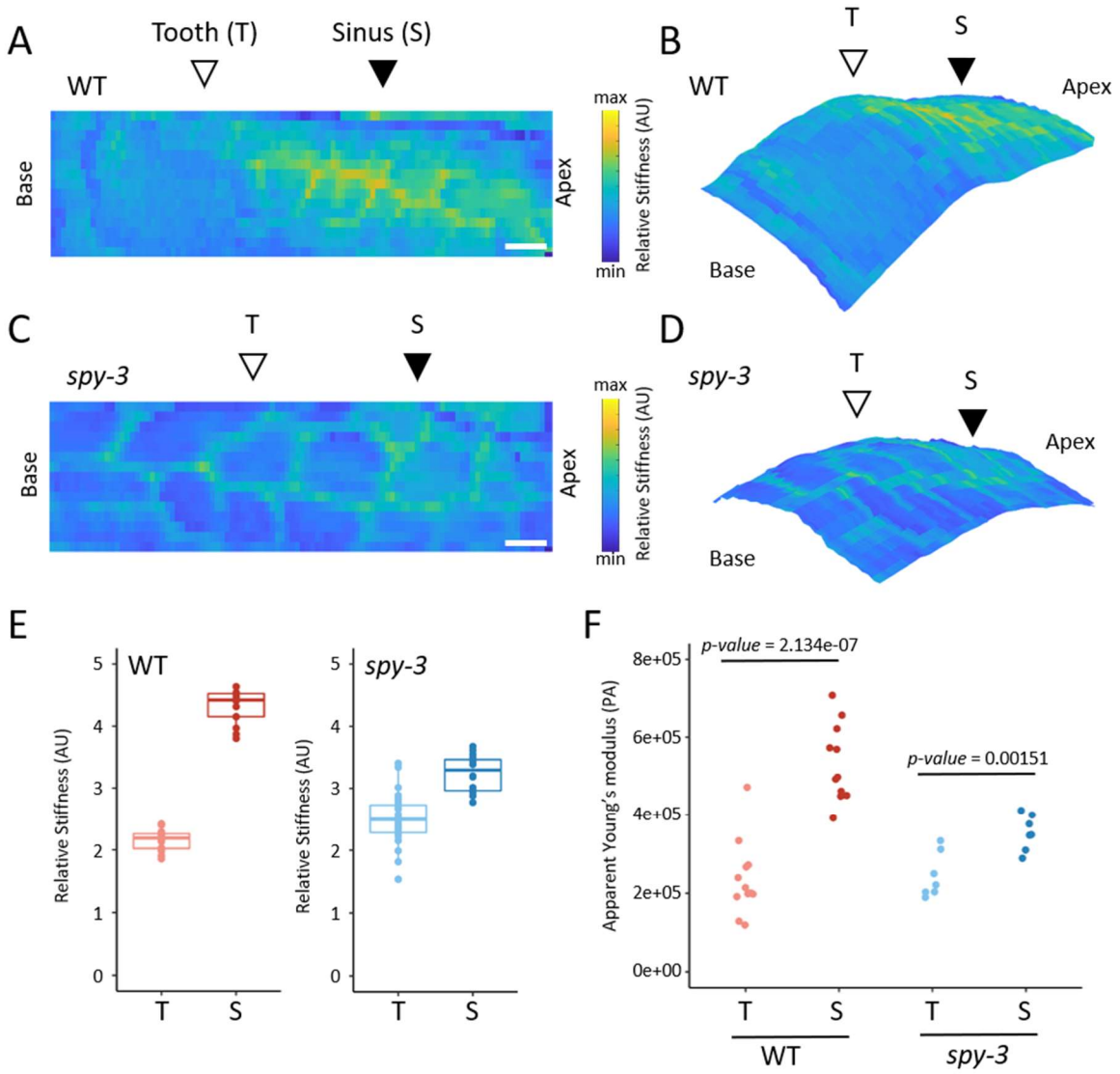

FIGURE 2-09: *spy-3* displays more flexible cell walls than the wild type in the sinus of young primordia

A,C. Representative maps of relative stiffness (arbitrary units) measured on the middle domain of an approximately 150µm-long growing primordium (rank 11-12-13) from wild-type (A) and *spy-3* (C) plants grown in SD conditions. Each pixel represents the relative stiffness calculated from a single force-indentation curve. Apico-basal polarity is indicated. Position of tooth (T) peak as well as sinus (S) are specified. Scale bars are 10 µm. B,D . Projection of relative stiffness (from A,C) on measured leaf topography for the wild type (B) and *spy-3* (D). E. Quantification of relative stiffness within a transversal cell wall of the tooth (T) or the sinus (S). Each point represents a measured pixel. F. Apparent Young's modulus (Pa) measured on transversal cell walls of wild type teeth (N=11) and sinuses (N=11) and *spy-3* teeth (N=7) and sinuses (N=7).

differential stiffness between teeth and sinuses than what was observed in the wild-type. (Figure 2-09C-D). Apparent Young's modulus quantification in another set of experiment in 7 independent young dissected leaves for *spy-3* confirms these results (Figure 2-09F). These data support the idea that the set of genes commonly downregulated by CUC2 and SPY may impact cell wall stiffness at the leaf margin. Reporter lines showing *EXLA1/2* and/or *XTH18/19* gene expression would be a nice addendum to these experiments, as their differential expression along the leaf margin would associate local gene expression data with local measured stiffness.

Furthermore, it is important to note that stiffness changes predate the cell morphological changes we observed in *spy-3* mutant and occur at early stages of leaf development suggesting that cell wall mechanics play a central role linking patterning and the subsequent differential growth. This is consistent with previous results that highlighted that mechanical heterogeneity predates morphological break of anisotropy (Peaucelle et al., 2015).

DISCUSSION

CUC2 modulates growth both locally and at distance

Interspersed CUC2 expression and auxin response maxima are both necessary and sufficient to initiate serrations at the leaf margin during development (Bilsborough et al., 2011). Consequently, a *cuc2-1* null mutant displays entirely smooth margins and does not initiate any tooth (Nikovics et al., 2006; Biot et al., 2016). Consistent with this, the *cuc2-1* mutant was used as a smooth control to better understand the processes that trigger serration formation. Developmental trajectories focusing on the leaf margins yielded that the first visible difference between a wild type and a *cuc2-1* growing leaf is the formation of two depressions at half of the blade (Biot et al., 2016). Hence, the first event in tooth formation seems to be associated with growth repression. Consistent with this, we showed that CUC2 is able to repress the expression of genes, namely *XTH18/19* and *EXLA1/2,* that were shown to modify the cell wall properties promoting cell expansion. Accordingly, CUC3 has been shown to inhibit cell expansion of sinus cell hence participating to the shaping of the leaf (Serra and Perrot-Rechenmann, 2020).

Here we propose that CUC2 inhibits cell expansion to repress leaf margin growth at the sinus and more generally in boundaries. However, CUC2-triggered growth repression could also involve other types of growth. BrdU immuno-labelling was used in developing inflorescences and in the floral meristem to reveal cell divisions (Breuil-Broyer et al., 2004). No labelling was observed in the boundary domains on the contrary to proliferating tissues, coinciding with CUC2 local expression. Hence, we can propose that CUC2 may locally repress cell division. However, mitotic index was evaluated in the floral meristem using Histone H4-GFP fusion protein visualization, and yielded that the boundary domain displays mitotic indexes that are similar to that of the meristem itself (Laufs et al., 2004). As a consequence, it is not clear whether CUC2 is able to locally modify cell division. Still, CUCs-expressing cells were associated with the lowest relative growth difference index following a comparative analysis of gene expression and growth patterns in floral meristems (Refahi et al., 2021). Since lines that have high CUC2 levels also have much larger teeth, it was proposed that CUC2 promote tooth outgrowth *via* cell division promotion at distance (Kawamura et al., 2010). It was then confirmed that CUC2 has a growth-triggering effect at distance through the promotion of *KLUH* expression (Maugarny-Calès et al., 2019), which was shown to promote cell proliferation in the leaf (Anastasiou et al., 2007; Kazama et al., 2010).

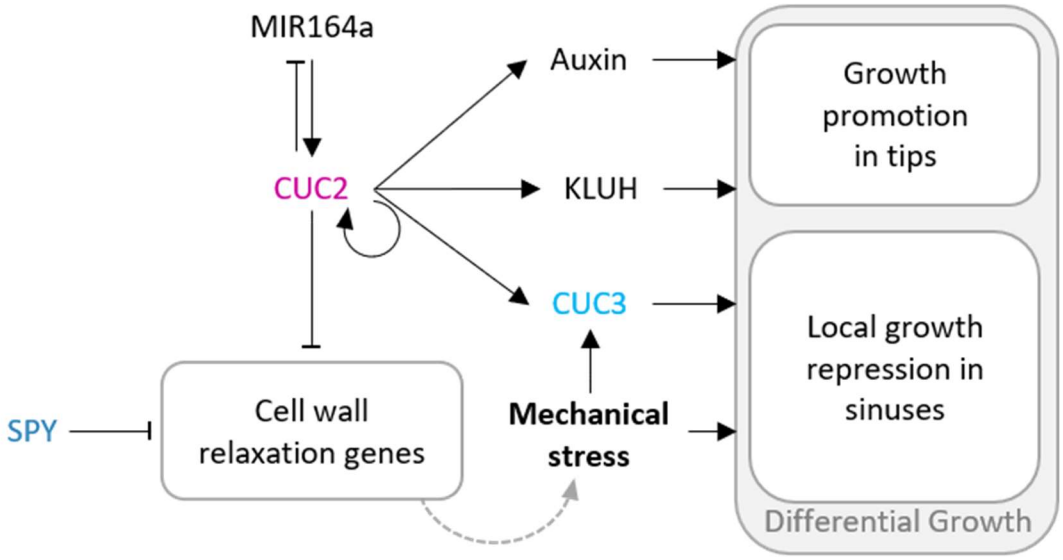

FIGURE 2-10: Operating concept of CUC2 model.

In this model, SPY and CUC2 could trigger local growth repression by repressing genes involved in cell wall relaxation and cell elongation. This growth repression would be associated with a local increase in mechanical stress that would further induce CUC3 expression.

CUC2 triggers a growth pathway partially impacting cell wall mechanical properties.

Transcript level analysis upon CUC2 induction revealed that, during leaf margin development, *CUC3* maximal expression level is observed around 48 hours following an 8 hours-long CUC2 induction showing that CUC3 acts downstream of CUC2 (Maugarny-Calès et al., 2019). Unpublished data obtained in the lab suggest that CUC3 may not be a direct CUC2 target. Moreover, *CUC3* transcript levels decrease from 48 hours post ethanol induction (Maugarny-Calès et al., 2019). This indicates that CUC2 is able to transiently activate *CUC3* expression, and that *CUC3* expression needs to be maintained through time. Here, we propose a model in which CUC2 modifies cell wall mechanical properties in the leaf boundary domains through the repression of the expression of cell wall-relaxing proteins. We propose, following our quantification of cell wall Young's Modulus at the leaf margin, that *CUC2* expression triggers a local tension at the sinuses. Such tensions were already reported in the SAM boundaries where *CUC2* is expressed (Hamant et al., 2008). As *CUC3* expression was shown to be triggered by mechanical stress (Fal et al., 2016), we suggest that CUC2 could indirectly trigger CUC3 expression locally through mechanical stress. This is consistent with the observation that *CUC2* pattern of expression is much wider than that of *CUC3*. Indeed, since CUC2 was previously shown to induce *CUC3* expression indirectly and after a delay (Maugarny-Calès et al., 2019), once would expect *CUC3* expression pattern to overlap or even exceed *CUC2* domain of expression (except, if CUC2-triggered expression of *CUC3* is dependent of a certain threshold of CUC2 level that is only achieved in a few cells). On the contrary, *CUC3* expression domain is more restricted than that of *CUC2*. We hence suppose that an intermediate process is necessary to explain this specific expression pattern. Here, CUC2 drives a local tension that would be maximal at the sinus. That mechanical stress then acts as a threshold-based cue that triggers local gene expression (Fal et al., 2016). Once *CUC3* is expressed, it is able to repress cell expansion locally (Serra and Perrot-Rechenmann, 2020) which participates in shaping the teeth. It is also possible that CUC2 and CUC3 form a positive feedback loop where CUC3-induced tension reinforces *CUC3* expression. The model we propose for CUC2 direct repression of growth and indirect induction of *CUC3* is represented in Figure 2-10.

Other processes could explain the induction of gene expression in relation to mechanical stress. Strong mechanical stress in the meristem boundaries triggers nuclei elongation due to local cell deformation (Fal et al., 2021). These deformations were shown to induce Histone3.1

expression and modify chromatin architecture. Chromatin state modification could subsequently trigger boundary-specific gene expression (Fal et al., 2021), thus specifying boundary cell fate.

As presented in the introduction, the formation of leaf primordia is associated with a decrease in cell wall stiffness due to the increased activity of pectin methyl-esterases (Peaucelle et al., 2008). Furthermore, the cell wall properties modifications associated with primordium emergence were shown to originate from inner cell layers L2-L3 rather than the outer one L1 (Peaucelle et al., 2011). Hence, the decrease in stiffness could start earlier than anticipated inside of the growing primordia. It would be interesting to test whether *CUC3* expression promotion by mechanical stress also depends on the differential behavior of cells from inner layers. Conversely, the epidermis acts as a load-bearing layer that is submitted to the tension from beneath cell layers, and it is said to be crucial for organ shaping (Verger et al., 2018). Hence, the outer layer is often submitted to the highest tension. We could thus predict that the outer L1 layer in the boundary domain is the one triggering the strongest *CUC3* expression, which is coherent with the fact that drug-induced tension triggered higher *CUC3* expression (Fal et al., 2016). Only a dynamic visualization of a *CUC3* reporter line in three dimensions would show which cells start expressing *CUC3* at first in the boundary domain.

Perspectives to better understand cell wall mechanics

Our data on leaf mechanical properties show that sinuses and teeth display differential cell wall stiffness even at early stage of leaf development. This differential stiffness was reduced in the *spy-3* mutant where sinuses cell wall resembles more to teeth cell wall. As SPY and CUC2 act on a common molecular network related to cell wall loosening, we suggest that the *spy-3* mutant allows us to partly decompose the CUC2 function at stiffening the cell wall from its other growth-promoting and -repressing functions (promotion of targets like *KLUH* or *MIR164a*…). Our work reveals the contribution of cell wall mechanics to leaf morphogenesis, as local cell wall parameters will grandly impinge on the growth of the whole organ.

As said earlier, primordium emergence is associated with mechanical stresses that originate from inner cell layers (Peaucelle et al., 2011). Deciphering the mechanical stresses in volume in the SAM would give rise to a better resolution in a system that is often considered as a topological surface only. Even if the AFM is a very powerful tool to measure mechanical properties in the epidermis, its high resolution diminishes greatly as larger beads are used to

analyze inner cell layers. Hence, the use of the AFM is limited inside of organs. New mechanosensing tools would be of a great interest to report for mechanical changes. For example, in vertebrates, the tool GenEPi was developed based on animal *Piezo1* which encodes a stretch-activated Ca^{2+} channel. GenEPi is a powerful reporter line that provides a fluorescent signal that is proportionate to mechanical stress (Yaganoglu et al., 2019). Recently, Piezo1 homolog in plants was shown to have mechanosensing functions in the roots of *Arabidopsis* (Mousavi et al., 2021). Therefore, adapting this reporter line in plants would be of a great interest for future research in the domain of mechanical stress.

Since the boundary domain in the SAM was associated with re-orientation of the microtubules, a visualization of the microtubules orientation below the first layer, where mechanical stress emerges, would also constitute an interesting feature. In the leaf model, microtubules orientation observation in the marginal cells was not assessed so far to our knowledge. Establishing whether there are differences between sinuses and teeth microtubules would potentially provide a better understanding of how serrations are patterned at the margin.

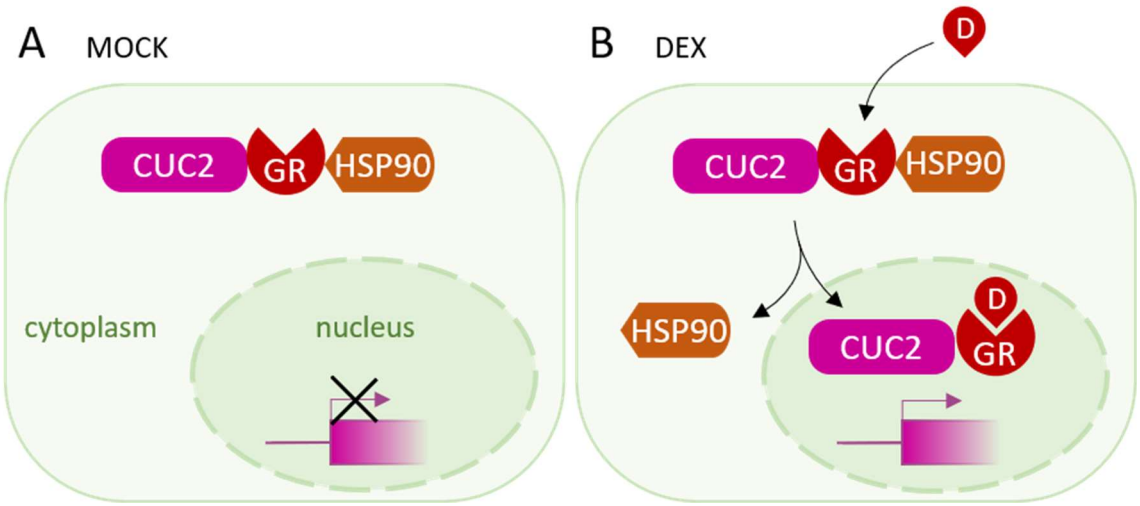

FIGURE 2-11: Operating concept of the *p35S:CUC2-GR* construction.
CUC2 is fused to the glucocorticoid receptor (GR) and ectopically expressed in the whole organism because of the ubiquitous *p35S* strong promoter. In the absence of dexamethasone (DEX, D), a synthetic steroid hormone specific to the glucocorticoid receptor (GR), the CUC2-GR fusion interacts with the heat shock protein 90 (HSP90) complex and is kept in the cytoplasm in an inactive state (Dalman et al., 1991). DEX treatment leads to disruption of the GR-HSP90 interaction, and ultimately allows CUC2-GR entrance into the nucleus. Once in the nucleus, the CUC2-GR fusion protein can bind to its DNA targets and trigger or repress transcription.

MATERIAL AND METHODS

Plant material and growth conditions

All plants used in this study are in the Columbia (Col-0) background except the *cuc2-1* mutant which was originally obtained in the Landsberg (Ler-0) background and back-crossed 5 times to Col-0. For dark grown hypocotyls experiments, seeds were surface sterilized and subsequently dispatched on 1% agar (w/v) Arabidopsis media with DEX or Mock treatment. DEX (Sigma, D1756) was dissolved in EtOH and used at a final concentration of 10 µM. The functioning of DEX induction is explained in Figure 2-11. Upon DEX application, the protein fused with the glucocorticoid receptor (GR) is freed from the HSP90 heat shock protein and is translocated into the nucleus. After 48 hours in the dark at 4°C, plates were transferred to growth chamber for 6 hours (21°C, light 50µM/m^2/s) before being placed vertically in the dark at 21°C. Plates were scanned after 72 hours of dark growth using a Perfection V800 Photo scanner (Epson) at 1600dpi.

Confocal imaging

pCUC2:RFP (Gonçalves et al., 2017) and *pCUC3:CFP* (Gonçalves et al., 2015) reporter lines were previously described. Confocal imaging was performed on F1 progeny from a *pSPY:SPY-GFP* in *spy-23* crossing with *pCUC2:RFP*, or from a *pSPY:SPY-GFP* in *spy-23* crossing with *pCUC3:CFP*. 3 weeks-old leaves of ranks 11-12-13 grown under SD conditions were dissected and mounted in confocal buffer containing TrisHCL, 10mM, pH = 8.5, Triton 0.01% (v/v). Samples were observed with a Leica SP5 inverted microscope (Leica Microsystems, Wetzlar, Germany; http://www.leica-microsystems.com/). GFP was excited at 514nm and detected within [524-630] nm using a hybrid detector. pCUC2:RFP was excited at 514nm and detected within [524-630] nm with a PMT detector. pCUC3:CFP was excited at 461nm and detected with a PMT detector within [524-630] nm.

Hypocotyl and cell length quantifications

Hypocotyl sizes were measured using the NeuronJ plugin from Fiji and data were analyzed using R software (R Core Team, 2016). For hypocotyl cell length measurements, samples were harvested from previously measured plates and fixed in paraformaldehyde (PFA 4%, triton 0,1%). Samples were fixed under vacuum for 1 hour after 3 vacuum breaks. Then, three 5 minutes-long rinses were performed in PBS, prior transferring in Clearsee (xylitol 10%, urea 25%, deoxycholate15% (Ursache et al., 2018)) + Direct red23 (0,01%) for one week at room temperature. Samples were mounted in Clearsee and observed with a Leica SP5 inverted or Leica TCS SP8X upright laser scanning confocal. Direct Red 23 was observed following a 561-nm excitation and using a [580–615] nm detection spectrum.

Expression level quantification

15 days-old seedlings grown in LD conditions on plates were pulled in 1.5 mL ependorf tubes up to 100µm of total mass and instantly immersed in liquid nitrogen. Alternatively, the 72-hours-old hypocotyls from DEX induction and length measurements in the dark were used. Total RNAs were isolated using RNAeasy Plant Mini Kit (Qiagen) following the manufacturer recommendation for plant tissue. For transient induction using DEX, 35S::CUC2-GR seedlings were grown in liquid Arabidopsis medium with constant shaking. After 10 days of growth under constant light, seedlings were treated with 10µM DEX for 6 h and then frozen in liquid nitrogen. Total RNA extraction was performed with the miRvana extraction kit (Ambion) following the manufacturer's recommendations. In both cases, reverse transcription was performed using RevertAid H Minus

M-MuLV Reverse transcriptase (Fermentas) followed by a RNAse H treatment was performed for 20 min 37°C to eliminate DNA-RNA duplexes. Real time PCR analysis was performed on a 384-well QuantStudio™ 5 Real-Time PCR System, using the SsoAdvance Universal SYBR Green Supermix with the following PCR conditions: 95˚C 3min; (95˚C 15s; 63˚C 30s) x40 cycles. Raw data was analyzed using Design & Analysis 2.2 software. Primers used for real time PCR analysis are available in S1 Table. Expression data were normalized using the ΔΔCt method using at three independent reference genes (*qREF*, *Actin2* and *EF1α*).

Cell wall mechanical properties quantification

For mechanical characterization of leaf cell walls, col-0 and *spy-3* plants were grown on soil in SD conditions (see material & methods, chapter 1). About 100-200 µm-long young leaf primordia from rank higher than 10 were hand-dissected under a stereomicroscope and collected. Samples were plasmolyzed by immersion in sorbitol 10% (m/v) and the excess was dried just before imaging. An AFM cantilever loaded with a 1µm tip was used in these measurements, for which 100µm*30µm areas were scanned with a fixed indentation value of 800 nm (maximum authorized deformation for each point of data). Apparent Young's modulus (Ea) was determined by a Hertzian indentation model on each indentation point. Cells topography was reconstructed using the height at each point of contact. Data were analyzed and maps were plotted using Matlab.

Chapter 3

Integration of local growth repression to leaf hormonal signaling

INTRODUCTION

So far, our investigations brought us to the study of the control of cell elongation dependent on CUC activity. In the previous chapter, we used the hypocotyl as a model for the study of CUC2 effect on cell elongation and demonstrated that CUC2 induction is able to induce cell growth repression. As CUC2 induced overexpression negatively regulates genes that are involved in cell elongation in dark grown hypocotyl, we suggest that CUC2 might be intervening in the control of cell elongation in various developmental contexts.

Recent studies have demonstrated that hypocotyl growth in dark conditions is mainly driven by the activation of phytohormonal pathways (Gendreau et al., 1997; Oh et al., 2014). In addition, mutant lines that exhibit impaired phytohormonal pathway often display shortened hypocotyls in the dark. For example, GAs regulate hypocotyl elongation in the dark as *ga1* GA-deficient mutants display smaller hypocotyls than the wild type (Cowling and Harberd, 1999). In addition, this phenotype can be rescued by bioactive GA supplementation. Similarly, BR biosynthetic mutants such as *de-etiolated 2 (det2)* display dwarf hypocotyls (Li et al., 1996; Clouse and Sasse, 1998). Finally, auxin also mediates cell elongation in darkness (Franklin et al., 2011; Reed et al., 2018; Ma and Li, 2019). Furthermore, hypocotyl elongation in the dark is triggered by the activity of PHYTOCHROME INTERACTING FACTORs (PIFs) which control dark/light environment perception (Choi and Oh, 2016). Several evidences indicate that these hormonal pathways intertwine to promote hypocotyl growth (Franklin et al., 2011; Zhou et al., 2013). Furthermore, the sets of genes targeted by these different pathways largely overlap (Oh et al., 2014). As CUC2 overexpression is able to inhibit hypocotyl growth in the dark, we suggest that CUC2 could interfere with the growth-promoting phytohormonal pathways and act as a major growth negative regulator.

As growth in other developmental contexts is also driven by phytohormones, we propose that CUC2 could modify hormonal pathways in other organs as well. In the following chapter, we want to test whether CUC2 is also able to modulate hormonal responses. For every hormone, multiple hypotheses are to take into consideration. Indeed, CUC2 could directly antagonize growth-promoting effects by binding to and/or repressing specific DNA targets of TFs triggering phytohormones responses. Conversely, CUC2 could target key TFs through protein-protein interactions to prevent them from binding to their DNA targets. Another possibility is that CUC2 directly impinges upon phytohormones metabolism. For this reason, we decided to mainly focus on two hormonal pathways strongly linked with growth: the gibberellin pathway and the auxin pathway.

RESULTS

CUC2 signaling pathway interferes with GA

CUC2 negatively regulates GA biosynthesis

Over the previous chapters, we demonstrated that CUC2 is genetically linked with SPY, probably because they share common targets and both trigger modifications of the cell wall properties that ultimately modify cell growth. Yet, as SPY is described as a major GA repressing enzyme, one can suggest that the GA signaling pathway and CUC2 have opposing and competing effects on growth.

The two main hypotheses in consideration when suggesting CUC2 negatively interferes with GA pathways, are that CUC2 interferes with GA metabolism or response pathway. In order to test the former, our transcriptomic data were re-observed and showed a slight over-representation of GA signaling pathway-related genes (10 genes were listed among 1877 mapped genes IDs from the list of 2569 genes that are down-regulated upon CUC2 induction. Enrichment fold was 3.25, p-value 2.35E-03 (Fisher exact test), FDR=3.38E-02). Among those genes, we chose to verify whether *GA3ox1* expression is reduced upon *CUC2* induction (Figure 3-01). *GA3ox1* encodes ARABIDOPSIS THALIANA GIBBERELLIN 3 BETA-HYDROXYLASE 1, a key gene for GA biosynthesis as it is responsible for the last step of bioactive GA_4 biosynthesis.

We measured gene expression levels for *GA3ox1* in a *p35S:CUC2-GR cuc2-3* line and found out that transcript levels were decreased by about 70% upon DEX-induced CUC2 expression (Figure 3-01). No significant change in gene expression was observed in the *cuc2-3* control upon DEX treatment. However, *GA3ox1* transcripts level was significantly higher in a *cuc2-3* mutant than in the wild type (Figure3-01A). We then wanted to test whether CUC2 directly targets *GA3ox1* to repress its expression. To do so, liquid grown *p35S:CUC2-GR cuc2-3* 10 days-old seedlings were treated with cycloheximide prior to a 6 hours-long DEX induction, in order to prevent *de novo* protein translation and reveal the TF-targets interactions. While untreated DEX-induced samples displayed a decrease in *GA3ox1* transcript level, samples treated with cycloheximide did not exhibit any change in expression level, indicating that CUC2 effect on *GA3ox1* expression may be indirect (Figure 3-01). However, these last measurements also show that a 6 hours induction is sufficient to observe a difference in *GA3ox1* expression.

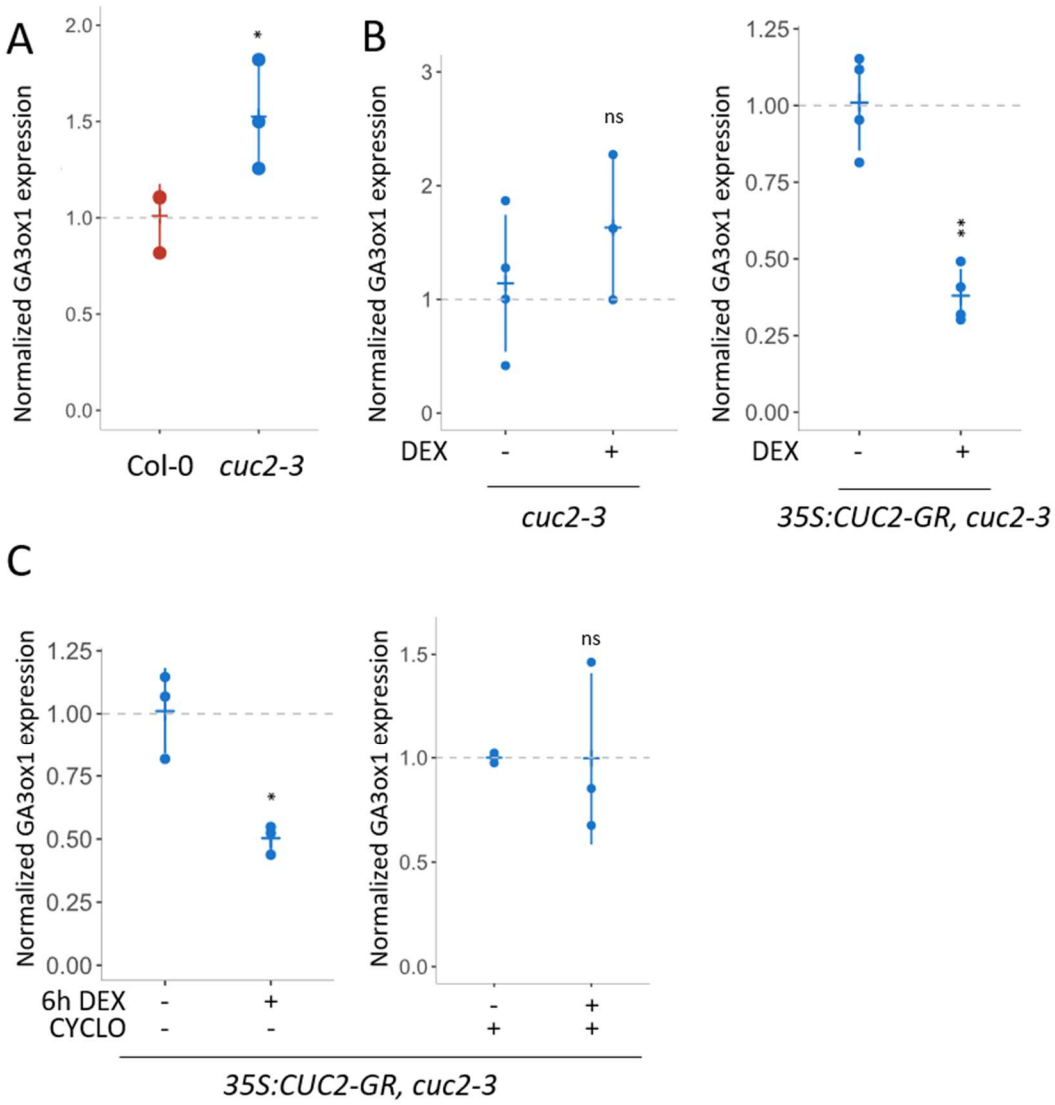

FIGURE 3-01: *GA3ox1* expression is indirectly repressed by CUC2.

A. Expression level of *GA3ox1* in *cuc2-3* and wildtype B. Expression level of *GA3ox1* in *cuc2-3* and *p35S:CUC2-GR, cuc2-3* treated with mock or 1µM dexamethasone. C. Expression level of *GA3ox1* in *p35S:CUC2, cuc2-3 in vitro* cultures induced or not with 10µM DEX for 6 hours. In the right panel, seedlings were treated 6 hours with 10µM cycloheximide, to inhibit translation. A,B,C. Each dot represents a biological RNA sample. *GA3ox1* transcript levels were measured by real-time quantitative RT-PCR and normalized by *EF1α* and *Actin2.* Statistical significance (Student's test) is designated by ns=not significant, * $p<0.05$, ** $p<0.01$.

Still, it is possible that GA pathways are negatively regulated locally in the CUC2 expressions domain due to a local but indirect repression of GA biosynthesis. A dosage of the different GA metabolites would help to determine whether GA biosynthesis pathway is modified in CUC2 expression domains. If our hypothesis is correct, we could potentially observe a decrease in the concentration of bioactive GA_4 in favor of an increase in the concentration of its precursors GA_9 (as well as GA_9 alternative products GA_{20}, $GA_{16/17}$, GA_{51}). Another way to visualize GA signaling levels *in vivo* would be the use of reporter lines. As DELLA proteins are rapidly degraded upon GA application (Ueguchi-Tanaka et al., 2007; Suzuki et al., 2009; Hirano et al., 2010), a visualization of dynamic DELLA protein levels disappearance would allow deciphering domains where GA are active. I used a pRGA:RGA-GFP reporter line to visualize RGA expression pattern in the leaf (data not shown), however this live observation did not allow to quantify the dynamic of DELLA disappearance, because of the sample thickness that did not let us determine if RGA-GFP signal was lower locally. One possibility would be to use a DELLA reporter in concert with a ubiquitous reporter. Hence, DELLA dynamic would be indicated as the ratio between a translational-fusion DELLA construct and the ubiquitous reporter. Such constructs are under development in other labs. Their observation in leaves will be critical to provide a better understanding of the contribution of GA to leaf morphogenesis.

Two *della* mutants display leaf margin phenotypes

SPY has been initially described as a major GA signaling repressor (Jacobsen and Olszewski, 1993; Jacobsen et al., 1996). Indeed, SPY was soon characterized as an activator of DELLA protein activity (Silverstone et al., 2007). Most recent data indicate that SPY could O-fucosylate DELLA protein to promote their folding into a more active conformation (Zentella et al., 2017). Hence, it is thought that in a *spy* null mutant, DELLA proteins remain in an inactive state, thus triggering the GA constitutive phenotype exhibited by *spy* mutant plants. In order to test whether *spy-3* leaf phenotypes are mediated by the DELLA post-translational modification pathway, two *della* mutant leaf phenotypes were analyzed. Since RGA and GAI are the most studied DELLA proteins as well as the most expressed in the leaf (Schmid et al., 2005, data visualized in ePlant tool of the Bio-Analystic Resource for Plant Biology), the two loss-of-function mutants for RGA and GAI namely *rga-28* and *gai-t6* were used (Figure 3-02). The morphology of 6 weeks-old, SD grown mature leaves of ranks 11 to 13 was quantified between the two *della* mutants. The two mutants did not display any particular differences in term of global shape, neither in terms of blade length (29.81 mm ± 3.17 mm for col-0, 29.89 mm ± 3.01 mm for *rga-28,* 31.88 mm ± 1.50 mm for *gai-t6*, no significant differences in ANOVA),

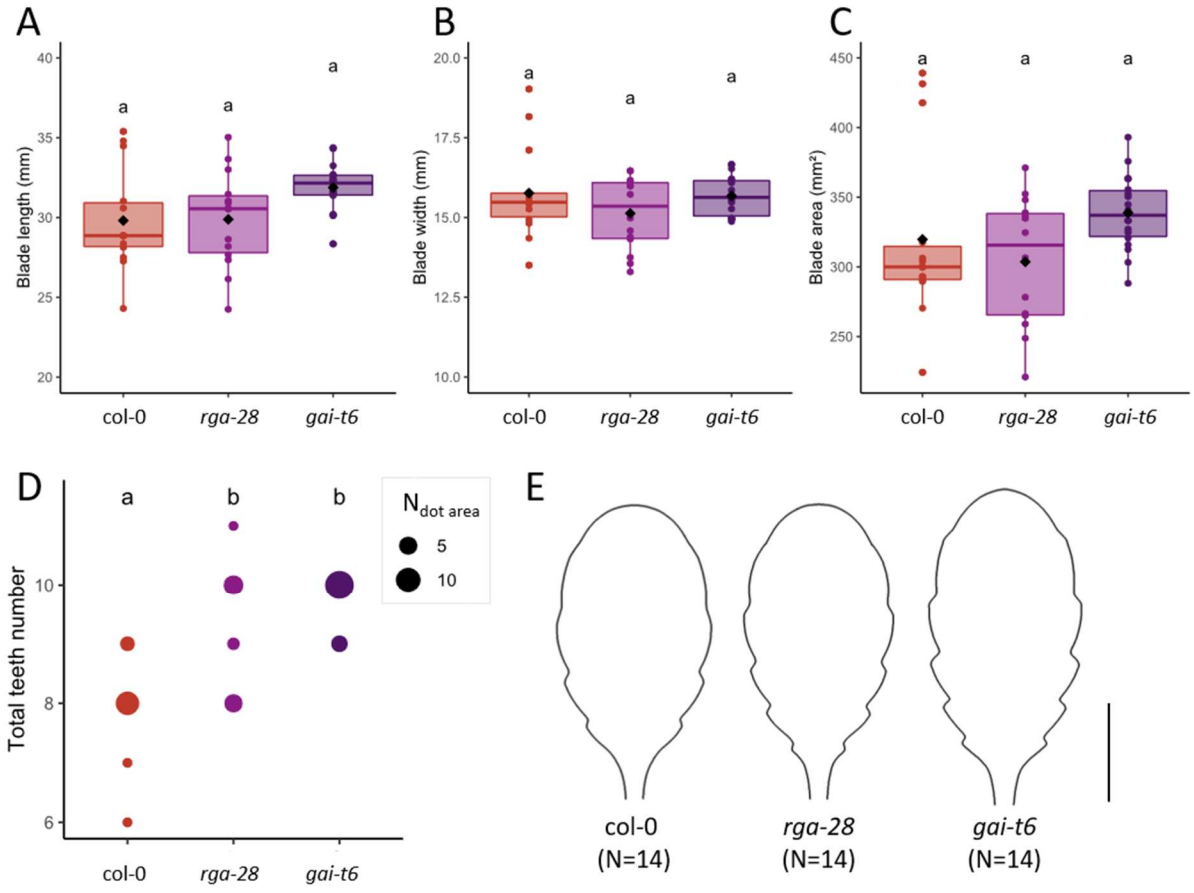

FIGURE 3-02: Two loss-of-function *DELLA* mutants display over-serrated phenotype

A. Maximal blade length of col-0, *rga-28* and *gai-t6* (mm) B. Blade width of col-0, *rga-28* and *gai-t6* (mm) C. Blade area of col-0, *rga-28* and *gai-t6* (mm^2). D. Counts of total teeth number in col-0, *rga-28* and *gai-t6.* The more leaves in the total population display a given number of teeth, the larger the point. E. Mean contours of the mature leaves for each genotype generated with Morpholeaf software (Biot et al., 2016). Scale bar is 1cm. A, B, C, D, E. col-0 (N=14), col-0, *rga-28* (N=14) and *gai-t6* (N=14) 6 weeks-old leaves grown in short-day condition L11/12/13 were used. Statistical one-way ANOVA analysis, followed by Tukey comparison test.

nor for blade width (15.76 mm ± 1.45 mm for col-0, 15.13 mm ± 1.13 mm for *rga-28*, 15.68 mm ± 0.61 mm for *gai-t6*, no significant differences in ANOVA). Consequently, leaves displayed similar areas (319.7 mm^2 ± 63.4 mm^2 for col-0, 303.7 mm^2 ± 46.4 mm^2 for *rga-28*, 338.8 mm^2 ± 26.5 mm^2 for *gai-t6*, no significant differences in ANOVA).

Remarkably, *rga-28* and *gai-t6* both exhibited higher total number of teeth on their margins (8 ± 0.8 for col-0, 9.2 ± 1.1 for *rga-28*, 9.7 ± 0.4 for *gai-t6*, $p\text{-value}_{rga\text{-}28/\text{col-}0}<0.001$, $p\text{-value}_{gai\text{-}t6/\text{col-}0}<0.001$, post-hoc TUKEY test). This result suggests that a partial lack of DELLA activity (since DELLA act partially redundantly in all organs (Gallego-Bartolomé et al., 2010; Lantzouni et al., 2020)) leads to increased teeth initiation at the leaf margin. In other words, DELLA seems to act as tooth initiation repressor in the leaf. Interestingly, in the leaf developmental trajectories we performed in chapter 1 on wild type and *spy-3* plants, differences of total teeth number were already observed but not consistently across development. In addition, total teeth number quantification is not possible in mature *spy-3* leaves as the margins are very smooth. Hence, it is possible that *spy-3* also has a slight effect on tooth initiation through the modulation of DELLA proteins activity. However, we may not have been able to count teeth accurately at late developmental stages.

As *della* mutants do not exhibit as many teeth as in the *spy-3* mutant, teeth positions are altered along the leaf margin. Hence, we chose not to perform further teeth morphology comparison as teeth ranks are not likely to be properly conserved. Moreover, since *della* mutants did not display an overall *spy*-like phenotype, we must consider that the repressive tooth outgrowth effect of SPY that we described in chapter 1 and 2 is independent from SPY activity towards DELLA proteins. Alternatively, it is also possible that the functional redundancy of DELLA proteins prevented us from observing any stronger phenotypes. Still, *in vitro* demonstration of DELLA fucosylation by SPY protein was only demonstrated on RGA and RGL1 (Zentella et al., 2017). Hence, we suggest that SPY is involved in a mechanism that is linked either with leaf global growth and/or GA-triggered proliferation/differentiation switch.

GA could repress tooth outgrowth

Next, we aimed at understanding the effect of GA on tooth outgrowth. To do so, we performed treatments on seedlings grown either on Paclobutrazol (which inhibits an early step in the GA biosynthesis), mock medium, or medium supplemented with 1µM GA_3. Plants grew *in vitro* in these conditions and were then dissected and imaged to quantify their leaf phenotype (Figure 3-03). As GA are involved in the overall growth of organs (Cowling and Harberd, 1999; Ubeda-Tomás et al.,

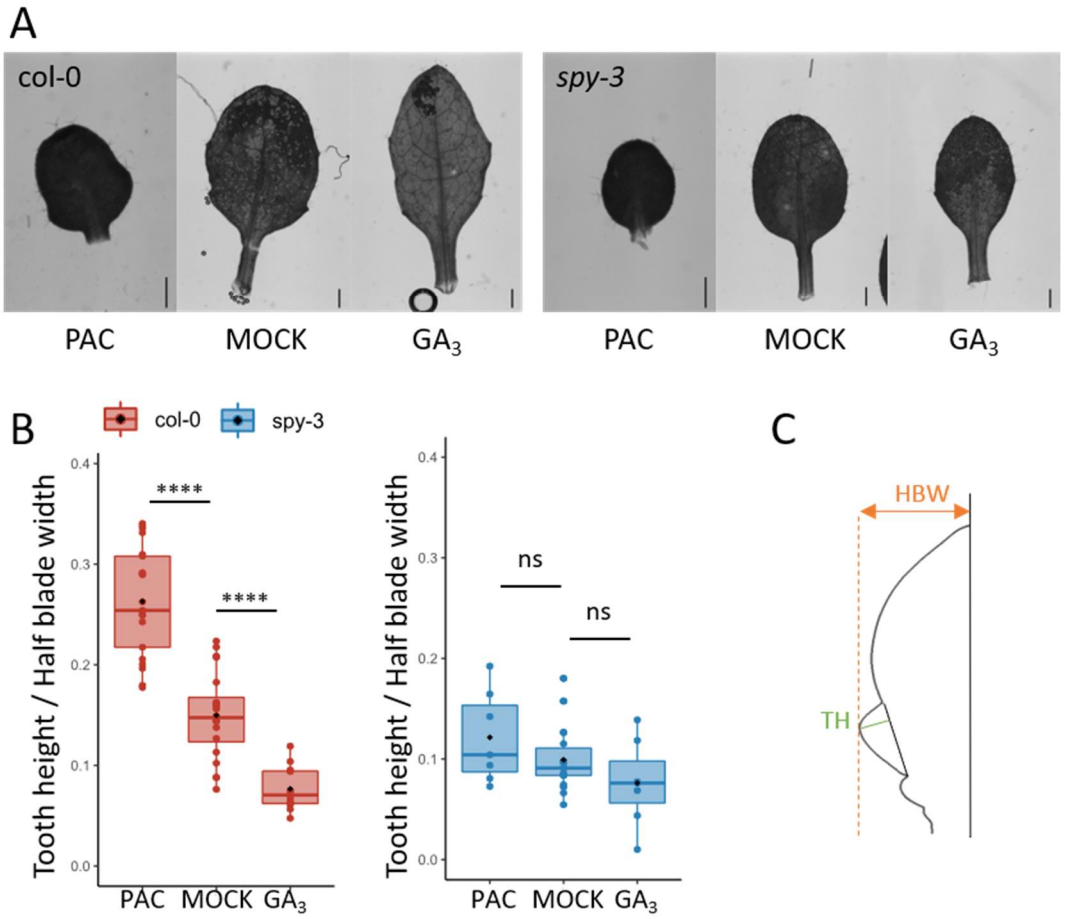

FIGURE 3-03: The effects of GA levels on tooth outgrowth are abolished in *spy-3* mutant.

A. Representative images of leaves of rank 4 from 15 days-old col-0 and *spy-3* seedlings grown *in vitro* in mock medium or treated either with 1µM Paclobutrazol or with 1µM GA_3. Scale bar is 500µm. B. Representation of lateral tooth outgrowth, as the first tooth height over blade half width for col-0 and *spy-3* leaves, either sown *in vitro* on mock medium or treated either with 1 µM of Paclobutrazol or with 1µM of GA_3. C. Schematic representation of the first tooth height and half blade width used to calculate tooth outgrowth in panel B.

2008; Achard et al., 2009; Sauret-Güeto et al., 2012), it was not surprising to observe intense changes in leaf global shapes. Indeed, PAC-treated leaves of rank 4 were very small, while GA_3-treated plants exhibited longer leaves. In the *spy-3* mutant, GA_3-treated plants did not exhibit much longer leaves compared to the untreated wild type plants in our growth conditions, meaning that leaf growth is not responsive to bioactive GA treatments in *spy-3*, which is already GA-constitutive (even if previous results demonstrates that in some contexts, *spy* mutant are still responsive to GA treatments (Jacobsen et al., 1996)). However, in our growth conditions, PAC-treated *spy-3* mutants displayed dwarf phenotypes as in col-0, suggesting that other routes exist down-stream of GA and independently from SPY to promote organ growth.

With such different global leaf shapes, a new proxy to quantify tooth growth was established. Hence, lateral tooth outgrowth, as the first tooth height over the half blade width (HBW), was used to quantify shape (Figure 3-03C). The second tooth was not used in this experiment because PAC-treated wild type plants did not initiate any. Furthermore, blade length was not used as a normalization tool to quantify tooth outgrowth, first because this value varies enormously between treatments. Second, blade length elongation is perpendicular to tooth outgrowth while tooth height and blade width elongate in the same direction. HBW is thus a better criterion than blade length to normalize tooth outgrowth in such diverse leaf samples. Consequently, when plotting lateral tooth outgrowth, PAC-treated col-0 leaves yielded to significantly higher ratios than the mock-treated plants. On the contrary, GA_3-treated plants exhibited significantly lower ratios than the control (Figure 3-03B). This suggests that bioactive GA negatively regulates tooth growth, since the first tooth becomes smaller relative to the leaf size as GA concentration increases. Conversely, GA concentration has no influence on tooth outgrowth in the *spy-3* background, since no significant differences was observed between treatments. This indicates that SPY is necessary for GA effect on tooth outgrowth, but not on global leaf shape and size. Hence, we can suppose that in our growth conditions SPY is not involved in the GA-mediated control of leaf growth, but is locally involved in the control of leaf margin development. This hypothesis is consistent with results obtained on untreated, mature leaf shapes observed in chapter 1 (Figure1-03). No differences were observed neither on blade length nor on its width between *spy-3* and the wild type, while teeth were much smoother in the mutant.

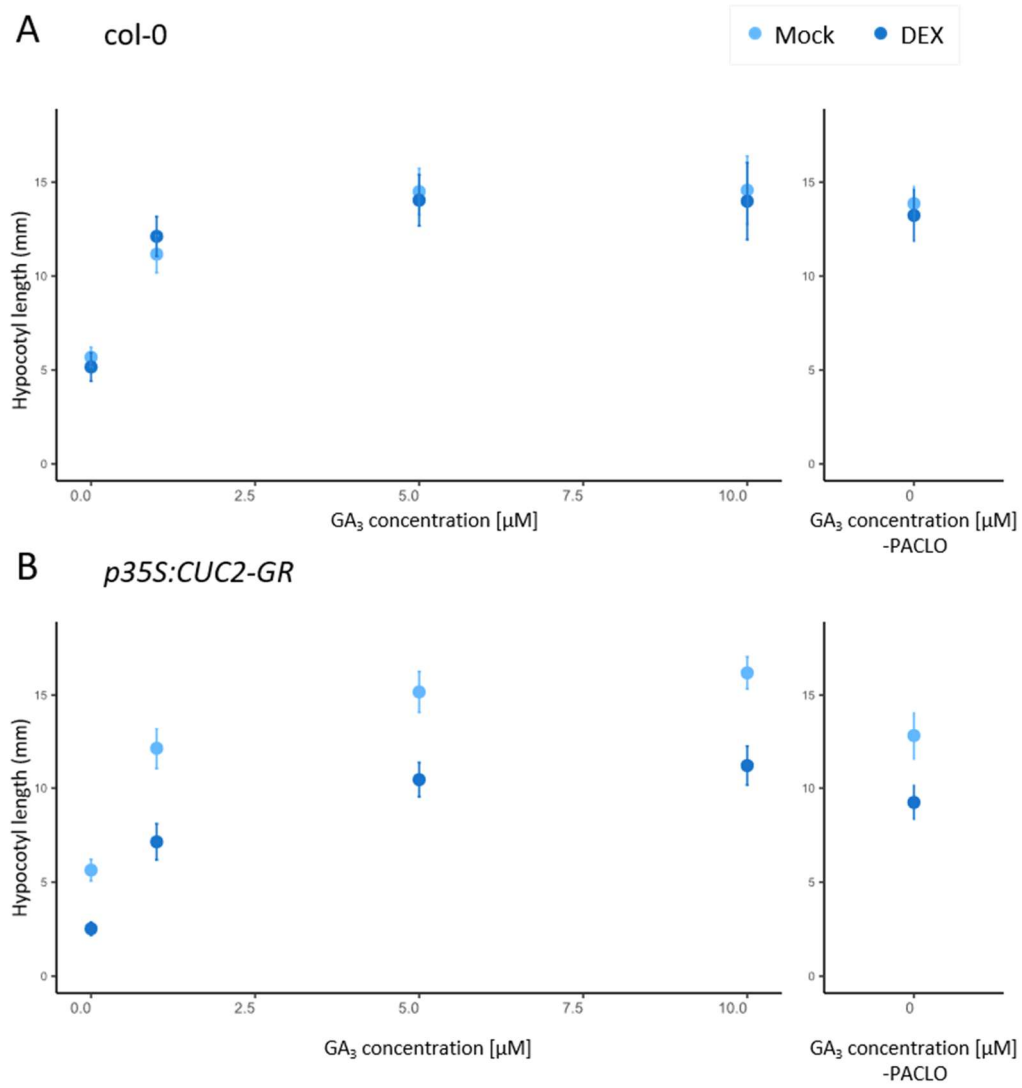

FIGURE 3-04: Dynamics of response to GA is unchanged over CUC2 induction

A. Mean hypocotyl length in col-0 three days-old seedlings treated with 1µM Paclobutrazol and with increasing concentrations 0, 1, 5 and 10 µM of GA_3. The right panel represents PACLO/GA_3 untreated control. B. Mean hypocotyl length in *p35S:CUC2-GR* three days-old seedlings treated with 1µM Paclobutrazol and increasing concentrations of GA_3. Right panel represent untreated hypocotyls. A, B. On left panels, 1 µM Paclobutrazol was used to inhibit endogenous GA production. Seeds were either sown on mock medium (light blue) or on 1µM dexamethasone containing medium (darker blue). Error bars represent standard deviation.

CUC2 induction does not alter the hypocotyl growth responses to GA

Next, in order to further study the interaction between CUC2 and GA hormonal pathway at controlling cell growth, we chose to quantify dark-grown hypocotyl elongation in response to various GA concentrations. Experiments were performed on Paclobutrazol-containing plates to get rid of endogenous bioactive GA_4 supplemented with various GA_3 concentrations (Figure 3-04). In col-0, increasing levels of GA_3 yielded to longer hypocotyls. After 6 days of growth in the dark, hypocotyl from 5 µM GA_3-treated seedlings were about 15 mm of total length. Higher GA_3 concentration did not trigger longer hypocotyls, suggesting GA response was maximal from 5 µM GA_3. Paclobutrazol untreated, GA_3 untreated, dark-grown hypocotyls displayed about 14 mm-long hypocotyls, which suggests GA response is maximal in those growth conditions. This result indicates that dark-grown hypocotyls contain endogenous GA, which justified the use of Paclobutrazol to suppress endogenous GA. Conversely, Paclobutrazol treatment with no or low GA_3 treatment yielded to smaller hypocotyls, indicating that bioactive GA are necessary to proper hypocotyl elongation in dark conditions. Paclobutrazol-treated seedlings were responsive to exogenous GA until a certain threshold, while higher exogenous GA levels did not trigger even longer hypocotyls. We calculate that 600nM of GA_3 are sufficient to trigger 50% of the total hypocotyl response to GA. We suggest that hypocotyls respond to GA in a dose-dependent manner, and that the GA concentration threshold for elongation response corresponds to the endogenous response that we observe in Paclobutrazol-untreated plants. In addition, DEX treatment had no influence on col-0 hypocotyl length in those growth conditions (Figure 3-04A). Conversely, 1µM DEX treatment was sufficient to inhibit hypocotyl elongation in *p35S:CUC2-GR* (Figure 3-04B). Paclobutrazol and DEX had additive, repressive effects on hypocotyl lengths as 1 µM DEX, 1 µM PACLO hypocotyls are about 2.5 mm-long in those conditions. Nevertheless, DEX-treated seedlings were still able to respond to GA. We calculated that the dose that allows 50% of the hypocotyl response is still around 600 nM of GA_3, which suggest the dynamic of response to bioactive GA is unchanged in DEX-induced *p35S:CUC2-GR*. Based on previous experiments, where CUC2 negatively regulated the expression of GA biosynthesis genes, we could speculate that CUC2 induction reduced growth in the dark by repressing GA biosynthesis. However, CUC2 repression of GA biosynthesis would imply a restoration of wild type hypocotyl length at high exogenous GA levels. Here, a new growth limit is set for hypocotyl growth upon CUC2 induction, which suggests CUC2 has GA-independent, growth-limiting effects on hypocotyl elongation.

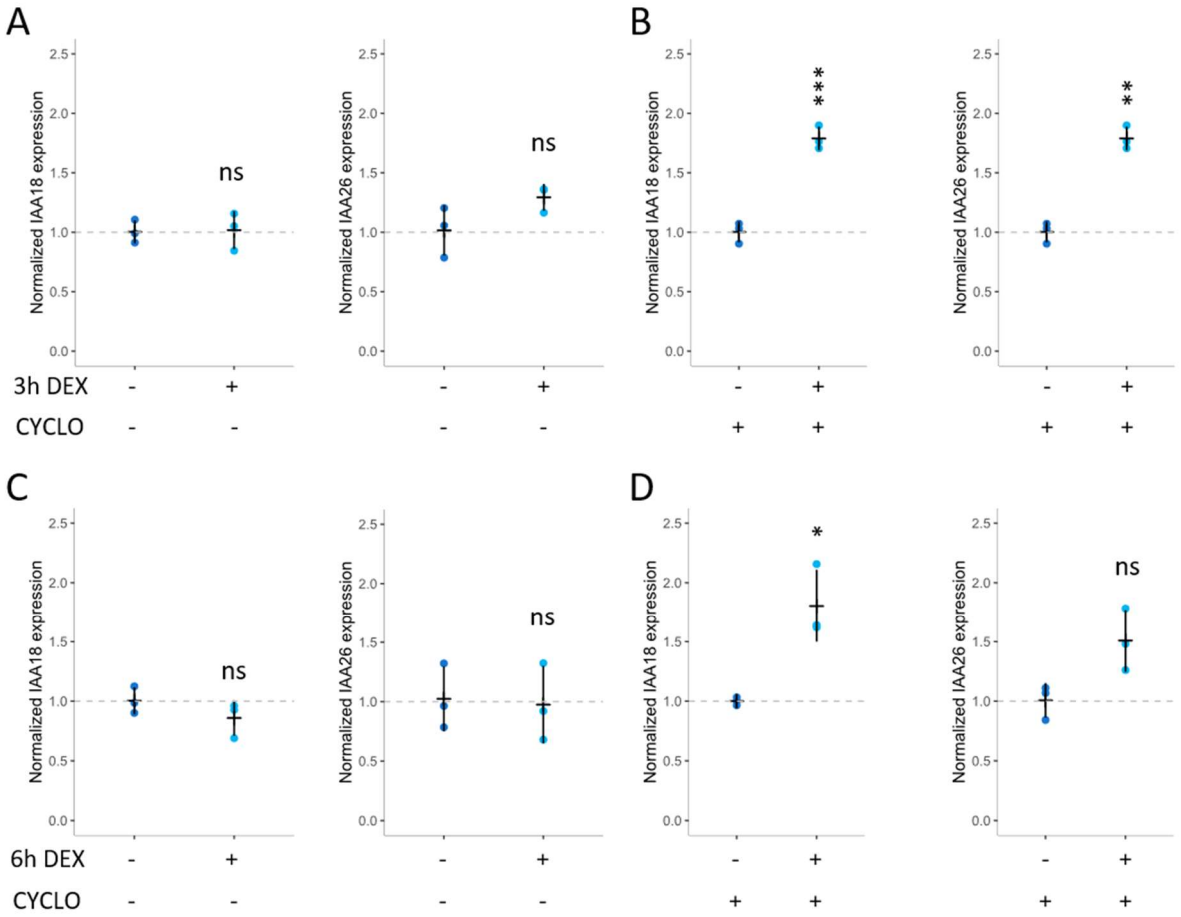

FIGURE 3-05: IAA18 and IAA26 are direct targets of CUC2.

A. Expression level of *IAA18* and *IAA26 p35S:CUC2-GR, cuc2-3* treated with mock or 10µM dexamethasone for 3 hours. B. Expression level of *IAA18* and *IAA26 p35S:CUC2-GR, cuc2-3* treated with 10µM of Cycloheximide and either mock or 10µM dexamethasone for 3 hours C. Expression level of *IAA18* and *IAA26 p35S:CUC2-GR, cuc2-3* treated with mock or 10µM dexamethasone for 6 hours. D. Expression level of *IAA18* and *IAA26 p35S:CUC2-GR, cuc2-3* treated with 10µM of Cycloheximide and either mock or 10µM dexamethasone for 6 hours A-D. Each dot represents a biological replicate. *IAA18 and IAA26* transcript levels were measured by real-time quantitative RT-PCR and normalized by *EF1α, REFA* and *qREF.* Statistical significance (Student's test) is designated by ns=not significant, * $p<0.05$, ** $p<0.01$, *** $p<0.001$.

Taken together, our data suggest that CUC2 and GA signaling have opposite, independent effects on cell elongation in the dark-grown hypocotyl model.

CUC2 signaling interferes with Auxin signaling

We then investigated whether CUC2 is able to impinge on auxin-mediated hypocotyl growth. Indeed, auxin is directly involved in the wall modifications at the origin of cell elongation and we have shown that CUC2 has effects on wall rigidity as well as on the expression of proteins modifying wall properties. Furthermore, the combination of three AUXIN RESPONSE FACTORS (ARFs) mutants was sufficient to repress hypocotyl growth in the dark and yield CUC2-overexpression-like hypocotyls (Reed et al., 2018). As described in chapter 2, previous results indicate that the auxin pathway acts downstream of CUC2 to trigger serration formation. Indeed, CUC2 induction was shown to trigger the expression of *DR5* auxin response gene at the tip (Maugarny-Calès et al., 2019). In addition, CUC2 is necessary for PIN1 auxin efflux transport local relocalization (Bilsborough et al., 2011), hence for interspersed auxin maxima. Therefore, auxin responsive genes are good candidates to study an interaction with CUC2.

CUC2 positively regulates IAA18 and IAA26

IAA18 and *IAA26* are two auxin responsive genes that were identified as induced CUC2 targets in our transcriptomic study. AUX/IAA are nuclear-localized, early auxin responsive proteins that negatively regulates ARF transcription factors through direct protein-protein interactions. Upon auxin application, AUX/IAA are rapidly targeted by E3 ubiquitin ligases and consequently degraded by the 26S proteasome. If *IAA18* and *IAA26* are up-regulated upon CUC2 induction, then we suppose that CUC2 could negatively regulate auxin signaling pathway. We thus measured gene expression levels for *IAA18* and *IAA26* upon CUC2 induction using quantitative RT-PCR (Figure 3-05). Experiments were conducted either with or without a cycloheximide treatment, to test whether the transcriptional activation is direct. In addition, several DEX treatment durations were performed to evaluate the dynamic of CUC2 induction response. In presence of cycloheximide, both *IAA18* and *IAA26* were upregulated when inducing CUC2, no matter the duration of treatment (three or six hours-long treatments) (Figure 3-05B, D). The increase in gene expression was not significant for *IAA26* after 6 hours of DEX treatment but all three measured gene expression varied towards an upregulation. Together, our gene expression quantification in presence of cycloheximide show that CUC2 directly upregulates both *IAA18* and *IAA26,* confirming our transcriptomic data. Surprisingly, no such increase in gene expression was observed, for neither of the two genes, in the absence of

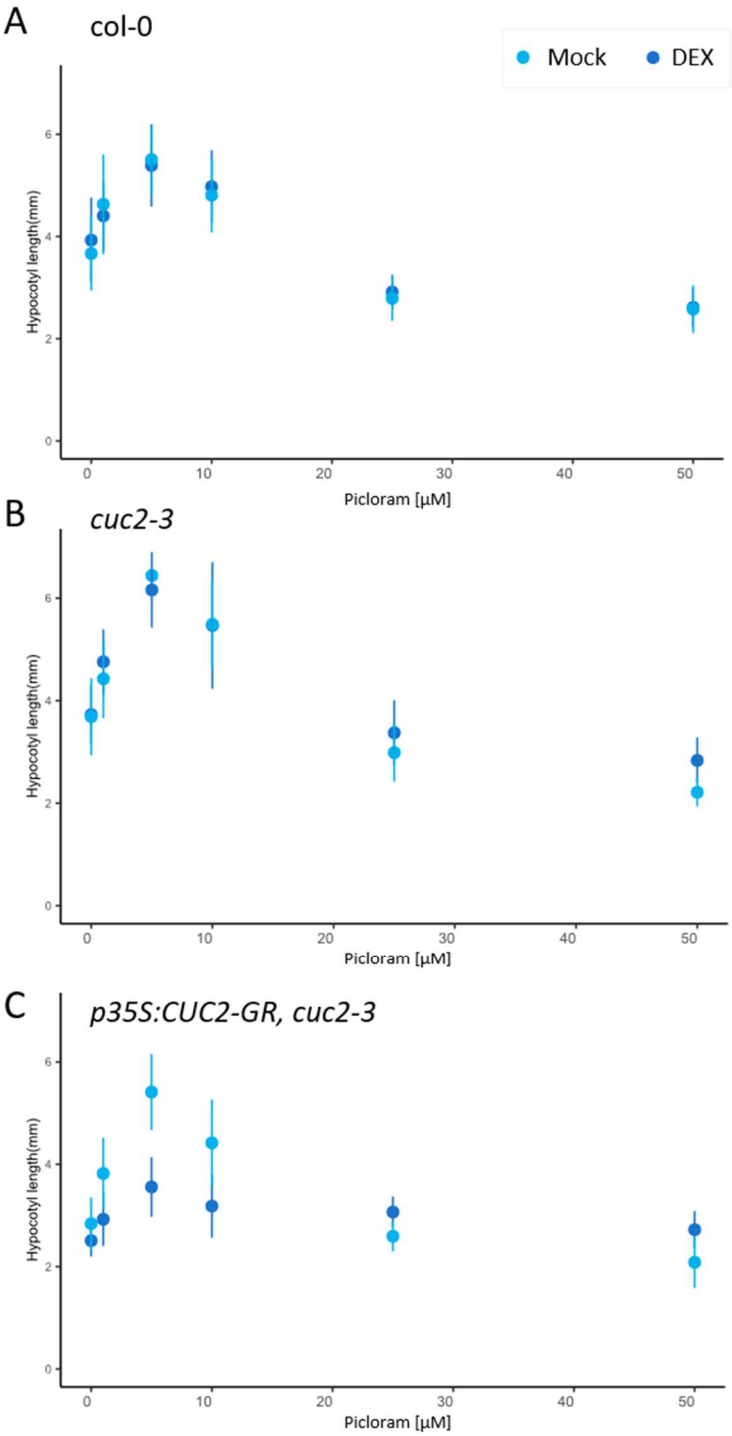

FIGURE 3-06: Dynamics of response to Picloram decreases over CUC2 induction

A. Mean hypocotyl length in col-0 three days-old seedlings treated with increasing concentrations 0, 1, 5, 10, 25 and 50 µM of Picloram. B. Mean hypocotyl length in *cuc2-3* three days-old seedlings treated with increasing concentrations of Picloram. C. Mean hypocotyl length in *p35S:CUC2-GR, cuc2-3* three days-old seedlings treated with increasing concentrations of GA_3. A, B. Seeds were sown *in vitro* on medium containing 1 µM Paclobutrazol to inhibit endogenous GA production. Seeds were either sown on mock medium (light blue) or on 1µM dexamethasone containing medium (darker blue). Error bars represent standard deviation.

cycloheximide (Figure 3-05A, C). This might be due to some indirect mechanism, potentially some feedback, by which CUC2 is not able to repress the expression of IAA 18 and IAA 26 genes in a cycloheximide-free context.

Hypocotyl elongation in response to auxin is altered upon CUC2 induction

As CUC2 might directly promote the expression of two repressors of auxin signaling, we wanted to test whether CUC2 functionally interacts with auxin response pathway. To do so, we used once more p*35S::CUC2-GR /* hypocotyl system and applied increasing picloram concentrations in presence or absence of CUC2 (Figure 3-06). Picloram is an auxin analog known to stimulate hypocotyl growth (Chapman et al., 2012). We observed a dose response curve with increasing Picloram concentrations, confirming that Picloram treatments are able to trigger -and repress at higher concentration- hypocotyl growth and in our experimental conditions. In both col-0 and *cuc2-3*, mock and DEX-treated hypocotyls yielded to very similar lengths (Figure 3-06A, B). From mock to 10µM, Picloram had a positive effect on hypocotyl growth. Both mock and DEX-treated wild type hypocotyls were longer by about 2 mm when treated with 5µM Picloram ($L_{\text{col Mock 5µM piclo}}$=5.5 ±0.7 mm) compared to untreated hypocotyls ($L_{\text{col Mock 0µM piclo}}$=3.6 ±0.7 mm). Remarkably, *cuc2-3* increased even more than the wild type in response to 5µM Picloram ($L_{\textit{cuc2-3}\text{ Mock 5µM piclo}}$=6.4 ±0.7 mm) compared to untreated hypocotyls ($L_{\textit{cuc2-3}\text{ Mock 0µM piclo}}$=3.7 ±0.7 mm).

Furthermore, a similar increase in hypocotyl length has been observed in DEX-untreated, 5µM Picloram *p35S:CUC2-GR, cuc2-3* hypocotyls compared to Picloram-untreated hypocotyls ($L_{\textit{p35S:CUC2-GR, cuc2-3}\text{ Mock 5µM piclo}}$=5.4 ±0.7 mm and $L_{\textit{p35S:CUC2-GR, cuc2-3}\text{ Mock 0µM piclo}}$=2.8 ±0.5 mm) (Figure 3-06C). This result is still consistent with CUC2 acting as a break towards auxin signaling-triggered growth. DEX-treated *p35S:CUC2-GR cuc2-3* hypocotyls responded to Picloram treatment to a lesser extent than in the mock treated condition. At 5µM Picloram, hypocotyl length increased less in DEX-induced *p35S:CUC2-GR cuc2-3* than in any other conditions ($L_{\textit{p35S:CUC2-GR, cuc2-3}\text{ DEX 5µM piclo}}$=3.6 ±0.6 mm and $L_{\textit{p35S:CUC2-GR, cuc2-3}\text{ DEX 0µM piclo}}$=2.5 ±0.3 mm). This result suggests that in presence of high levels of CUC2, auxin effects on hypocotyl length are weaker. Here again, CUC2 interferes negatively with auxin response pathway and reduces its effects on hypocotyl elongation. Based on the foregoing results, we can hypothesize that CUC2 negatively interferes with auxin signaling by increasing the expression of IAAs which, in turn, negatively regulate the auxin response.

From 10µM picloram, we observed that Picloram had repressive effects on growth in both the wild type, *cuc2-3* and *p35S:CUC2-GR cuc2-3*. A 25µM treatment was sufficient to get shorter hypocotyls than those that grew with no Picloram ($L_{col\ Mock\ 25\mu M\ piclo}$=2.8 ±0.4 mm, $L_{cuc2\text{-}3\ Mock\ 25\mu M\ piclo}$=3.0 ±0.6 mm and $L_{p35S:CUC2\text{-}GR\ cuc2\text{-}3\ Mock\ 25\mu M\ piclo}$=2.6 ±0.3 mm, respectively). Notably, *p35S:CUC2-GR cuc2-3* hypocotyls not treated with DEX were more affected by picloram-related toxicity, leading to slightly shorter lengths than those treated with DEX ($L_{p35S:CUC2\text{-}GR\ cuc2\text{-}3\ DEX\ 25\mu M\ piclo}$=3.0 ±0.3 mm). This suggests that CUC2 induction may have a buffering effect picloram-related toxicity.

Taken together, our data suggest that CUC2 interferes negatively with the auxin response pathway. However, several regulating loops and additional regulatory layers could add up with the described interaction.

DISCUSSION

The tremendous diversity in plant architecture relies on the tight coordination between growth axes initiation and the growth magnitude. This is especially true for leaf development: new axes initiation determines the complexity and the arrangement of the growing blades and growth rates and timing finely tunes the extent each formed blade grows. The perturbation of growth initiation and magnitude due to the accumulation of mutations involved in those processes produces staggering leaf phenotypes (Blein et al., 2013; Challa et al., 2021). Moreover, those processes are supported by a tight control of growth, which is either suppressed in boundary domains or promoted in growing blades. Cell expansion is critical for leaf morphogenesis as it is required for both initiation and the subsequent growth of leaves. Research on growth control highlights that phytohormones are key for the control of growth in various organs (Oh et al., 2014; Bouré et al., 2019).

CUC2 has opposite effects on growth compared to GA and other growth-promoting hormones.

CUC2 indirect repression of GA biosynthesis

Our results suggest that CUC2 could indirectly influence GA biosynthesis through the control of expression of *GA3ox1*. In the SAM, KNOX1 proteins indeed activate CK signaling, thus inhibiting GA locally (Jasinski et al., 2005). KNOX1 was shown to inhibit *GA20ox1* expression (Hay et al., 2002). In maize, KNOX directly promotes the expression of *GA2ox1*, which encodes a bioactive GA (Bolduc and Hake, 2009). However, no inhibition of *GA3ox1* was reported so far. STM was shown to be necessary for normal CUC2 expression (Balkunde et al., 2017) and STM tunes CUCs expression locally (Spinelli et al., 2011). These results indicate that CUC2 and KNOX1 coordinate GA repression in the SAM, and that the control of *GA3ox1* expression could be involved in that tight coordination.

Our quantification of gene expression was conducted in *Arabidopsis* 15d-old seedlings, and still no data is available for the leaf only, especially not at lower scales. It is possible that, using localized, dissected samples from microdissected leaf margins, more precise data could be obtained to infer whether GA metabolism is impaired in leaf sinuses. In addition, local bioactive GAs quantification would be informative of GA signaling dynamics in the leaf. However, these experiments require a lot of material and optimization and were not conducted within this PhD.

Local GA modulation

In order to infer whether CUC2 and GA signaling pathway interfere with one another during serration development, we aimed at locally modifying GA metabolism at the leaf margins. We produced several transgenic lines in order to locally alter GA levels. First, we introduced a construct *pCUC3:GA3ox1-t35S* in wild type background. As *GA3ox1* encodes the enzyme responsible for the last step of bioactive GA synthesis, we aimed at locally increasing GA levels within *CUC3* expression domain, *i.e.* leaf sinuses. We were expecting to locally promote GA-triggered promotion of growth in the domain were both CUC2 and CUC3 repress cell growth, and wanted to verify whether the construct was sufficient to decrease leaf dissection in the wild type. Simultaneously, we transformed *cuc3-105* smooth mutants with a *pCUC3:GA2ox1-t35S* construct. *GA2ox1* encodes a gibberellin 2-oxidase that is responsible for the first step of bioactive GA catabolism. Hence, we aimed at locally decreasing GA levels in the *CUC3* expression domain, in order to observe if such decrease in GA activity would be sufficient to trigger local growth repression and increase leaf dissection.

For both transgenic lines more than 25 independent primary transformants were selected. Lines containing single insertions were selected to provide about 10 independent, homozygous lines for each construct. Nevertheless, none of the selected lines displayed any obvious phenotype at first glance, and we chose not to push these experiments any further. With the benefit of hindsight, we suggest that *GA3ox1* and *GA2ox1* expressions were too weak and expressed in a domain that was too small, due to the use of the *pCUC3* promoter. Moreover, as very little is known about GA metabolism in leaves, it is not possible to know whether modifying the expression of the last anabolism enzyme or the first catabolism enzyme would be sufficient to inflect GA levels locally. Leaf microdissection and GA quantification would have been interesting to address this problem, but the implementation of such experiments is long and requires a lot of optimization. Like before, a dynamic observation of DELLA protein levels using ratiometric fluorescence would also give rapid knowledge on GA local activity in leaves, but first, such a reporter line is still under development, second, the construct would also have to be introduced in that line.

Acceleration of the leaf proliferation front arrest lead to more teeth initiation

In the model proposed by (Kierzkowski et al., 2019), the more teeth are initiated for a given final size of the blade, the closer and thinner the outgrowths. They suggest that an increase of the rate of teeth initiation is due to an earlier stop of the longitudinal growth of the tooth (*i.e.* tooth width). This

is consistent with the role of GA signaling towards the proliferation arrest front. Indeed, in leaves GAs promote the switch between cell proliferation and cell differentiation on a basipetal gradient. During leaf growth, this proliferation arrest front progresses basipetally. In *della* mutants, we can hypothesize that the active GA signaling domain is wider and extends faster due to the lack of a negative regulator. Hence, the proliferation/differentiation switch would be occurring sooner during leaf development and stop tooth longitudinal extension. Since teeth are formed iteratively along the leaf margin, the reduction of tooth longitudinal extension would consecutively trigger the formation of additional serrations.

A putative complex molecular feedback between auxin and gibberellins.

Auxin was shown to promote hypocotyl elongation in the light (Chapman et al., 2012). *Aux/IAA* mutants showed reduced response to applied auxin, indicating that most auxin promotion of hypocotyl elongation involves the canonical auxin pathway. In a nutshell, in absence of auxin, Aux/IAA repressors interacts with AUXIN RESPONSE FACTORS (ARFs) to inhibit their transcriptional activity. In presence of auxin, auxin binds to a member of the TRANSPORT INHIBITOR RESPONSE 1 and AUXIN F-BOX 1 to 5 (TIR/AFBs) F-box subfamily that forms a co-receptor together with Aux/IAA repressors, triggering Aux/IAA polyubiquitination and consecutive degradation by the 26S proteasome. Hence, auxin activates ARFs transcriptional activity through a "repressing a repressor" model.

Microarray experiments were conducted to identify auxin-responsive genes that are associated with hypocotyl elongation (Chapman et al., 2012). Gene ontology was consecutively performed on the established list of genes and revealed a significant enrichment in cell expansion-related and hormone-related genes. Picloram treatment was associated with an increase in GA biosynthesis-associated genes. Furthermore, paclobutrazol significantly reduced picloram effects on hypocotyl growth, and *ga20ox1/ga20ox2* double mutant response to auxin was weakened. Together, these experiments suggest that normal bioactive GA levels are necessary for auxin response in the hypocotyl and that part of auxin promotion of growth is GA-dependent. In addition, clock-controlled genes were also up-regulated upon picloram application in the microarray experiments. As PIF TFs are involved in the control of dark-induced hypocotyl growth, the effect of auxin on the *pif4pif5* double mutant was investigated. However, PIF4 and PIF5 were not necessary for the hypocotyl

response to applied auxin, as *pif4pif5* exhibited the same response as the wildtype (Chapman et al., 2012).

As we demonstrated that CUC2 interferes with auxin signaling through positive regulation of two auxin repressive *Aux/IAA* genes, and since CUC2 was able to alter hypocotyl response to picloram in our growing conditions, we suggest that CUC2 could be an additional, negative effector of growth-regulating hubs in the plant. Because we showed CUC2 indirectly represses GA3ox1 expression, it is possible that this repression is mediated by other pathways, such as auxin.

CUC2 could balance the response of other phytohormones

Antagonism with BR in the meristem

BZR1 directly represses CUC family genes expression (Gendron et al., 2012). Increased brassinosteroids (BR) concentrations were linked with organ fusion while BR-defective lines exhibited ectopic boundaries leading to ectopic organ formation (Gendron et al., 2012). BES1 also represses *CUC3* expression through the recruitment of the TOPLESS (TPL) co-repressor on CUC3 promoter (Espinosa-Ruiz et al., 2017). In the boundary domain, BR levels are low because of LATERAL ORGAN BOUNDARIES (LOB) TF, which activates the expression of BAS1 BR-degrading enzyme (Bell et al., 2012). Taken together, these results indicate that CUC and BR have opposite effects on growth in various contexts. In addition, BR are part of the molecular hub that was shown to be decisive for growth promotion in the hypocotyl (Oh et al., 2014). We compared the genes that were down-regulated upon CUC2 induction with the list of genes that were up-regulated upon brassinolide (BL) induction (Oh et al., 2014). A 4.38-fold enrichment was obtained in the intersection of the two lists compared with a random draw in *Arabidopsis* total genes ($N_{intersection}$=541, p-value = $5.97e^{-124}$), corresponding to almost a third of BL positively-regulated genes.

Therefore, we suggest that BR signaling and CUC2 downstream pathways are probably linked with one another. We suggest that experiments should be performed to infer the extent of that interaction. For example, increasing concentrations of BL could be applied on dark-grown hypocotyls with or without CUC2 being induced. Else, we could use BR signaling reporter lines and BR quantification in various CUC2 mutant, in order to infer whether variations in CUC2 levels are able to trigger a modulation in BR responses.

CUC2 and SPY could be associated with cytokinins pathways.

Studying the role of CUC TFs during ovule primordia development, RNA-seq experiments have been performed on a transgenic line with reduced CUC2 and CUC1 activity, and identified that CUC genes down-regulates genes involved in CK degradation (Cucinotta et al., 2018). Functionally, defects in ovule initiation were observed in a line exhibiting low levels for both CUC1 and CUC2, and were subsequently rescued by CK treatment (Cucinotta et al., 2018). CK was shown to induce PIN1 expression in growing pistils, which could be mediated by CUC TFs (Galbiati et al., 2013). While previous data suggest that CUC2 modifies PIN1 polarization (Bilsborough et al., 2011), the effects of CUC2 on PIN1 protein level was not properly investigated yet. In a *cuc2-1* mutant, observation of *pPIN1::PIN1-GFP* expression pattern showed that PIN1 proteins do not look polarized in marginal cells, and were partially contained in vesicles (Galbiati et al., 2013). Since CUC2 and CK are both involved ovule development, it is therefore temping to suggest that CUC2 and CK act together also during leaf development.

In inflorescences, both CUC2 and CUC3 were up-regulated in a line with high CK levels (Li et al., 2010). These results suggest that CK and CUCs probably regulate each other in a regulatory loop. Yet, testing the genetic interactions between CUC2 and CK remains an interesting perspective in our study.

Our work revealed that SPY and CUC2 both promote local growth repression through modification of the expression of genes involved in cell wall modification. Interestingly, SPY was also shown to be essential for CK signaling as *spy* mutant do not respond to CK (Greenboim-Wainberg et al., 2005). Moreover, it seems that SPY is involved early in CK response pathway as it acts upstream of *GIS2* and *GL1* CK-responsive genes (Gan et al., 2007). It is then possible, since CUC2 and SPY both seem to interact with CK pathway, that both CUC2 and SPY repression on growth involved CK.

Furthermore, CK-treated plants exhibit highly serrated leaves, which could suggest their participation in shaping the leaves during development (Maymon et al., 2009). Serrations were lowered in CK-treated *spy-4* mutant, thus confirming that SPY is critical for CK responses. However, the teeth positioning is erratic in CK-treated plants and leaves do not look like the highly serrated leaves that result from high CUC2 levels.

CUC2 could be a major repressor of growth-promoting molecular hub

Together, our data suggest that CUC2 acts in an antagonist way toward GA and auxin. GAs and auxin have partly independent but also mutually dependent effects on hypocotyl growth promotion. A BRASSINAZOLE RESISTANT 1 (BZR1), AUXIN RESPONSE FACTOR 6 (ARF6), and PHYTOCHROME INTERACTING FACTOR 4 (PIF4) (BAP) module was shown to orchestrate growth in hypocotyls (Oh et al., 2014). PIF4, ARF6 and BZR1 have indeed largely overlapping targets but each TF also has its own set of specific targets (Oh et al., 2014).

PIF4 and BZR1 were shown regulate common targets via binding to the same cis-regulatory element (Oh et al., 2012). It is worthy to note that BZR1 and PIF4 binding sites resemble that of NAC TFs (Lindemose et al., 2014). This suggests that CUC2 could directly bind to several targets of the BAP module. Besides, *PACLOBUTRAZOL RESISTANCE1 (PRE1),* which encodes a cell growth-promoting bHLH TF that functions downstream of the BAP module, could be a CUC2 target as well since CUC2 was able to reduce *PACLOBUTRAZOL RESISTANCE1 (PRE1)* mRNA accumulation (data not shown). Accordingly, ChipSeq experiments yielded that CUC2, PIF4 and ARF6 peaks on PRE1 promoter coincide (Nicolas Arnaud, personal communication; (citation)). This experiment suggests that CUC2 could repress growth through repression of the BAP module activity, by competitive binding with its targeted genes. Further experiments to better characterize CUC2 binding sites would be necessary to understand how CUC2 and the BAP module TFs activities are integrated during development.

As CUC2 overexpression was able to interfere with auxin and GA growth promotion, we suggest that CUC2 could be involved in a larger, complex system centered on the BAP module, that involves multiple feedback loops to control growth in various developmental contexts. In the course of my PhD, I wrote a review on the BAP module signal integration and the environmental responses. This review provides an integrative point of view on the way the BAP module integrates endogenous and exogenous cues to provide appropriate growth decision.

MATERIALS & EXPERIMENTAL PROCEDURES

Gene expression quantification

15 days-old *p35S:CUC2-GR, cuc2-3* seedlings grown on plates were used with or without transient induction using DEX and pulled in 1.5 mL ependorf tubes up to 100µm of total mass and instantly immersed in liquid nitrogen. Alternatively, *p35S:CUC2-GR, cuc2-3* seeds were placed in liquid medium under long day conditions at 23°C for ten days at the end of which the plants were treated for 30 minutes of treatment with 10µM cycloheximide in order to prevent protein translation and to reveal direct interactions followed by 3 or 6 hours of 10µM DEX treatment to induce CUC2 nuclear relocalization.
Total RNAs were isolated using RNAeasy Plant Mini Kit (Qiagen) or alternatively the miRvana extraction kit (Ambion) following the manufacturer recommendation for plant tissue. In both extractions, reverse transcription was performed using RevertAid H Minus M-MuLV Reverse transcriptase (Fermentas) followed by a RNAse H treatment was performed for 20 min 37°C to eliminate DNA-RNA duplexes. Real time PCR analysis was performed on a 384-well QuantStudio™ 5 Real-Time PCR System, using the SsoAdvance Universal SYBR Green Supermix with the following PCR conditions: 95˚C 3min; (95˚C 15s; 63˚C 30s) x40 cycles. Raw data was analyzed using Design & Analysis 2.2 software. Primers used for real time PCR analysis are available in S1 Table. Expression data were normalized using the ΔΔCt method using at three independent reference genes (*qREF*, *Actin2* and *EF1α*).

Morphometric analysis

For *gai-t6* (Peng et al., 1997) and *rga-28* (Salk_089146) mutants mature leaf shape quantification, data were acquired and treated as in chapter 1. Both mutants were provided by Patrick Achard (IBMP, Strasbourg).
For col-0 and *spy-3* leaf shape quantification in media containing various GA levels, seeds were sown in vitro on mock medium or treated either with 1µM Paclobutrazol or with 1µM GA3. 15 days-old col-0 and *spy-3* seedlings were dissected and leaves of rank 4 were imaged using an Axio Zoom.V16 microscope (Carl Zeiss Microscopy, Jena, Germany; http://www.zeiss.com/). Quantification of leaf shape was performed as in chapter 1, see Material and Methods.

Hypocotyl size quantification

Seeds were sown on media containing various concentration of GA_3 or Picloram. Hypocotyls were scanned at 1600 dpi using a Perfection V800 Photo scanner (Epson) after three days of *in vitro* growth in LD conditions. The hypocotyl length was semi-automatically measured with the NeuronJ plugin on ImageJ.

CONCLUSION & PERSPECTIVES

The involvement of *CUC* genes in defining the organs that emerge from the meristem has been known for almost 30 years. Since then, their role has been largely clarified, and elements acting upstream and downstream of CUCs have been identified (Maugarny-Calès et al., 2019). Phylogenetic studies have shown that the *NAC* family, which *CUCs* are a part of, is highly conserved during evolution (Hasson et al., 2011; Maugarny et al., 2016). In several species, CUCs and their homologues are involved in the definition of boundary domains, and particularly in the establishment of serrations at the leaf margin. Over the course of my PhD, I took part in gathering new data on the functions of CUCs and the involved molecular processes.

Hence, I proposed in this manuscript a molecular framework by which CUC2 connects patterning with the control of cell growth. In this model, we suggest that CUC2 could trigger local growth repression, independently of its previously known targets such as CUC3, by repressing genes that are involved in cell wall relaxation, hence cell elongation. We suggest that CUC2 is able to modulate the cell wall mechanical properties locally, thus creating *CUC3* expression-promoting conditions (Fal et al., 2016). Previous studies pointed out that CUC2 is necessary for serration initiation, while the role of CUC3 is to maintain differential growth (Hasson et al., 2011; Serra and Perrot-Rechenmann, 2020). Here, I showed that CUC2 also leads to local growth repression independently from CUC3. In the literature, mechanical stress was already demonstrated to be essential in the SAM to trigger specific gene expression programs (Landrein et al., 2015; Fal et al., 2016). A better knowledge of mechanical traits and constrains will be key to understand development and patterning of the leaf.

Our focus on the *spindly* mutant phenotypes revealed that SPY and CUC2 can repress the expression of a common set of genes involved in cell elongation. However, on the contrary to CUC2 and CUC3 local expression domains, SPY is widely expressed throughout the leaf. Despite their differences in expression pattern, *cuc3* and *spy* mutations lead to very similar phenotype at sinuses. This observation suggests that the local defect we saw in the *spy-3* mutant may reflect different activity of SPY depending on the tissue where it is expressed and/or that leaf cells do not respond uniformly to SPY activity alterations.

Since hormones are master regulators of organs development and cell growth, and because CUC2 seems to be able to repress growth, I investigated the interactions between CUC2, auxin and

GA hormonal pathways. The interactions with some other phytohormones, such as BR or CK were not explored over the course of my PhD but could constitute a nice perspective for my work. Besides, preliminary data already indicates that CUC and BR interfere with one another, since the boundary domains are depleted in BR and since BZR1 was shown to negatively regulate CUCs (Gendron et al., 2012). Numerous crosstalks however connect hormonal pathways with one another and make it challenging to explore interactions between CUCs and individual hormones. Even if the distribution and pathways of main hormones is well described in the SAM, little is known about the fine regulation of hormonal pathways at the leaf margin, since leaves are very often considered as a whole. A combination of gene expression spatio-temporal quantification and modelling, that includes hormonal pathway reporter lines, will surely enlighten our knowledge on margin development dynamic with a better resolution. Such a comparative tool is currently being developed in the lab in collaboration with the *modélisation et images numériques* (MIN) group at IJPB.

During my PhD, I mainly focused on local growth repression at the leaf sinuses. However, growth-promoting effects have also been described at distance for CUC2 (Bilsborough et al., 2011; Maugarny-Calès et al., 2019). KLUH, a cytochrome P450 which expression is activated by CUC2, could generate a mobile signal to trigger cell growth promotion within the tooth tip (Anastasiou et al., 2007). A better understanding of the molecular pathways downstream of KLUH could potentially provide new data on leaf patterning and teeth growth promotion. In addition, the study of CUC2-triggered PIN1 repolarization and auxin response maxima in the teeth tip, which were previously described (Bilsborough et al., 2011), could also represent an interesting feature in future experiments.

Furthermore, in addition to CUC TFs, other actors are able to induce and maintain auxin response maxima in the teeth. Indeed, auxin maintains its own signaling in tooth through a feedback mechanism involving EPIDERMAL PATTERNING FACTOR-LIKE2 (EPFL2) interaction and its receptor ERECTA (ER). While ER is expressed widely in the leaf, its ligand EPFL2 is excluded from the tooth as its expression is repressed by auxin signaling. At the same time, outside of the tooth, EPFL2-ER interaction negatively regulates auxin response (Tameshige et al., 2016b). This feedback mechanism contributes to leaf serration development as it allows sharpening auxin signaling to the tooth tip. Like *cuc* mutants, *erecta* mutants display smoother leaves than the wild type as a result of defective tooth growth maintenance (Torii et al., 1996; Tameshige et al., 2016a). In addition, since fused carpels were reported in an *epfl2* mutant (Kawamoto et al., 2020), similarly to what was previously described in *cuc2cuc3* double mutants (Gonçalves et al., 2015), it is tempting to suggest that CUC2 somehow

modulates ER/EPFL pathways. Together, these data suggest that EPFL2, like CUC2, is involved in several developmental contexts to trigger the organization and patterning of boundary domains in plant.

The role of CUC2 is very conserved in simple leaves, but it is also the case during the development of other species, since NAM/CUC genes were found to delimit leaflets formation in species that carry compound leaves (Blein et al., 2008). Other actors seem to be important for leaflet formation, like *REDUCED COMPLEXITY (RCO)* which encodes a HD-ZIP TF that triggers differential growth in compound leaves. In addition, loss of *RCO* was shown to be responsible for *Arabidopsis thaliana* leaf simplification (Sicard et al., 2014; Vlad et al., 2014). RCO, like CUC2, seems to be crucial for leaf complexity development through sharp growth repression between individual leaflets. Once more, it seems that the study of phytohormones will be essential to understand how leaf diversity is established, since RCO was recently shown to control CK homeostasis to repress growth (Hajheidari et al., 2019). Finally, modeling the GRN at the basis of margin development yielded that variations in gene expression timing, pattern and intensity can trigger extensive variations in leaf shape and be responsible for the apparent leaf diversity within and between species (Kierzkowski et al., 2019).

REFERENCES

1. Achard P, Baghour M, Chapple A, Hedden P, Van Der Straeten D, Genschik P, Moritz T, Harberd NP (2007) The plant stress hormone ethylene controls floral transition via DELLA-dependent regulation of floral meristem-identity genes. Proc Natl Acad Sci U S A 104: 6484–6489
2. Achard P, Gusti A, Cheminant S, Alioua M, Dhondt S, Coppens F, Beemster GTS, Genschik P (2009) Gibberellin Signaling Controls Cell Proliferation Rate in Arabidopsis. Curr Biol 19: 1188–1193
3. Achard P, Vriezen WH, Van Der Straeten D, Harberd NP (2003) Ethylene Regulates Arabidopsis Development via the Modulation of DELLA Protein Growth Repressor Function. Plant Cell 15: 2816–2825
4. Aida M, Ishida T, Fukaki H, Fujisawa H, Tasaka M (1997) Genes involved in organ separation in Arabidopsis: an analysis of the cup-shaped cotyledon mutant. Plant Cell 9: 841–857
5. Alvarez JP, Furumizu C, Efroni I, Eshed Y, Bowman JL (2016) Active suppression of a leaf meristem orchestrates determinate leaf growth. eLife 5: e15023
6. An F, Zhang X, Zhu Z, Ji Y, He W, Jiang Z, Li M, Guo H (2012) Coordinated regulation of apical hook development by gibberellins and ethylene in etiolated Arabidopsis seedlings. Cell Res 22: 915–927
7. Anastasiou E, Kenz S, Gerstung M, MacLean D, Timmer J, Fleck C, Lenhard M (2007) Control of Plant Organ Size by KLUH/CYP78A5-Dependent Intercellular Signaling. Dev Cell 13: 843–856
8. Andriankaja M, Dhondt S, De Bodt S, Vanhaeren H, Coppens F, De Milde L, Mühlenbock P, Skirycz A, Gonzalez N, Beemster GTS, et al (2012) Exit from Proliferation during Leaf Development in Arabidopsis thaliana: A Not-So-Gradual Process. Dev Cell 22: 64–78
9. Arnaud N, Girin T, Sorefan K, Fuentes S, Wood TA, Lawrenson T, Sablowski R, Østergaard L (2010) Gibberellins control fruit patterning in Arabidopsis thaliana. Genes Dev 24: 2127–2132
10. Bai M-Y, Shang J-X, Oh E, Fan M, Bai Y, Zentella R, Sun T-P, Wang Z-Y (2012) Brassinosteroid, gibberellin and phytochrome impinge on a common transcription module in Arabidopsis. Nat Cell Biol 14: 810–817
11. Bainbridge K, Guyomarc'h S, Bayer E, Swarup R, Bennett M, Mandel T, Kuhlemeier C (2008) Auxin influx carriers stabilize phyllotactic patterning. Genes Dev 22: 810–823
12. Balkunde R, Kitagawa M, Xu XM, Wang J, Jackson D (2017) SHOOT MERISTEMLESS trafficking controls axillary meristem formation, meristem size and organ boundaries in Arabidopsis. Plant J 90: 435–446
13. Bar M, Ori N (2015) Compound leaf development in model plant species. Curr Opin Plant Biol 23: 61–69
14. Barbier de Reuille P, Routier-Kierzkowska A-L, Kierzkowski D, Bassel GW, Schüpbach T, Tauriello G, Bajpai N, Strauss S, Weber A, Kiss A, et al (2015) MorphoGraphX: A platform for quantifying morphogenesis in 4D. eLife 4: e05864
15. Barton MK (2010) Twenty years on: The inner workings of the shoot apical meristem, a developmental dynamo. Dev Biol 341: 95–113
16. Bell EM, Lin W, Husbands AY, Yu L, Jaganatha V, Jablonska B, Mangeon A, Neff MM, Girke T, Springer PS (2012) Arabidopsis LATERAL ORGAN BOUNDARIES negatively regulates brassinosteroid accumulation to limit growth in organ boundaries. Proc Natl Acad Sci 109: 21146–21151
17. Benková E, Michniewicz M, Sauer M, Teichmann T, Seifertová D, Jürgens G, Friml J (2003) Local, Efflux-Dependent Auxin Gradients as a Common Module for Plant Organ Formation. Cell 115: 591–602
18. Bennett T, van den Toorn A, Sanchez-Perez GF, Campilho A, Willemsen V, Snel B, Scheres B (2010) SOMBRERO, BEARSKIN1, and BEARSKIN2 regulate root cap maturation in Arabidopsis. Plant Cell 22: 640–654
19. Berger Y, Harpaz-Saad S, Brand A, Melnik H, Sirding N, Alvarez JP, Zinder M, Samach A, Eshed Y, Ori N (2009) The NAC-domain transcription factor GOBLET specifies leaflet boundaries in compound tomato leaves. Development 136: 823–832
20. Besnard F, Refahi Y, Morin V, Marteaux B, Brunoud G, Chambrier P, Rozier F, Mirabet V, Legrand J, Lainé S, et al (2014) Cytokinin signalling inhibitory fields provide robustness to phyllotaxis. Nature 505: 417–421
21. Bilsborough GD, Runions A, Barkoulas M, Jenkins HW, Hasson A, Galinha C, Laufs P, Hay A, Prusinkiewicz P, Tsiantis M (2011) Model for the regulation of Arabidopsis thaliana leaf margin development. Proc Natl Acad Sci U S A 108: 3424–3429
22. Biot E, Cortizo M, Burguet J, Kiss A, Oughou M, Maugarny-Calès A, Gonçalves B, Adroher B, Andrey P, Boudaoud A, et al (2016) Multiscale quantification of morphodynamics: MorphoLeaf software for 2D shape analysis. Dev Camb Engl 143: 3417–3428

23. Blanco-Touriñán N, Legris M, Minguet EG, Costigliolo-Rojas C, Nohales MA, Iniesto E, García-León M, Pacín M, Heucken N, Blomeier T, et al (2020a) COP1 destabilizes DELLA proteins in Arabidopsis. Proc Natl Acad Sci 117: 13792–13799
24. Blanco-Touriñán N, Serrano-Mislata A, Alabadí D (2020b) Regulation of DELLA Proteins by Post-translational Modifications. Plant Cell Physiol 61: 1891–1901
25. Blázquez MA, Green R, Nilsson O, Sussman MR, Weigel D (1998) Gibberellins Promote Flowering of Arabidopsis by Activating the LEAFY Promoter. Plant Cell 10: 791–800
26. Blein T, Hasson A, Laufs P (2010) Leaf development: what it needs to be complex. Curr Opin Plant Biol 13: 75–82
27. Blein T, Pautot V, Laufs P (2013) Combinations of Mutations Sufficient to Alter Arabidopsis Leaf Dissection. Plants 2: 230–247
28. Blein T, Pulido A, Vialette-Guiraud A, Nikovics K, Morin H, Hay A, Johansen IE, Tsiantis M, Laufs P (2008) A conserved molecular framework for compound leaf development. Science 322: 1835–1839
29. Bolduc N, Hake S (2009) The Maize Transcription Factor KNOTTED1 Directly Regulates the Gibberellin Catabolism Gene ga2ox1. Plant Cell 21: 1647–1658
30. Bonin CP, Potter I, Vanzin GF, Reiter W-D (1997) The MUR1 gene of Arabidopsis thaliana encodes an isoform of GDP-d-mannose-4,6-dehydratase, catalyzing the first step in the de novo synthesis of GDP-l-fucose. Proc Natl Acad Sci 94: 2085–2090
31. Boron AK, Van Loock B, Suslov D, Markakis MN, Verbelen J-P, Vissenberg K (2015) Over-expression of AtEXLA2 alters etiolated arabidopsis hypocotyl growth. Ann Bot 115: 67–80
32. Bouré N, Kumar SV, Arnaud N (2019) The BAP Module: A Multisignal Integrator Orchestrating Growth. Trends Plant Sci 24: 602–610
33. Braccini I, Pérez S (2001) Molecular Basis of Ca2+-Induced Gelation in Alginates and Pectins: The Egg-Box Model Revisited. Biomacromolecules 2: 1089–1096
34. Brand A, Shirding N, Shleizer S, Ori N (2007) Meristem maintenance and compound-leaf patterning utilize common genetic mechanisms in tomato. Planta 226: 941–951
35. Breuil-Broyer S, Morel P, Almeida-Engler JD, Coustham V, Negrutiu I, Trehin C (2004) High-resolution boundary analysis during Arabidopsis thaliana flower development. Plant J 38: 182–192
36. Brumos J, Robles LM, Yun J, Vu TC, Jackson S, Alonso JM, Stepanova AN (2018) Local Auxin Biosynthesis Is a Key Regulator of Plant Development. Dev Cell 47: 306-318.e5
37. Burian A, Raczyńska-Szajgin M, Borowska-Wykręt D, Piatek A, Aida M, Kwiatkowska D (2015) The CUP-SHAPED COTYLEDON2 and 3 genes have a post-meristematic effect on Arabidopsis thaliana phyllotaxis. Ann Bot 115: 807–820
38. Burk DH, Ye Z-H (2002) Alteration of oriented deposition of cellulose microfibrils by mutation of a katanin-like microtubule-severing protein. Plant Cell 14: 2145–2160
39. Byrne M, Timmermans M, Kidner C, Martienssen R (2001) Development of leaf shape. Curr Opin Plant Biol 4: 38–43
40. Caesar K, Elgass K, Chen Z, Huppenberger P, Witthöft J, Schleifenbaum F, Blatt MR, Oecking C, Harter K (2011) A fast brassinolide-regulated response pathway in the plasma membrane of Arabidopsis thaliana. Plant J 66: 528–540
41. Caggiano MP, Yu X, Bhatia N, Larsson A, Ram H, Ohno CK, Sappl P, Meyerowitz EM, Jönsson H, Heisler MG (2017) Cell type boundaries organize plant development. eLife. doi: 10.7554/eLife.27421
42. Caldana C, Li Y, Leisse A, Zhang Y, Bartholomaeus L, Fernie AR, Willmitzer L, Giavalisco P (2013) Systemic analysis of inducible target of rapamycin mutants reveal a general metabolic switch controlling growth in Arabidopsis thaliana. Plant J Cell Mol Biol 73: 897–909
43. Challa KR, Rath M, Sharma AN, Bajpai AK, Davuluri S, Acharya KK, Nath U (2021) Active suppression of leaflet emergence as a mechanism of simple leaf development. Nat Plants 1–12
44. Chan J, Eder M, Crowell EF, Hampson J, Calder G, Lloyd C (2011) Microtubules and CESA tracks at the inner epidermal wall align independently of those on the outer wall of light-grown Arabidopsis hypocotyls. J Cell Sci 124: 1088–1094
45. Chapman EJ, Greenham K, Castillejo C, Sartor R, Bialy A, Sun T-P, Estelle M (2012) Hypocotyl transcriptome reveals auxin regulation of growth-promoting genes through GA-dependent and -independent pathways. PloS One 7: e36210
46. Cheng X, Peng J, Ma J, Tang Y, Chen R, Mysore KS, Wen J (2012) NO APICAL MERISTEM (MtNAM) regulates floral organ identity and lateral organ separation in Medicago truncatula. New Phytol 195: 71–84
47. Chitwood DH, Nogueira FTS, Howell MD, Montgomery TA, Carrington JC, Timmermans MCP (2009) Pattern formation via small RNA mobility. Genes Dev 23: 549–554
48. Cho HT, Cosgrove DJ (2000) Altered expression of expansin modulates leaf growth and pedicel abscission in Arabidopsis thaliana. Proc Natl Acad Sci U S A 97: 9783–9788
49. Choi H, Oh E (2016) PIF4 Integrates Multiple Environmental and Hormonal Signals for Plant Growth Regulation in Arabidopsis. Mol Cells 39: 587–593

50. **Christenhusz MJM, Byng JW** (2016) The number of known plants species in the world and its annual increase. Phytotaxa **261**: 201–217–201–217
51. **Churchman ML, Brown ML, Kato N, Kirik V, Hülskamp M, Inzé D, De Veylder L, Walker JD, Zheng Z, Oppenheimer DG, et al** (2006) SIAMESE, a plant-specific cell cycle regulator, controls endoreplication onset in Arabidopsis thaliana. Plant Cell **18**: 3145–3157
52. **Claeys H, De Bodt S, Inzé D** (2014) Gibberellins and DELLAs: central nodes in growth regulatory networks. Trends Plant Sci **19**: 231–239
53. **Cleland R** (1973) Auxin-Induced Hydrogen Ion Excretion from Avena Coleoptiles. Proc Natl Acad Sci **70**: 3092–3093
54. **Clouse SD, Sasse JM** (1998) BRASSINOSTEROIDS: Essential Regulators of Plant Growth and Development. Annu Rev Plant Physiol Plant Mol Biol **49**: 427–451
55. **Conlon I, Raff M** (1999) Size control in animal development. Cell **96**: 235–244
56. **Corneillie S, De Storme N, Van Acker R, Fangel JU, De Bruyne M, De Rycke R, Geelen D, Willats WGT, Vanholme B, Boerjan W** (2019) Polyploidy Affects Plant Growth and Alters Cell Wall Composition. Plant Physiol **179**: 74–87
57. **Cosgrove DJ** (2005) Growth of the plant cell wall. Nat Rev Mol Cell Biol **6**: 850–861
58. **Cosgrove DJ** (2016) Catalysts of plant cell wall loosening. F1000Research. doi: 10.12688/f1000research.7180.1
59. **Cowling RJ, Harberd NP** (1999) Gibberellins control Arabidopsis hypocotyl growth via regulation of cellular elongation. J Exp Bot **50**: 1351–1357
60. **Cowling RJ, Kamiya Y, Seto H, Harberd NP** (1998) Gibberellin Dose-Response Regulation of GA4 Gene Transcript Levels in Arabidopsis. Plant Physiol **117**: 1195–1203
61. **Crowell EF, Gonneau M, Vernhettes S, Höfte H** (2010) Regulation of anisotropic cell expansion in higher plants. C R Biol **333**: 320–324
62. **Cucinotta M, Manrique S, Cuesta C, Benkova E, Novak O, Colombo L** (2018) CUP-SHAPED COTYLEDON1 (CUC1) and CUC2 regulate cytokinin homeostasis to determine ovule number in Arabidopsis. J Exp Bot **69**: 5169–5176
63. **Daher FB, Chen Y, Bozorg B, Clough J, Jönsson H, Braybrook SA** (2018) Anisotropic growth is achieved through the additive mechanical effect of material anisotropy and elastic asymmetry. eLife **7**: e38161
64. **Davière J-M, Achard P** (2013) Gibberellin signaling in plants. Development **140**: 1147–1151
65. **Davière J-M, Wild M, Regnault T, Baumberger N, Eisler H, Genschik P, Achard P** (2014) Class I TCP-DELLA Interactions in Inflorescence Shoot Apex Determine Plant Height. Curr Biol **24**: 1923–1928
66. **De Veylder L, Larkin JC, Schnittger A** (2011) Molecular control and function of endoreplication in development and physiology. Trends Plant Sci **16**: 624–634
67. **Dill A, Jung HS, Sun TP** (2001) The DELLA motif is essential for gibberellin-induced degradation of RGA. Proc Natl Acad Sci U S A **98**: 14162–14167
68. **Dobrenel T, Marchive C, Azzopardi M, Clément G, Moreau M, Sormani R, Robaglia C, Meyer C** (2013) Sugar metabolism and the plant target of rapamycin kinase: a sweet operaTOR? Front Plant Sci **4**: 93
69. **Dubois M, Selden K, Bediée A, Rolland G, Baumberger N, Noir S, Bach L, Lamy G, Granier C, Genschik P** (2018) SIAMESE-RELATED1 Is Regulated Posttranslationally and Participates in Repression of Leaf Growth under Moderate Drought. Plant Physiol **176**: 2834–2850
70. **Dubrovsky JG, Doerner PW, Colón-Carmona A, Rost TL** (2000) Pericycle Cell Proliferation and Lateral Root Initiation in Arabidopsis. Plant Physiol **124**: 1648–1657
71. **Emery JF, Floyd SK, Alvarez J, Eshed Y, Hawker NP, Izhaki A, Baum SF, Bowman JL** (2003) Radial Patterning of Arabidopsis Shoots by Class III HD-ZIP and KANADI Genes. Curr Biol **13**: 1768–1774
72. **Eriksson S, Stransfeld L, Adamski NM, Breuninger H, Lenhard M** (2010) KLUH/CYP78A5-dependent growth signaling coordinates floral organ growth in Arabidopsis. Curr Biol CB **20**: 527–532
73. **Espinosa-Ruiz A, Martínez C, de Lucas M, Fàbregas N, Bosch N, Caño-Delgado AI, Prat S** (2017) TOPLESS mediates brassinosteroid control of shoot boundaries and root meristem development in Arabidopsis thaliana. Dev Camb Engl **144**: 1619–1628
74. **Fahlgren N, Montgomery TA, Howell MD, Allen E, Dvorak SK, Alexander AL, Carrington JC** (2006) Regulation of AUXIN RESPONSE FACTOR3 by TAS3 ta-siRNA Affects Developmental Timing and Patterning in Arabidopsis. Curr Biol **16**: 939–944
75. **Fal K, Korsbo N, Alonso-Serra J, Teles J, Liu M, Refahi Y, Chabouté M-E, Jönsson H, Hamant O** (2021) Tissue folding at the organ–meristem boundary results in nuclear compression and chromatin compaction. Proc Natl Acad Sci. doi: 10.1073/pnas.2017859118
76. **Fal K, Landrein B, Hamant O** (2016) Interplay between miRNA regulation and mechanical stress for CUC gene expression at the shoot apical meristem. Plant Signal Behav **11**: e1127497

77. Feng S, Martinez C, Gusmaroli G, Wang Y, Zhou J, Wang F, Chen L, Yu L, Iglesias-Pedraz JM, Kircher S, et al (2008) Coordinated regulation of Arabidopsis thaliana development by light and gibberellins. Nature 451: 475–479
78. Fleet CM, Sun T (2005) A DELLAcate balance: the role of gibberellin in plant morphogenesis. Curr Opin Plant Biol 8: 77–85
79. Franklin KA, Lee SH, Patel D, Kumar SV, Spartz AK, Gu C, Ye S, Yu P, Breen G, Cohen JD, et al (2011) PHYTOCHROME-INTERACTING FACTOR 4 (PIF4) regulates auxin biosynthesis at high temperature. Proc Natl Acad Sci 108: 20231–20235
80. Fry SC, Smith RC, Renwick KF, Martin DJ, Hodge SK, Matthews KJ (1992) Xyloglucan endotransglycosylase, a new wall-loosening enzyme activity from plants. Biochem J 282: 821–828
81. Fu X, Harberd NP (2003) Auxin promotes Arabidopsis root growth by modulating gibberellin response. Nature 421: 740–743
82. Furumizu C, Alvarez JP, Sakakibara K, Bowman JL (2015) Antagonistic Roles for KNOX1 and KNOX2 Genes in Patterning the Land Plant Body Plan Following an Ancient Gene Duplication. PLOS Genet 11: e1004980
83. Galbiati F, Roy DS, Simonini S, Cucinotta M, Ceccato L, Cuesta C, Simaskova M, Benkova E, Kamiuchi Y, Aida M, et al (2013) An integrative model of the control of ovule primordia formation. Plant J 76: 446–455
84. Gallego-Bartolomé J, Minguet EG, Grau-Enguix F, Abbas M, Locascio A, Thomas SG, Alabadí D, Blázquez MA (2012) Molecular mechanism for the interaction between gibberellin and brassinosteroid signaling pathways in Arabidopsis. Proc Natl Acad Sci U S A 109: 13446–13451
85. Gallego-Bartolomé J, Minguet EG, Marín JA, Prat S, Blázquez MA, Alabadí D (2010) Transcriptional diversification and functional conservation between DELLA proteins in Arabidopsis. Mol Biol Evol 27: 1247–1256
86. Gan Y, Liu C, Yu H, Broun P (2007) Integration of cytokinin and gibberellin signalling by Arabidopsis transcription factors GIS, ZFP8 and GIS2 in the regulation of epidermal cell fate. Development 134: 2073–2081
87. Geisler M, Nadeau J, Sack FD (2000) Oriented Asymmetric Divisions That Generate the Stomatal Spacing Pattern in Arabidopsis Are Disrupted by the too many mouths Mutation. Plant Cell 12: 2075–2086
88. Gendreau E, Traas J, Desnos T, Grandjean O, Caboche M, Höfte H (1997) Cellular basis of hypocotyl growth in Arabidopsis thaliana. Plant Physiol 114: 295–305
89. Gendron JM, Liu J-S, Fan M, Bai M-Y, Wenkel S, Springer PS, Barton MK, Wang Z-Y (2012) Brassinosteroids regulate organ boundary formation in the shoot apical meristem of Arabidopsis. Proc Natl Acad Sci U S A 109: 21152–21157
90. Gonçalves B, Hasson A, Belcram K, Cortizo M, Morin H, Nikovics K, Vialette-Guiraud A, Takeda S, Aida M, Laufs P, et al (2015) A conserved role for CUP-SHAPED COTYLEDON genes during ovule development. Plant J Cell Mol Biol 83: 732–742
91. Gonçalves B, Maugarny-Calès A, Adroher B, Cortizo M, Borrega N, Blein T, Hasson A, Gineau E, Mouille G, Laufs P, et al (2017) GDP-L-fucose is required for boundary definition in plants. J Exp Bot 68: 5801–5811
92. Gonçalves B, Sechet J, Arnaud N (2018) Xyloglucans fucosylation defects do not alter plant boundary domain definition. Plant Signal Behav. doi: 10.1080/15592324.2018.1430545
93. González A, Hall MN (2017) Nutrient sensing and TOR signaling in yeast and mammals. EMBO J 36: 397–408
94. Gonzalez N, Bodt SD, Sulpice R, Jikumaru Y, Chae E, Dhondt S, Daele TV, Milde LD, Weigel D, Kamiya Y, et al (2010) Increased Leaf Size: Different Means to an End. Plant Physiol 153: 1261–1279
95. Gonzalez N, Pauwels L, Baekelandt A, De Milde L, Van Leene J, Besbrugge N, Heyndrickx KS, Cuéllar Pérez A, Durand AN, De Clercq R, et al (2015) A Repressor Protein Complex Regulates Leaf Growth in Arabidopsis. Plant Cell 27: 2273–2287
96. Grafi G (2004) How cells dedifferentiate: a lesson from plants. Dev Biol 268: 1–6
97. Greenboim-Wainberg Y, Maymon I, Borochov R, Alvarez J, Olszewski N, Ori N, Eshed Y, Weiss D (2005) Cross Talk between Gibberellin and Cytokinin: The Arabidopsis GA Response Inhibitor SPINDLY Plays a Positive Role in Cytokinin Signaling. Plant Cell 17: 92–102
98. Guan C, Wu B, Yu T, Wang Q, Krogan NT, Liu X, Jiao Y (2017) Spatial Auxin Signaling Controls Leaf Flattening in Arabidopsis. Curr Biol 27: 2940-2950.e4
99. Günl M, Neumetzler L, Kraemer F, Souza A de, Schultink A, Pena M, York WS, Pauly M (2011) AXY8 Encodes an α-Fucosidase, Underscoring the Importance of Apoplastic Metabolism on the Fine Structure of Arabidopsis Cell Wall Polysaccharides. Plant Cell 23: 4025–4040
100. Guo H, Li L, Ye H, Yu X, Algreen A, Yin Y (2009) Three related receptor-like kinases are required for optimal cell elongation in Arabidopsis thaliana. Proc Natl Acad Sci 106: 7648–7653
101. Ha CM, Jun JH, Nam HG, Fletcher JC (2007) BLADE-ON-PETIOLE1 and 2 Control Arabidopsis Lateral Organ Fate through Regulation of LOB Domain and Adaxial-Abaxial Polarity Genes. Plant Cell 19: 1809–1825

102. **Hajheidari M, Wang Y, Bhatia N, Vuolo F, Franco-Zorrilla JM, Karady M, Mentink RA, Wu A, Oluwatobi BR, Müller B, et al** (2019) Autoregulation of RCO by Low-Affinity Binding Modulates Cytokinin Action and Shapes Leaf Diversity. Curr Biol CB **29**: 4183-4192.e6
103. **Hamant O, Heisler MG, Jönsson H, Krupinski P, Uyttewaal M, Bokov P, Corson F, Sahlin P, Boudaoud A, Meyerowitz EM, et al** (2008) Developmental Patterning by Mechanical Signals in Arabidopsis. Science **322**: 1650–1655
104. **Harberd NP, Belfield E, Yasumura Y** (2009) The Angiosperm Gibberellin-GID1-DELLA Growth Regulatory Mechanism: How an "Inhibitor of an Inhibitor" Enables Flexible Response to Fluctuating Environments. Plant Cell **21**: 1328–1339
105. **Hartweck LM, Genger RK, Grey WM, Olszewski NE** (2006) SECRET AGENT and SPINDLY have overlapping roles in the development of Arabidopsis thaliana L. Heyn. J Exp Bot **57**: 865–875
106. **Hartweck LM, Scott CL, Olszewski NE** (2002) Two O-linked N-acetylglucosamine transferase genes of Arabidopsis thaliana L. Heynh. have overlapping functions necessary for gamete and seed development. Genetics **161**: 1279–1291
107. **Hasson A, Plessis A, Blein T, Adroher B, Grigg S, Tsiantis M, Boudaoud A, Damerval C, Laufs P** (2011) Evolution and diverse roles of the CUP-SHAPED COTYLEDON genes in Arabidopsis leaf development. Plant Cell **23**: 54–68
108. **Hauvermale AL, Steber CM** (2020) GA signaling is essential for the embryo-to-seedling transition during Arabidopsis seed germination, a ghost story. Plant Signal Behav **15**: 1705028
109. **Hay A, Barkoulas M, Tsiantis M** (2006) ASYMMETRIC LEAVES1 and auxin activities converge to repress BREVIPEDICELLUS expression and promote leaf development in Arabidopsis. Development **133**: 3955–3961
110. **Hay A, Kaur H, Phillips A, Hedden P, Hake S, Tsiantis M** (2002) The gibberellin pathway mediates KNOTTED1-type homeobox function in plants with different body plans. Curr Biol CB **12**: 1557–1565
111. **Hedden P** (2003) The genes of the Green Revolution. Trends Genet **19**: 5–9
112. **Heisler MG, Ohno C, Das P, Sieber P, Reddy GV, Long JA, Meyerowitz EM** (2005) Patterns of Auxin Transport and Gene Expression during Primordium Development Revealed by Live Imaging of the Arabidopsis Inflorescence Meristem. Curr Biol **15**: 1899–1911
113. **van Hengel AJ, Roberts K** (2002) Fucosylated arabinogalactan-proteins are required for full root cell elongation in arabidopsis. Plant J Cell Mol Biol **32**: 105–113
114. **Hernández-García J, Briones-Moreno A, Blázquez MA** (2021) Origin and evolution of gibberellin signaling and metabolism in plants. Semin Cell Dev Biol **109**: 46–54
115. **Hibara K, Karim MdR, Takada S, Taoka K, Furutani M, Aida M, Tasaka M** (2006) Arabidopsis CUP-SHAPED COTYLEDON3 Regulates Postembryonic Shoot Meristem and Organ Boundary Formation. Plant Cell **18**: 2946–2957
116. **Hill JL, Hammudi MB, Tien M** (2014) The Arabidopsis Cellulose Synthase Complex: A Proposed Hexamer of CESA Trimers in an Equimolar Stoichiometry[W]. Plant Cell **26**: 4834–4842
117. **Hirano K, Asano K, Tsuji H, Kawamura M, Mori H, Kitano H, Ueguchi-Tanaka M, Matsuoka M** (2010) Characterization of the molecular mechanism underlying gibberellin perception complex formation in rice. Plant Cell **22**: 2680–2696
118. **Höfte H, Voxeur A** (2017) Plant cell walls. Curr Biol CB **27**: R865–R870
119. **Holst K, Schmülling T, Werner T** (2011) Enhanced cytokinin degradation in leaf primordia of transgenic Arabidopsis plants reduces leaf size and shoot organ primordia formation. J Plant Physiol **168**: 1328–1334
120. **Hooper CM, Castleden IR, Tanz SK, Aryamanesh N, Millar AH** (2017) SUBA4: the interactive data analysis centre for Arabidopsis subcellular protein locations. Nucleic Acids Res **45**: D1064–D1074
121. **Hou X, Lee LYC, Xia K, Yan Y, Yu H** (2010) DELLAs modulate jasmonate signaling via competitive binding to JAZs. Dev Cell **19**: 884–894
122. **Husbands AY, Benkovics AH, Nogueira FTS, Lodha M, Timmermans MCP** (2015) The ASYMMETRIC LEAVES Complex Employs Multiple Modes of Regulation to Affect Adaxial-Abaxial Patterning and Leaf Complexity. Plant Cell **27**: 3321–3335
123. **Ikeda A, Ueguchi-Tanaka M, Sonoda Y, Kitano H, Koshioka M, Futsuhara Y, Matsuoka M, Yamaguchi J** (2001) slender Rice, a Constitutive Gibberellin Response Mutant, Is Caused by a Null Mutation of the SLR1 Gene, an Ortholog of the Height-Regulating Gene GAI/RGA/RHT/D8. Plant Cell **13**: 999–1010
124. **Ishida T, Aida M, Takada S, Tasaka M** (2000) Involvement of CUP-SHAPED COTYLEDON Genes in Gynoecium and Ovule Development in Arabidopsis thaliana. Plant Cell Physiol **41**: 60–67
125. **Israeli A, Burko Y, Shleizer-Burko S, Zelnik ID, Sela N, Hajirezaei MR, Fernie AR, Tohge T, Ori N, Bar M** (2020) Coordinating the morphogenesis-differentiation balance by tweaking the cytokinin-gibberellin equilibrium. bioRxiv 2020.12.14.422551
126. **Ito T, Okada K, Fukazawa J, Takahashi Y** (2018) DELLA-dependent and -independent gibberellin signaling. Plant Signal Behav **13**: e1445933
127. **Izhaki A, Swain SM, Tseng TS, Borochov A, Olszewski NE, Weiss D** (2001) The role of SPY and its TPR domain in the regulation of gibberellin action throughout the life cycle of Petunia hybrida plants. Plant J Cell Mol Biol **28**: 181–190

128. Jacobsen SE, Binkowski KA, Olszewski NE (1996) SPINDLY, a tetratricopeptide repeat protein involved in gibberellin signal transduction in Arabidopsis. Proc Natl Acad Sci **93**: 9292–9296
129. Jacobsen SE, Olszewski NE (1993) Mutations at the SPINDLY locus of Arabidopsis alter gibberellin signal transduction. Plant Cell **5**: 887–896
130. Jasinski S, Piazza P, Craft J, Hay A, Woolley L, Rieu I, Phillips A, Hedden P, Tsiantis M (2005) KNOX action in Arabidopsis is mediated by coordinate regulation of cytokinin and gibberellin activities. Curr Biol CB **15**: 1560–1565
131. Jewell JL, Russell RC, Guan K-L (2013) Amino acid signalling upstream of mTOR. Nat Rev Mol Cell Biol **14**: 133–139
132. Jones AR, Forero-Vargas M, Withers SP, Smith RS, Traas J, Dewitte W, Murray JAH (2017) Cell-size dependent progression of the cell cycle creates homeostasis and flexibility of plant cell size. Nat Commun **8**: 15060
133. Josse E-M, Halliday KJ (2008) Skotomorphogenesis: The Dark Side of Light Signalling. Curr Biol **18**: R1144–R1146
134. Juarez MT, Kui JS, Thomas J, Heller BA, Timmermans MCP (2004) microRNA-mediated repression of rolled leaf1 specifies maize leaf polarity. Nature **428**: 84–88
135. Katagiri Y, Hasegawa J, Fujikura U, Hoshino R, Matsunaga S, Tsukaya H (2016) The coordination of ploidy and cell size differs between cell layers in leaves. Development **143**: 1120–1125
136. Kawamoto N, Carpio DPD, Hofmann A, Mizuta Y, Kurihara D, Higashiyama T, Uchida N, Torii KU, Colombo L, Groth G, et al (2020) A Peptide Pair Coordinates Regular Ovule Initiation Patterns with Seed Number and Fruit Size. Curr Biol **30**: 4352-4361.e4
137. Kawamura E, Horiguchi G, Tsukaya H (2010) Mechanisms of leaf tooth formation in Arabidopsis. Plant J Cell Mol Biol **62**: 429–441
138. Kazama T, Ichihashi Y, Murata S, Tsukaya H (2010) The mechanism of cell cycle arrest front progression explained by a KLUH/CYP78A5-dependent mobile growth factor in developing leaves of Arabidopsis thaliana. Plant Cell Physiol **51**: 1046–1054
139. Kerstetter RA, Bollman K, Taylor RA, Bomblies K, Poethig RS (2001) *KANADI* regulates organ polarity in *Arabidopsis*. Nature **411**: 706–709
140. Kierzkowski D, Nakayama N, Routier-Kierzkowska A-L, Weber A, Bayer E, Schorderet M, Reinhardt D, Kuhlemeier C, Smith RS (2012) Elastic Domains Regulate Growth and Organogenesis in the Plant Shoot Apical Meristem. Science **335**: 1096–1099
141. Kierzkowski D, Runions A, Vuolo F, Strauss S, Lymbouridou R, Routier-Kierzkowska A-L, Wilson-Sánchez D, Jenke H, Galinha C, Mosca G, et al (2019) A Growth-Based Framework for Leaf Shape Development and Diversity. Cell. doi: 10.1016/j.cell.2019.05.011
142. Kim JH, Choi D, Kende H (2003) The AtGRF family of putative transcription factors is involved in leaf and cotyledon growth in Arabidopsis. Plant J **36**: 94–104
143. Klesen S, Hill K, Timmermans MCP (2020) Small RNAs as plant morphogens. Curr Top Dev Biol **137**: 455–480
144. Kohnen MV, Schmid-Siegert E, Trevisan M, Petrolati LA, Sénéchal F, Müller-Moulé P, Maloof J, Xenarios I, Fankhauser C (2016) Neighbor Detection Induces Organ-Specific Transcriptomes, Revealing Patterns Underlying Hypocotyl-Specific Growth. Plant Cell **28**: 2889–2904
145. Koini MA, Alvey L, Allen T, Tilley CA, Harberd NP, Whitelam GC, Franklin KA (2009) High Temperature-Mediated Adaptations in Plant Architecture Require the bHLH Transcription Factor PIF4. Curr Biol **19**: 408–413
146. Koyama T, Sato F, Ohme-Takagi M (2017) Roles of miR319 and TCP Transcription Factors in Leaf Development1[OPEN]. Plant Physiol **175**: 874–885
147. Kreppel LK, Blomberg MA, Hart GW (1997) Dynamic Glycosylation of Nuclear and Cytosolic Proteins CLONING AND CHARACTERIZATION OF A UNIQUE O-GlcNAc TRANSFERASE WITH MULTIPLE TETRATRICOPEPTIDE REPEATS. J Biol Chem **272**: 9308–9315
148. Kwiatkowska D, Dumais J (2003) Growth and morphogenesis at the vegetative shoot apex of Anagallis arvensis L. J Exp Bot **54**: 1585–1595
149. Lamb JR, Michaud WA, Sikorski RS, Hieter PA (1994) Cdc16p, cdc23p and cdc27p form a complex essential for mitosis. EMBO J **13**: 4321–4328
150. Landrein B, Kiss A, Sassi M, Chauvet A, Das P, Cortizo M, Laufs P, Takeda S, Aida M, Traas J, et al (2015) Mechanical stress contributes to the expression of the STM homeobox gene in Arabidopsis shoot meristems. eLife **4**: e07811
151. Lantzouni O, Alkofer A, Falter-Braun P, Schwechheimer C (2020) GROWTH-REGULATING FACTORS Interact with DELLAs and Regulate Growth in Cold Stress. Plant Cell **32**: 1018–1034
152. Laufs P, Peaucelle A, Morin H, Traas J (2004) MicroRNA regulation of the CUC genes is required for boundary size control in Arabidopsis meristems. Dev Camb Engl **131**: 4311–4322

153. Lee S, Cheng H, King KE, Wang W, He Y, Hussain A, Lo J, Harberd NP, Peng J (2002) Gibberellin regulates Arabidopsis seed germination via RGL2, a GAI/RGA-like gene whose expression is up-regulated following imbibition. Genes Dev 16: 646–658
154. Lev-Yadun S (2015) Plant development: cell movement relative to each other is both common and very important. Plant Signal Behav 10: e991566
155. Li J, Nagpal P, Vitart V, McMorris TC, Chory J (1996) A Role for Brassinosteroids in Light-Dependent Development of Arabidopsis. Science 272: 398–401
156. Li N, Liu Z, Wang Z, Ru L, Gonzalez N, Baekelandt A, Pauwels L, Goossens A, Xu R, Zhu Z, et al (2018) STERILE APETALA modulates the stability of a repressor protein complex to control organ size in Arabidopsis thaliana. PLOS Genet 14: e1007218
157. Li S, Zhao Y, Zhao Z, Wu X, Sun L, Liu Q, Wu Y (2016) Crystal Structure of the GRAS Domain of SCARECROW-LIKE7 in Oryza sativa. Plant Cell 28: 1025–1034
158. Li X, Cai W, Liu Y, Li H, Fu L, Liu Z, Xu L, Liu H, Xu T, Xiong Y (2017) Differential TOR activation and cell proliferation in Arabidopsis root and shoot apexes. Proc Natl Acad Sci U S A 114: 2765–2770
159. Li X, Zheng Y, Xing Q, Ardiansyah R, Zhou H, Ali S, Jing T, Tian J, Song XS, Li Y, et al (2020) Ectopic expression of the transcription factor CUC2 restricts growth by cell cycle inhibition in Arabidopsis leaves. Plant Signal Behav 15: 1706024
160. Li XG, Su YH, Zhao XY, Li W, Gao XQ, Zhang XS (2010) Cytokinin overproduction-caused alteration of flower development is partially mediated by CUC2 and CUC3 in Arabidopsis. Gene 450: 109–120
161. Liang Y, Basu D, Pattathil S, Xu W, Venetos A, Martin SL, Faik A, Hahn MG, Showalter AM (2013) Biochemical and physiological characterization of fut4 and fut6 mutants defective in arabinogalactan-protein fucosylation in Arabidopsis. J Exp Bot 64: 5537–5551
162. Lindemose S, Jensen MK, de Velde JV, O'Shea C, Heyndrickx KS, Workman CT, Vandepoele K, Skriver K, Masi FD (2014) A DNA-binding-site landscape and regulatory network analysis for NAC transcription factors in Arabidopsis thaliana. Nucleic Acids Res 42: 7681–7693
163. Lionetti V, Raiola A, Camardella L, Giovane A, Obel N, Pauly M, Favaron F, Cervone F, Bellincampi D (2007) Overexpression of Pectin Methylesterase Inhibitors in Arabidopsis Restricts Fungal Infection by Botrytis cinerea. Plant Physiol 143: 1871–1880
164. Lis H, Sharon N (1993) Protein glycosylation. Structural and functional aspects. Eur J Biochem 218: 1–27
165. Locascio A, Blázquez MA, Alabadí D (2013) Dynamic regulation of cortical microtubule organization through prefoldin-DELLA interaction. Curr Biol CB 23: 804–809
166. Lodha M, Marco CF, Timmermans MCP (2013) The ASYMMETRIC LEAVES complex maintains repression of KNOX homeobox genes via direct recruitment of Polycomb-repressive complex2. Genes Dev 27: 596–601
167. Long JA, Moan EI, Medford JI, Barton MK (1996) A member of the KNOTTED class of homeodomain proteins encoded by the STM gene of Arabidopsis. Nature 379: 66–69
168. de Lucas M, Davière J-M, Rodríguez-Falcón M, Pontin M, Iglesias-Pedraz JM, Lorrain S, Fankhauser C, Blázquez MA, Titarenko E, Prat S (2008) A molecular framework for light and gibberellin control of cell elongation. Nature 451: 480–484
169. Ma L, Li G (2019) Auxin-Dependent Cell Elongation During the Shade Avoidance Response. Front Plant Sci. doi: 10.3389/fpls.2019.00914
170. MacKinnon IM, Sturcová A, Sugimoto-Shirasu K, His I, McCann MC, Jarvis MC (2006) Cell-wall structure and anisotropy in procuste, a cellulose synthase mutant of Arabidopsis thaliana. Planta 224: 438–448
171. Malamy JE, Benfey PN (1997) Organization and cell differentiation in lateral roots of Arabidopsis thaliana. Dev Camb Engl 124: 33–44
172. Malinowski R, Kasprzewska A, Fleming AJ (2011) Targeted manipulation of leaf form via local growth repression. Plant J 66: 941–952
173. Marin E, Jouannet V, Herz A, Lokerse AS, Weijers D, Vaucheret H, Nussaume L, Crespi MD, Maizel A (2010) miR390, Arabidopsis TAS3 tasiRNAs, and Their AUXIN RESPONSE FACTOR Targets Define an Autoregulatory Network Quantitatively Regulating Lateral Root Growth. Plant Cell 22: 1104–1117
174. Marín-de la Rosa N, Pfeiffer A, Hill K, Locascio A, Bhalerao RP, Miskolczi P, Grønlund AL, Wanchoo-Kohli A, Thomas SG, Bennett MJ, et al (2015) Genome Wide Binding Site Analysis Reveals Transcriptional Coactivation of Cytokinin-Responsive Genes by DELLA Proteins. PLOS Genet 11: e1005337
175. Maris A, Kaewthai N, Eklöf JM, Miller JG, Brumer H, Fry SC, Verbelen J-P, Vissenberg K (2011) Differences in enzymic properties of five recombinant xyloglucan endotransglucosylase/hydrolase (XTH) proteins of Arabidopsis thaliana. J Exp Bot 62: 261–271

176. Maugarny A, Gonçalves B, Arnaud N, Laufs P (2016) Chapter 15 - CUC Transcription Factors: To the Meristem and Beyond. *In* DH Gonzalez, ed, Plant Transcr. Factors. Academic Press, Boston, pp 229–247
177. Maugarny-Calès A, Cortizo M, Adroher B, Borrega N, Gonçalves B, Brunoud G, Vernoux T, Arnaud N, Laufs P (2019) Dissecting the pathways coordinating patterning and growth by plant boundary domains. PLoS Genet **15**: e1007913
178. Maugarny-Calès A, Laufs P (2018) Getting leaves into shape: a molecular, cellular, environmental and evolutionary view. Dev Camb Engl. doi: 10.1242/dev.161646
179. Maymon I, Greenboim-Wainberg Y, Sagiv S, Kieber JJ, Moshelion M, Olszewski N, Weiss D (2009) Cytosolic activity of SPINDLY implies the existence of a DELLA-independent gibberellin-response pathway. Plant J **58**: 979–988
180. McConnell JR, Emery J, Eshed Y, Bao N, Bowman J, Barton MK (2001) Role of *PHABULOSA* and *PHAVOLUTA* in determining radial patterning in shoots. Nature **411**: 709–713
181. McGinnis KM, Thomas SG, Soule JD, Strader LC, Zale JM, Sun T, Steber CM (2003) The Arabidopsis SLEEPY1 gene encodes a putative F-box subunit of an SCF E3 ubiquitin ligase. Plant Cell **15**: 1120–1130
182. McKenna ST, Kunkel JG, Bosch M, Rounds CM, Vidali L, Winship LJ, Hepler PK (2009) Exocytosis Precedes and Predicts the Increase in Growth in Oscillating Pollen Tubes. Plant Cell **21**: 3026–3040
183. McQueen-Mason S, Durachko DM, Cosgrove DJ (1992) Two endogenous proteins that induce cell wall extension in plants. Plant Cell **4**: 1425–1433
184. Melaragno JE, Mehrotra B, Coleman AW (1993) Relationship between Endopolyploidy and Cell Size in Epidermal Tissue of Arabidopsis. Plant Cell **5**: 1661–1668
185. Meyer HM, Teles J, Formosa-Jordan P, Refahi Y, San-Bento R, Ingram G, Jönsson H, Locke JCW, Roeder AHK (2017) Fluctuations of the transcription factor ATML1 generate the pattern of giant cells in the Arabidopsis sepal. eLife **6**: e19131
186. Miedes E, Suslov D, Vandenbussche F, Kenobi K, Ivakov A, Van Der Straeten D, Lorences EP, Mellerowicz EJ, Verbelen J-P, Vissenberg K (2013) Xyloglucan endotransglucosylase/hydrolase (XTH) overexpression affects growth and cell wall mechanics in etiolated Arabidopsis hypocotyls. J Exp Bot **64**: 2481–2497
187. Milani P, Gholamirad M, Traas J, Arnéodo A, Boudaoud A, Argoul F, Hamant O (2011) In vivo analysis of local wall stiffness at the shoot apical meristem in Arabidopsis using atomic force microscopy. Plant J **67**: 1116–1123
188. Monna L, Kitazawa N, Yoshino R, Suzuki J, Masuda H, Maehara Y, Tanji M, Sato M, Nasu S, Minobe Y (2002) Positional Cloning of Rice Semidwarfing Gene, sd-1: Rice "Green Revolution Gene" Encodes a Mutant Enzyme Involved in Gibberellin Synthesis. DNA Res **9**: 11–17
189. Mora C, Tittensor DP, Adl S, Simpson AGB, Worm B (2011) How Many Species Are There on Earth and in the Ocean? PLOS Biol **9**: e1001127
190. Mousavi SAR, Dubin AE, Zeng W-Z, Coombs AM, Do K, Ghadiri DA, Keenan WT, Ge C, Zhao Y, Patapoutian A (2021) PIEZO ion channel is required for root mechanotransduction in Arabidopsis thaliana. Proc Natl Acad Sci. doi: 10.1073/pnas.2102188118
191. Murase K, Hirano Y, Sun T, Hakoshima T (2008) Gibberellin-induced DELLA recognition by the gibberellin receptor GID1. Nature **456**: 459–463
192. Mutanwad KV, Zangl I, Lucyshyn D (2020) Arabidopsis O-fucosyltransferase SPINDLY regulates root hair patterning independently of gibberellin signalling. bioRxiv 2020.04.23.057083
193. Mutasa-Göttgens E, Hedden P (2009) Gibberellin as a factor in floral regulatory networks. J Exp Bot **60**: 1979–1989
194. Nakata M, Matsumoto N, Tsugeki R, Rikirsch E, Laux T, Okada K (2012) Roles of the Middle Domain–Specific WUSCHEL-RELATED HOMEOBOX Genes in Early Development of Leaves in Arabidopsis. Plant Cell **24**: 519–535
195. Nakayama H, Kimura S (2015) Leaves may function as temperature sensors in the heterophylly of Rorippa aquatica (Brassicaceae). Plant Signal Behav **10**: e1091909
196. Nath U, Crawford BCW, Carpenter R, Coen E (2003) Genetic control of surface curvature. Science **299**: 1404–1407
197. Nikovics K, Blein T, Peaucelle A, Ishida T, Morin H, Aida M, Laufs P (2006) The Balance between the MIR164A and CUC2 Genes Controls Leaf Margin Serration in Arabidopsis. Plant Cell **18**: 2929–2945
198. Nogueira FTS, Madi S, Chitwood DH, Juarez MT, Timmermans MCP (2007) Two small regulatory RNAs establish opposing fates of a developmental axis. Genes Dev **21**: 750–755
199. Nohales MA, Kay SA (2019) GIGANTEA gates gibberellin signaling through stabilization of the DELLA proteins in Arabidopsis. Proc Natl Acad Sci **116**: 21893–21899
200. Norberg M, Holmlund M, Nilsson O (2005) The BLADE ON PETIOLE genes act redundantly to control the growth and development of lateral organs. Development **132**: 2203–2213
201. Oh E, Zhu J-Y, Bai M-Y, Arenhart RA, Sun Y, Wang Z-Y (2014) Cell elongation is regulated through a central circuit of interacting transcription factors in the Arabidopsis hypocotyl. eLife. doi: 10.7554/eLife.03031

202. Oh E, Zhu J-Y, Wang Z-Y (2012) Interaction between BZR1 and PIF4 integrates brassinosteroid and environmental responses. Nat Cell Biol 14: 802–809
203. Okada K, Ueda J, Komaki MK, Bell CJ, Shimura Y (1991) Requirement of the Auxin Polar Transport System in Early Stages of Arabidopsis Floral Bud Formation. Plant Cell 3: 677–684
204. O'Leary BM, Oh GGK, Lee CP, Millar AH (2020) Metabolite Regulatory Interactions Control Plant Respiratory Metabolism via Target of Rapamycin (TOR) Kinase Activation[OPEN]. Plant Cell 32: 666–682
205. Olszewski NE, West CM, Sassi SO, Hartweck LM (2010) O-GlcNAc protein modification in plants: Evolution and function. Biochim Biophys Acta 1800: 49–56
206. Ori N, Cohen AR, Etzioni A, Brand A, Yanai O, Shleizer S, Menda N, Amsellem Z, Efroni I, Pekker I, et al (2007) Regulation of LANCEOLATE by miR319 is required for compound-leaf development in tomato. Nat Genet 39: 787–791
207. Otsuga D, DeGuzman B, Prigge MJ, Drews GN, Clark SE (2001) REVOLUTA regulates meristem initiation at lateral positions. Plant J Cell Mol Biol 25: 223–236
208. Palatnik JF, Allen E, Wu X, Schommer C, Schwab R, Carrington JC, Weigel D (2003) Control of leaf morphogenesis by microRNAs. Nature 425: 257–263
209. Park J, Oh D-H, Dassanayake M, Nguyen KT, Ogas J, Choi G, Sun T (2017) Gibberellin Signaling Requires Chromatin Remodeler PICKLE to Promote Vegetative Growth and Phase Transitions1[OPEN]. Plant Physiol 173: 1463–1474
210. Pauly M, Albersheim P, Darvill A, York WS (1999) Molecular domains of the cellulose/xyloglucan network in the cell walls of higher plants. Plant J 20: 629–639
211. Peaucelle A, Braybrook SA, Le Guillou L, Bron E, Kuhlemeier C, Höfte H (2011) Pectin-Induced Changes in Cell Wall Mechanics Underlie Organ Initiation in Arabidopsis. Curr Biol 21: 1720–1726
212. Peaucelle A, Louvet R, Johansen JN, Höfte H, Laufs P, Pelloux J, Mouille G (2008) Arabidopsis phyllotaxis is controlled by the methyl-esterification status of cell-wall pectins. Curr Biol CB 18: 1943–1948
213. Peaucelle A, Wightman R, Höfte H (2015) The Control of Growth Symmetry Breaking in the Arabidopsis Hypocotyl. Curr Biol 25: 1746–1752
214. Peng J, Carol P, Richards DE, King KE, Cowling RJ, Murphy GP, Harberd NP (1997) The Arabidopsis GAI gene defines a signaling pathway that negatively regulates gibberellin responses. Genes Dev 11: 3194–3205
215. Peng J, Richards DE, Hartley NM, Murphy GP, Devos KM, Flintham JE, Beales J, Fish LJ, Worland AJ, Pelica F, et al (1999) "Green revolution" genes encode mutant gibberellin response modulators. Nature 400: 256–261
216. Pfeiffer A, Janocha D, Dong Y, Medzihradszky A, Schöne S, Daum G, Suzaki T, Forner J, Langenecker T, Rempel E, et al (2016) Integration of light and metabolic signals for stem cell activation at the shoot apical meristem. eLife 5: e17023
217. Phokas A, Coates JC (2021) Evolution of DELLA function and signaling in land plants. Evol Dev n/a: e12365
218. Pillitteri LJ, Guo X, Dong J (2016) Asymmetric cell division in plants: mechanisms of symmetry breaking and cell fate determination. Cell Mol Life Sci CMLS 73: 4213–4229
219. Popper ZA, Fry SC (2008) Xyloglucan-pectin linkages are formed intra-protoplasmically, contribute to wall-assembly, and remain stable in the cell wall. Planta 227: 781–794
220. del Pozo JC, Diaz-Trivino S, Cisneros N, Gutierrez C (2006) The Balance between Cell Division and Endoreplication Depends on E2FC-DPB, Transcription Factors Regulated by the Ubiquitin-SCFSKP2A Pathway in Arabidopsis. Plant Cell 18: 2224–2235
221. Qi J, Wang Y, Yu T, Cunha A, Wu B, Vernoux T, Meyerowitz E, Jiao Y (2014) Auxin depletion from leaf primordia contributes to organ patterning. Proc Natl Acad Sci 111: 18769–18774
222. Qi J, Wu B, Feng S, Lü S, Guan C, Zhang X, Qiu D, Hu Y, Zhou Y, Li C, et al (2017) Mechanical regulation of organ asymmetry in leaves. Nat Plants 3: 724–733
223. Qi R, John PCL (2007) Expression of Genomic AtCYCD2;1 in Arabidopsis Induces Cell Division at Smaller Cell Sizes: Implications for the Control of Plant Growth. Plant Physiol 144: 1587–1597
224. Qin F, Kodaira K-S, Maruyama K, Mizoi J, Tran L-SP, Fujita Y, Morimoto K, Shinozaki K, Yamaguchi-Shinozaki K (2011) SPINDLY, a negative regulator of gibberellic acid signaling, is involved in the plant abiotic stress response. Plant Physiol 157: 1900–1913
225. Quante M, Wang TC (2009) Stem cells in gastroenterology and hepatology. Nat Rev Gastroenterol Hepatol 6: 724–737
226. Rautengarten C, Ebert B, Liu L, Stonebloom S, Smith-Moritz AM, Pauly M, Orellana A, Scheller HV, Heazlewood JL (2016) The Arabidopsis Golgi-localized GDP- L -fucose transporter is required for plant development. Nat Commun 7: 12119
227. Rayon C, Cabanes-Macheteau M, Loutelier-Bourhis C, Salliot-Maire I, Lemoine J, Reiter WD, Lerouge P, Faye L (1999) Characterization of N-glycans from Arabidopsis. Application to a fucose-deficient mutant. Plant Physiol 119: 725–734
228. Reddy GV, Heisler MG, Ehrhardt DW, Meyerowitz EM (2004) Real-time lineage analysis reveals oriented cell divisions associated with morphogenesis at the shoot apex of Arabidopsis thaliana. Development 131: 4225–4237

229. **Reed JW, Wu M-F, Reeves PH, Hodgens C, Yadav V, Hayes S, Pierik R** (2018) Three Auxin Response Factors Promote Hypocotyl Elongation. Plant Physiol **178**: 864–875
230. **Refahi Y, Zardilis A, Michelin G, Wightman R, Leggio B, Legrand J, Faure E, Vachez L, Armezzani A, Risson A-E, et al** (2021) A multiscale analysis of early flower development in Arabidopsis provides an integrated view of molecular regulation and growth control. Dev Cell **56**: 540-556.e8
231. **Reinhardt D, Frenz M, Mandel T, Kuhlemeier C** (2005) Microsurgical and laser ablation analysis of leaf positioning and dorsoventral patterning in tomato. Development **132**: 15–26
232. **Reinhardt D, Kuhlemeier C** (2002) Plant architecture. EMBO Rep **3**: 846–851
233. **Reinhardt D, Mandel T, Kuhlemeier C** (2000) Auxin regulates the initiation and radial position of plant lateral organs. Plant Cell **12**: 507–518
234. **Reinhardt D, Pesce E-R, Stieger P, Mandel T, Baltensperger K, Bennett M, Traas J, Friml J, Kuhlemeier C** (2003) Regulation of phyllotaxis by polar auxin transport. Nature **426**: 255–260
235. **Reiter WD, Chapple CC, Somerville CR** (1993) Altered growth and cell walls in a fucose-deficient mutant of Arabidopsis. Science **261**: 1032–1035
236. **Ren M, Qiu S, Venglat P, Xiang D, Feng L, Selvaraj G, Datla R** (2011) Target of rapamycin regulates development and ribosomal RNA expression through kinase domain in Arabidopsis. Plant Physiol **155**: 1367–1382
237. **Ridley BL, O'Neill MA, Mohnen D** (2001) Pectins: structure, biosynthesis, and oligogalacturonide-related signaling. Phytochemistry **57**: 929–967
238. **Robaglia C, Thomas M, Meyer C** (2012) Sensing nutrient and energy status by SnRK1 and TOR kinases. Curr Opin Plant Biol **15**: 301–307
239. **Robert HS, Grunewald W, Sauer M, Cannoot B, Soriano M, Swarup R, Weijers D, Bennett M, Boutilier K, Friml J** (2015) Plant embryogenesis requires AUX/LAX-mediated auxin influx. Development **142**: 702–711
240. **Robertson M, Swain SM, Chandler PM, Olszewski NE** (1998) Identification of a Negative Regulator of Gibberellin Action, HvSPY, in Barley. Plant Cell **10**: 995–1007
241. **Robinson DO, Coate JE, Singh A, Hong L, Bush M, Doyle JJ, Roeder AHK** (2018) Ploidy and Size at Multiple Scales in the Arabidopsis Sepal. Plant Cell **30**: 2308–2329
242. **Rodriguez RE, Mecchia MA, Debernardi JM, Schommer C, Weigel D, Palatnik JF** (2010) Control of cell proliferation in Arabidopsis thaliana by microRNA miR396. Development **137**: 103–112
243. **Roeder AHK, Chickarmane V, Cunha A, Obara B, Manjunath BS, Meyerowitz EM** (2010) Variability in the Control of Cell Division Underlies Sepal Epidermal Patterning in Arabidopsis thaliana. PLOS Biol **8**: e1000367
244. **Sarnowska EA, Rolicka AT, Bucior E, Cwiek P, Tohge T, Fernie AR, Jikumaru Y, Kamiya Y, Franzen R, Schmelzer E, et al** (2013) DELLA-interacting SWI3C core subunit of switch/sucrose nonfermenting chromatin remodeling complex modulates gibberellin responses and hormonal cross talk in Arabidopsis. Plant Physiol **163**: 305–317
245. **Sasaki A, Itoh H, Gomi K, Ueguchi-Tanaka M, Ishiyama K, Kobayashi M, Jeong D-H, An G, Kitano H, Ashikari M, et al** (2003) Accumulation of Phosphorylated Repressor for Gibberellin Signaling in an F-box Mutant. Science **299**: 1896–1898
246. **Sassi M, Ali O, Boudon F, Cloarec G, Abad U, Cellier C, Chen X, Gilles B, Milani P, Friml J, et al** (2014) An Auxin-Mediated Shift toward Growth Isotropy Promotes Organ Formation at the Shoot Meristem in Arabidopsis. Curr Biol **24**: 2335–2342
247. **Sauret-Güeto S, Calder G, Harberd NP** (2012) Transient gibberellin application promotes Arabidopsis thaliana hypocotyl cell elongation without maintaining transverse orientation of microtubules on the outer tangential wall of epidermal cells. Plant J **69**: 628–639
248. **Sawa S, Watanabe K, Goto K, Liu YG, Shibata D, Kanaya E, Morita EH, Okada K** (1999) FILAMENTOUS FLOWER, a meristem and organ identity gene of Arabidopsis, encodes a protein with a zinc finger and HMG-related domains. Genes Dev **13**: 1079–1088
249. **Scheller HV, Ulvskov P** (2010) Hemicelluloses. Annu Rev Plant Biol **61**: 263–289
250. **Schepetilnikov M, Dimitrova M, Mancera-Martínez E, Geldreich A, Keller M, Ryabova LA** (2013) TOR and S6K1 promote translation reinitiation of uORF-containing mRNAs via phosphorylation of eIF3h. EMBO J **32**: 1087–1102
251. **Schepetilnikov M, Makarian J, Srour O, Geldreich A, Yang Z, Chicher J, Hammann P, Ryabova LA** (2017) GTPase ROP2 binds and promotes activation of target of rapamycin, TOR, in response to auxin. EMBO J **36**: 886–903
252. **Schepetilnikov M, Ryabova LA** (2018) Recent Discoveries on the Role of TOR (Target of Rapamycin) Signaling in Translation in Plants. Plant Physiol **176**: 1095–1105
253. **Schiessl K, Kausika S, Southam P, Bush M, Sablowski R** (2012) JAGGED Controls Growth Anisotropy and Coordination between Cell Size and Cell Cycle during Plant Organogenesis. Curr Biol **22**: 1739–1746
254. **Schmid M, Davison TS, Henz SR, Pape UJ, Demar M, Vingron M, Schölkopf B, Weigel D, Lohmann JU** (2005) A gene expression map of Arabidopsis thaliana development. Nat Genet **37**: 501–506

255. Schruff MC, Spielman M, Tiwari S, Adams S, Fenby N, Scott RJ (2006) The AUXIN RESPONSE FACTOR 2 gene of Arabidopsis links auxin signalling, cell division, and the size of seeds and other organs. Development 133: 251–261
256. Scofield S, Murison A, Jones A, Fozard J, Aida M, Band LR, Bennett M, Murray JAH (2018) Coordination of meristem and boundary functions by transcription factors in the SHOOT MERISTEMLESS regulatory network. Development. doi: 10.1242/dev.157081
257. Sénéchal F, Habrylo O, Hocq L, Domon J-M, Marcelo P, Lefebvre V, Pelloux J, Mercadante D (2017) Structural and dynamical characterization of the pH-dependence of the pectin methylesterase–pectin methylesterase inhibitor complex. J Biol Chem 292: 21538–21547
258. Sénéchal F, Mareck A, Marcelo P, Lerouge P, Pelloux J (2015) Arabidopsis PME17 Activity can be Controlled by Pectin Methylesterase Inhibitor4. Plant Signal Behav 10: e983351
259. Serra L, Perrot-Rechenmann C (2020) Spatiotemporal control of cell growth by CUC3 shapes leaf margins. Development. doi: 10.1242/dev.183277
260. Shi J, Dong J, Xue J, Wang H, Yang Z, Jiao Y, Xu L, Huang H (2017) Model for the role of auxin polar transport in patterning of the leaf adaxial–abaxial axis. Plant J 92: 469–480
261. Shibaoka H (1993) Regulation by Gibberellins of the Orientation of Cortical Microtubules in Plant Cells. Funct Plant Biol 20: 461–470
262. Shimada A, Ueguchi-Tanaka M, Nakatsu T, Nakajima M, Naoe Y, Ohmiya H, Kato H, Matsuoka M (2008) Structural basis for gibberellin recognition by its receptor GID1. Nature 456: 520–523
263. Shimada A, Ueguchi-Tanaka M, Sakamoto T, Fujioka S, Takatsuto S, Yoshida S, Sazuka T, Ashikari M, Matsuoka M (2006) The rice SPINDLY gene functions as a negative regulator of gibberellin signaling by controlling the suppressive function of the DELLA protein, SLR1, and modulating brassinosteroid synthesis. Plant J Cell Mol Biol 48: 390–402
264. Sicard A, Thamm A, Marona C, Lee YW, Wahl V, Stinchcombe JR, Wright SI, Kappel C, Lenhard M (2014) Repeated evolutionary changes of leaf morphology caused by mutations to a homeobox gene. Curr Biol CB 24: 1880–1886
265. Silverstone AL, Jung HS, Dill A, Kawaide H, Kamiya Y, Sun TP (2001) Repressing a repressor: gibberellin-induced rapid reduction of the RGA protein in Arabidopsis. Plant Cell 13: 1555–1566
266. Silverstone AL, Mak PYA, Martinez EC, Sun T (1997) The New Rga Locus Encodes a Negative Regulator of Gibberellin Response in Arabidopsis Thaliana. Genetics 146: 1087–1099
267. Silverstone AL, Tseng T-S, Swain SM, Dill A, Jeong SY, Olszewski NE, Sun T (2007) Functional Analysis of SPINDLY in Gibberellin Signaling in Arabidopsis. Plant Physiol 143: 987–1000
268. Simon MLA, Platre MP, Marquès-Bueno MM, Armengot L, Stanislas T, Bayle V, Caillaud M-C, Jaillais Y (2016) A PI4P-driven electrostatic field controls cell membrane identity and signaling in plants. Nat Plants 2: 16089
269. Skopelitis DS, Benkovics AH, Husbands AY, Timmermans MCP (2017) Boundary Formation through a Direct Threshold-Based Readout of Mobile Small RNA Gradients. Dev Cell 43: 265-273.e6
270. Smit ME, Weijers D (2015) The role of auxin signaling in early embryo pattern formation. Curr Opin Plant Biol 28: 99–105
271. Smith DK, Jones DM, Lau JBR, Cruz ER, Brown E, Harper JF, Wallace IS (2018) A Putative Protein O-Fucosyltransferase Facilitates Pollen Tube Penetration through the Stigma–Style Interface. Plant Physiol 176: 2804–2818
272. Sothern RB, Tseng T-S, Orcutt SL, Olszewski NE, Koukkari WL (2002) GIGANTEA and SPINDLY genes linked to the clock pathway that controls circadian characteristics of transpiration in Arabidopsis. Chronobiol Int 19: 1005–1022
273. Spartz AK, Ren H, Park MY, Grandt KN, Lee SH, Murphy AS, Sussman MR, Overvoorde PJ, Gray WM (2014) SAUR Inhibition of PP2C-D Phosphatases Activates Plasma Membrane H+-ATPases to Promote Cell Expansion in Arabidopsis. Plant Cell 26: 2129–2142
274. Sperry J (2015) Evolution of Water Transport and Xylem Structure. Int J Plant Sci. doi: 10.1086/368398
275. Spinelli SV, Martin AP, Viola IL, Gonzalez DH, Palatnik JF (2011) A Mechanistic Link between STM and CUC1 during Arabidopsis Development. Plant Physiol 156: 1894–1904
276. Stanislas T, Platre MP, Liu M, Rambaud-Lavigne LES, Jaillais Y, Hamant O (2018) A phosphoinositide map at the shoot apical meristem in Arabidopsis thaliana. BMC Biol 16: 20
277. Steiner E, Efroni I, Gopalraj M, Saathoff K, Tseng T-S, Kieffer M, Eshed Y, Olszewski N, Weiss D (2012) The Arabidopsis O-linked N-acetylglucosamine transferase SPINDLY interacts with class I TCPs to facilitate cytokinin responses in leaves and flowers. Plant Cell 24: 96–108
278. Steiner E, Livne S, Kobinson-Katz T, Tal L, Pri-Tal O, Mosquna A, Tarkowská D, Muller B, Tarkowski P, Weiss D (2016) SPINDLY inhibits class I TCP proteolysis to promote sensitivity to cytokinin. Plant Physiol. doi: 10.1104/pp.16.00343
279. Stratilová B, Šesták S, Mravec J, Garajová S, Pakanová Z, Vadinová K, Kučerová D, Kozmon S, Schwerdt JG, Shirley N, et al (2020) Another building block in the plant cell wall: Barley xyloglucan xyloglucosyl transferases link covalently xyloglucan and anionic oligosaccharides derived from pectin. Plant J Cell Mol Biol 104: 752–767

280. **Sugimoto-Shirasu K, Roberts K** (2003) "Big it up": endoreduplication and cell-size control in plants. Curr Opin Plant Biol **6**: 544–553
281. **Suzuki H, Park S-H, Okubo K, Kitamura J, Ueguchi-Tanaka M, Iuchi S, Katoh E, Kobayashi M, Yamaguchi I, Matsuoka M, et al** (2009) Differential expression and affinities of Arabidopsis gibberellin receptors can explain variation in phenotypes of multiple knock-out mutants. Plant J **60**: 48–55
282. **Swain SM, Tseng TS, Olszewski NE** (2001) Altered expression of SPINDLY affects gibberellin response and plant development. Plant Physiol **126**: 1174–1185
283. **Swain SM, Tseng T-S, Thornton TM, Gopalraj M, Olszewski NE** (2002) SPINDLY Is a Nuclear-Localized Repressor of Gibberellin Signal Transduction Expressed throughout the Plant. Plant Physiol **129**: 605–615
284. **Takeda T, Furuta Y, Awano T, Mizuno K, Mitsuishi Y, Hayashi T** (2002) Suppression and acceleration of cell elongation by integration of xyloglucans in pea stem segments. Proc Natl Acad Sci **99**: 9055–9060
285. **Tameshige T, Okamoto S, Lee JS, Aida M, Tasaka M, Torii KU, Uchida N** (2016a) A Secreted Peptide and Its Receptors Shape the Auxin Response Pattern and Leaf Margin Morphogenesis. Curr Biol **26**: 2478–2485
286. **Tameshige T, Okamoto S, Tasaka M, Torii KU, Uchida N** (2016b) Impact of *erecta* mutation on leaf serration differs between *Arabidopsis* accessions. Plant Signal Behav **11**: e1261231
287. **Thornton T, Kreppel L, Hart G, Olszewski N** (1999) Genetic and Biochemical analysis of arabidopsis SPY. *In* A Altman, M Ziv, S Izhar, eds, Plant Biotechnol. Vitro Biol. 21st Century Proc. IXth Int. Congr. Int. Assoc. Plant Tissue Cult. Biotechnol. Jerus. Isr. 14–19 June 1998. Springer Netherlands, Dordrecht, pp 445–448
288. **Tibbits CW, MacDougall AJ, Ring SG** (1998) Calcium binding and swelling behaviour of a high methoxyl pectin gel. Carbohydr Res **310**: 101–107
289. **Torii KU, Mitsukawa N, Oosumi T, Matsuura Y, Yokoyama R, Whittier RF, Komeda Y** (1996) The Arabidopsis ERECTA gene encodes a putative receptor protein kinase with extracellular leucine-rich repeats. Plant Cell **8**: 735–746
290. **Tseng T-S, Salomé PA, McClung CR, Olszewski NE** (2004) SPINDLY and GIGANTEA Interact and Act in Arabidopsis thaliana Pathways Involved in Light Responses, Flowering, and Rhythms in Cotyledon Movements. Plant Cell **16**: 1550–1563
291. **Tseng T-S, Swain SM, Olszewski NE** (2001) Ectopic Expression of the Tetratricopeptide Repeat Domain of SPINDLY Causes Defects in Gibberellin Response. Plant Physiol **126**: 1250–1258
292. **Tsuda K, Kurata N, Ohyanagi H, Hake S** (2014) Genome-Wide Study of KNOX Regulatory Network Reveals Brassinosteroid Catabolic Genes Important for Shoot Meristem Function in Rice. Plant Cell **26**: 3488–3500
293. **Tsukaya H** (2002) Interpretation of mutants in leaf morphology: Genetic evidence for a compensatory system in leaf morphogenesis that provides a new link between cell and organismal theories. Int. Rev. Cytol. Academic Press, pp 1–39
294. **Ubeda-Tomás S, Swarup R, Coates J, Swarup K, Laplaze L, Beemster GTS, Hedden P, Bhalerao R, Bennett MJ** (2008) Root growth in Arabidopsis requires gibberellin/DELLA signalling in the endodermis. Nat Cell Biol **10**: 625–628
295. **Ueguchi-Tanaka M, Ashikari M, Nakajima M, Itoh H, Katoh E, Kobayashi M, Chow T, Hsing YC, Kitano H, Yamaguchi I, et al** (2005) GIBBERELLIN INSENSITIVE DWARF1 encodes a soluble receptor for gibberellin. Nature **437**: 693–698
296. **Ueguchi-Tanaka M, Nakajima M, Katoh E, Ohmiya H, Asano K, Saji S, Hongyu X, Ashikari M, Kitano H, Yamaguchi I, et al** (2007) Molecular Interactions of a Soluble Gibberellin Receptor, GID1, with a Rice DELLA Protein, SLR1, and Gibberellin. Plant Cell **19**: 2140–2155
297. **Ursache R, Andersen TG, Marhavý P, Geldner N** (2018) A protocol for combining fluorescent proteins with histological stains for diverse cell wall components. Plant J **93**: 399–412
298. **Van Sandt VST, Suslov D, Verbelen J-P, Vissenberg K** (2007) Xyloglucan Endotransglucosylase Activity Loosens a Plant Cell Wall. Ann Bot **100**: 1467–1473
299. **Vanzin GF, Madson M, Carpita NC, Raikhel NV, Keegstra K, Reiter W-D** (2002) The mur2 mutant of Arabidopsis thaliana lacks fucosylated xyloglucan because of a lesion in fucosyltransferase AtFUT1. Proc Natl Acad Sci **99**: 3340–3345
300. **Vaux DL, Korsmeyer SJ** (1999) Cell Death in Development. Cell **96**: 245–254
301. **Verger S, Chabout S, Gineau E, Mouille G** (2016) Cell adhesion in plants is under the control of putative O-fucosyltransferases. Dev Camb Engl **143**: 2536–2540
302. **Verger S, Long Y, Boudaoud A, Hamant O** (2018) A tension-adhesion feedback loop in plant epidermis. eLife. doi: 10.7554/eLife.34460
303. **Vernoux T, Kronenberger J, Grandjean O, Laufs P, Traas J** (2000) PIN-FORMED 1 regulates cell fate at the periphery of the shoot apical meristem. Dev Camb Engl **127**: 5157–5165
304. **Vialette-Guiraud ACM, Adam H, Finet C, Jasinski S, Jouannic S, Scutt CP** (2011) Insights from ANA-grade angiosperms into the early evolution of CUP-SHAPED COTYLEDON genes. Ann Bot **107**: 1511–1519

305. Vlad D, Kierzkowski D, Rast MI, Vuolo F, Ioio RD, Galinha C, Gan X, Hajheidari M, Hay A, Smith RS, et al (2014) Leaf Shape Evolution Through Duplication, Regulatory Diversification, and Loss of a Homeobox Gene. Science 343: 780–783
306. Walker JD, Oppenheimer DG, Concienne J, Larkin JC (2000) SIAMESE, a gene controlling the endoreduplication cell cycle in Arabidopsis thaliana trichomes. Dev Camb Engl 127: 3931–3940
307. Wan J-X, Zhu X-F, Wang Y-Q, Liu L-Y, Zhang B-C, Li G-X, Zhou Y-H, Zheng S-J (2018) Xyloglucan Fucosylation Modulates Arabidopsis Cell Wall Hemicellulose Aluminium binding Capacity. Sci Rep 8: 428
308. Wang Y, He Y, Su C, Zentella R, Sun T-P, Wang L (2019) Nuclear Localized O-fucosyltransferase SPY Facilitates PRR5 Proteolysis to Fine-tune the Pace of Arabidopsis Circadian Clock. Mol Plant. doi: 10.1016/j.molp.2019.12.013
309. Wang Z, Li N, Jiang S, Gonzalez N, Huang X, Wang Y, Inzé D, Li Y (2016) SCFSAP controls organ size by targeting PPD proteins for degradation in Arabidopsis thaliana. Nat Commun 7: 11192
310. White PB, Wang T, Park YB, Cosgrove DJ, Hong M (2014) Water–Polysaccharide Interactions in the Primary Cell Wall of Arabidopsis thaliana from Polarization Transfer Solid-State NMR. J Am Chem Soc 136: 10399–10409
311. Willats WGT, Orfila C, Limberg G, Buchholt HC, Alebeek G-JWM van, Voragen AG, Marcus SE, Christensen TMIE, Mikkelsen JD, Murray BS, et al (2001) Modulation of the Degree and Pattern of Methyl-esterification of Pectic Homogalacturonan in Plant Cell Walls: IMPLICATIONS FOR PECTIN METHYL ESTERASE ACTION, MATRIX PROPERTIES, AND CELL ADHESION *. J Biol Chem 276: 19404–19413
312. Willige BC, Ghosh S, Nill C, Zourelidou M, Dohmann EMN, Maier A, Schwechheimer C (2007) The DELLA Domain of GA INSENSITIVE Mediates the Interaction with the GA INSENSITIVE DWARF1A Gibberellin Receptor of Arabidopsis. Plant Cell 19: 1209–1220
313. Wilson RN, Somerville CR (1995) Phenotypic Suppression of the Gibberellin-Insensitive Mutant (gai) of Arabidopsis. Plant Physiol 108: 495–502
314. Wolf S, Hématy K, Höfte H (2012) Growth control and cell wall signaling in plants. Annu Rev Plant Biol 63: 381–407
315. Wormit A, Usadel B (2018) The Multifaceted Role of Pectin Methylesterase Inhibitors (PMEIs). Int J Mol Sci 19: 2878
316. Wu G, Lin W-C, Huang T, Poethig RS, Springer PS, Kerstetter RA (2008) KANADI1 regulates adaxial-abaxial polarity in Arabidopsis by directly repressing the transcription of ASYMMETRIC LEAVES2. Proc Natl Acad Sci U S A 105: 16392–16397
317. Wu S, O'Lexy R, Xu M, Sang Y, Chen X, Yu Q, Gallagher KL (2016) Symplastic signaling instructs cell division, cell expansion, and cell polarity in the ground tissue of Arabidopsis thaliana roots. Proc Natl Acad Sci 113: 11621–11626
318. Wu Y, Williams M, Bernard S, Driouich A, Showalter AM, Faik A (2010) Functional Identification of Two Nonredundant Arabidopsis α(1,2)Fucosyltransferases Specific to Arabinogalactan Proteins*. J Biol Chem 285: 13638–13645
319. Xiang H, Okamura H, Kezuka Y, Katoh E (2018) Physical and thermodynamic characterization of the rice gibberellin receptor/gibberellin/DELLA protein complex. Sci Rep 8: 17719
320. Xiong Y, McCormack M, Li L, Hall Q, Xiang C, Sheen J (2013) Glucose-TOR signalling reprograms the transcriptome and activates meristems. Nature 496: 181–186
321. Yaganoglu S, Helassa N, Gaub BM, Welling M, Shi J, Müller DJ, Török K, Pantazis P (2019) GenEPi: Piezo1-based fluorescent reporter for visualizing mechanical stimuli with high spatiotemporal resolution. bioRxiv 702423
322. Yamaguchi S, Kamiya Y (2001) Gibberellins and Light-Stimulated Seed Germination. J Plant Growth Regul 20: 369–376
323. Yanai O, Shani E, Dolezal K, Tarkowski P, Sablowski R, Sandberg G, Samach A, Ori N (2005) Arabidopsis KNOXI Proteins Activate Cytokinin Biosynthesis. Curr Biol 15: 1566–1571
324. Yoshizumi T, Tsumoto Y, Takiguchi T, Nagata N, Yamamoto YY, Kawashima M, Ichikawa T, Nakazawa M, Yamamoto N, Matsui M (2006) INCREASED LEVEL OF POLYPLOIDY1, a Conserved Repressor of CYCLINA2 Transcription, Controls Endoreduplication in Arabidopsis. Plant Cell 18: 2452–2468
325. Yu H, Takeuchi H (2019) Protein O-glucosylation: another essential role of glucose in biology. Curr Opin Struct Biol 56: 64–71
326. Yu S, Galvão VC, Zhang Y-C, Horrer D, Zhang T-Q, Hao Y-H, Feng Y-Q, Wang S, Schmid M, Wang J-W (2012) Gibberellin regulates the Arabidopsis floral transition through miR156-targeted SQUAMOSA promoter binding-like transcription factors. Plant Cell 24: 3320–3332
327. Zentella R, Hu J, Hsieh W-P, Matsumoto PA, Dawdy A, Barnhill B, Oldenhof H, Hartweck LM, Maitra S, Thomas SG, et al (2016) O-GlcNAcylation of master growth repressor DELLA by SECRET AGENT modulates multiple signaling pathways in Arabidopsis. Genes Dev 30: 164–176
328. Zentella R, Sui N, Barnhill B, Hsieh W-P, Hu J, Shabanowitz J, Boyce M, Olszewski NE, Zhou P, Hunt DF, et al (2017) The Arabidopsis O-fucosyltransferase SPINDLY activates nuclear growth repressor DELLA. Nat Chem Biol 13: 479–485
329. Zhang F, Tadege M (2015) Repression of AS2 by WOX family transcription factors is required for leaf development in Medicago and Arabidopsis. Plant Signal Behav 10: e993291

330. **Zhang N, Meng Y, Li X, Zhou Y, Ma L, Fu L, Schwarzländer M, Liu H, Xiong Y** (2019a) Metabolite-mediated TOR signaling regulates the circadian clock in Arabidopsis. Proc Natl Acad Sci U S A **116**: 25395–25397
331. **Zhang T, Tang H, Vavylonis D, Cosgrove DJ** (2019b) Disentangling loosening from softening: insights into primary cell wall structure. Plant J Cell Mol Biol **100**: 1101–1117
332. **Zhao F, Du F, Oliveri H, Zhou L, Ali O, Chen W, Feng S, Wang Q, Lü S, Long M, et al** (2020) Microtubule-Mediated Wall Anisotropy Contributes to Leaf Blade Flattening. Curr Biol **30**: 3972-3985.e6
333. **Zhiponova MK, Vanhoutte I, Boudolf V, Betti C, Dhondt S, Coppens F, Mylle E, Maes S, González-García M-P, Caño-Delgado AI, et al** (2013) Brassinosteroid production and signaling differentially control cell division and expansion in the leaf. New Phytol **197**: 490–502
334. **Zhou X-Y, Song L, Xue H-W** (2013) Brassinosteroids Regulate the Differential Growth of Arabidopsis Hypocotyls through Auxin Signaling Components IAA19 and ARF7. Mol Plant **6**: 887–904
335. **Zykwinska AW, Ralet M-CJ, Garnier CD, Thibault J-FJ** (2005) Evidence for In Vitro Binding of Pectin Side Chains to Cellulose. Plant Physiol **139**: 397–407

Résumé de la thèse en français

Les végétaux forment de nouveaux organes toute leur vie grâce à l'activité de leurs méristèmes, au sein desquels un pool central de cellules souches alimente la production de nouveaux organes à la périphérie. Ces structures permettent l'émergence d'organes latéraux qui contribuent fortement à l'architecture de la plante. Les feuilles sont ainsi initiées successivement à des intervalles de temps réguliers (plastochron) et avec une disposition régulière (phyllotaxie). Le début du développement d'une nouvelle feuille est marqué par la création d'un nouvel axe de croissance par lequel un primordium en formation se sépare du reste du méristème apical caulinaire. La formation de cet axe de croissance implique la mise en place d'un domaine intermédiaire, appelé domaine frontière. Ce domaine possède une croissance réduite par rapport au primordium formant ainsi un différentiel de croissance au sein du tissu, à la base de la morphogénèse chez les végétaux. Des différences de croissance apparaissent également peu à peu à la marge de la feuille en croissance et permettent de définir des serrations comme la répétition le long de cette marge de protrusions appelées dents et de creux appelés sinus. Au niveau des feuilles, les sinus tiennent le rôle de domaine frontière entre deux dents successives.

Les facteurs de transcription CUP-SHAPED COTYLEDON participent à la définition de l'architecture de la plante dans différents contextes développementaux. Dans la feuille, les gènes *CUC2* et *CUC3* sont exprimés dans les sinus et ils permettent l'initiation des dents et leur croissance. Des résultats récents ont montré que CUC3 agit en aval de CUC2 et permet de maintenir la répression de croissance aux sinus. En plus de son rôle de répresseur de croissance local *via* CUC3, il a aussi été montré que CUC2 promeut la croissance de la dent à distance. Cette promotion de croissance à distance se fait à la fois au travers d'une activation de la signalisation auxinique, mais aussi par des relais moléculaires, tels que le gène *KLUH,* qui est impliqué dans la prolifération des cellules. L'effet de CUC2 sur la croissance est ainsi double, combinant un effet de répresseur local de croissance et un effet de promotion de la croissance à distance.

Des travaux récents ont cherché à identifier des relais supplémentaires et ont mis en évidence l'importance du fucose dans la mise en place de la serration. En effet un crible génétique suppresseur de l'activité de CUC2 a conduit à l'identification d'un nouvel allèle du gène *MURUS1* qui code une enzyme impliquée dans la synthèse du GDP-fucose. Ces travaux m'ont amenée à considérer le gène *SPINDLY (SPY),* qui code une O-fucosyl-transferase, comme un acteur de la morphogénèse foliaire car des mutants *spindly* ont la particularité de posséder des marges de feuilles lisses. Ces résultats constituent ainsi le point de départ de mes travaux de thèse.

Une première partie de mon travail a consisté à établir une caractérisation fine des phénotypes foliaires au cours du développement de la feuille du mutant *spy-3*. Cette caractérisation a notamment permis de montrer que le mutant *spy-3* phénocopie le mutant *cuc3-105* en présentant des feuilles dont les dents sont moins hautes que chez un individu sauvage, et ce dès le début de la croissance de la feuille. Mon attention s'est par la suite portée sur les cellules du sinus des feuilles du mutant *spy-3*, pour lesquelles j'ai montré une augmentation de surface significativement plus importante que chez le sauvage, suggérant ainsi que la restriction de croissance aux sinus n'est pas maintenue chez ce mutant. Une cinétique de croissance d'un double mutant *cuc3-105 spy-3* a permis d'écarter le fait que SPINDLY agisse dans une voie commune à CUC3, cependant plusieurs phénotypes foliaires de doubles mutants montrent que l'activité de SPINDLY est requise pour une mise en place correcte des dents dépendante de CUC2. Des quantifications de phénotypes de fusion de cotylédons montrent par ailleurs qu'il existe une redondance fonctionnelle entre les CUC et SPINDLY.

Des quantifications de l'expression de *SPINDLY* dans différentes lignées avec des niveaux de CUC2 contrastés suggèrent que l'expression de *SPINDLY* n'est pas activée par CUC2. En parallèle, la comparaison d'une liste de gènes dont l'expression est plus forte dans un mutant *spy-3* avec une liste de gènes négativement régulés suite à une forte induction ectopique de l'activité de CUC2 révèle l'existence de 100 gènes communs, dont un nombre important de gènes impliqués dans les modifications des parois et la croissance des cellules. L'effet de CUC2 sur l'expression de certains de ces gènes a été confirmé par quantification de leurs transcrits dans un contexte d'hypocotyles placés à l'obscurité, induits ou non-induits. Dans le même temps, des mesures de la taille des hypocotyles mettent en évidence que l'expression ectopique de CUC2 dans l'hypocotyle cause une forte diminution de l'élongation des cellules. Ces deux quantifications ayant été réalisées dans un fond mutant *cuc2-3* mais aussi double mutant *cuc2-3 cuc3-105*, j'ai proposé que CUC2 soit capable d'agir négativement sur l'élongation des cellules, et ce indépendamment de CUC3.

Enfin, des expériences de microscopie à force atomique (AFM) sur de très jeunes feuilles m'ont permis de montrer que bien que la taille des cellules des sinus et des dents ne soit pas différentes à ces stades, (i) il existe une rigidité différentielle des parois entre les futurs sinus et les futures dents, les sinus étant plus rigides et (ii) le mutant *spy-3* présente une perte de rigidité au sinus par rapport au sauvage. L'absence de contraste de rigidité entre les cellules de la future dent et du futur sinus d'un mutant *spy-3* pourrait ainsi causer l'apparition des phénotypes foliaires quantifiés au cours de mon travail.

Ces expériences suggèrent que dans le mutant *spy-3*, le niveau d'expression des gènes régulés de façon commune par SPINDLY et CUC2 soit plus élevé ce qui permettrait aux cellules d'avoir des parois plus lâches et ainsi une croissance moins contrainte. Par ailleurs, cela suggère que la mutation *spy-3* est capable de découpler l'activité de CUC2 sur les gènes de relâchement de la paroi de ses autres activités présentées plus haut.

Des expériences préliminaires réalisées à la fin de mon doctorat pourraient indiquer l'existence d'antagonismes entre CUC2 et diverses voies hormonales impliquées dans la croissance, telle que l'auxine. Notamment, CUC2 régule positivement l'expression de deux répresseurs de la voie auxinique *IAA18* et *IAA26* et la réponse à une auxine de synthèse semble altérée lors d'une induction ectopique de CUC2 dans un contexte d'hypocotyles placés à l'obscurité. Ces expériences constituent une base de travail pour de futurs travaux de recherche.

APPENDIX 1

List of the 100 genes that are both down-regulated in *p35S:CUC2-GR* and up-regulated in *spy-3*. 15 genes that are involved in cell wall-related processes are highlighted.

At3g30260	AGL79, AGAMOUS-like 79
At5g56970	ATCKX3, CKX3, cytokinin oxidase 3
At1g62500	Bifunctional inhibitor/lipid-transfer protein/seed storage 2S albumin superfamily protein
At5g26660	ATMYB86, MYB86, myb domain protein 86
At3g57520	AtSIP2, SIP2, seed imbibition 2
At5g04120	Phosphoglycerate mutase family protein
At5g24580	Heavy metal transport/detoxification superfamily protein
At1g79180	ATMYB63, MYB63, myb domain protein 63
At5g42180	Peroxidase superfamily protein
At4g14130	XTH15, XTR7, xyloglucan endotransglucosylase/hydrolase 15
At3g22740	HMT3, homocysteine S-methyltransferase 3
At1g11740	ankyrin repeat family protein
At1g31720	Protein of unknown function (DUF1218)
At5g09970	CYP78A7, cytochrome P450, family 78, subfamily A, polypeptide 7
At4g16270	Peroxidase superfamily protein
At1g14390	Leucine-rich repeat protein kinase family protein
At2g06850	EXGT-A1, EXT, XTH4, xyloglucan endotransglucosylase/hydrolase 4
At1g23760	JP630, PG3, BURP domain-containing protein
At3g02500	unknown protein
At3g29370	unknown protein
At3g29430	Terpenoid synthases superfamily protein
At4g29030	Putative membrane lipoprotein
At4g23680	Polyketide cyclase/dehydrase and lipid transport superfamily protein
At3g58850	HLH2, PAR2, phy rapidly regulated 2
At5g48560	basic helix-loop-helix (bHLH) DNA-binding superfamily protein
At5g20740	Plant invertase/pectin methylesterase inhibitor superfamily protein
At3g15400	ATA20, anther 20
At2g16980	Major facilitator superfamily protein
At1g49450	Transducin/WD40 repeat-like superfamily protein
At5g14090	unknown protein
At3g15990	SULTR3;4, sulfate transporter 3;4
At1g13600	AtbZIP58, bZIP58, basic leucine-zipper 58
At1g77530	O-methyltransferase family protein
At1g60060	Serine/threonine-protein kinase WNK (With No Lysine)-related
At3g50630	ICK2, KRP2, KIP-related protein 2
At5g33370	GDSL-like Lipase/Acylhydrolase superfamily protein
At5g54240	Protein of unknown function (DUF1223)

Appendix 1

At3g59010	PME61, pectin methylesterase 61
At2g38090	Duplicated homeodomain-like superfamily protein
At1g44970	Peroxidase superfamily protein
At1g48750	Bifunctional inhibitor/lipid-transfer protein/seed storage 2S albumin superfamily protein
At1g66350	RGL, RGL1, RGA-like 1
At1g80120	Protein of unknown function (DUF567)
At5g60760	P-loop containing nucleoside triphosphate hydrolases superfamily protein
At4g08160	glycosyl hydrolase family 10 protein / carbohydrate-binding domain-containing protein
At4g38400	ATEXLA2, ATEXPL2, ATHEXP BETA 2.2, EXLA2, EXPL2, expansin-like A2
At5g27220	Frigida-like protein
At5g65390	AGP7, arabinogalactan protein 7
At1g30760	FAD-binding Berberine family protein
At1g74430	ATMYB95, ATMYBCP66, MYB95, myb domain protein 95
At1g62480	Vacuolar calcium-binding protein-related
At5g49330	ATMYB111, MYB111, PFG3, myb domain protein 111
At4g21850	ATMSRB9, MSRB9, methionine sulfoxide reductase B9
At1g27920	MAP65-8, microtubule-associated protein 65-8
At3g13960	AtGRF5, GRF5, growth-regulating factor 5
At4g32460	Protein of unknown function, DUF642
At4g30290	ATXTH19, XTH19, xyloglucan endotransglucosylase/hydrolase 19
At1g76180	ERD14, Dehydrin family protein
At1g56430	ATNAS4, NAS4, nicotianamine synthase 4
At1g02205	CER1, Fatty acid hydroxylase superfamily
At1g52750	alpha/beta-Hydrolases superfamily protein
At5g42600	MRN1, marneral synthase
At1g13635	DNA glycosylase superfamily protein
At3g12710	DNA glycosylase superfamily protein
At5g24910	CYP714A1, cytochrome P450, family 714, subfamily A, polypeptide 1
At3g09910	ATRAB18C, ATRABC2B, RABC2b, RAB GTPase homolog C2B
At2g31900	ATMYO5, ATXIF, XIF, myosin-like protein XIF
At1g13670	unknown protein
At5g17420	ATCESA7, CESA7, IRX3, MUR10, Cellulose synthase family protein
At1g53160	SPL4, squamosa promoter binding protein-like 4
At4g13300	ATTPS13, TPS13, terpenoid synthase 13
At1g52030	F-ATMBP, MBP1.2, MBP2, myrosinase-binding protein 2
At4g30280	ATXTH18, XTH18, xyloglucan endotransglucosylase/hydrolase 18
At4g17220	ATMAP70-5, MAP70-5, microtubule-associated proteins 70-5
At2g14890	AGP9, arabinogalactan protein 9
At1g09540	ATMYB61, MYB61, myb domain protein 61
At1g12570	Glucose-methanol-choline (GMC) oxidoreductase family protein
At5g02170	Transmembrane amino acid transporter family protein

Appendix 1

At3g20450	B-cell receptor-associated protein 31-like
At1g14960	Polyketide cyclase/dehydrase and lipid transport superfamily protein
At1g19940	AtGH9B5, GH9B5, glycosyl hydrolase 9B5
At4g02290	AtGH9B13, GH9B13, glycosyl hydrolase 9B13
At3g45970	ATEXLA1, ATEXPL1, ATHEXP BETA 2.1, EXLA1, EXPL1, expansin-like A1
At5g50790	Nodulin MtN3 family protein
At1g20160	ATSBT5.2, Subtilisin-like serine endopeptidase family protein
At2g37280	ATPDR5, PDR5, pleiotropic drug resistance 5
At3g13520	AGP12, ATAGP12, arabinogalactan protein 12
At1g11080	scpl31, serine carboxypeptidase-like 31
At1g80760	NIP6, NIP6;1, NLM7, NOD26-like intrinsic protein 6;1
At1g78970	ATLUP1, LUP1, lupeol synthase 1
At4g29150	IQD25, IQ-domain 25
At1g69690	TCP family transcription factor
At4g23420	NAD(P)-binding Rossmann-fold superfamily protein
At5g19740	Peptidase M28 family protein
At5g44700	EDA23, GSO2, Leucine-rich repeat transmembrane protein kinase
At1g04660	glycine-rich protein
At1g06350	Fatty acid desaturase family protein
At5g06930	unknown protein
At5g10430	AGP4, ATAGP4, arabinogalactan protein 4
At5g22460	alpha/beta-Hydrolases superfamily protein

APPENDIX 2

List of the 30 genes that are both up-regulated in *p35S:CUC2-GR* and down-regulated in *spy-3*.

At4g12500	Bifunctional inhibitor/lipid-transfer protein/seed storage 2S albumin superfamily protein
At5g20250	DIN10, Raffinose synthase family protein
At1g33840	Protein of unknown function (DUF567)
At4g12310	CYP706A5, cytochrome P450, family 706, subfamily A, polypeptide 5
At3g14760	unknown protein
At2g38390	Peroxidase superfamily protein
At5g64750	ABR1, Integrase-type DNA-binding superfamily protein
At4g12480	pEARLI 1, Bifunctional inhibitor/lipid-transfer protein/seed storage 2S albumin superfamily protein
At1g06160	ORA59, octadecanoid-responsive Arabidopsis AP2/ERF 59
At3g23550	MATE efflux family protein
At1g69160	unknown protein
At5g44260	Zinc finger C-x8-C-x5-C-x3-H type family protein
At3g55240	Plant protein 1589 of unknown function
At1g57990	ATPUP18, PUP18, purine permease 18
At1g53870	Protein of unknown function (DUF567)
At1g71030	ATMYBL2, MYBL2, MYB-like 2
At5g59130	Subtilase family protein
At4g01250	AtWRKY22, WRKY22, WRKY family transcription factor
At4g13410	ATCSLA15, CSLA15, Nucleotide-diphospho-sugar transferases superfamily protein
At2g32660	AtRLP22, RLP22, receptor like protein 22
At4g36670	Major facilitator superfamily protein
At3g08970	ATERDJ3A, TMS1, DNAJ heat shock N-terminal domain-containing protein
At3g15356	Legume lectin family protein
At3g51660	Tautomerase/MIF superfamily protein
At5g28770	AtbZIP63, BZO2H3, bZIP transcription factor family protein
At2g04040	ATDTX1, TX1, MATE efflux family protein
At1g28010	ABCB14, ATABCB14, PGP14, P-glycoprotein 14
At4g12470	AZI1, azelaic acid induced 1
At2g29170	NAD(P)-binding Rossmann-fold superfamily protein
At2g40330	PYL6, RCAR9, PYR1-like 6

APPENDIX 4

List of primers used in this PhD manuscript for real-time quantitative RT-PCR:

Target	Primer 1	Primer 2
qREF	AACTCTATGCAGCATTTGATCCACT	TGATTGCATATCTTTATCGCCATC
EF1a	ATGCCCCAGGACATCGTGATTTCAT	TTGGCGGCACCCTTAGCTGGATCA
Actin2	GGAAGGATCTGTACGGTAAC	GGACCTGCCTCATCATACT
SPY	GTAGTTTCAACAACCTCGCA	CGAGAATTGGGAACTGCAC
CUC2	CTTGGCAACTTCCCGGGAGA	CCAGCCTCAGTTGCTCTGTTAGTT
CUC3	GGCGGAGGAGGACAGCTTGTT	TGAGGCCACGTGGAGCCCTA
XTH18	GCAAAGCCGAGGTTCAAATG	CCGGAGACTTAAGATAGAATGTTGTTAC
XTH19	ATCTCATCCCATGTAGTTCCCGG	CTTGTCCCTGGTAACTCTGCTG
EXLA1	GGCTAAACCTATTGTTGGTGCTGAC	CTTGTTGCCGTAATCGCAAGGAAC
EXLA2	CTTGTCCTTAGCAGCAGAGCC	GGTACAAGAGCTTTATCGCC
GA3ox1	GCGGGCTCTGGTTTGGTTA	ACCGTGCCACCGTTTCCT
IAA18	TCGCTGGCAAATACTTCTCTC	CACTGGACCAGGAGCAGTTC
IAA26	GTTTCATCTGTGAAGAGACTGCG	TTGCTTACTGCATCCAAATGTCAAG

List of primers used in this PhD manuscript genotyping:

Genotype	Allele	Primer1	Primer 2
spy-22	WT	GTTAAACCCTAAGTATCGGAC	TTGGCATAAGAAAGTGTATC
	Mutant	ATTTTGCCGATTTCGGAAC	TTGGCATAAGAAAGTGTATC
spy-23	WT	ATGGTGGGACTGGAAGATGATAC	CAGCTTCTACGAGGCGTCCTTC
	Mutant	ACGGTCGGGAAACTAGCTCTA	CAGCTTCTACGAGGCGTCCTTC
CUC2g-m4	WT	GCAATCTACGCCGCAGTCAAC	AATTCTTCCGCCATTGTCGTT
	Mutant	CAGCCGTAGCACCAACACAA	GGAAACAGCTATGACCATGAT
cuc2-1	WT	GGATCCGGAGGCTAAAGAAGTACCA	ATCCACATTATTACCACGCCCC
	Mutant	GGATCCGGAGGCTAAAGAAGTACCA	CTCGAGAGATTGAGTCGCCGTTTG
cuc2-3	WT	GGATCCGGAGGCTAAAGAAGTACCA	ATCCACATTATTACCACGCCCC
	Mutant	GGATCCGGAGGCTAAAGAAGTACCA	TCCATAACCAATCTCGATACAC
cuc3-105	WT	CTGTCCTCCCCATACTAAGCC	AGATGTGTTAAGCGAACTCGC
	Mutant	CTGTCCTCCCCATACTAAGCC	ATATTGACCATCATACTCATTGC
mir164a-4	WT	TCAATGCGTTACATATGCTG	CCATGCCATAGAGTAGATGC
	Mutant	TCAATGCGTTACATATGCTG	CAACCACGTCTTCAAAGCAA
gai-t6	WT	CTAGATCCGACATTGAAGGA	AGCATCAAGATCAGCTAAAC
	Mutant	CTAGATCCGACATTGAAGGA	TCGGGTACGGGATTTTCGCAT
rga-28	WT	ATGAAGAGAGATCATCACCAA	GCGTGGACCGCTTGCTGCAACT
	Mutant	ATGAAGAGAGATCATCACCAA	CGGCGGAGAGAGACGGTAG
spy-3		GCTCCCCTTACGCATCATGATTA	ACCAGCTCCTCGACCTGCCTGCA
mur1-1		ATGAAACTCCACTACGCCGA	GCCACAACGTAATCATCTGG

The *spy-3* and *mur1-1* mutants carry point mutations. Hence, genotyping was performed using sequencing for *spy-3* (WT: TTGGATC**A**G; Mutant: TTGGATC**G**G) as well as *mur1-1* (WT: CCGGAT**T**T; Mutant: CCGGAT**C**T).

université PARIS-SACLAY
ÉCOLE DOCTORALE
Sciences du végétal : du gène à l'écosystème (SEVE)

Résumé

Titre : Analyse Multi-Échelle de la Fonction des Facteurs de Transcription CUP-SHAPED COTYLEDON

Mots clés : Développement, Morphogenèse, Domaines frontières, CUP-SHAPED COTYLEDON, SPINDLY.

Au cours du développement des plantes, la croissance différentielle est essentielle pour façonner l'organisme. Les cellules végétales sont délimitées par une paroi cellulaire et ne peuvent pas migrer. Ainsi, la mise en place de l'architecture repose uniquement sur la production de nouveaux axes de croissance séparés les uns des autres par des domaines frontières qui délimitent et organisent la croissance. A l'échelle cellulaire, les domaines frontières présentent une croissance locale réduite, tandis qu'à distance ils contrôlent la croissance et le devenir cellulaire des tissus adjacents de manière non-cellule-autonome. Malgré l'identification de plusieurs leviers moléculaires, la façon dont les domaines frontières réalisent ces deux fonctions est encore mal comprise.

Au cours de cette thèse, des données morphométriques ainsi que la quantification de paramètres cellulaires ont permis de démontrer que le développement du domaine frontière à la marge de la feuille nécessite l'activité de SPINDLY (SPY) comme répresseur de croissance. J'ai montré que SPY agit de manière redondante avec les facteurs de transcription CUP-SHAPED COTYLEDON (CUC2 et CUC3) qui sont des déterminants majeurs du développement des domaines frontières. Au niveau moléculaire, SPY et CUC2 répriment un ensemble commun de gènes impliqués dans le relâchement de la paroi cellulaire. L'inhibition de l'expression de ces gènes pourrait expliquer la répression de croissance aux domaines frontières. Des mesures d'hypocotyles cultivés à l'obscurité valident ces données moléculaires et révèlent une nouvelle fonction de CUC2 dans la restriction de l'expansion cellulaire indépendamment de CUC3. Des mesures au microscope à force atomique confirment que les parois cellulaires des cellules des sinus de jeunes feuilles sont plus rigides que celles des dents. Cette rigidité différentielle de la paroi cellulaire se trouve réduite chez le mutant spy-3, renforçant l'idée que SPY permet de partiellement décomposer les fonctions de CUC2. Des régulateurs de la voie de l'auxine et des gibbérellines ont également été identifiés parmi les cibles de CUC2. Sachant que l'auxine et les gibbérellines régulent positivement l'expansion cellulaire, j'ai cherché à observer d'éventuelles interactions entre CUC2 et ces différentes voies hormonales.

L'ensemble de ces données montre que SPINDLY est impliqué dans la mise en place et le maintien des domaines frontières dans la feuille au cours du développement. La démonstration d'une nouvelle fonction de CUC2 indépendante de CUC3 précise le réseau de gènes centré sur CUC2. Enfin, CUC2 pourrait interagir négativement avec diverses voies hormonales.

Abstract

Title : Multi-Scale Analysis of CUP-SHAPED COTYLEDON Transcription Factors Function

Keywords : Development, leaf morphogenesis, Boundary domains, CUP-SHAPED COTYLEDON, SPINDLY.

In plants, differential growth is key to shape the developing organism as cells are delimited by cell wall and cannot migrate. The establishment of plant architecture relies on the production of new growth axes, that are separated by boundary domains that delimit and organize organ growth. At the cell level, boundary domains display reduced growth locally, while they orchestrate growth and fate of adjacent tissues in a non-cell autonomous manner. How these two functions are achieved remains elusive despite the identification of several molecular levers.

During my PhD, morphometrics as well as quantification of cellular parameters were used to show that leaf boundary domain development requires the activity of SPINDLY (SPY) as cell growth repressor. I show that SPY acts redundantly with CUP-SHAPED COTYLEDON transcription factors (CUC2 and CUC3) which are crucial for boundary domain development. Accordingly, at the molecular level, SPINDLY and CUC2 repress a common set of genes involved in cell wall loosening providing a molecular network for growth repression at boundary domains. Dark grown hypocotyl measurements validate molecular data and further reveal a new function for CUC2 at restricting cell expansion independently from CUC3. Atomic force microscopy confirmed that young leaf boundary domain cells have stiffer cell walls than marginal outgrowths. This differential cell wall stiffness was reduced in spy-3 mutant pushing the idea that SPY activity allows to partly decompose CUC2 local and remote functions Auxin and gibberellins have been shown to positively regulate cell expansion. As regulators of these hormonal pathways were found among CUC2 targets, I started to investigate the interactions between CUC2 and these hormonal pathways.

Taken together these data highlight a role for SPINDLY during boundary domain development and reveal a concealed part of the CUC2-centered gene network underlying boundary domain development, in relation with the regulation of hormone signaling pathways.